NASA Contractor Report 3275

Practical Optimal Flight Control System Design for Helicopter Aircraft

Volume I - Technical Report

L. G. Hofmann, Susan A. Riedel,
and Duane McRuer

CONTRACT NAS2-9946
MAY 1980

NASA

NASA Contractor Report 3275

Practical Optimal Flight Control System Design for Helicopter Aircraft

Volume I - Technical Report

L. G. Hofmann, Susan A. Riedel,
and Duane McRuer
Systems Technology, Inc.
Hawthorne, California

Prepared for
Ames Research Center
under Contract NAS2-9946

NASA
National Aeronautics
and Space Administration

**Scientific and Technical
Information Office**

1980

TABLE OF CONTENTS

LIST OF FIGURES

LIST OF TABLES

SECTION I

INTRODUCTION AND SUMMARY

A. INTRODUCTION

This report presents an eclectic flight control system design methodology which is characterized by highly integrated and synergistic use of modern and classical control theory techniques. The classical flight control aspects follow conventional practice, e.g., as covered in Ref. 10, while the optimal control component of the methodology is simply one viable approach among the several that have been suggested (e.g., Refs. 1-5). It is the intermix of techniques that promises improved effectiveness and more widespread consideration of practical matters in the design process. Practicality is viewed herein as satisfaction of design qualities which are explicit or implied by traditional flight control system specifications and structures. In this context practicality indicates compliance with flight control system objectives which have a history of success, such as requirements upon closed-loop bandwidth, and a desire for low-order controllers.

The class of problem addressed is in the province of stationary, linear, Gaussian, stochastic systems. Modern control theory results for linear, stationary stochastic optimal control [i.e., linear, quadratic, Gaussian (LQG) theory, e.g., Refs. 6-8] are the primary system synthesis tools. Classical control theory results [i.e., transfer functions, frequency response (Bode) plots, transient response plots, s-plane and Bode root locus techniques, and multiloop analysis (e.g., Refs. 9-11)] are the primary analytical and interpretative tools. Again, the integrated use of these modern and classical techniques is crucial in this design procedure.

One feature typical of flight control systems is that measurements provided by many sensors (with the possible exception of accelerometers) are practically free from broadband noise. This presents a problem and

an opportunity in the modern control framework wherein the controller comprises a Kalman filter and regulator combination. The absence of broadband measurement noise requires solution of a singular Kalman filter problem (treated in Appendix A). The singular filter solutions are of lower order than those with full measurement noise. Thus, the ability to solve the singular filter problem is a key point in attaining low-order controllers, which are desirable for practical solutions.

The design methodology presented is approached in a case study format so that examples of each step are available directly as that step is presented. The example applications use a UH-1H helicopter as the object of control. Two complete syntheses are available:

- Longitudinal rate of climb command, airspeed hold system for cruise.
- Longitudinal rate of climb command, groundspeed hold system for hover.

The details of these examples are summarized in appendices, i.e., the equations of motion for the UH-1H and its actuation system in Appendix B, the hover example in Appendix C, and the 100 kt cruise example in Appendix D. Appropriate material is drawn from these data bases to illustrate the technique and methodological developments in the main body of the report. This procedure is presented in a more general fashion so as to apply with little change to flight control designs for conventional takeoff and landing, and vertical/short takeoff and landing aircraft.

B. PREVIEW OF THE REPORT

The flight control system design synthesis starts as all syntheses must with design requirements. These are treated in Section II both generally and specifically. At the outset the analytical synthesis and design assessment phases are placed in context with the overall design process. The distinguishing features of optimal stochastic control and conventional control techniques in accomplishing these phases are then drawn. With the differences and distinguishing characteristics between optimal and traditional concepts delineated, the next step in an eclectic

approach is to establish some connections. This is accomplished using a simple idealized control system in which analytical relationships can be developed between open-loop function crossover frequency and optimal control cost function coefficients. This permits the conventional design goal of bandwidth to be related to cost function parameters for an equivalent optimal system. Design goals are then identified as primary (essential for feasibility) and secondary (degree of system quality and viability relative to alternatives). Control system bandwidth is primary, while degree of stability, detailed responses of primary and secondary controlled variables, control activity, sensitivity, etc., are examples of secondary design goals. In the synthesis methodology presented here the primary bandwidth goals are associated with the synthesis procedure using LQG optimal controller synthesis techniques. The secondary design goals are treated primarily via conventional controls analysis. There is of course potential, even essential, interaction required between the direct synthesis and analysis procedures to evolve a suitable design compromise, so these roles are not independent.

Although the theory of LQG stochastic optimal control is well advanced, the necessary engineering art required to permit practical flight control solutions as straightforward results from theory application is not well established. Section III describes some of the more important problem formulation details which we have found can make the difference between practical and nonsense solutions. These range from such mundane features as actuator command and disturbance representation to the subtle but extremely important selection of the control rates as the control features to be accounted for in the performance index.

With design goals established and the problem formulation details in hand, the controller synthesis itself is presented in Section IV. This is divided into the distinct steps of filter-observer synthesis, regulator synthesis, and combination to form the controller. At the beginning, some important facts about linear stochastic control are reviewed as needed to define the synthesis problem and solution. The singular filter problems and the implications of requiring a solution which does not require a differentiation are considered as an important aspect for flight

control system synthesis. These provide the last of the background needed in the synthesis steps, so the remainder, which is the bulk of the section, is devoted to specific recommended procedures for the synthesis of flight control systems and illustrative examples of their application. Some of the syntheses are repeated for different parameter sets to illustrate the sensitivity of the designs to various weightings.

The design assessment is presented in Section V as an examination and expansion of the synthesis results into a composite total picture of system properties, behavior, and design margins. In our optimal synthesis method the bandwidths of various loops were central issues, and these were "automatically" met by direct (or perhaps iterative) exercise of the optimal design procedure. The design assessment uses a combination of analytical techniques from classical and optimal control theory to expand the scope of the results, highlight the dominant properties, and reveal the sensitivity of the system's characteristics to uncertainties. In the process of the detailed design assessment the optimal synthesis design results can be better appreciated in that the relative importance of the various terms in the control laws and factors which contribute to particular control behavior can be clearly identified. This detailed assessment and broadened understanding lead directly to simplifications of the design which may lead to a simpler and more practical controller and other aspects of detailed implementation of the system. Section V begins with an outline of the system and controller properties to be examined and a systematic checklist-like method for exposing the properties of the system and controller. The major content of the section is then devoted to a close look at many of the techniques for the design evaluation illustrated with the helicopter hovering system example. When all this is done, the design is not only assessed but simplified implementations have also been considered, together with their implications on system behavior.

Various technical details required for completeness or reference are contained in the appendices. These include, as mentioned previously, the development of the singular Kalman filter solution, aircraft equations of motion and numerical data, and data summaries for the example applications.

C. SOFTWARE

The extensive computations required to accomplish numerical solutions are a necessary adjunct to the methodology presented. Volume II of this report contains the user's manual for the software package developed in the course of this work. The software integrates the design principles from optimal control theory with those from classical control theory, permitting the user to design and analyze a control system. The highly interactive and modular design philosophy employed permits the user to develop a "hands on" appreciation and close connection with each aspect of the synthesis and assessment process. In addition, the flexibility of the software permits the design to proceed in exactly that sequence of steps deemed most appropriate for the particular problems.

Figure 1 illustrates the block structure which forms the backbone of the software package. Each block is a separate executable file which performs the specific task noted in the figure. The underlying file system structure allows the various blocks to communicate information to one another. At each block, a "problem file" is read and/or written. These problem files store all intermediate results, which the user may access via the service routine. The service routine selectively reads and formats to a line printer any user-requested elements in a given problem file. In this way, the user can examine not only the final synthesis results but also those intermediate results of interest which might provide increased understanding of the results obtained.

Two types of blocks comprise Fig. 1. The first type (Blocks 1, 3, 4, 5, 6, 7, 10) implements various aspects of the optimal control design process using software adapted from Slater's version of Bryson and Hall's OPTSYS (Ref. 29). The output from these blocks is stored on problem files. The second type of block (Blocks 2, 8, 9) provides links between the optimal control design and the classical control analysis techniques. The classical control software is organized in a similar fashion, as shown in Fig. 2.

A typical sequence of steps in designing an optimal control system is to begin with Block 1 at the top of Fig. 1 and work clockwise through

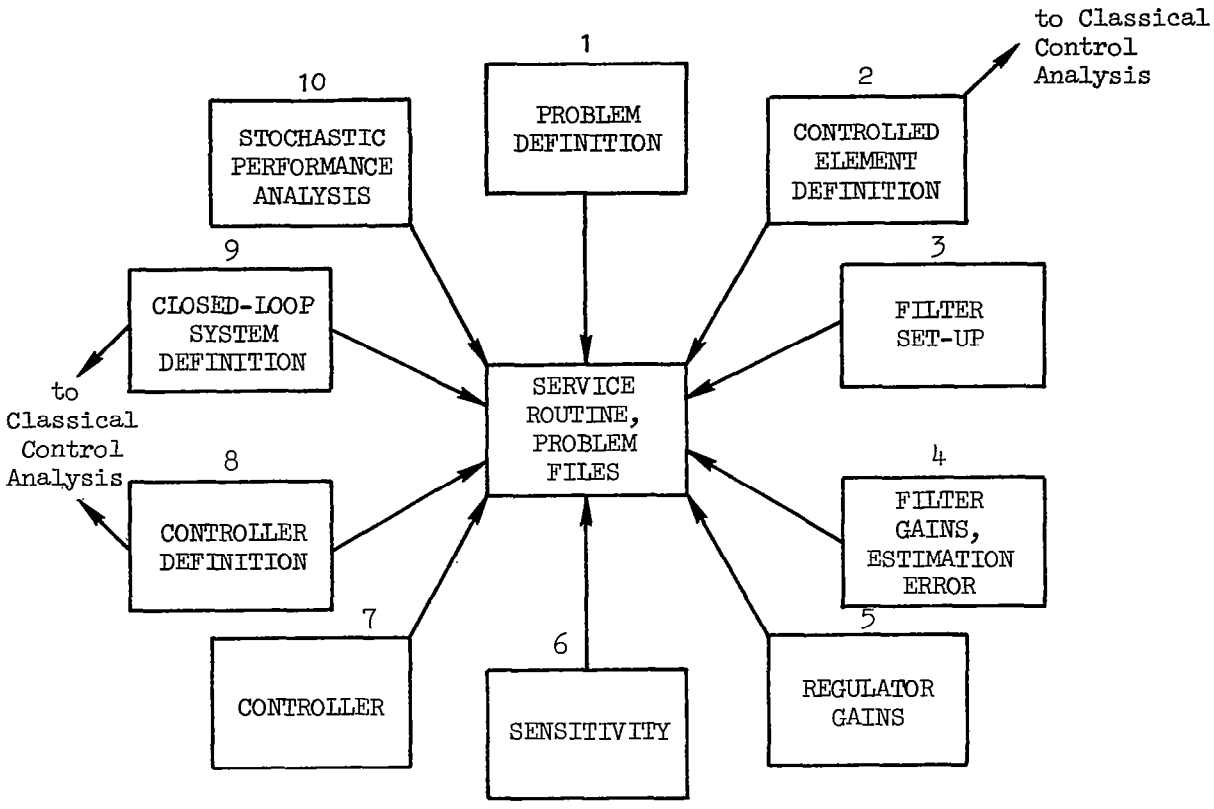

Figure 1. Software Structure, Optimal Control

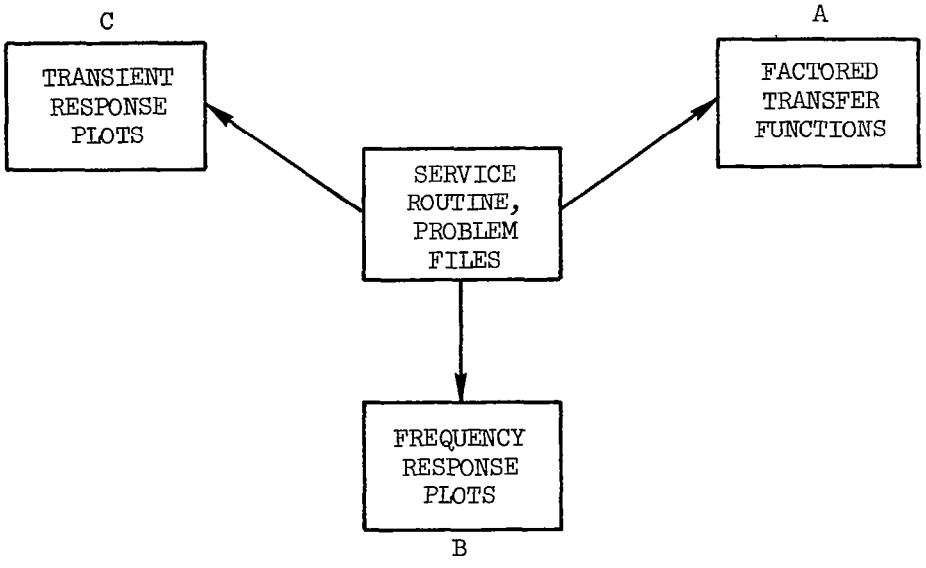

Figure 2. Software Structure, Classical Control

all blocks, making the appropriate indicated excursions to the blocks in Fig. 2 to use the classical control analysis techniques. Blocks may be repeated to cycle a portion of the design, while some blocks (such as the sensitivity block, for example) may be bypassed altogether.

A complete description of the use of this package, along with a simple, but illustrative, example is given in Vol. II (Ref. 23).

SECTION II

FLIGHT CONTROL SYSTEM DESIGN REQUIREMENTS

A. INTRODUCTION

The flight control system's (FCS) basic overall function is to provide:

- Stability.
- Desired responses to specified inputs.
- Suppression of the effects of disturbances, component variations, and uncertainties.
- Modification or elimination of vehicle cross-coupling effects.

Each specific function can be achieved by appropriate application of control techniques in a manner consistent with overall system requirements.

It is, of course, necessary to have a keen understanding of what is "appropriate" and "consistent." This is best arrived at via the overview of the design process given in the next three paragraphs (from Ref. 10).

> The aim of the FCS design is to produce a functional system that performs its assigned tasks "satisfactorily." The design process leading to this end can be broken into several phases that are more or less chronological, yet are extensively interrelated and interconnected. A typical set of such phrases might include the following.
>
> 1) Establishment of System Purpose and Overall System Requirements. At the design stage, system purpose can be equated with the mission phase or task definitions. Requirements are partially derivable from the functions needed to be performed to accomplish these mission phases (operational requirements), and less directly from the characteristics of the interconnected components and the environment in which they operate (implied requirements).
>
> 2) Determination of Unalterable Element, Command, and Disturbance Environment Characteristics. Typically, the characteristics of some component parts of the system

are not easily changed by the system designer. In aeronautical control and guidance such relatively "unalterable" elements often include the vehicle itself and possibly the control surface actuators and some of the motion quantity sensors. The "structure" of the commands and disturbances is not subject to the choice of the designer but is instead a direct consequence of the mission or task and the environment. The latter may, however, be open to some interpretation.

3) Evolution of Competing Feasible Systems. Usually, requirements can be met in more than one way, e.g., with different sensed motion quantities and equalization elements which are completely alterable within the limits of physical realizability and practicality. Then it is possible to evolve competing systems that become candidates for selection on the basis of their various desirable properties.

4) Competing System Assessment, System Selection. The competing systems can be compared on a very large number of bases which can be divided into two categories: design quantities and design qualities. Design quantities include the dynamic performance (relative stability, accuracy, speed of response or bandwidth, etc.) and the physical characteristics (weight, volume, power or energy consumption, etc.). Design qualities, the so-called "-ilities," include safety, operational capability, reliability, maintainability, cost, etc. An optimum system is one that has some "best" combination of all these features.

5) Detailed Study of the Selected System. Once a best system has been selected, it is still necessary to validate it for all nominal and abnormal operating conditions. The components that do not yet exist as hardware must be specified, designed, fabricated and tested as components. As many of these as possible should be assembled in a series of system simulations which culminate in flight tests of the complete system in its actual operating environment. At each stage of the testing process the assumptions that were made in previous phases of the design should be checked for validity. If actual conditions violate the assumptions, a new iteration of the design should be begun at the point at which the incorrect assumption was made.

The above steps in the orderly process of evolving, or synthesizing, a system that satisfactorily meets all its objectives are governed initially by a set of functional requirements stemming (see Item 1 above) from operational needs and system integration

implications. These latter, implied, requirements depend on the final system selected (see Item 4) which is then completely specified functionally by the total set of (functional) requirements. The converting of these requirements on each element of the system into usable hardware generally requires a specification that includes not only the functional requirements but also applicable specifications relating to hardware design and fabrication practices, including extreme environmental factors.

In any aeronautical system design the requirements for subsystems evolve in a pyramidal fashion, and become more numerous and detailed as definition of the actual equipment is approached. The apex of the pyramid is the mission purpose and definition (see Fig. 3). Immediately below this central point are three blocks involving considerations that interact strongly in the earliest preliminary design stages: mission phases, vehicle operating point profile, and guidance possibilities. When the mission is realistic, one or more feasible vehicle operating-point profiles are joined with one or more guidance possibilities to enable the overall system to perform through the constituent phases of the mission.

It is within this larger context that practical flight control system design must be considered. This project, while restricted in scope to the analytical/quantitative aspects of design, must remain responsive to, and compatible with, this context. Within this scope, it is clear that we are mainly concerned with the quantitative aspects of the

Determination of Unalterable Element Command and Disturbance Environment Characteristics

Evolution of Competing Feasible Systems

Competing System Assessment, System Selection

phases of the overall design process.

Address of these design phases using a non-traditional flight control system synthesis technique, such as linear quadratic, Gaussian (LQG) optimal control, requires that we have the distinguishing features with respect to the more traditional techniques firmly in mind. These distinguishing features are summarized in Table 1. As shown by the table the differences are confined largely to the Evolution of Competing Systems design phase. Conventional control theory considers the entire entourage of inputs and disturbances ab initio, whereas the optimal formulation leaves direct consideration of transients until a later phase of design. Control point

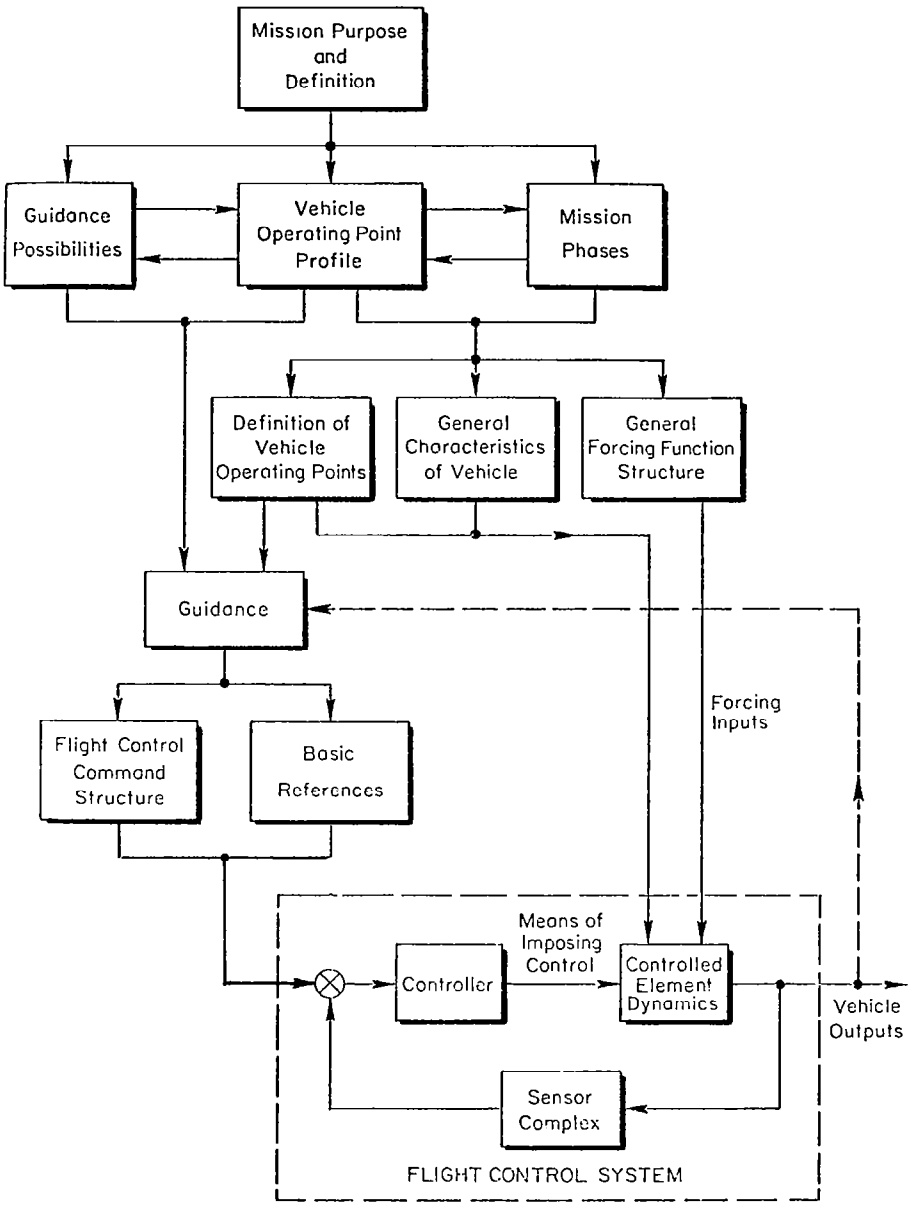

Figure 3. Evolution of Flight Control Requirements (from Ref. 10)

TABLE 1

DISTINGUISHING FEATURES OF CONTROL SYSTEM
ANALYSIS/SYNTHESIS TECHNIQUES

DESIGN PROCESS PHASES	ANALYSIS/SYNTHESIS TECHNIQUES	
	LQG OPTIMAL STOCHASTIC CONTROL	CONVENTIONAL CONTROL THEORY
Determination of Unalterable Element, Command and Disturbance Environment Characteristics	Similar linearized, constant coefficient equations of motion and Gaussian statistics for random commands/disturbances are needed	Entire ensemble of discrete command input forms
Evolution of Competing Feasible Systems	Measurements: Similar alternatives based on traditional/feasible sensors are applicable.	
	Control Point Utilization: Determined by solution based upon cost function parameters. Alternative solutions obtained by varying cost function parameters.	Control Point Utilization: Determined by considerations of: typical operational utilization (e.g., by pilots); design-conducted transfer function survey based on multivariable control theory; separation of trim and high-frequency control actions; controls coordination and/or decoupling.
	Controller Equalization: Determined by solution of optimal filter-observer problem. Alternative solution obtained by altering measurement noise and/or disturbance environment assumptions.	Controller Equalization: Determined using combinations of: s-plane and Bode root loci and conventional frequency response synthesis procedures with multivariable control theory, response/error coefficients, and indicial (sometimes ramp) responses.
	Realization: Designer-conducted reconfigurations of standard regulator plus filter-observer realizations.	Realization: Inherent in synthesis procedure.
Competing System Assessment, System Selection	Transient Response: Same transient response characteristics required.	
	RMS Response: Same rms response characteristics required.	
	System Sensitivity: Same insensitivity characteristics required.	
	RMS State Estimation Error: Additional basis for selecting sensor complement.	
	Economy of Controller Equalization: Direct result of sensor complement selection and measurement noise assumptions.	Economy of Controller Equalization: Inherent in synthesis procedure.

utilization factors at first glance appear to be quite different — yet the considerations used in the conventional approach must ultimately be reflected into the optimal if an adequate design is to be achieved. LQG optimal control techniques provide an additional basis for selecting a sensor complement (via rms state estimation error evaluation) and permit an automated controller solution (albeit ordinarily in a form requiring considerable manipulation before the flight control system implementation). The automated solution feature is achieved at the expense of having to specify sets of cost function parameters. We shall show later that this can be analogous to selection of control loop bandwidths when conventional frequency response synthesis techniques are used. Additional features of the LQG optimal control technique are that closed-loop system stability is inherent in every controller solution (but acceptable insensitivity to component variations and uncertainties is by no means assured), and that the closed-loop system can be designed specifically for a given command and disturbance input environment.

The assessments needed at the completion of a trial synthesis to evaluate the degree of system adequacy are substantially identical and any shortcomings must be corrected by additional iterations. Thus, in the larger context, the impact of using one or another control system analysis/synthesis technique should be nil. The two techniques are simply systematic methods for evolving and assessing competing system designs. On the other hand, the impact will not be nil if the two techniques are not equally effective in evolving practical candidate competing systems. This in turn emphasizes the importance of technique in applying LQG optimal stochastic control to the flight control problem when one chooses to take advantage of this more highly automatic design procedure.

These aspects of technique fall into four areas:

- Establishing design goals consistent with operational and implied requirements.
- Formulating the problem (equations of motion and input and disturbance environment models) in terms appropriate to control requirements determined by mission phase tasks.

- Selecting appropriate sensor complements.
- Selecting appropriate cost function parameters.

These matters of technique are discussed in this and the following section.

B. CONNECTIONS BETWEEN OPTIMAL AND TRADITIONAL CONTROL CONCEPTS FOR A SIMPLE IDEAL SYSTEM

The last section explored the differences and distinguishing characteristics between optimal and more traditional concepts; the present one will emphasize their connecting relationships. This will be accomplished in the guise of a very simple idealized control system. Simplicity permits the development of analytical relationships among bandwidth, open-loop function crossover frequency, transient and stochastic system response characteristics, sensitivity, and optimal control cost function coefficients. The idealized system is chosen not only for its analytical simplicity but also for its practical significance in the application of frequency response synthesis techniques. The system, in fact, serves as a prototype or ideal solution which the designer attempts to emulate in far more complex applications.

1. Relationships Between System Response Characteristics and Sensitivity to Crossover Frequency and Bandwidth

A block diagram for a single-loop feedback control system is given in Fig. 4. Limiting forms of the closed-loop system transfer functions in terms of the magnitude of the open-loop function, $|G(s)|$, are given in Table 2. The key point of these limiting forms is that three regions exist. In the first, when $|G| >> 1$ feedback control is fully active, and the system output follows the system input closely with little error. The second regime is at the other extreme, $|G| << 1$, where feedback control is essentially not operating and the system error and input are nearly the same. The third frequency regime, characterized by $|G|$ of the order of 1, is the region where feedback relationships are most complex in that the controller and controlled element dynamics interact to create the dominant closed-loop system modes. In a typical closed-loop system which

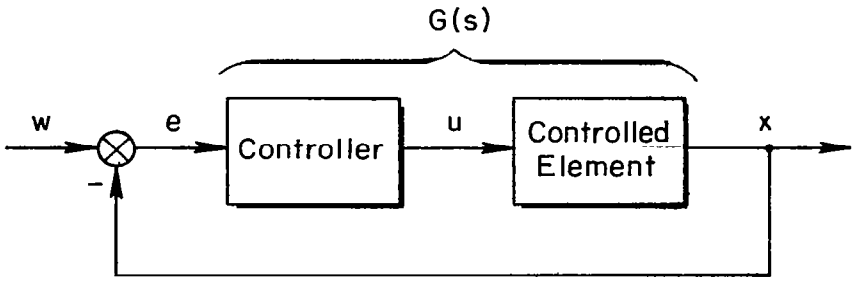

Open-Loop Transfer Function

$$G(s) = \frac{X(s)}{E(s)}$$

Closed-Loop Transfer Functions

Response/Command Relationship

$$\frac{X(s)}{W(s)} = \frac{G(s)}{1 + G(s)}$$

Error/Command Relationship

$$\frac{E(s)}{W(s)} = \frac{1}{1 + G(s)}$$

Figure 4. Prototype Closed-Loop Control System

TABLE 2. LIMITING FORMS FOR TRANSFER FUNCTIONS

TRANSFER FUNCTION	$\|G\|$		
	$>> 1$	$O(1)$	$<< 1$
X/W	1	$\frac{G}{1 + G}$	G
E/W	1/G	$\frac{1}{1 + G}$	1

is low pass in character, these three regimes correspond to low frequency, very high frequency, and crossover frequency regions, respectively.

A key point to appreciate in Table 2 is that $|G(s)| = 1$ provides a clear demarcation between the limiting form approximations. Further, while the limiting forms represent idealizations of the response characteristics desired for the controlled variable, x, and for the error variable, e, these particular idealizations are essentially independent of the details of $G(s)$ in the regimes where the limiting forms apply.

On the other hand, the form of $G(s)$ in the crossover region about $|G(s)| = 1$, which constitutes a transition between the limiting cases, is of great importance. It is here that the battle between high performance and stability is joined. The ideal form for $G(s)$ in this crossover region approximates $G(s) = \omega_c/s$, where the gain, ω_c, coincides with the crossover frequency (i.e., $|\omega_c/s|_{s=j\omega_c} = 1$). A basic design principle in classical frequency response design is to adjust $G(s)$ so that:

$$\begin{aligned} G(s) &\doteq \omega_c/s && \text{for} \quad s \doteq j\omega_c \\ |G(j\omega)| &>> 1 && \text{for} \quad \omega << \omega_c \\ |G(j\omega)| &<< 1 && \text{for} \quad \omega >> \omega_c \end{aligned} \tag{1}$$

The closed-loop consequences of this type of adjustment include good response following of commands and good error reduction over an input frequency range less than ω_c, with adequate closed-loop system stability. These characteristics will be obtained regardless of the detailed nature of $G(s)$ in the limiting form regimes. This prescription can be generalized in a straightforward way for multivariable control applications (Refs. 10 and 11). It can be modified to take more precise account of phase margins significantly less than $\pi/2$ rad by adding an $e^{-\tau s}$ term to the approximation for $G(s)$ in the crossover band (Refs. 10 and 12). The optimal controllers with which we shall be concerned here tend inherently to be highly stable, so our simple form $G(s) = \omega_c/s$ remains an appropriate ideal.

The dynamics, open- and closed-loop frequency response, and indicial response characteristics of the idealized system are summarized in Fig. 5.

The closed-loop frequency response functions in Fig. 5 show that crossover frequency coincides with the classical definition of signal bandwidth. That is, bandwidth is associated with the −3.01 dB point of the frequency response. Notice that for this particular choice for G(s) the error suppression bandwidth and controlled variable response bandwidth are <u>both</u> equal to ω_c. If $\angle G(j\omega) \neq -\pi/2$ when $|G(j\omega)| = 1$, these bandwidths are unequal, but both are still approximated by ω_c when adequate phase (stability) margin is provided for in G(s). [That is, when $|G(j\omega)| = 1$, $(0 - \varphi_M) \geq \angle G(j\omega) \geq (\varphi_M - \pi/2)$ in order to insure a phase margin of at least φ_M radians.]

The transient response characteristics for this prototype system are illustrated by the indicial responses in Fig. 5. These are:

$$x = 1 - \exp(-\omega_c t) \tag{2}$$

$$e = \exp(-\omega_c t) \tag{3}$$

The responses to a unit initial condition on the controlled variable (considered to be the state) are:

$$x = \exp(-\omega_c t) = -e \tag{4}$$

The transient responses are smooth, free from overshoot, and are characterized by a response time, $3/\omega_c$. The steady-state error response to the step input is zero.

Consider next the root-mean-square (rms) response characteristics for this prototype system. The block diagram for the system is in Fig. 6. The stochastic input is generated by low-pass filtering unit white noise. Normalized rms controlled variable (σ_x/σ_w) and error (σ_e/σ_w) responses are plotted in Fig. 7 as a function of the normalized stochastic input half-power frequency (ω_i/ω_c). For stochastic input half-power frequencies ω_i which are less than the crossover frequency, Fig. 7 indicates that

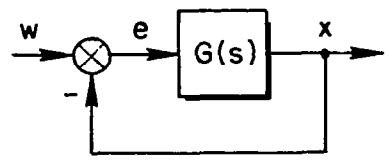

$$G(s) = \frac{\omega_c}{s}$$

$$\frac{X(s)}{W(s)} = \frac{G}{1+G} = \frac{\omega_c}{s+\omega_c}$$

$$\frac{E(s)}{W(s)} = \frac{1}{1+G} = \frac{s}{s+\omega_c}$$

a) System Transfer Function

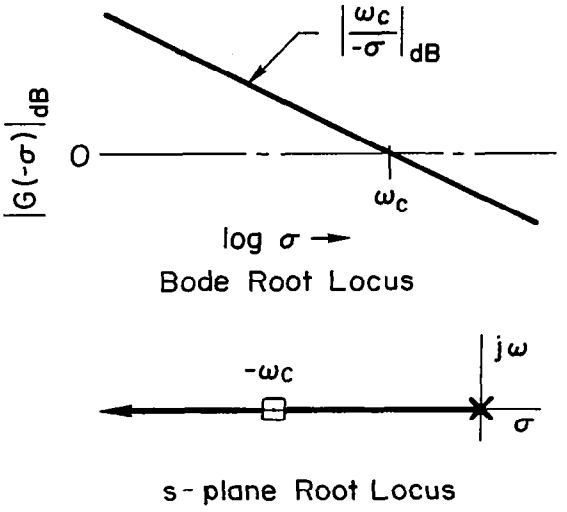

b) System Dynamics : Root Loci

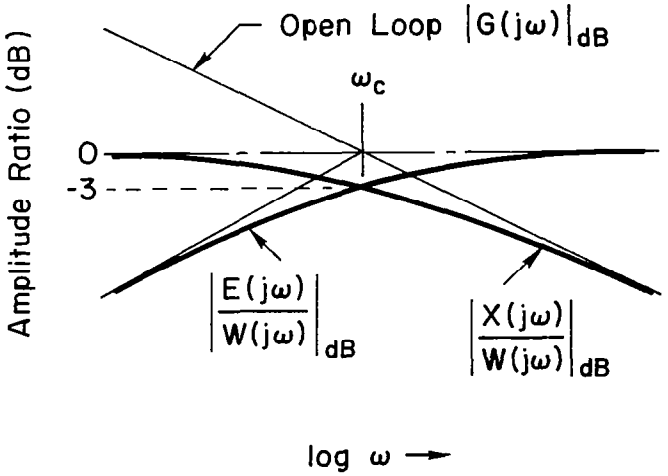

c) Open and Closed-Loop Frequency Response

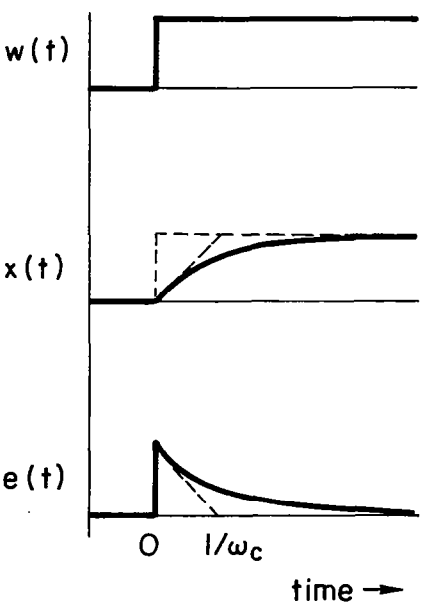

d) Closed-Loop System Indicial Responses

Figure 5. Characteristics of Idealized System

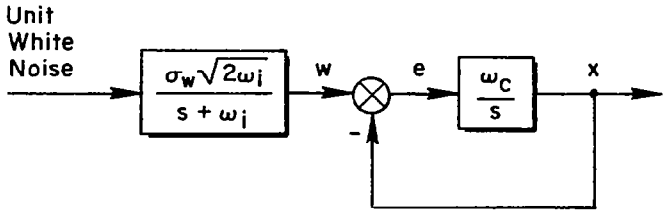

$$\sigma^2_{(\cdot)} \triangleq \frac{1}{2\pi}\int_{-\infty}^{\infty} \Phi_{(\cdot)}\, d\omega$$

$$\Phi_{(\cdot)} = \left[F_{(\cdot)}(s)\, F_{(\cdot)}(-s)\right]_{s=j\omega}$$

$$F_x = \frac{\omega_c\sqrt{2\omega_i}}{(s+\omega_c)(s+\omega_i)}$$

$$F_e = \frac{\sqrt{2\omega_i}\, s}{(s+\omega_c)(s+\omega_i)}$$

Figure 6. Block Diagram for Prototype System RMS Performance Evaluation

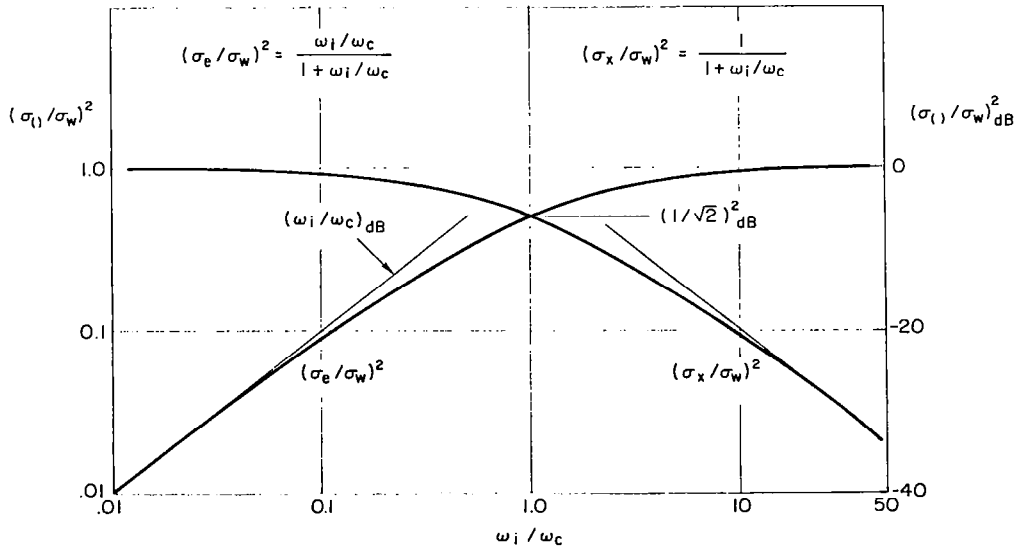

Figure 7. Relationship Among Bandwidth/Crossover Frequency/ Stochastic Performance

attenuation of the controlled variable rms response with respect to the rms input does not exceed $1/\sqrt{2}$, while attenuation of the rms error response with respect to the rms input always exceeds the lesser of $1/\sqrt{2}$ and $\sqrt{\omega_i/\omega_c}$. This demonstrates that stochastic system performance for the prototype is consistent with desired design properties.

Because the open-loop system phase lag is confined to −90 deg, this ideal system is stable for all values of gain. Its response characteristics will, however, be affected by changes in system features. These are conveniently treated using first-order sensitivity factors which relate shifts in open-loop parameters to their consequences as closed-loop pole shifts. In general, the variation $d\lambda_i$ in a closed-loop pole (λ_i), due to changes in open-loop gain ($d\kappa$), open-loop zeros (dz_i) and open-loop poles (dp_i) is given by (Ref. 10):

$$d\lambda_i = S^i_\kappa \frac{d\kappa}{\kappa} + \sum_{j=1}^{n} S^i_{z_j} dz_i + \sum_{j=1}^{m+n} S^i_{p_i} dp_i \tag{5}$$

The S^i quantities are the first-order sensitivity factors. The subscript and superscript notation indicates that a differential increment in the open-loop parameter (defined by the subscript) results in a differential increment of the ith closed-loop root (denoted in the superscript) which is equal to the sensitivity factor times the open-loop parametric variation. Provision is made for an excess of m poles over zeros in the open-loop transfer function. The gain sensitivity is given by,

$$S^i_\kappa = \left[\frac{1}{\partial G/\partial s}\right]_{s=\lambda_i} \tag{6}$$

which for this simple ideal system is $-\omega_c$. This leads to the obvious result:

$$d\lambda_i = -\omega_c \frac{d\kappa}{\kappa} \tag{7}$$

The crossover frequency is thus the gain sensitivity factor which relates proportional changes in open-loop gain to closed-loop root shifts.

At this point we have established connections among open-loop function crossover frequency, closed-loop system transient responses, stochastic input responses, and performance and system sensitivity to parameter variations. In all cases the bandwidth or crossover frequency is the significant (in this case solitary) design variable. These results can be summarized by the design aphorism "with stability assured, everything else is related to bandwidth." This is of course the complete story for the case at hand.

2. Connections Between Desired Open-Loop Function Crossover Frequency and Optimal Control System Cost Function Coefficients

Given the goal that the resulting system exhibit the favorable properties enumerated above, let us now turn to the task of designing a controller $C(s)$, using linear-quadratic-Gaussian optimal control procedures. For the system to be optimal requires that a cost function, such as

$$J = \int_0^\infty [q_R e^2 + r_R \dot{u}^2] \, dt \tag{8}$$

be minimized. Assume that the controlled element component of the system $Y_c(s)$ has a form in the frequency region near ω_c which can be approximated by:

$$Y_c = \frac{K_c}{s^{n+1}} \quad , \quad n \geq 0 \tag{9}$$

The desired controller properties are to be such that the total open-loop function $G(s) = C(s)Y_c(s)$ exhibits the three properties enumerated above, i.e., $|G(s)| >> 1$, $|G(s)| \doteq |\omega_c/s|$, and $|G(s) << 1$ at frequencies below, near, and above the crossover frequency, ω_c, respectively. The optimal control procedure can accomplish this only if the weighting factors in the performance index or cost function can be selected to reflect these desires.

Fortunately, this problem has been solved, and it has been shown in Ref. 13 that if the cost function coefficients, q_R and r_R, are chosen to satisfy

$$q_R = \frac{(2^n \omega_c^2)^{n+1}}{K_c^2} r_R \tag{10}$$

then the open-loop function G(s) will tend to have the three desired properties. Figure 8 presents the approximate asymptotes for the G(s) amplitude ratio frequency response resulting when q_R and r_R satisfy Eq. 10. Notice that crossover frequency, ω_c, for the low-frequency asymptote is maintained regardless of the controlled element characteristics in the frequency region near ω_c.

The actual frequency response can be expected to be close to its asymptotes, and controlled variable and error response bandwidths are

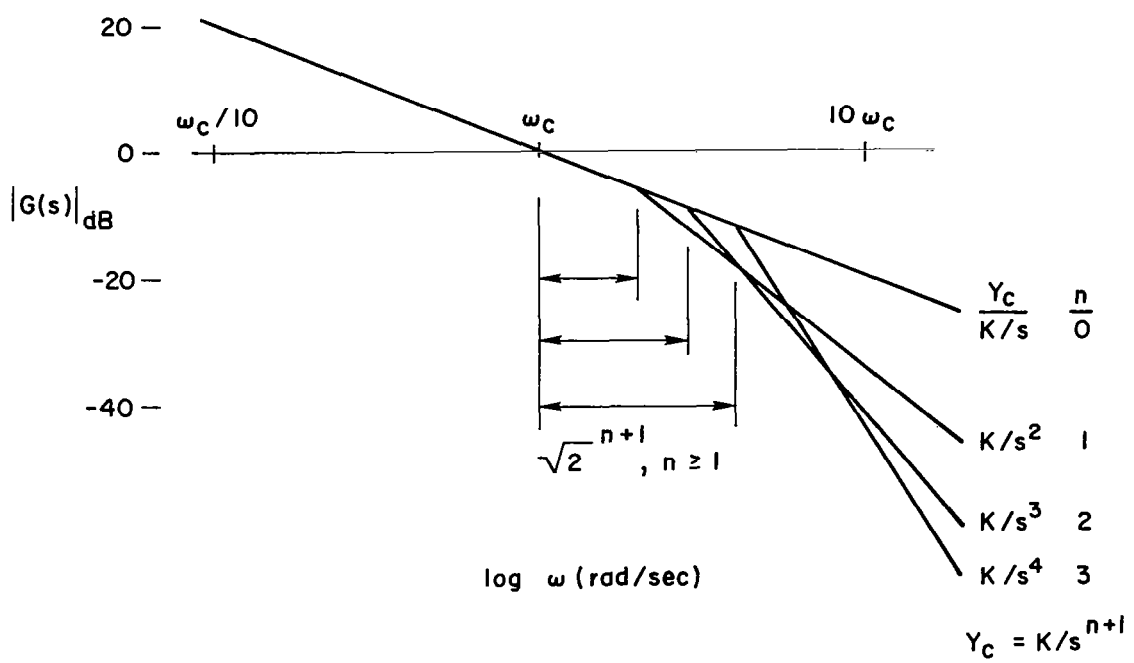

Figure 8. Relationships Between Crossover Frequency and Cost Function Coefficients

approximately equal to the open-loop function crossover frequency. Thus, we have here the basis for specifying q_R and r_R in a cost function that induces an optimal control system which satisfies a given bandwidth requirement. This observation is the cornerstone of the method presented in later sections for design of practical, optimal flight control systems.

C. DESIGN GOALS

Design goals are deduced from mission tasks by considering what is required to perform the task (e.g., the landing approach task requires speed and path control). Design goals can be identified as primary (task cannot be accomplished satisfactorily if not satisfied) or secondary (degree to which minimum standards of task performance are exceeded). That primary design criteria be satisfied is essential for feasibility, whereas secondary design criteria satisfaction is more a matter of system quality and viability relative to the alternatives. The design goals elaborated below are not unique or exhaustive. They merely represent one recommendation which has been tested successfully.

1. Elementary Mission Task Requirements

Experience and mission task analysis (e.g., Ref. 10) have demonstrated that certain modes of flight control system operation are required on virtually all rotorcraft missions. In our demonstration here of practical optimal rotorcraft flight control system design we shall focus on these more or less standard modes of operation and disregard special modes peculiar to less universal mission tasks. (The same approach and philosophy for determination of requirements and for design development carry over for these special modes, of course.)

Table 3 lists standard operational modes of interest for rotorcraft. These are grouped mainly by control axis, although no distinction between the pitch and vertical axes is made because of the significant differences in appropriate control technique at hover and at cruise. Entries in Table 3 are ordered to roughly reflect increasing level of flight control system responsibility (in distinction to pilot responsibility) in the overall conduct of these mission tasks.

TABLE 3

STANDARD FLIGHT CONTROL SYSTEM
MODES FOR ROTORCRAFT

Longitudinal (pitch and/or vertical control axes)

- Damping augmentation
- Rate command/attitude hold
- Attitude command
- Airspeed hold
- Translational rate command
- Rate-of-climb command
- Altitude hold/path track
- Hover (longitudinal and vertical position hold)

Lateral (roll control axis)

- Damping augmentation
- Rate command/attitude hold
- Attitude command
- Heading command/hold (at mid and high speeds)
- Translational rate command
- Path track

Directional (yaw control axis)

- Damping augmentation
- Rate command/attitude hold
- Heading command/hold (at low speeds)

2. Primary Design Criteria

Primary design criteria involve two considerations:

- Identification of outer-loop error variables pertinent to a mission task (e.g., for "follow commanded rate of climb," rate of climb error is the pertinent outer-loop error variable to control to zero).
- Specification of the bandwidths over which outer-loop errors and other key variables (e.g., pitch attitude) are to be controlled.

The first item is fundamental to accomplishing the mission task. The second is, in effect, a catch-all specification of the performance required. This was demonstrated previously in presenting the relationships among bandwidth, open-loop crossover frequency, closed-loop system dynamic steady-state, and stochastic performance. Stability per se is not identified here as a primary design criterion because the design will be evolved using an optimal control formulation which assures stability. Thus we return again to the aphorism "with stability assured, all else relates to bandwidth."

The other key variables in the second item require further explanation. If bandwidths are specified for outer-loop error control only, then the bandwidths (or crossover frequencies) provided by the optimal control design algorithm for all other variables will be at the minimum levels required to achieve the outer-loop error bandwidth objective. Modes participating significantly in the outer-loop error response may be separated from the outer loop's dominant mode frequency by as little as a factor of two, while non-participating modes may be changed hardly at all. Frequently a factor of two separation is not adequate. For example, it is usually inadequate for path error and attitude modal separation in view of customary flying qualities requirements related to motion harmony and the partitioning of attitude and path control frequency bands. It can also be inappropriate when the effective actuator bandwidth is fixed because of an unalterable hardware selection or when significantly higher actuator bandwidth is required for other reasons. In either event, modal separation may be at the designer's choice merely by specifying target bandwidths for control of these other key variables.

Selection of outer-loop error variables is subject to fundamental limitations. The number of outer-loop error variables which may be controlled independently cannot exceed the number of independent controlled element control points. Further, these outer-loop error variables must be controllable via the independent control points. Selection of the outer-loop error variables must be consistent with these two fundamental limitations.

Outer-loop error and other key variables for helicopter flight control are summarized in Table 4. Entries in this table correspond to the Standard Flight Control System Modes for Rotorcraft listed in Table 3. The outer-loop error variable for each mode is the right-most entry in each string not appearing under an integral. Variables to the left of the outer-loop error in each string are the "other key variables." In several instances the integral of the outer-loop error appears at the extreme right of the string. These integrals are included to assure zero steady-state error to a step command input. Integral terms are required only when a command input is explicit in the outer-loop error.

Tables 5 and 6 recommend bandwidth requirements for the outer-loop and other key variables. In several instances alternative recommendations are given for precision and other (non-precision) tasks. The recommendations generally are in the form of a lower bound on bandwidth. These lower bound values have been found to be reasonably adequate (albeit lower than optimum) in practice. Larger bandwidths generally correspond to increased performance (faster response, smaller rms error). However, larger bandwidth systems, because they are more sensitive to parasitic nonlinearities and to the influence of higher frequency modes, may produce "twitchy" system response characteristics to which pilots object. Furthermore, increases in bandwidth tend to equate with increased control authority and rate requirements. Therefore, extreme caution should be exercised when requiring more than twice the bandwidth lower bounds listed.

Tables 5 and 6 do not include bandwidth recommendations for the integrals of outer-loop error variables. These low frequency integral modes cause "tails" in the transient response. We have found that the bandwidth for the integral should be 0.2 to 0.5 of the bandwidth for the outer-loop

TABLE 4

OUTER-LOOP ERROR AND OTHER KEY VARIABLES [a]

Pitch Control Axis

Actuator:	$\dot{\delta}_B$, δ_B
Damping augmentation:	$\dot{\delta}_B$, δ_B, q
Rate command/attitude hold:	$\dot{\delta}_B$, δ_B, q_e, $\int q_e \, dt$
Attitude command:	$\dot{\delta}_B$, δ_B, q^b, θ_e, $\int \theta_e \, dt$
Airspeed hold:	$\dot{\delta}_B$, δ_B, q^b, θ, u_{AS_e}, $\int u_{AS_e} \, dt$
Translational rate command:	$\dot{\delta}_B$, δ_B, q^b, θ, $\dot{x}_e$, $\int \dot{x}_e \, dt$
Hover (longitudinal position hold):	$\dot{\delta}_B$, δ_B, q^b, θ, $\dot{x}^b$, x_e, $\int x_e \, dt$

Vertical Control Axis

Actuator:	$\dot{\delta}_C$, δ_C
Damping augmentation:	$\dot{\delta}_C$, δ_C, $\dot{h}$
Rate-of-climb command:	$\dot{\delta}_C$, δ_C, $\dot{h}_e$, $\int \dot{h}_e \, dt$
Altitude hold/path track:	$\dot{\delta}_C$, δ_C, $\dot{h}^b$, h_e, $\int h_e \, dt$

[a] See Appendix B for variable definitions.

[b] Used only when adjustments to the closed-loop damping are required.

(continued on following page)

TABLE 4 (CONCLUDED)

Lateral Control Axis	
Actuator:	$\dot{\delta}_A$, δ_A
Damping augmentation:	$\dot{\delta}_A$, δ_A, p
Rate command/attitude hold:	$\dot{\delta}_A$, δ_A, p_e, $\int p_e \, dt$
Attitude command:	$\dot{\delta}_A$, δ_A, p^b, φ_e, $\int \varphi_e \, dt$
Heading command:	$\dot{\delta}_A$, δ_A, p^b, φ, ψ_e, $\int \psi_e \, dt$
Translational rate command:	$\dot{\delta}_A$, δ_A, p^b, φ, $\dot{Y}_e$, $\int \dot{Y}_e \, dt$
Path track/hover (lateral position command):	$\dot{\delta}_A$, δ_A, p^b, φ, $\dot{Y}^b$, Y_e, $\int Y_e \, dt$
Directional Control Axis	
Actuator:	$\dot{\delta}_R$, δ_R
Damping augmentation:	$\dot{\delta}_R$, δ_R, r
Rate command/attitude hold:	$\dot{\delta}_R$, δ_R, r_e, $\int r_e \, dt$
Heading command:	$\dot{\delta}_R$, δ_R, r^b, ψ_e, $\int \psi_e \, dt$

[b]Used only when adjustments to the closed-loop damping are required.

TABLE 5

LONGITUDINAL DESIGN BANDWIDTH OBJECTIVE

Function	Lower Bound Desired Bandwidth (rad/sec)
Path Tracking	
Course	≥ 0.10
Glide Slope	≥ 0.25
Precision Hover	0.50
Rate-of-Climb	
Precision	1.0
Other	≥ 0.30
Speed	≥ 0.10
Pitch Attitude	≥ 2.0
Actuators	
Cyclic	≥ 10.0[a]
Collective	≥ 10.0[a]

TABLE 6

LATERAL-DIRECTIONAL DESIGN BANDWIDTH OBJECTIVE

Function	Lower Bound Desired Bandwidth (rad/sec)
Path Tracking	
Course	≥ 0.1
Localizer	≥ 0.25
Precision Hover	0.50
Heading Hold	
Precision	≥ 1.0
Other	≥ 0.30
Roll Attitude	≥ 2.0
Actuators	
Cyclic	≥ 10.0[a]
Tail Rotor Collective	> 10.0[a]

[a]These are minimum values. Actuator bandwidths are usually considerably larger in typical installations. Actuator bandwidths may be specified rather than being design parameters.

error variable. A good compromise or starting value is 0.3. Smaller values tend to produce "tails" in transient responses which have smaller magnitude but longer duration, and vice versa for larger values.

Next, consider the secondary design criteria.

3. Secondary Design Criteria

The secondary design requirements involve a great many considerations. These may be classified into two categories: verification that primary design criteria are satisfied, and investigation of system characteristics determining the quality of performance. Secondary criteria in both categories are applied after the fact (or at least after the first iteration) as far as the optimal control synthesis is concerned. Therefore, they may be thought of as design assessment or evaluation criteria.

Verification that primary design criteria are satisfied is necessary because the relationships between bandwidth, crossover frequency and the cost function coefficients given previously are approximate. While we have found these approximate relationships to be robust, verification that desired bandwidths and crossover frequencies are actually obtained is recommended.

The second category includes the numerous items which have been found effective in exposing the strengths and weaknesses of control system designs. A complete list of system design features and properties which should be considered in this context is given in Table 44. The system features listed there, and exemplified in Section V, include:

- System stability characteristics and margins
- Responses
  - Primary controlled variables
  - Secondary controlled variables
  - Control activity
- Sensitivity
  - Key modes
  - Parasitic nonlinearities
- Gain levels
- Sensor/equalization economy

The investigation of system characteristics to determine the quality of performance and to quantify these system features primarily involve, but are not confined to, such items as:

- Closed-loop frequency response
- Steady-state error response
- Transient response
- RMS response
- Actuator displacement and rate limits and activity
- System insensitivity

Closed-loop frequency responses are used to determine that physical responses of the system are free from resonant peaks, that the response band is flat, etc. Steady-state error characteristics can be determined by examining the very low frequency closed-loop transfer function for the outer-loop error response to the command input as $s \rightarrow 0$. Transient responses can be inspected for overshoot, slow "tails," smoothness, etc. RMS responses of the errors, controls and other key variables can be compared against specifications and error budgets. In particular, three times the rms actuator displacement (σ_x) and rms actuator rate ($\sigma_{\dot{x}}$) can be compared with the available displacement and rate capability to insure that the fraction of time these capabilities are expected to be exceeded is less than 0.26 percent. Control activity in terms of positive-going zero crossings of the trim setting can be calculated using $\sigma_{\dot{x}}/2\pi\sigma_x$.

System sensitivity characteristics can be examined from several points of view. The optimal control solution itself facilitates computation of the closed-loop regulator pole first-order sensitivity to plant coefficient changes and to regulator gain changes. The dual relationships between the regulator and filter solutions can be used to evaluate the closed-loop filter pole first-order sensitivity to plant model coefficient changes and to filter gain changes. First-order sensitivity effects are also available via the partial fraction expansions of the closed-loop transfer functions used in computing transient responses. The modal response coefficients of the partial fraction expansions are gain sensitivities

(Ref. 10). Finally, sensitivity to use of the designed controller at flight conditions other than the design case, to use with more comprehensive models of plant dynamics, and to use of simplified approximate versions of the designed controller can be evaluated.

D. APPLICATION OF THE DESIGN CRITERIA IN SYNTHESIS

Primary and secondary classes of the design checklist items for rotorcraft flight control systems have been presented above. In the synthesis routine the primary requirements are to be addressed directly via the LQG optimal controller synthesis procedure. This is accomplished first by formulating the problem so that appropriate outer-loop error quantities are included, and second by making use of fundamental relationships between response bandwidth and cost function coefficient values.

Design evaluation for satisfaction of the secondary criteria is after the fact of the optimal design. To the extent that any changes are needed, secondary requirements are reflected indirectly in the next design cycle via the LQG optimal controller synthesis procedure. Connections between secondary requirements and the cost function coefficient changes required tend to be straightforward. (For example, if activity of one control point is excessive, increase the cost function coefficient family weighting that control and those variables which are affected sensitively by that control, by a common factor.) In addressing secondary requirements, primary requirements must remain satisfied. Thus primary requirements act as constraints. If both sets of requirements cannot be satisfied simultaneously, then it will be necessary to modify the sensor array, provide additional controlled element capability or adjust bandwidth requirements downward. If simultaneous satisfaction still cannot be obtained after maximum compromise, then it is not feasible to accomplish the mission task with the available resources.

The single most important point to appreciate in connection with this design checklist is that only a very few design requirements are addressed directly in applying the LQG optimal controller synthesis procedure. Yet, because many of the secondary requirements are closely connected with

bandwidth, these requirements tend to be satisfied as well. Satisfaction of the remaining design requirements is still an artful process which requires a full appreciation of the requirements and of their cause-effect connection with the dynamical physics and mathematics of the particular application. This is the case even though LQG optimal controller synthesis techniques are used. Therefore, the ultimate suitability of flight control system designs will remain keenly dependent upon the designer's experience. Nevertheless, modern synthesis techniques can contribute very significantly and effectively by providing candidate flight control system designs for complex tasks and plants, which are responsive to primary design goals.

SECTION III

PROBLEM FORMULATION

A. GENERAL

Synthesis of practical optimal flight control systems depends upon appropriate formulation of the problem to an extent which we find surprising. Careful attention to actuator representation, integrated errors, etc., can make the difference between practical and nonsense solutions.

In formulating the plant, i.e., the model of the fixed or unalterable elements of the system, we adopt the viewpoint that we are dealing with a closed, stochastic system. This means, for example, that all significant elements of the command and disturbance input environment must be included, and that all variables which may be used in the cost function must be provided. The subsections which follow attempt to summarize practices we have found effective. Figure 9 (page 35) provides the generalized form into which the flight control synthesis problems are ultimately cast. Figure 9 can be partitioned into several subsections, as explained below.

- Stochastic Command and Disturbance Input. The subsystem having matrices with S subscripts (Fig. 9a, below) is used to generate the command and disturbance vector, y_S, by providing shaping for the white process noise vector, w.

$$\dot{x}_S = F_S x_S + \Gamma_S w \tag{11}$$

$$y_S = H_S x_S + t_S \tag{12}$$

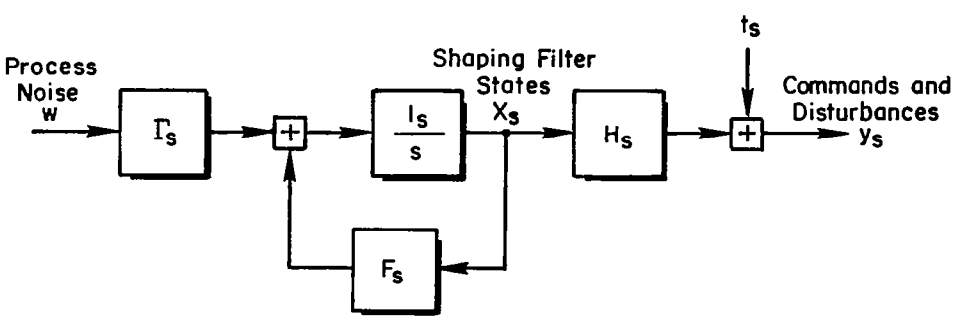

Figure 9a. Stochastic Command and Disturbance Subsystem

$$J_R = \int_0^\infty (y' Q_R y + u' R_R u)\,dt \qquad J_F = E\left[(\hat{x}_c - x_c)'(\hat{x}_c - x_c) + (\hat{x}_s - x_s)'(\hat{x}_s - x_s)\right]$$

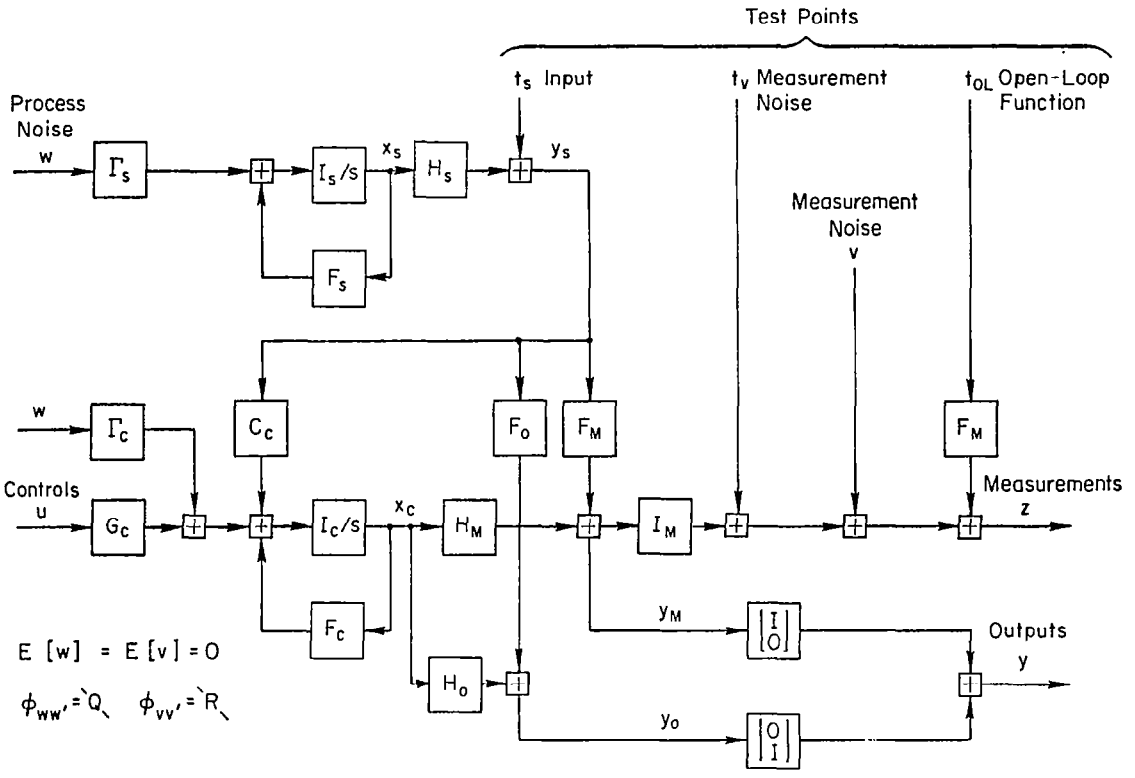

Figure 9. Formulation of Problem

- Controlled Element State Variables. The subsystem having matrices with C subscripts (Fig. 9b) is used to generate the controlled element state variables, x_C. Provision is made for excitation of the controlled element via control variables, u, commands and disturbances, y_S, and white process noise, w.

$$\dot{x}_C = F_C x_C + G_C u + C_C y_S + \Gamma_C w \tag{13}$$

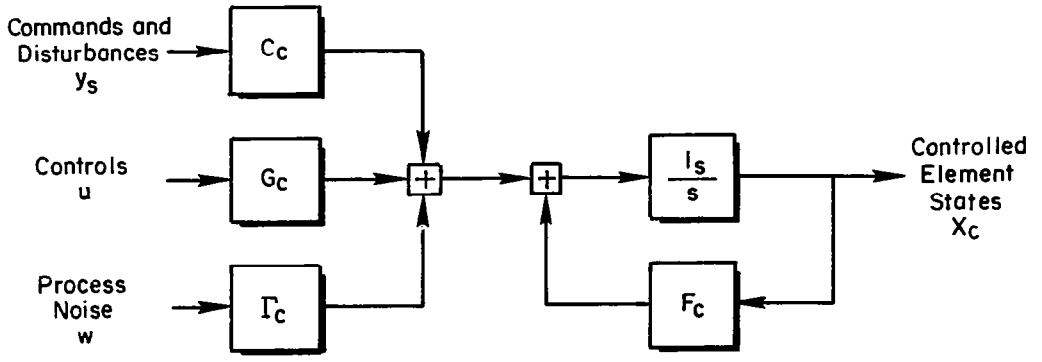

Figure 9b. Controlled Element Subsystem

- Measurements. The subsystem having matrices with M subscripts (Fig. 9c) is used to model output variables, y_M, and sensor outputs, z. Sensor outputs may be linear combinations of the commands and disturbances, y_S, the controlled element state, x_C, and the white measurement noise, w.

$$y_M = F_M y_S + H_M x_C \tag{14}$$

$$z = I_M y_M + v + t_v + F_M t_{OL} \tag{15}$$

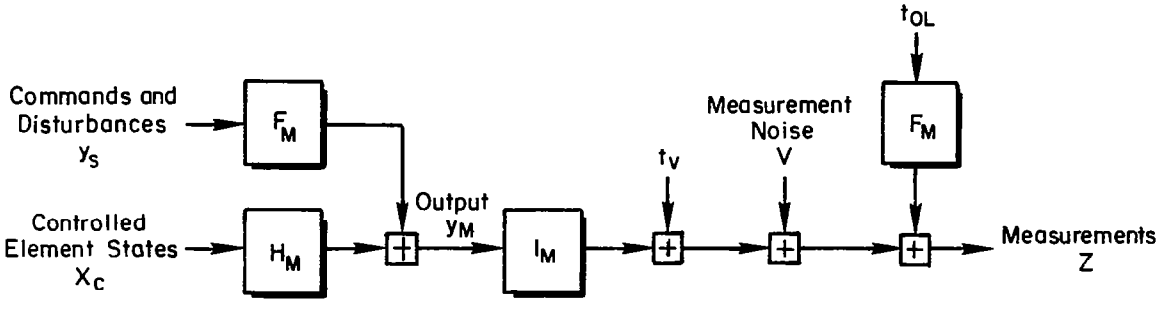

Figure 9c. Measurement Subsystem

- Other Output Variables. Variables of interest which are not the objective of measurement (i.e., which are not in y_M) are included in y_O. The subsystem having matrices with O subscripts (Fig. 9d) provides these variables.

$$y_O = H_O x_C + F_O y_S \tag{16}$$

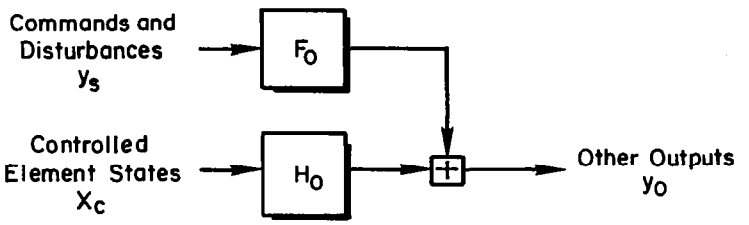

Figure 9d. Other Output Subsystem

- Outputs. The outputs, y (Fig. 9e), consist of the variables which are the objects of measurement, y_M, plus the other output variables, y_O. Notice that all variables potentially of interest in the cost function must be included at the outset in formulation.

$$y = \begin{bmatrix} y_M \\ y_O \end{bmatrix} \tag{17}$$

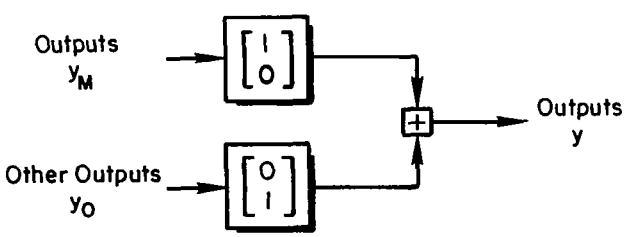

Figure 9e. Outputs Subsystem

- Loop Opening Points. The input, y_M, to every sensor (i.e., the kinematic portion of every measurement, z) may be interrupted individually by setting elements of the identity matrix, I_M, to zero (Fig. 9f). This feature provides the ability to examine closed-loop system transfer functions with some or all

feedback loops open at the measurement point. This central feature permits the calculation of optimal system properties in a form consonant with the criteria and considerations used to evaluate conventionally designed systems.

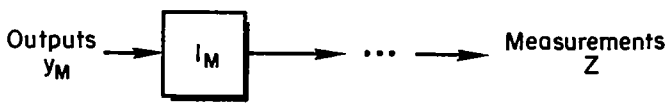

Figure 9f. Loop Opening Subsystem

- Test Points. Three types of test input points are provided, shown in Fig. 9g. The test input vector, t_S, enables computation of closed- and open-loop system transfer functions between every command and disturbance input to the controlled element, y_S, and every state, x_C, and output, y. The test input vector, t_V, enables computation of closed- and open-loop system transfer functions between every measurement noise input, v, and every state, x_C, and output, y. (In cases where

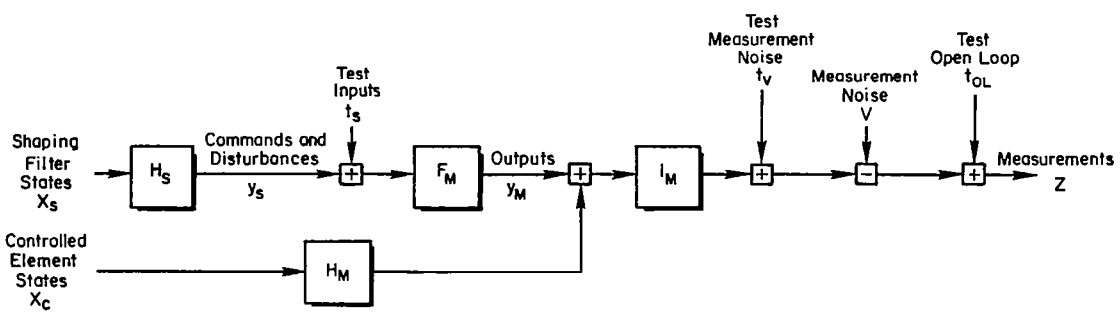

Figure 9g. Test Point Subsystem

the outer-loop function is regulation to a constant value, or where effective inner-loop error regulation properties are of interest, the test input vector, t_V, can be used to supply surrogate command inputs.) The test input vector, t_{OL}, enables computation of open-loop system transfer functions when outer-loop error feedbacks are interrupted. Transfer functions between error points corresponding to every command component of y_S and every output variable y can be obtained.

- Cost Function. The cost function is in the form

$$J_C = E[y' Q_R y + u' R_R u] \tag{18}$$

where Q_R and R_R are diagonal matrices. The fact that Q_R and R_R matrices are diagonal results in a cost function integrand which is a weighted sum of squares of the elements of y and u. This restriction stems from our belief that the cost function should be interpreted as an index of performance, and to this end should consist of a weighted sum of squares of variables indicative of performance for each particular application. This set of variables must be contained in the output and control vectors, y and u, by virtue of their respective definitions.

The separability principal is used in obtaining the optimal controller solution. This leads to the use of two separate cost functions, J_R and J_F:

$$J_R = \int_0^\infty (y'Q\, y + u'R\, u)\, dt \tag{19}$$

$$J_F = E[(\hat{x}_C - x_C)'(\hat{x}_C - x_C) + (\hat{x}_S - x_S)'(\hat{x}_S - x_S)]$$

Minimization of these functions permits the separate solution of the optimal regulator and filter problems, as an alternative to combined solution using J_C.

The process noise vector, w, and measurement noise vector, v, are independent, zero-mean Gaussian white noise processes. Their intensities are given by the diagonal Q and R matrices, respectively, i.e.,

$$E[w] = E[v] = 0 \tag{20}$$

$$\varphi_{ww'} = Q \tag{21}$$

$$\varphi_{vv'} = R \tag{22}$$

To this point, the matters dealing with optimal control are more or less standard. Here, however, we need to recognize that many measurements in flight control systems are, for all practical purposes, noise

free. Thus, some or all of the measurement noise components may have zero intensity. This, in turn, implies an ability to solve the singular Kalman filter problem.

In the following paragraphs the definitions of the partitions of the problem formulation shown in Fig. 9 are specialized for the flight control system application.

B. RECOMMENDED FORMULATION FOR FLIGHT CONTROL SYSTEMS

1. Stochastic Commands and Disturbances

Stochastic commands may be represented by first- or second-order shaped white noise. First-order shaping can be used to represent maneuver requirements, guidance source inaccuracies, or inadvertent pilot inputs. One form of the second-order shaping filter equations is:

$$\dot{x}_{S1} = -\omega_{S1} x_{S1} + \sqrt{2\omega_{S1}}\, w_1 \tag{23}$$

$$\dot{x}_{S2} = -\omega_{S2} x_{S2} + \sqrt{2\omega_{S2}}\, w_2 \tag{24}$$

$$y_{S1} = x_{S1} + x_{S2} \tag{25}$$

$$Q_{w_1} = \sigma^2_{x_{S1}} \quad , \quad Q_{w_2} = \sigma^2_{x_{S2}} \tag{26}$$

To obtain first-order shaping merely omit the equations for $\dot{x}_{S2}$ and Q_{w_2}.

The output, y_{S1}, is the sum of two independent first-order shaped processes. One process might represent maneuvering commands and have moderate level and low bandwidth. The second process might represent guidance source inaccuracies, and have low level and moderate bandwidths. Relatively little numerical data are available to guide selection of level and bandwidth. Some data are contained in Ref. 14 and further suggestions appear in Appendix B. Stochastic disturbances are mainly due to gust effects. Gusts may be modeled by the Dryden form of the power spectral

densities (Ref. 15). These power spectral densities correspond to first- and second-order shaped white noise. The longitudinal (u_g) and effective rolling (p_g) gust components are first-order forms:

$$\dot{x}_S = -\omega_S x_S + \sqrt{2\omega_S}\, w \tag{27}$$

$$y_S = x_S \tag{28}$$

$$Q_w = \sigma^2_{x_S} \quad , \quad x_S = u_g \text{ or } p_g \tag{29}$$

Side and normal gust components are second-order forms:

$$\dot{x}_{S1} = -\omega_S x_{S1} + \sqrt{2\omega_S}\, w \tag{30}$$

$$\dot{x}_{S2} = -\omega_S x_{S2} + \omega_S/\sqrt{2}\, x_{S1} \tag{31}$$

$$y = \sqrt{3/2}\, x_{S1} - (\sqrt{3} - 1)x_{S2} \tag{32}$$

$$Q_w = \sigma_{y_S} \quad , \quad y_S = v_g \text{ or } w_g$$

In each case ω_S represents the characteristic frequency of the particular gust component. Second-order shaping may be approximated by first-order shaping for simplicity. The form is:

$$\dot{x}_S = -1.594\,\omega_S x_S + \sqrt{2(1.594)\omega_S}\, w \tag{33}$$

$$y_S = x_S \tag{34}$$

$$Q_w = \sigma^2_{y_S} \quad , \quad y_S = v_g \text{ or } w_g \tag{35}$$

This approximation preserves the half-power frequency, $1.594\omega_S$, and the rms value, σ_{y_S}, of the second-order power spectral density.

Additional background and numerical data can be found in pages 417-461 of Ref. 15, pages 654-660 of Ref. 10, and in Appendix B.

2. Actuators

Actuation dynamics, activity, displacement limits and rate limits almost always provide the main limitations on automatic flight control system performance and frequently contribute to performance limitations in manual control. For this reason inclusion of an actuation dynamic model at some point in the optimal flight control system design cycle is essential. Fortunately, actuation dynamics need not be modeled in detail. Simple approximations capture the essential effects.

Consider the NASA VSTOLAND UH-1H helicopter actuation system (Ref. 16) in Fig. 10. An approximation adequate for design purposes is shown in Fig. 11. The approximation in Fig. 11 results in a reduction in order for the actuation system model of three. The effective actuation lag is computed by the method given in Appendix B. We have found it to be good practice to represent the effective actuation lag by its open-loop element, $1/s$, and supply the actuator feedback gain via the optimal design process. This practice results in accurate representation of the mean square (boost actuator) control deflection and control rate in the cost function.

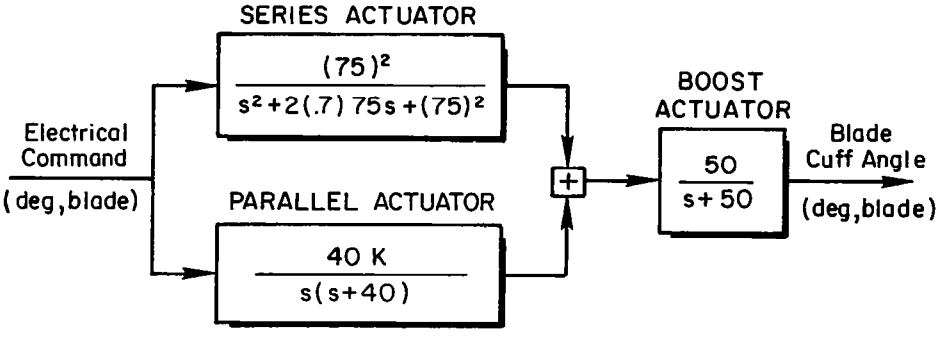

Figure 10. Actuation System Block Diagram

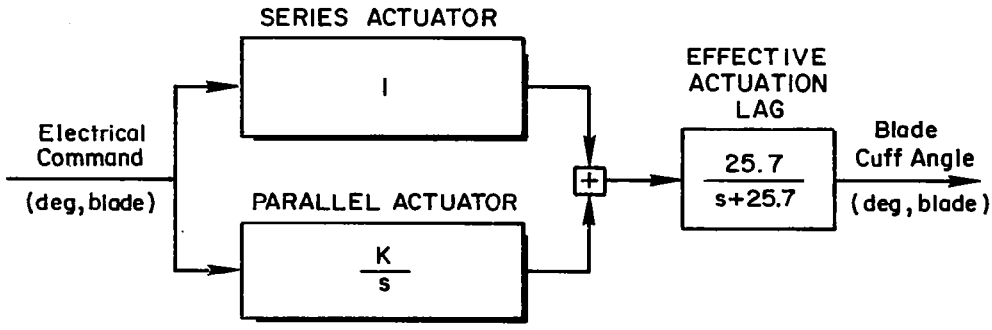

Figure 11. Approximation to Actuation System

Other quantities in the actuation system are frequently subject to physical limitations. Series actuator displacement and parallel actuator rate are usually in this category, since both quantities are ordinarily limited for safety-of-flight reasons. These quantities can either be evaluated directly using variables existing in the plant formulation, or by including additional state and output equations as described in Appendix B.

3. Airframe

The airframe can be represented by uncoupled longitudinal and lateral-directional sets of equations. Longitudinal equations may be written conveniently in terms of states u, w, q, θ, δ_B, δ_C, x_{BAR}, and the lateral-directional equations in terms of states v, p, r, φ, δ_A, δ_P, x_{BAR}. The last state in each set represents the stabilizer bar state. Crosscoupling between longitudinal and lateral-directional systems has been found to be relatively unimportant in connection with flight control systems design. Specific sets of state equations for the UH-1H used in our examples are given in Appendix B.

Airframe models which are more, or less, detailed than the one described above may be appropriate for a particular application. The problem most often faced is that of obtaining a simplified model for flight control

system design purposes from a very high-order, detailed model of the airframe. We shall assume that the high-order model is linear and stationary. Simplification of this model is accomplished by making low-frequency approximations to very high-frequency modes. This process is called "aggregation," e.g., Ref. 17. "High" frequency is interpreted relative to the usual range of flight control system modes, typically the band 0.0 to 50.0 rad/sec. There are at least two methods for developing the simplified model. In the first (e.g., Refs. 18 and 19), a modal representation of the system is constructed in terms of its eigenvalues and eigenvectors. Derivatives of modal coordinates having eigenvalues with modulus larger than 50.0 are approximated by zero. The approximated representation is reconstituted to the original coordinates after algebraic equations* of the system are eliminated by substitution. These algebraic equations become additional output equations for the reduced-order model. Dependencies of the measurement and original output equations upon the variables of these additional output equations must be eliminated by substitution. A compact exposition of this method is given on pages 34-36 of Ref. 18.

The second method is in the spirit of the first but does not require construction of a modal representation of the system. It is frequently the case that modal subsystems which couple only weakly with the rest of the system can be identified by inspection of the equations of motion. (Inspection may be by comparing eigenvalues of the subsystem with eigenvalues for the total system, for example. If subsystem eigenvalues are nearly equal to corresponding total system eigenvalues, then coupling is weak.) Weakly coupled subsystems having eigenvalues larger than 50.0 rad/sec may be replaced in the equations of motion by approximate algebraic equations which represent the static (low-frequency) characteristics of the subsystem. This approximation has been applied in Ref. 20 and in Appendices C through H of Ref. 21, for example.

---

*These algebraic equations result from those equations for which derivatives of modal coordinates are set to zero.

4. Kinematics

It is essential that all kinematic relationships which are in differential equation form be included in the plant. These may include not only obvious kinematic relationships such as

$$\dot{h} = u \sin \Theta_o - w \cos \Theta_o + V_{T_o} \theta \tag{36}$$

$$\dot{\psi} = r/\cos \Theta_o \tag{37}$$

but also error integrals which may be required in the cost function such as

$$h_{eI} = h_c - h \tag{38}$$

$$\dot{\psi}_{eI} = \psi_c - \psi \tag{39}$$

5. Measurements

Equations for the measurements assumed available must be accurate with respect to sensor location and orientation effects. Sensor noise characteristics must be represented with reasonable fidelity. Most flight control system measurements are free from broadband (i.e., "measurement") noise as a practical matter. Accelerometer measurements are a possible exception, however, especially when installed in a vibratory environment. Some flight control measurements, such as glide slope error for example, have correlated noise (e.g., Ref. 22, Appendix B). It is essential for proper formulation of the problem that correlated noise be represented by shaped process noise rather than by white measurement noise.

A list of the conventional sensors which have been found useful in flight control systems is given in Table 7. A summary of special considerations in using, orienting and locating certain of these sensors follows Table 7.

TABLE 7. CONVENTIONAL FLIGHT CONTROL SENSORS

Longitudinal Axes	
q	Body axis pitching velocity
$\dot{\theta}$	Pitch attitude rate
θ	Pitch attitude
$\dot{h}$	Rate-of-climb (barometric or baro-inertial)
h	Altitude (barometric or radar)
η	Glide slope deviation (angular measure)
R	DME or IRS derived slant range
$\dot{R}$	Derived DME or IRS slant range rate
V_g	IRS ground speed
a'_x	Body-fixed longitudinal acceleration
a'_z	Body-fixed normal acceleration
$(\alpha - \alpha_g)$	Aerodynamic angle of attack
V_{AS}	Airspeed
δ_B/δ_e	Longitudinal cyclic pitch or elevator deflection
δ_C/δ_t	Collective pitch or power lever deflection
Lateral	
p	Body-fixed rolling velocity
$\dot{\varphi}$	Bank angle rate
φ	Bank angle
r	Body-fixed yawing velocity
$\dot{\psi}$	Heading rate
ψ	Heading (magnetic or gyro compass)
ν	Localizer or VOR deviation (angular measure)
$(\psi - \lambda)$	IRS drift angle
a'_y	Body-fixed lateral acceleration
$(\beta - \beta_g)$	Aerodynamic angle of sideslip
δ_A/δ_a	Lateral cyclic pitch or aileron deflection
δ_R/δ_r	Tail rotor collective pitch or rudder deflection

Special Considerations

a_x': Body-fixed longitudinal acceleration is sensitive to orientation and location effects in the airframe. Location effects are secondary, but near c.g. alignment is preferred. Orientation effects are important and are usually dictated by alignment with the flight path in the flight regime where close groundspeed or airspeed control is desired. In these instances it is often desirable to use "longitudinal acceleration independent of pitch," i.e., let $a_x' \triangleq a_x - g \sin \theta$ be the effective measurement, by combining a_x and $g \sin \theta$ at the outset. This results in an approximate measurement of $\dot{V}_T$ when both quantities are referenced to/aligned with the reference flight path.

a_y': Lateral acceleration is sensitive to location effects. This is frequently used to advantage in flight control systems in order to create a surrogate β measurement. By locating the accelerometer a distance $\ell_x = -Y_{\delta R}/N_{\delta R}$ ahead of the aircraft c.g.,* one obtains a_y' and β transfer functions for δ_R inputs which are identical over a broad range of frequencies except for a scale factor.

a_z': Normal acceleration is sensitive to both orientation and location effects. Preferred values depend upon the particular application.

a_z may be used to extend the bandwidth of the barometric rate of climb measurement which has an inherent lagging characteristic. In this case, the accelerometer should be located close to the aircraft c.g. and should be oriented so that its sensitive axis is near vertical at trim for the flight regime where close rate-of-climb control is desired. This same location and orientation is appropriate when the a_z measurement is fed back to collective pitch in order to alter the apparent mass of the aircraft for flight path control.

Normal acceleration can also be used to create a surrogate α measurement via proper location. By locating the accelerometer a distance

*That is, at the instantaneous center of rotation with respect to the tail rotor collective control.

$\ell_x = Z_{\delta_B}/M_{\delta_B}$ ahead of the aircraft c.g.,* one obtains a_z' and α transfer functions for δ_B inputs which are identical over a broad range of frequencies except for a scale factor. This use of normal acceleration is frequently impractical for rotorcraft application because Z_{δ_B} may change by more than an order of magnitude between hover and maximum speed and is usually positive.

For all of the above uses of normal acceleration, it is necessary to wash out, bias out or cancel the gravitational component of the acceleration measurement. This requirement is not evident in the control design problem because linearized perturbation equations are typically used wherein the constant gravitational component does not appear.

q, r, $\dot{\theta}$, $\dot{\psi}$: Airframes requiring large amounts of artificial damping or which must execute gross maneuvers must make careful use of superficially equivalent measurements, i.e., of q and $\dot{\theta}$ or of r and $\dot{\psi}$. For example, an airframe requiring heavy pitch axis damping will lose that damping augmentation in steeply banked turns if $\dot{\theta}$ is used in lieu of q since

$$\dot{\Theta} = q \cos \Phi - r \sin \Phi$$

On the other hand, use of q in lieu of $\dot{\theta}$ when the requirement is for vertical path equalization will result in opposition of steady turns since

$$q = \dot{\Theta} \cos \Phi + \dot{\Psi} \cos \Theta \sin \Phi$$

$(\alpha - \alpha_g)$, $(\beta - \beta_g)$: Measurements of aerodynamic angle of attack and angle of sideslip are frequently unsatisfactory in rotorcraft applications. These measurements, when used, require correction for installation and location effects.

---

*That is, at the instantaneous center of rotation with respect to the longitudinal cyclic pitch control.

6. Outputs

Numerous linear combinations of the state variables in a given application are of interest because of their relevance to the physics of the problem, to performance or flying qualities specifications or because of their potential use in the cost function. Our recommendation is that all measurement kinematic components (y_M in Fig. 9), and candidate measurement quantities, all candidate quantities for use in the cost function, all quantities which may encounter physical or specification limits be included in the output vector, y. Virtually all of the variables in Table 7 may be included in the output vector. Additional variables associated with the actuation system such as series actuator displacements and parallel trim actuator rates must be included when appropriate to the particular application.

C. EXAMPLE FORMULATION

Application for design of a longitudinal flight control for the UH-1H helicopter at hover is used for illustrative purposes. Pertinent data for the primary design objectives are summarized in Table 8. Vector definition

TABLE 8

UH-1H LONGITUDINAL FLIGHT CONTROL SYSTEM

Flight Condition:	
Hover	
Functions:	
Rate-of-climb command	
Groundspeed hold	
Bandwidths:	rad/sec
Cyclic (DB)	25.73
Collective (DC)	25.73
Pitch (TH)	2.0
Rate-of-climb error (HDE)	1.0
Integral of HDE (HDI)	0.82
Groundspeed error (XD)	0.5
Integral of XD (XDI)	0.1

for the plant, measurements and outputs are given in Table 9. Note that each variable has an associated computer mnemonic, as indicated below each vector. With the exception of the state variables, the mnemonics are input to the software (Ref. 23) by the user, and are used to produce the data from the software in report-ready form. In the case of the state variables, however, the mnemonics are internally generated by the software. The names X01, X02, ..., X05 are reserved for the shaping filter states, while X06, X07, ..., X15 are reserved for the controlled element states. Most matrix data in the remainder of this report were produced by the software just described, and the mnemonic conventions apply throughout.

Throughout this report, it is important for the reader to maintain the distinction between variables which are states and variables which are measurements, even though the same variable names are used. This confusion could arise with the variables q, θ, δ_B and δ_C. For instance, we see that the state variable δ_B (the actual longitudinal cyclic deflection) is defined as the integral of the control variable $\dot{\delta}_B$, via the equation $\dot{\mathbf{x}} = \mathbf{F}\mathbf{x} + \mathbf{G}\mathbf{u} + \Gamma\mathbf{w}$. Once the controller has been defined, though, we will see that the measurement variable δ_B (which may only exist as a quantity inside a processor) is <u>not</u> the integral of the control variable $\dot{\delta}_B$. We will continue to point out this distinction in the text.

The software and its associated mnemonics do not suffer from these ambiguities. For example, the state variables q, θ, δ_B and δ_C are X08, X09, X10, and X11, whereas the measurements q, θ, δ_B and δ_C are Q, TH, DB and DC (see Table B-1).

Table 10 presents the literal form for the F, G, Γ, and H_R matrices for the example problem. These matrices are composites of the matrices which comprise the problem formulation (Fig. 9) as indicated in the table. The numerical data for the example problem in terms of these problem formulation matrices are given in Table 11. The numerical data for the F, G, Γ and H_R matrices are given in Appendix C.

Throughout the report it will be useful to present factored transfer functions. The notation used is explained in Table 12. Table 13 presents selected factored transfer functions for the example controlled element.

TABLE 9. EXAMPLE PLANT DATA

VECTORS

Shaping Filter States

$$x'_S \triangleq \{u_g \quad w_g \quad \dot{h}_c\}$$
$$= \{XO1 \quad XO2 \quad XO3\}$$

Controlled Element States

$$x'_C \triangleq \{u \quad w \quad q \quad \theta \quad \delta_B \quad \delta_C \quad \int \dot{h}_e\,dt \quad x_{BAR} \quad \int \dot{x}\,dt\}$$
$$= \{XO6 \quad XO7 \quad XO8 \quad XO9 \quad X10 \quad X11 \quad X12 \quad X13 \quad X14\}$$

Process Noise

$$w' \triangleq \{w_{u_g} \quad w_{w_g} \quad w_{\dot{h}_c} \quad w_u \quad w_w \quad w_q \quad w_\theta \quad w_{\delta_B} \quad w_{\delta_C} \quad w_{\int \dot{h}_e dt} \quad w_{x_{BAR}} \quad w_{\int \dot{x}\,dt}\}$$
$$= \{PUG \quad PWG \quad PHC \quad PU \quad PW \quad PQ \quad PTH \quad PDB \quad PDC \quad PHD \quad PXB \quad PXD\}$$

Controls

$$u' \triangleq \{\dot{\delta}_B \quad \dot{\delta}_C\}$$
$$= \{DBD \quad DCD\}$$

Shaping Output

$$y'_S \triangleq \{u_g \quad w_g \quad \dot{h}_c\}$$
$$= \{UG \quad WG \quad HDC\}$$

Measurements

$$z' \triangleq \{\dot{h} \quad q \quad \theta \quad \delta_B \quad \delta_C \quad \dot{h}_e \quad \int \dot{h}_e\,dt \quad \dot{x} \quad \int \dot{x}\,dt\}$$
$$= \{HD \quad Q \quad TH \quad DB \quad DC \quad HDE \quad HDI \quad XD \quad XDI\}$$

Outputs

$$y' \triangleq \{\dot{h} \quad q \quad \theta \quad \delta_B \quad \delta_C \quad \dot{h}_e \quad \int \dot{h}_e\,dt \quad \dot{x} \quad \int \dot{x}\,dt \quad \alpha \quad u_{AS_e}\}$$
$$= \{HD \quad Q \quad TH \quad DB \quad DC \quad HDE \quad HDI \quad XD \quad XDI \quad AOA \quad ASE\}$$

TABLE 10. LITERAL FORMS FOR F, G, Γ AND H_R MATRICES

$$F = \begin{array}{c} \begin{array}{cccccccccccccc} \text{UG} & \text{WG} & \text{HDC} & \text{U} & \text{W} & \text{Q} & \text{TH} & \text{DB} & \text{DC} & \text{HDI} & \text{XBR} & \text{XDI}^a & \text{ASI}^a & \end{array} \\ \left[\begin{array}{cccccccccccccc} -\lvert V_{A_o}\rvert/L_u & 0 & 0 & 0 & 0 & 0 & 0 & 0 & 0 & 0 & 0 & 0 & 0 & \text{UG} \\ 0 & -1.594\lvert V_{A_o}\rvert/L_w & 0 & 0 & 0 & 0 & 0 & 0 & 0 & 0 & 0 & 0 & 0 & \text{WG} \\ 0 & 0 & -\omega_{hc} & 0 & 0 & 0 & 0 & 0 & 0 & 0 & 0 & 0 & 0 & \text{HDC} \\ \hline -X_u & -X_w & 0 & X_u & X_w & X_q - W_o & -g\cos\theta_o & X_{\delta_B} & X_{\delta_C} & 0 & X_{\delta_B} & 0 & 0 & \text{U} \\ -Z_u & -Z_w & 0 & Z_u & Z_w & Z_q + U_o & -g\sin\theta_o & Z_{\delta_B} & Z_{\delta_C} & 0 & Z_{\delta_B} & 0 & 0 & \text{W} \\ -M_u & -M_w & 0 & M_u & M_w & M_q & 0 & M_{\delta_B} & M_{\delta_C} & 0 & M_{\delta_B} & 0 & 0 & \text{Q} \\ 0 & 0 & 0 & 0 & 0 & 1 & 0 & 0 & 0 & 0 & 0 & 0 & 0 & \text{TH} \\ 0 & 0 & 0 & 0 & 0 & 0 & 0 & 0 & 0 & 0 & 0 & 0 & 0 & \text{DB} \\ 0 & 0 & 0 & 0 & 0 & 0 & 0 & 0 & 0 & 0 & 0 & 0 & 0 & \text{DC} \\ 0 & 0 & 1. & -\sin\theta_o & -\cos\theta_o & 0 & -V_{T_o} & 0 & 0 & -\epsilon & 0 & 0 & 0 & \text{HDI} \\ 0 & 0 & 0 & 0 & 0 & 4.97 & 0 & 0 & 0 & 0 & -.333 & 0 & 0 & \text{XBR} \\ 0 & 0 & 0 & \cos\theta_o & \sin\theta_o & 0 & 0 & 0 & 0 & 0 & 0 & -\epsilon & x & \text{XDI}^a \\ -\cos\theta_o & -\sin\theta_o & 0 & \cos\theta_o & \sin\theta_o & 0 & 0 & 0 & 0 & 0 & 0 & x & -\epsilon & \text{ASI}^a \end{array}\right] \end{array}$$

$$F = \begin{bmatrix} F_s & 0 \\ C_c H_s & F_c \end{bmatrix} \qquad H_s = I$$

[a]XDI used in hover example;
ASI used in 100 kt example

(continued on following page)

TABLE 10. (Continued)

$$G = \begin{array}{c} \begin{matrix} \text{DBD} & \text{DCD} & \end{matrix} \\ \left[\begin{array}{cc|l} 0 & 0 & \text{UG} \\ 0 & 0 & \text{WG} \\ 0 & 0 & \text{HDC} \\ \hline 0 & 0 & \text{U} \\ 0 & 0 & \text{W} \\ 0 & 0 & \text{Q} \\ 0 & 0 & \text{TH} \\ 1. & 0 & \text{DB} \\ 0 & 1. & \text{DC} \\ 0 & 0 & \text{HDI} \\ 0 & 0 & \text{XBR} \\ 0 & 0 & \text{XDI}^{a} \\ 0 & 0 & \text{ASI}^{a} \end{array}\right] \end{array} = \begin{bmatrix} 0 \\ G_C \end{bmatrix}$$

$$\Gamma = \begin{array}{c} \begin{matrix} \text{PUG} & \text{PWG} & \text{PHC} & \text{PU} & \text{PW} & \text{PQ} & \text{PTH} & \text{PDB} & \text{PDC} & \text{PHI} & \text{PXB} & \text{PXI}^{a} & \text{PSE}^{a} & \end{matrix} \\ \left[\begin{array}{ccc|cccccccccccc|l} \sqrt{2\lvert V_{T_0}\rvert/L_u} & 0 & 0 & 0 & 0 & 0 & 0 & 0 & 0 & 0 & 0 & 0 & 0 & 0 & \text{UG} \\ 0 & \sqrt{2\times 1.594\lvert V_{T_0}\rvert/L_u} & 0 & 0 & 0 & 0 & 0 & 0 & 0 & 0 & 0 & 0 & 0 & 0 & \text{WG} \\ 0 & 0 & \sqrt{2\omega\dot{h}_c} & 0 & 0 & 0 & 0 & 0 & 0 & 0 & 0 & 0 & 0 & 0 & \text{HDC} \\ \hline 0 & 0 & 0 & 1. & 0 & 0 & 0 & 0 & 0 & 0 & 0 & 0 & 0 & 0 & \text{U} \\ 0 & 0 & 0 & 0 & 1. & 0 & 0 & 0 & 0 & 0 & 0 & 0 & 0 & 0 & \text{W} \\ 0 & 0 & 0 & 0 & 0 & 1. & 0 & 0 & 0 & 0 & 0 & 0 & 0 & 0 & \text{Q} \\ 0 & 0 & 0 & 0 & 0 & 0 & 1. & 0 & 0 & 0 & 0 & 0 & 0 & 0 & \text{TH} \\ 0 & 0 & 0 & 0 & 0 & 0 & 0 & 1. & 0 & 0 & 0 & 0 & 0 & 0 & \text{DB} \\ 0 & 0 & 0 & 0 & 0 & 0 & 0 & 0 & 1. & 0 & 0 & 0 & 0 & 0 & \text{DC} \\ 0 & 0 & 0 & 0 & 0 & 0 & 0 & 0 & 0 & 1. & 0 & 0 & 0 & 0 & \text{HDI} \\ 0 & 0 & 0 & 0 & 0 & 0 & 0 & 0 & 0 & 0 & 1. & 0 & 0 & 0 & \text{XBR} \\ 0 & 0 & 0 & 0 & 0 & 0 & 0 & 0 & 0 & 0 & 0 & 1. & 0 & 0 & \text{XDI}^{a} \\ 0 & 0 & 0 & 0 & 0 & 0 & 0 & 0 & 0 & 0 & 0 & 0 & 1. & 0 & \text{ASI}^{a} \end{array}\right] \end{array} = \begin{bmatrix} \Gamma_S \\ \Gamma_C \end{bmatrix}$$

[a]XDI used in hover example; ASI used in 100 kt example.

(concluded on following page)

TABLE 10. (Concluded)

UG	WG	HDC	U	W	Q	TH	DB	DC	HDI	XBR	XDI[a]	ASI[a]	
0	0	0	$\sin\theta_o$	$-\cos\theta_o$	0	V_{T_o}	0	0	0	0	0	0	HD
0	0	0	0	0	1.0	0	0	0	0	0	0	0	Q
0	0	0	0	0	0	1.0	0	0	0	0	0	0	TH
0	0	0	0	0	0	0	1.0	0	0	0	0	0	DB
0	0	0	0	0	0	0	0	1.0	0	0	0	0	DC
0	0	1.0	$-\sin\theta_o$	$\cos\theta_o$	0	$-V_{T_o}$	0	0	0	0	0	0	HDE
0	0	0	0	0	0	0	0	0	1.0	0	0	0	HDI
0	0	0	$\cos\theta_o$	$\sin\theta_o$	0	0	0	0	0	0	0	0	XD[b]
0	0	0	0	0	0	0	0	0	0	0	1.0	0	XDI[a]
0	0	0	0	0	0	0	0	0	0	0	0	1.0	ASI[a]
$-\cos\theta_o$	$-\sin\theta_o$	0	$\cos\theta_o$	$\sin\theta_o$	0	0	0	0	0	0	0	0	ASE[b]
$-X_u$	$-X_w$	0	X_u	X_w	X_q	$-g\cos\theta_o$	X_{δ_B}	X_{δ_C}	0	X_{δ_B}	0	0	AXP[c]
$-(Z_u - \ell_x M_u)$	$-(Z_w - \ell_x M_w)$	0	$Z_u - \ell_x M_u$	$Z_w - \ell_x M_w$	$Z_q - \ell_x M_q$	0	$Z_{\delta_B} - \ell_x M_{\delta_B}$	$Z_{\delta_C} - \ell_x M_{\delta_C}$	0	$Z_{\delta_B} - \ell_x M_{\delta_B}$	0	0	AZP[c]
0	$-1/V_{T_o}$	0	0	$1/V_{T_o}$	0	0	0	0	0	0	0	0	AOA

$$= H_R = \begin{bmatrix} F_M H_S & H_M \\ F_O H_S & H_O \end{bmatrix},$$

$$H_S = I$$

[a]XDI used in hover example; ASI used in 100 kt cruise.

[b]XD used as measurement in hover, output at 100 kt; ASE used as measurement at 100 kt, output in hover.

[c]Used to investigate acceleration measurements in 100 kt case.

MATRICES

Shaping

TABLE 11. PROBLEM FORMULATION MATRICES, UH-1H HOVER EXAMPLE

FS MATRIX

1 X01	2 X02	3 X03	
-0.117E-02	0.000	0.000	1 X01
0.000	-0.269E-02	0.000	2 X02
0.000	0.000	-0.100	3 X03

GAMMAS MATRIX

1 PUG	2 PWG	3 PHC	4 P U	5 P W	6 P Q	7 PTH	8 PDB	9 PDC	10 PHD	11 PXB	12 PXD	
0.483E-01	0.000	0.000	0.000	0.000	0.000	0.000	0.000	0.000	0.000	0.000	0.000	1 X01
0.000	0.734E-01	0.000	0.000	0.000	0.000	0.000	0.000	0.000	0.000	0.000	0.000	2 X02
0.000	0.000	0.447	0.000	0.000	0.000	0.000	0.000	0.000	0.000	0.000	0.000	3 X03

HS MATRIX

1 X01	2 X02	3 X03	
1.00	0.000	0.000	1 UG
0.000	1.00	0.000	2 WG
0.000	0.000	1.00	3 HDC

TABLE 11. (Continued)

Controlled Element

FC MATRIX

1 X06	2 X07	3 X08	4 X09	5 X10	6 X11	7 X12	8 X13	9 X14		
-0.340E-02	0.250E-01	0.460	-32.1	1.04	0.691	0.000	1.04	0.000	1	X06
-0.991E-01	-0.385	1.97	-2.27	0.321	-9.77	0.000	0.321	0.000	2	X07
0.190E-02	-0.380E-02	-0.190	0.000	-0.169	-0.330E-02	0.000	-0.169	0.000	3	X08
0.000	0.000	1.00	0.000	0.000	0.000	0.000	0.000	0.000	4	X09
0.000	0.000	0.000	0.000	0.000	0.000	0.000	0.000	0.000	5	X10
0.000	0.000	0.000	0.000	0.000	0.000	0.000	0.000	0.000	6	X11
-0.705E-01	0.998	0.000	-1.69	0.000	0.000	0.000	0.000	0.000	7	X12
0.000	0.000	4.97	0.000	0.000	0.000	0.000	-0.333	0.000	8	X13
0.998	0.705E-01	0.000	0.000	0.000	0.000	0.000	0.000	0.000	9	X14

GC MATRIX

1 DBD	2 DCD		
0.000	0.000	1	X06
0.000	0.000	2	X07
0.000	0.000	3	X08
0.000	0.000	4	X09
1.00	0.000	5	X10
0.000	1.00	6	X11
0.000	0.000	7	X12
0.000	0.000	8	X13
0.000	0.000	9	X14

TABLE 11. (Continued)

GAMMAC MATRIX

1 PUG	2 PWG	3 PHC	4 P U	5 P W	6 P Q	7 PTH	8 PDB	9 PDC	10 PHD	11 PXB	12 PXD	
0.000	0.000	0.000	1.00	0.000	0.000	0.000	0.000	0.000	0.000	0.000	0.000	1 X06
0.000	0.000	0.000	0.000	1.00	0.000	0.000	0.000	0.000	0.000	0.000	0.000	2 X07
0.000	0.000	0.000	0.000	0.000	1.00	0.000	0.000	0.000	0.000	0.000	0.000	3 X08
0.000	0.000	0.000	0.000	0.000	0.000	1.00	0.000	0.000	0.000	0.000	0.000	4 X09
0.000	0.000	0.000	0.000	0.000	0.000	0.000	1.00	0.000	0.000	0.000	0.000	5 X10
0.000	0.000	0.000	0.000	0.000	0.000	0.000	0.000	1.00	0.000	0.000	0.000	6 X11
0.000	0.000	0.000	0.000	0.000	0.000	0.000	0.000	0.000	1.00	0.000	0.000	7 X12
0.000	0.000	0.000	0.000	0.000	0.000	0.000	0.000	0.000	0.000	1.00	0.000	8 X13
0.000	0.000	0.000	0.000	0.000	0.000	0.000	0.000	0.000	0.000	0.000	1.00	9 X14

TABLE 11. (Continued)

Measurement

CC MATRIX

1 UG	2 WG	3 HDC		
0.340E-02	-0.250E-01	0.000	1	X06
0.991E-01	0.385	0.000	2	X07
-0.190E-02	0.380E-02	0.000	3	X08
0.000	0.000	0.000	4	X09
0.000	0.000	0.000	5	X10
0.000	0.000	0.000	6	X11
0.000	0.000	1.00	7	X12
0.000	0.000	0.000	8	X13
0.000	0.000	0.000	9	X14

FM MATRIX

1 UG	2 WG	3 HDC		
0.000	0.000	0.000	1	HD
0.000	0.000	0.000	2	Q
0.000	0.000	0.000	3	TH
0.000	0.000	0.000	4	DB
0.000	0.000	0.000	5	DC
0.000	0.000	1.00	6	HDE
0.000	0.000	0.000	7	HDI
0.000	0.000	0.000	8	XD
0.000	0.000	0.000	9	XDI

TABLE 11. (Concluded)

HM MATRIX

1 X06	2 X07	3 X08	4 X09	5 X10	6 X11	7 X12	8 X13	9 X14	
0.705E-01	-0.998	0.000	1.69	0.000	0.000	0.000	0.000	0.000	1 HD
0.000	0.000	1.00	0.000	0.000	0.000	0.000	0.000	0.000	2 Q
0.000	0.000	0.000	1.00	0.000	0.000	0.000	0.000	0.000	3 TH
0.000	0.000	0.000	0.000	1.00	0.000	0.000	0.000	0.000	4 DB
0.000	0.000	0.000	0.000	0.000	1.00	0.000	0.000	0.000	5 DC
-0.705E-01	0.998	0.000	-1.69	0.000	0.000	0.000	0.000	0.000	6 HDE
0.000	0.000	0.000	0.000	0.000	0.000	1.00	0.000	0.000	7 HDI
0.998	0.705E-01	0.000	0.000	0.000	0.000	0.000	0.000	0.000	8 XD
0.000	0.000	0.000	0.000	0.000	0.000	0.000	0.000	1.00	9 XDI

Output (Auxiliary Only)

FO MATRIX

1 UG	2 WG	3 HDC	
0.000	-0.592	0.000	1 AOA
-0.998	-0.705E-01	0.000	2 ASE

HO MATRIX

1 X06	2 X07	3 X08	4 X09	5 X10	6 X11	7 X12	8 X13	9 X14	
0.000	0.592	0.000	0.000	0.000	0.000	0.000	0.000	0.000	1 AOA
0.998	0.705E-01	0.000	0.000	0.000	0.000	0.000	0.000	0.000	2 ASE

TABLE 12. NOTATION FOR FACTORED TRANSFER FUNCTIONS

```
CASE:  UH1H HOVER 122LONG 31-JAN-79 CONTROLLED ELEMENT TF'S  <-- Title

DENOMINATOR:

  1.0000  <-- High-frequency gain
( .00000  ) ( .00000  ) ( .00000  ) ( .00000  )
( .38494  )                                      <-- Real poles
(( .10339  , .18934  , .19576E-01, .18833  ))
(( .26279  , .92717  , .24365  , .89459  ))      <-- Complex poles
< .11863E-01>  <-- Low-frequency gain

NUMERATOR:  TH/DBD  <-- Numerator title

 -.16910  <-- High-frequency gain
( .00000  ) ( .00000  ) ( .00000  ) (-.79065E-02)
( .33300  ) ( .39184  )                          <-- Real zeros
< .17445E-03>  <-- Low-frequency gain
```

$$\frac{\dot{\theta}}{\delta_B} = \frac{-.1691s^3(s-.0079)(s+.333)(s+.39184)}{s^4(s+.38494)[s^2+2(.10339)(.18934)s+(.18934)^2][s^2+2(.26279)(.92717)s+(.92717)^2]}$$

$$= \frac{-.1691(s+.333)}{[s^2+2(.10339)(.18934)s+(.8934)^2][s^2+2(.26279)(.92717)s+(.92717)^2]}$$

Alternately, the notation can be considered shorthand for expressing factored polynomials:

```
K
(z)
((ζ, ω, ζω, ω √(1-ζ²) ))
<Kzω²>
```

corresponds to

$$K(s+z)(s^2+2\zeta\omega s+\omega^2)$$

Note that the complex poles and zeros have four components:

((damping ratio, undamped natural frequency, real part, imaginary part))

TABLE 13

SELECTED CONTROLLED ELEMENT TRANSFER FUNCTIONS

CASE: UH1H HOVER 122LONG 31-JAN-79 CONTROLLED ELEMENT TF'S

DENOMINATOR:

```
  1.0000
( .00000    ) ( .00000    ) ( .00000    ) ( .00000    )
( .38494    )
(( .10339    , .18934    , .19576E-01, .18833    ))
(( .26279    , .92717    , .24365    , .89459    ))
< .11863E-01>
```

NUMERATOR: TH/DBD

```
 -.16910
( .00000    ) ( .00000    ) ( .00000    ) (-.79065E-02)
( .33300    ) ( .39184    )
< .17445E-03>
```

NUMERATOR: TH/DCD

```
 -.33000E-02
( .00000    ) ( .00000    ) ( .00000    ) ( .10854E-01)
( .33300    ) (-11.270    )
< .13442E-03>
```

Shorthand notation is used to express factored polynomials. For example,

$$K(s + z)(s^2 + 2\zeta\omega s + \omega^2)$$

corresponds to

$$K\ (z)\ ((\zeta,\ \omega,\ \zeta\omega,\ \omega\sqrt{1-\zeta^2}))\ \langle Kz\omega^2\rangle$$

SECTION IV

CONTROLLER SYNTHESIS

The controller optimal synthesis can be divided into three distinct steps:

- Filter-observer synthesis
- Regulator synthesis
- Combination of the above into the controller

This section starts by reviewing some important linear stochastic control facts in order to define the synthesis problem and solution. The solution of the singular filter problem, and the implications of requiring a solution which does not use differentiation, are considered. This is followed by specific recommended procedures for the synthesis of flight control systems and illustrative examples of their application.

A. STOCHASTIC OPTIMAL CONTROL FACTS

Stationary plant state and measurement equations and process and measurement noise characteristics for the system which is the object of optimal control are summarized in Table 14. The notation and definitions used follow those customary in the literature (e.g., Ref. 1). We have made specific provision in Table 14 for noise-free measurements via the z_2 partition of the measurement vector.

It is well known (e.g., Ref. 6) that the linear stochastic optimal control solution with respect to the cost function

$$J_C = E[y' Q_R y + u' R_R u] \tag{40}$$

where the plant outputs are

$$y = H_R x$$

TABLE 14. LINEAR PROBLEM MODEL

States

$$\dot{x} = Fx + Gu + \Gamma w \quad , \quad x(0) = x_0$$

Measurements

$$z = \begin{Bmatrix} z_1 \\ z_2 \end{Bmatrix} = Hx + v$$

$$z_1 = H_1 x + v_1$$

$$z_2 = H_2 x + \cancel{v_2}^{0}$$

Noise Characteristics

$$E[w] = 0 \quad , \quad E[v] = 0$$

$$E[w(t_1)\, w'(t_2)] = Q\delta(t_2 - t_1)$$

$$E[v(t_1)\, v'(t_2)] = R\delta(t_2 - t_1)$$

can be partitioned into solution of two separate problems. These are the (Kalman) filter and regulator problems. The combined solution, shown in Fig. 12, results in the linear optimal stochastic controller.

The filter problem is solved to minimize the mean square estimation error via the cost function:

$$J_F = E[(\hat{x} - x)'\,(\hat{x} - x)] \tag{41}$$

Solution results in the filter gain matrix, K. In formulating the problem we have assumed that some or all of the measurements are noise free. Thus,

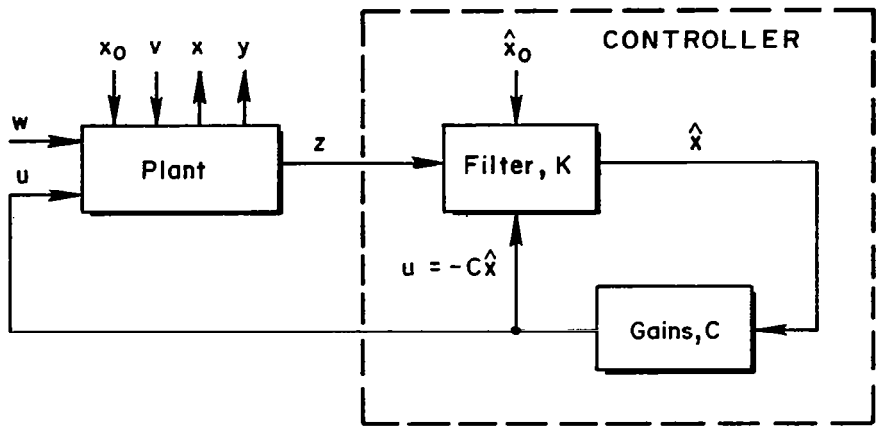

Figure 12. Form of Linear Stochastic Optimal Control Solution

the measurement noise intensity matrix R may be singular. This, in turn, implies difficulty in obtaining the filter solution by computational methods which depend on the existence of R^{-1}. Appendix A presents an alternative solution technique which yields the required partitions, K_{11} and K_{12}, of the filter matrix, K, for this singular case. Solution of this singular filter problem is a key contribution for optimal flight controllers because most measurements in flight control applications are practically noise free. It also enables us to obtain lower-order controllers which are necessary for practical flight control systems.

The regulator problem is solved to minimize the cost function:

$$J_R = \int_o^\infty (y' Q_R y + u' R_R u)\, dt \qquad (42)$$

Solution results in the regulator gain matrix, C. To be consistent with the physical constraints on control use in flight control applications we shall require R_R to be non-singular. The central issue in the regulator problem is the selection of appropriate Q_R and R_R matrices. The selection must produce adequate performance yet not waste control resources. A methodology for their rational selection is another key contribution of this research.

As depicted in Fig. 12 the "controller" is defined by the filter gain matrix (K), the regulator gain matrix (C), and the equation:

$$u = -C\hat{x} \tag{43}$$

In the flight control application we elect additional restrictions. We shall require the plant to be stabilizable with respect to the available control points, and detectable with respect to those elements of y which have non-zero weighting in Q_R (Ref. 8)

The cost function shall be a weighted sum of mean square values of variables having operational significance for each application. Therefore, Q_R and R_R are restricted to be diagonal matrices because the measurement matrix, H_R, can be used to generate all variables having operational significance except for the controls. However, the controls are available in their operationally significant form by virtue of their definition. Further, we shall require R_R to be positive definite.

Singular filters have order (number of states) which is less than or equal to $(n - m_2)$, where n is the number of plant states and m_2 is the number of independent noise-free measurements. When the order is less than $(n - m_2)$, differentiation of the noise-free measurements may be required. Differentiation is undesirable for the flight control application because very low level, broadband noise components of measurements are a virtual certainty even if negligible from all other viewpoints. In order to make differentiation of the noise-free measurements unattractive as an optimal solution we resort to the artifice of augmenting the process noise excitation of the plant. The added noise is specifically chosen to cause the derivative of every noise-free measurement to contain an independent process noise component. Mathematically, this is equivalent to requiring $\Gamma_2 Q \Gamma_2'$ to be nonsingular (Appendix A).* The levels of the

*This solution for the filter problem having noise-free measurements was reported by Uttam and O'Halloran, Ref. 25, pp. 327-332, but is not recognized as the optimal filter.

augmenting noise can be made very low, although numerical roundoff in computation imposes lower bounds. When $\Gamma_2 Q \Gamma_2'$ is nonsingular, the filter order is exactly $(n-m_2)$ and the filter can be realized using that number of integrators. The levels of the augmenting process noise can be manipulated to affect the closed-loop filter eigenvalues. This can be used to advantage in controlling the range for the closed-loop filter eigenvalues. It is also the reason we refer to the singular filter as the "filter-observer."

Although augmenting the process noise excitation of the plant is an artifice, it can be rationalized. The stationary, linearized, perturbation plant equations we tend to regard as a true model are in fact an approximation. Nonlinear, nonstationary effects and small terms in the equations are neglected, as is the uncertainty in the values for the coefficients in terms we retain. One may look upon the augmenting process noise as an aggregated representation of these conveniently neglected effects.

When $\Gamma_2 Q \Gamma_2'$ is nonsingular, the optimal filter-observer has the structure shown in Fig. 13. (Figure 13 assumes for simplicity, and without loss of generality, that the plant state definition includes the noise-free measurements, z_2, as the x_2 partition.)

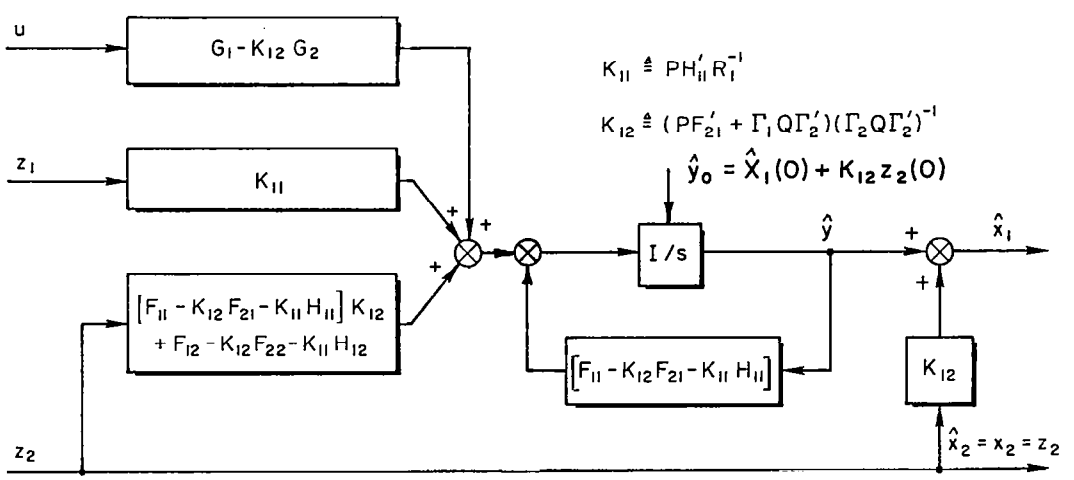

Figure 13. Optimal Filter-Observer Structure

Given the regulator gains, C, in terms of the same state vector, the controller structure and equations can be shown as in Fig. 14. The coefficient matrices in Fig. 14 are given by

$$A_F = [F_{11} - K_{12}F_{21} - K_{11}H_{11} + (G_1 - K_{12}G_2)C_F]$$

$$B_F = [K_{11},\ (F_{11} - K_{12}F_{21} - K_{11}H_{11})K_{12} + F_{12} - K_{12}F_{22} - K_{11}H_{12}]$$

$$C_F = -C \begin{bmatrix} I \\ 0 \end{bmatrix}$$

$$D_F = -C \begin{bmatrix} 0 & K_{12} \\ 0 & I \end{bmatrix}$$

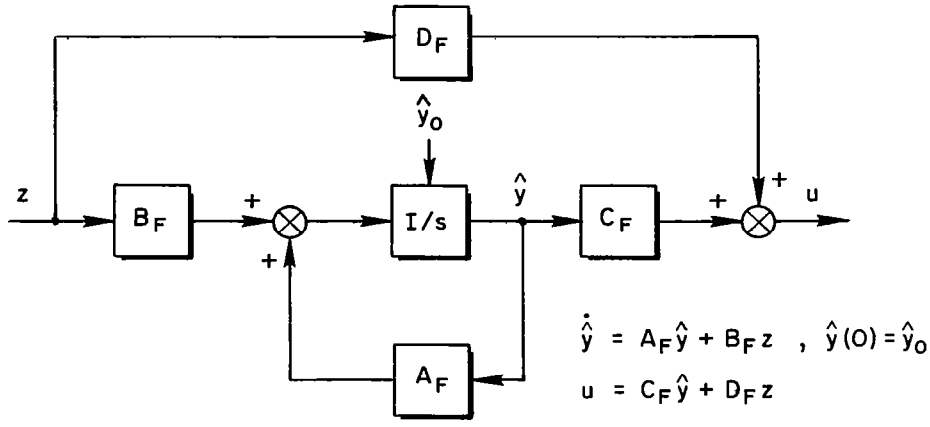

Figure 14. Form of Controller Solution
(Filter-Observer + Regulator)

This block diagram, and the matrices therein, corresponds to the simplest form of the generalized controller equations. This form, including the A_F, B_F, C_F and D_F matrices, is used in the optimal design software. Figure 15a shows this same controller, but here the block diagram structure more clearly delineates the filter-observer and regulator

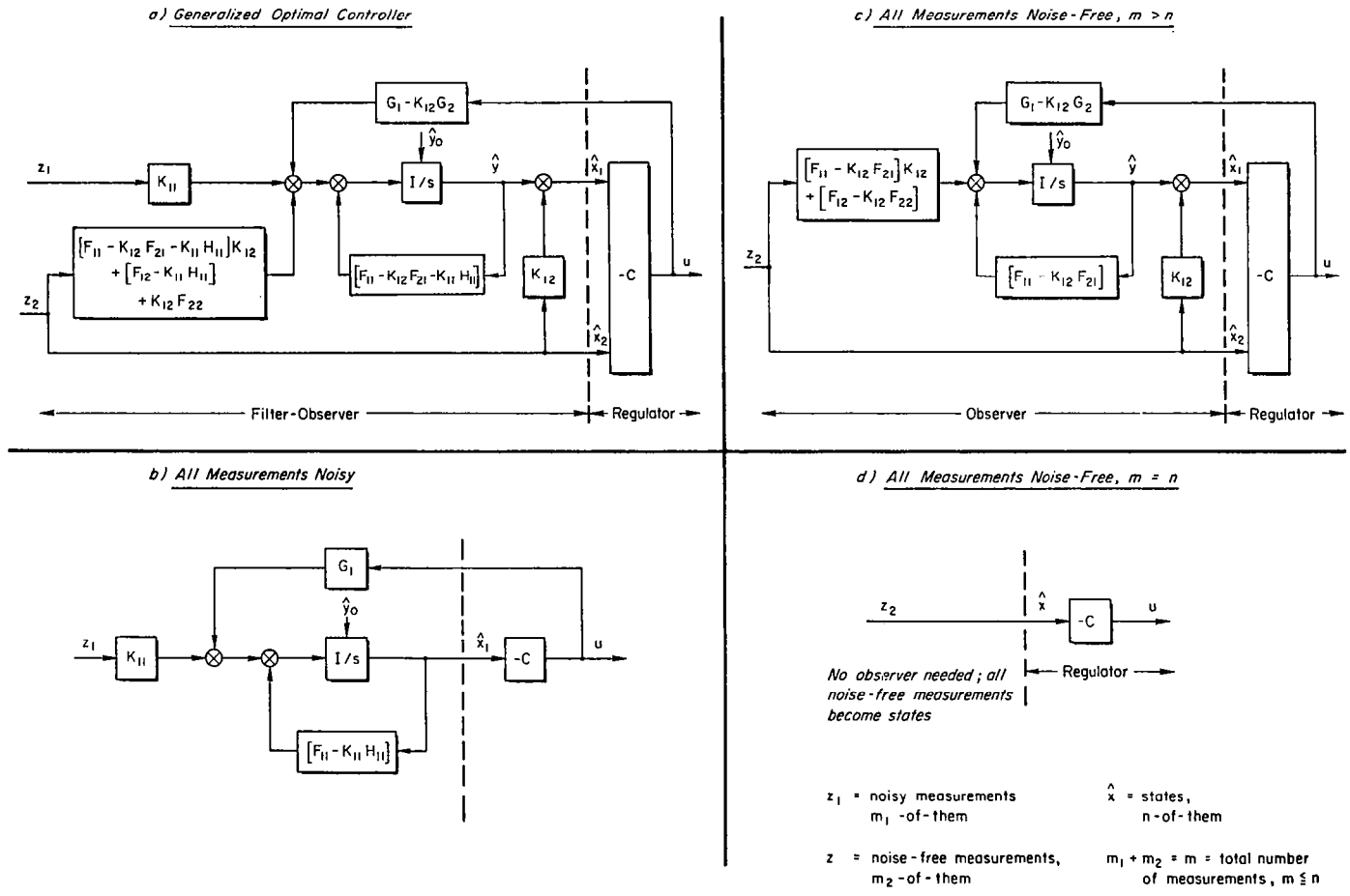

Figure 15. Form of Controller Solution — Special Cases

components. Two limiting cases are also of interest. When all the measurements are noisy the controller reduces to the block diagram of Fig. 15b; the filter-observer reduces to the familiar Kalman filter, while the regulator is unchanged. With all measurements noise-free, and with fewer measurements than states, the filter-observer becomes a pure observer, used to estimate those states for which measurements are unavailable (Fig. 15c). If the number of measurements equals the number of states, however, an observer is not needed at all; the noise-free measurements constitute alternative states, and are subsequently fed to the usual regulator (Fig. 15d).

The recitation of stochastic optimal control facts given above establishes the mechanics for obtaining solutions. The following subsections present the techniques for purposeful application and illustrative examples. These subsections focus on two key questions:

- How should one choose the diagonal Q_R and R_R matrix elements for practical designs?
- How should one augment the process noise input to avoid differentiators in the filter solution?

Answers to these questions complete the data required to synthesize an optimal flight control system responsive to primary design goals. All other data required are obtained from the physics of the problem.

B. FILTER-OBSERVER SYNTHESIS

In defining the shaping and controlled element states, the measurements, and the outputs in preparation for optimal controller design we have attempted to use experience and foresight to make the actual optimal control calculations straightforward. For example, we have chosen to include the integrals of variables when the indicial error response for those variables must approach zero as time approaches infinity. Also, care has been taken to insure that all pertinent variables are included in the output vector.

Still, there are certain fine points which remain elusive. Foremost among these is the definition of a desirable group of measurements,

together with the corollary question of the adequacy of the associated sensor array. The synthesis of the filter-observer permits these points to be resolved. In particular, the synthesis provides a definitive measure of the sensor array performance for a particular measurement set. The order of the controller will also be finalized because it is determined by the order of the filter-observer.

It is recommended that the filter-observer synthesis be addressed before the regulator synthesis. This is mainly for the reason that once the rms state estimation error and filter-observer eigenvalues are in acceptable ranges (specified later) the designer need not reconsider the filter-observer design in the later stage of optimal closed-loop system assessment. (The same cannot be said for the regulator solution.) Furthermore, controller transfer functions are immediately available at each cycle of the regulator solution when the filter-observer solution is already in hand. In this way, the controller tends to proceed in a top-down fashion.

The filter-observer has three main functions:

- It defines the quality of the instrumental complex used to make measurements, via the rms state estimation error. This is the primary reason cited above for beginning the controller design with the filter-observer synthesis. A stage is set upon which several alternate sensor arrays may compete, and the best one be chosen.

- It provides the best estimate of the total state vector, given the available measurements, to use as input to the regulator.

- It is the only place where the detailed properties of the noise and disturbances can affect the controller design.

This final function is perhaps the most important. In essence, the noise and disturbance properties directly affect the closed-loop system in that the filter-observer poles are closed-loop system poles. Filter-observer poles are a function of the process and measurement noise levels. These poles are the equivalent of the compensator poles in a conventional design in that they adjust the controller behavior as a function of the disturbance environment. This is analogous to the adjustment of washout and

complementary filter break frequencies appropriate to the command, disturbance and noise environment in conventional design practice. In the course of the filter-observer discussion we will see how these same poles affect the controller in the command environment.

Steps in the filter-observer synthesis are summarized in Table 15 for ready reference. These five steps are elaborated in the following paragraphs and are illustrated by examples.

TABLE 15. FILTER-OBSERVER SYNTHESIS

Specify process and measurement noise levels based on physics (Q and R)
Augment process noise to get independent noise on the derivative of every noise-free measurement
Compute closed-loop filter eigenvalues and rms estimation error
Change sensor array if rms estimation error is extreme
Adjust augmenting process noise if eigenvalue range is unacceptable

1. Physical Components of Process and Measurement Noise

The process noise components which are used to generate shaped command and disturbance inputs to the controlled element have levels which are determined by the physics of the operating environment. In practice, these levels may be definitively established, as in the case of gusts, or may merely be estimates, as in the case of some commands. Here, we assume the noise levels which are features of the environment are known. Measurement noise components should also be based upon the physical situation. For example, it is reasonable to assume that rate and attitude gyros and actuator position pickoffs provide noise-free measurements.

Measurement noise on body-mounted accelerometers may or may not be regarded as significant depending upon factors specific to the application. If significant, measurement noise levels may be inferred from the threshold and linearity specifications for the particular accelerometer instrument. In the case of Microwave Landing System (MLS) guidance, for example, the measurement noise (power spectral density) level can be calculated from either the levels of error budget power spectral densities (e.g., Ref. 25) for the broadband sources, or from measured power spectral densities.

2. Augmenting Process Noise Components

The requirement to differentiate any noise-free measurement can be avoided if the derivative of every noise-free measurement contains an independent component of process noise.* One means by which this condition may be satisfied is to simply include an identity partition in the controlled element Γ_c matrix (refer to Table 11). This identity partition is in addition to any columns of the Γ_c matrix which arise from the problem physics. A corresponding null partition must be included in the shaping Γ_s matrix to insure dimensional compatibility. Subject only to the assumption that no command or disturbance input is a noise-free measurement, this provision and the ability to specify the levels of the augmenting process noise arbitrarily are sufficient to provide an independent component of process noise in the derivative of every noise-free measurement. That this is so is verified by the following equations.

*Alternatively, there will never be a requirement to differentiate any measurement containing measurement noise. However, adding measurement noise for the sole purpose of avoiding differentiation of a measurement is unattractive because it increases the order of the filter-observer. The order increases by one for each measurement so treated. Practically, this would require an increase in controller complexity.

$$\dot{x} = \begin{Bmatrix} \dot{x}_S \\ \dot{x}_C \end{Bmatrix} = \cdots + \begin{bmatrix} \Gamma_S \\ \Gamma_C \end{bmatrix} w \tag{44}$$

$$z = [F_M H_S \quad H_M] \begin{Bmatrix} x_S \\ x_C \end{Bmatrix} + v \tag{45}$$

$$\dot{z} = \cdots + [F_M H_S \Gamma_S + H_M \Gamma_C] w + \cdots \tag{46}$$

Inspection of $[F_M H_S \Gamma_S + H_M \Gamma_C]$ reveals which augmenting process noise components must have non-zero levels. This inspection proceeds row-by-row for only those rows which are associated with noise-free measurements. An array formed of these rows can be constructed.* This array must have rank m_2, where m_2 is the number of noise-free measurements. Up to $n - m_2$ columns of this array may be eliminated without reduction of the array rank. Any set of columns which are coefficients of the augmenting process noise and which can be eliminated without reducing the array rank, may have corresponding zero levels in the diagonal process noise intensity matrix, Q. The values for the remaining augmenting process noise levels must be greater than zero, but are otherwise arbitrary.

The above approach to augmenting the process noise has been adequate for all applications made to date. However, it is clear that augmentation of the Γ_C and Γ_S matrices by identity and null partitions, respectively, is not required. Indeed, these augmentation partitions may be completely arbitrary subject only to the restriction that Γ_2 have full rank.

3. Filter Eigenvalues and RMS Estimation Error

The third step, that is, the computation of closed-loop filter-observer eigenvalues and rms estimation error, is accomplished using the software package (Ref. 23).

*This array is computed by the software as Γ_2.

4. Changes to Sensor Array

Next, the rms estimation error is compared with target values for closed-loop system performance. Since rms estimation error establishes a lower bound on achievable closed-loop system performance, it is essential that no target rms performance value be exceeded by its corresponding estimation error component and that significant margins exist. If target values are exceeded, this is an indication that the sensor array is inadequate with respect to variables measured, quality of measurement,* location/orientation of sensors, or any combination of these factors. Changes to the sensor array with respect to one or more of the above characteristics should be made before continuing the controller synthesis. On the other hand, if rms estimation error is exceedingly small with respect to target values, this may be regarded as an invitation to explore use of fewer or lower quality* sensors. Use of fewer noise-free measurements, of course, requires use of a correspondingly higher-order filter-observer. This tradeoff aspect must be borne in mind when exploring the possibility for reducing the number of sensors.

5. Adjusting Augmenting Process Noise

The final step is to inspect the eigenvalue range for the closed-loop filter-observer. Eigenvalues with very large modulus (say, greater than 50. rad/sec) indicate that large gains will be required in filter implementation and may indicate excessive dynamic range requirements. Eigenvalues with very small modulus (say, less than 0.1 rad/sec) indicate that very slow closed-loop response modes arising in the filter-observer may be present. These modes may be excited by command or disturbance inputs, or as the result of differences between the real-world plant and the plant model for which the filter-observer is designed. Some closed-loop filter eigenvalues may be altered when some or all of the measurements are noise-free. This can be accomplished by adjusting the augmenting process noise

*Lower quality measurements can only be explored when noise effects are explicitly modeled.

via changes in the appropriate columns of the Γ and Q matrices. Our experience in application is that changes in the augmenting process noise levels via the diagonal Q matrix are usually sufficient to obtained closed-loop filter eigenvalues in the desired range.

6. Filter-Observer Synthesis Examples

This subsection provides illustrative examples for the filter-observer considerations addressed in previous paragraphs. The application to be described in detail is to the longitudinal dynamics of the UH-1H for the hover flight condition. Table 16 is a data summary for the final filter-observer design.

Consider the elements of the diagonal process noise intensity matrix, Q, in Table 16. The associated mnemonics have P prefixes to denote process noise. The remainder of each mnemonic has been used to designate the differential equation each process noise component forces. The first three element values are fixed by the physics of the assumed operating environment. The values given are $\sigma^2_{u_g}$, $\sigma^2_{w_g}$, and $\sigma^2_{\dot{h}_c}$, respectively, because the shaping filter gains, $\sqrt{2\omega_{u_g}}$, $\sqrt{2\omega_{w_g}}$, and $\sqrt{2\omega_{\dot{h}_c}}$ are contained in Γ_S. The remaining nine elements of the Q matrix diagonal are augmenting process noise intensities. Notice that one of these intensities is zero.

Next, consider the elements of the diagonal measurement noise intensity matrix, R. The associated mnemonics indicate the measurement in which that measurement noise component appears. All elements of the diagonal R matrix are zero because all nine measurements are assumed to be noise-free in this application.

Consider the rms estimation error in Table 16. Only two of the 12 rms state estimation errors are non-zero. Those two values are for estimates of the longitudinal and normal gust velocities. We can compare these rms errors to the input rms gust velocities:

$$\sigma_{u_g} = 2.06 \qquad \sigma_{E_{u_g}} = .173 \qquad \sigma_{E_{u_g}} \Rightarrow 8.4\% \ \sigma_{u_g}$$

$$\sigma_{w_g} = 1.71 \qquad \sigma_{E_{w_g}} = .054 \qquad \sigma_{E_{w_g}} \Rightarrow 3.2\% \ \sigma_{w_g}$$

TABLE 16. UH-1H, HOVER, FINAL FILTER DESIGN

Q MATRIX DIAGONAL, FILTER 1

4.24	1 PUG
2.92	2 PWG
1.00	3 PHC
0.100E-04	4 P U
0.100E-04	5 P W
0.100E-04	6 P Q
0.100E-05	7 PTH
0.100E-04	8 PDB
0.100E-04	9 PDC
0.100E-04	10 PHD
0.000	11 PXB
0.100E-04	12 PXD

R MATRIX DIAGONAL, FILTER 1

0.000	1 HD
0.000	2 Q
0.000	3 TH
0.000	4 DB
0.000	5 DC
0.000	6 HDE
0.000	7 HDI
0.000	8 XD
0.000	9 XDI

RMS STATE EST ERROR, FILTER 1

0.173	1 X01
0.541E-01	2 X02
0.000	3 X03
0.000	4 X06
0.000	5 X07
0.000	6 X08
0.000	7 X09
0.000	8 X10
0.000	9 X11
0.000	10 X12
0.000	11 X13
0.000	12 X14

CLOSED LOOP EIGENVALUES, FILTER 1

0.333 180.	1 E13
15.6 180.	2 E01
0.315 180.	3 E02

K12 GAIN MATRIX, FILTER

1 HD	2 Q	3 TH	4 DB	5 DC	6 HDE	7 HDI	8 XD	9 XDI	
0.941E-08	-0.679E-09	-0.159E-07	0.000	0.000	-0.286E-16	0.000	0.195E-08	0.000	1 E13
-6.07	-8.57	10.3	0.000	0.000	0.184E-07	0.000	29.5	0.000	2 E01
-38.9	2.54	65.8	0.000	0.000	0.118E-06	0.000	-7.16	0.000	3 E02

Because the estimation error is a small percentage of the rms gust velocities, the sensor array is judged to be adequate. In other applications, it may be desirable to compute the rms estimation error as reflected in the output vector, y, in order to verify that design performance target values are not exceeded.

Consider the filter gain matrices K_{11} and K_{12}. K_{11} does not appear in Table 16. This is the case because K_{11} has zero columns when all measurements are noise free. The K_{12} matrix in Table 16 (and other plant data) is used in the structure shown in Fig. 13 to define the filter-observer design.

Next, we focus attention on the filter eigenvalues, in the center of Table 16. Previously, we identified a rather arbitrary range of 0.1 to 50.0 rad/sec for "acceptable" eigenvalues. Clearly, the eigenvalues from this example fall within the acceptable range. Concerns with eigenvalues on the high end of the range centered around the high gains which might appear in the filter as a result. From the K_{12} filter gain matrix we see that all gains are at moderate levels, thus corroborating the acceptability of the eigenvalue at 15.6 rad/sec.

On the other hand, the eigenvalues at the low end of the range were of concern because, in general, the filter eigenvalues become closed-loop system roots. Closed-loop roots with modulus less than 0.1 rad/sec clearly are undesirable. For example, they produce long tails in some of the transient response characteristics of the system. In fact, even the eigenvalues at 0.315 rad/sec and 0.333 rad/sec, for the example, could cause unacceptable transient response tails. But we shall see presently that, for this example and many other systems, these eigenvalues are not an important concern.

This example constitutes a very interesting special case which has practical value. Notice that the filter-observer structure shown in Fig. 13 implies that the controller and closed-loop filter eigenvalues can differ only if $[G_1 - K_{12}G_2]$ is not null.* However, the data for K_{12}, G_1 and G_2

*This is the case because all filter modes are uncontrollable with respect to all elements of the plant control vector.

in Tables 16 and 17 indicate that $[G_1 - K_{12}G_2]$ is null. Therefore, the controller and closed-loop filter eigenvalues are the same, and the closed-loop filter eigenvalues are independent of the regulator solution. Furthermore, in this special case the controller eigenvalues are therefore guaranteed to be stable. Stability of the controller-alone is usually desired in traditional flight control system synthesis. It is therefore important for us to recognize the causal factors which lead to similar optimal controller designs.

One factor is the application of control through serially coupled actuation subsystems. Another factor is noise-free measurement of the actuator outputs. Together, these result in G_1 being null and G_2 being sparse. Additionally, we observe that the only non-zero elements of G_2 occur in the actuator state equations. Finally, we have observed in numerous applications that the coefficients of the actuator output measurements in K_{12} are zero as long as no noise-free measurement (other than actuator output itself) depends explicitly upon the actuator output states. $K_{12}G_2$ is null when these two observations apply. We have already observed that when $[G_1 - K_{12}G_2]$ is a null matrix, the filter eigenvalues and the controller eigenvalues are identical.

The filter eigenvalues are, in general, closed-loop system poles. They do not, however, necessarily affect all aspects of closed-loop behavior. For instance, those inputs which drive the plant controls directly through a gain matrix result in closed-loop transfer functions in which zeros cancel the closed-loop filter-observer poles exactly. (These inputs are those commands wherein error and integral error are noise-free, and have gains in the B_F matrix equal to zero.) This reduces, to some extent, the importance of the filter eigenvalue location, since the modes they represent are not present in some of the command transfer functions of the closed-loop system. There remain, however, three areas where the filter eigenvalues do play a role:

- The filter eigenvalues become roots of the controller transfer functions. If the controller is used apart from the total FCS (e.g., in a checkout phase) the eigenvalue locations will partially determine the controller's response characteristics.

TABLE 17. CONTROL DISTRIBUTION MATRIX PARTITIONS

G1 MATRIX

1 DBD	2 DCD	
Ø.ØØØ	Ø.ØØØ	1 E13
Ø.ØØØ	Ø.ØØØ	2 EØ1
Ø.ØØØ	Ø.ØØØ	3 EØ2

G2 MATRIX

1 DBD	2 DCD	
Ø.ØØØ	Ø.ØØØ	1 HD
Ø.ØØØ	Ø.ØØØ	2 Q
Ø.ØØØ	Ø.ØØØ	3 TH
1.ØØ	Ø.ØØØ	4 DB
Ø.ØØØ	1.ØØ	5 DC
Ø.ØØØ	Ø.ØØØ	6 HDE
Ø.ØØØ	Ø.ØØØ	7 HDI
Ø.ØØØ	Ø.ØØØ	8 XD
Ø.ØØØ	Ø.ØØØ	9 XDI

- The poles of the closed-loop system identified as filter eigenvalues will not be cancelled exactly in general by closed-loop system zeros for transfer functions where the input is a disturbance. Often, however, they nearly cancel with zero, and are thus not much of a concern.

- In the next chapter we will consider the behavior of the closed-loop system in the face of various nonlinearities and component degradation. These off-nominal conditions have the effect of opening or changing one or more of the feedback loops. This will naturally destroy the cancellation of filter eigenvalue poles by closed-loop zeros. Consideration of filter eigenvalue location then becomes quite important.

Turn attention now to the matter of augmenting process noise excitation of the plant in such a way that differentiation of any noise-free measurement is not required. Consider the process noise distribution matrix, Γ, in Table 18. The upper and lower partitions of Γ are Γ_S and Γ_C, respectively. The left and right partitions of Γ contain the coefficients of the process noise components arising from the problem physics and arising from augmentation, respectively. Notice that the upper right partition of Γ is null in accordance with our recommendation for augmenting Γ_S, and the lower right partition is identity in accordance with our recommendation for augmenting Γ_C.

Consider the Γ_2 matrix for this example application in Table 19. The first three columns of Γ_2 distribute those process noise components which have a basis in the problem physics into the derivatives of the noise-free measurements. The first two columns cannot contribute to the rank of Γ_2. The last nine columns of Γ_2 distribute the augmenting process noise components. Column 11 cannot contribute to the rank of Γ_2; therefore, the PXB component of the process noise intensity can be zero. (This is the eleventh element in the diagonal Q matrix.) The remaining nine columns of Γ_2 are linearly independent; therefore, Γ_2 has full rank. Eight of these nine columns are associated with augmenting process noise components. The levels for these eight components must be greater than zero in the diagonal Q matrix.

TABLE 18. PROCESS NOISE DISTRIBUTION MATRIX

Coefficients of Process Noise Components Arising from Problem Physics

Coefficients of Augmenting Process Noise

GAMMA MATRIX

1 PUG	2 PWG	3 PHC	4 P U	5 P W	6 P Q	7 PTH	8 PDB	9 PDC	10 PHD	11 PXB	12 PXD	
0.483E-01	0.000	0.000	0.000	0.000	0.000	0.000	0.000	0.000	0.000	0.000	0.000	1 X01
0.000	0.734E-01	0.000	0.000	0.000	0.000	0.000	0.000	0.000	0.000	0.000	0.000	2 X02
0.000	0.000	0.447	0.000	0.000	0.000	0.000	0.000	0.000	0.000	0.000	0.000	3 X03
0.000	0.000	0.000	1.00	0.000	0.000	0.000	0.000	0.000	0.000	0.000	0.000	4 X06
0.000	0.000	0.000	0.000	1.00	0.000	0.000	0.000	0.000	0.000	0.000	0.000	5 X07
0.000	0.000	0.000	0.000	0.000	1.00	0.000	0.000	0.000	0.000	0.000	0.000	6 X08
0.000	0.000	0.000	0.000	0.000	0.000	1.00	0.000	0.000	0.000	0.000	0.000	7 X09
0.000	0.000	0.000	0.000	0.000	0.000	0.000	1.00	0.000	0.000	0.000	0.000	8 X10
0.000	0.000	0.000	0.000	0.000	0.000	0.000	0.000	1.00	0.000	0.000	0.000	9 X11
0.000	0.000	0.000	0.000	0.000	0.000	0.000	0.000	0.000	1.00	0.000	0.000	10 X12
0.000	0.000	0.000	0.000	0.000	0.000	0.000	0.000	0.000	0.000	1.00	0.000	11 X13
0.000	0.000	0.000	0.000	0.000	0.000	0.000	0.000	0.000	0.000	0.000	1.00	12 X14

TABLE 19. PROCESS NOISE DISTRIBUTION MATRIX FOR DERIVATIVES OF NOISE-FREE MEASUREMENTS

GAMMA2 MATRIX

1 PUG	2 PWG	3 PHC	4 P U	5 P W	6 P Q	7 PTH	8 PDB	9 PDC	10 PHD	11 PXB	12 PXD	
0.000	0.000	0.000	0.705E-01	-0.998	0.000	1.69	0.000	0.000	0.000	0.000	0.000	1 HD
0.000	0.000	0.000	0.000	0.000	1.00	0.000	0.000	0.000	0.000	0.000	0.000	2 Q
0.000	0.000	0.000	0.000	0.000	0.000	1.00	0.000	0.000	0.000	0.000	0.000	3 TH
0.000	0.000	0.000	0.000	0.000	0.000	0.000	1.00	0.000	0.000	0.000	0.000	4 DB
0.000	0.000	0.000	0.000	0.000	0.000	0.000	0.000	1.00	0.000	0.000	0.000	5 DC
0.000	0.000	0.447	-0.705E-01	0.998	0.000	-1.69	0.000	0.000	0.000	0.000	0.000	6 HDE
0.000	0.000	0.000	0.000	0.000	0.000	0.000	0.000	0.000	1.00	0.000	0.000	7 HDI
0.000	0.000	0.000	0.998	0.705E-01	0.000	0.000	0.000	0.000	0.000	0.000	0.000	8 XD
0.000	0.000	0.000	0.000	0.000	0.000	0.000	0.000	0.000	0.000	0.000	1.00	9 XDI

The final filter-observer design summarized in Table 16 is the result of three filter-observer design trials. The initial filter-observer design is summarized in Table 20. This initial design differs from the final only with respect to levels used for the augmenting process noise. Thus, Table 20 can be compared with Table 16 to demonstrate the substantial influence adjustment of augmenting process noise levels may have upon closed-loop filter eigenvalues. Initial design levels are larger for most components, and especially so for the u state equation. The initial design has a range of eigenvalues which is unacceptable because the smallest eigenvalue modulus is less than 0.1 rad/sec. This design also is characterized by somewhat larger rms estimation error and larger gains in the K_{12} matrix. Adjustment of the augmenting process noise levels (by trial and error) brings the low modulus eigenvalue well into the acceptable range (refer to Table 16).

Another interesting and practical dimension to filter-observer synthesis involves use of different sensor complements. The study described below explores the results of incorporating measurements of longitudinal acceleration independent of pitch and normal acceleration. Application in this case is for longitudinal dynamics of the UH-1H at a 100 kt level flight condition. The baseline sensor complex includes noise-free measurement of instantaneous vertical speed, pitch rate, pitch attitude, longitudinal cyclic actuator output, main rotor collective actuator output, rate-of-climb error, integral rate-of-climb error, airspeed error, and integral airspeed error. Five additional cases are considered in terms of measurements added to the baseline measurement set. The characteristics of these cases are summarized in Table 21.

Table 22 summarizes the design parameters, closed-loop filter eigenvalues, rms estimation error performance and the filter gain matrix for the baseline case of the UH-1H at 100 kt. In the process noise intensity diagonal matrix, Q, the fourth and subsequent elements are augmenting process noise components. The intensities of these augmenting components are kept constant in this study to the extent that the addition of noise-free measurements permits. The baseline filter design is third order; its eigenvalue range is acceptable, and the rms state estimation error

TABLE 20. UH-1H, HOVER, INITIAL FILTER DESIGN

Q MATRIX DIAGONAL, FILTER 1

4.24	1 PUG
2.92	2 PWG
1.00	3 PHC
10.0	4 P U
0.100E-03	5 P W
0.100E-03	6 P Q
0.100E-05	7 PTH
0.100E-03	8 PDB
0.100E-03	9 PDC
0.100E-03	10 PHD
0.000	11 PXB
0.100E-03	12 PXD

R MATRIX DIAGONAL, FILTER 1

0.000	1 HD
0.000	2 Q
0.000	3 TH
0.000	4 DB
0.000	5 DC
0.000	6 HDE
0.000	7 HDI
0.000	8 XD
0.000	9 XDI

RMS STATE EST ERROR, FILTER 1

0.569	1 X01
0.157	2 X02
0.000	3 X03
0.000	4 X06
0.000	5 X07
0.000	6 X08
0.000	7 X09
0.000	8 X10
0.000	9 X11
0.000	10 X12
0.000	11 X13
0.000	12 X14

CLOSED LOOP EIGENVALUES, FILTER 1

0.333 180.	1 E13
4.93 180.	2 E01
0.281E-01 180.	3 E02

K12 GAIN MATRIX, FILTER

1 HD	2 Q	3 TH	4 DB	5 DC	6 HDE	7 HDI	8 XD	9 XDI	
0.000	0.000	0.000	0.000	0.000	0.000	0.000	0.000	0.000	1 E13
-2.16	-9.30	3.65	0.000	0.000	0.172E-07	0.000	0.153	0.000	2 E01
-12.2	2.50	20.6	0.000	0.000	0.970E-07	0.000	0.862	0.000	3 E02

TABLE 21. SENSOR COMPLEMENT STUDY

CASE / TABLE	MEASUREMENTS	MEASUREMENT NOISE	NORMAL ACCELEROMETER LOCATION, ℓ_x (ft)
Baseline / 22	$\dot{h}$, q, θ, δ_B, δ_C, $\dot{h}_e$, $\int \dot{h}_e\, dt$, u_{AS_e}, $\int u_{AS_e}\, dt$	None	—
AZP1 / 23	Baseline + a_z' at pilot's location	None	7.3
AZP2 / 24	Baseline + a_z' at ICRB[a]	None	-29.86
AZP3 / 25	Baseline + a_z' at pilot's location	$R_{AZP} = 10^{-4}$ $(ft/sec^2)^2/Hz$	7.3
AXP1 / 26	Baseline + $(a_x - g \sin \Theta)$	None	—
AXP1 + AZP1 / 24	Baseline + $(a_x - g \sin \Theta)$ + a_z' at pilot's location	None	7.3

[a]ICRB denotes the instantaneous center of rotation location for longitudinal cyclic pitch control inputs, $Z_{\delta_B}/M_{\delta_B}$.

TABLE 22. BASELINE FILTER DESIGN, UH-1H, 100 KT

Q MATRIX DIAGONAL, FILTER 1

4.24	1 PUG
2.92	2 PWG
1.00	3 PHC
10.0	4 P U
0.000	5 P W
0.100E-03	6 P Q
0.100E-05	7 PTH
0.100E-03	8 PDB
0.100E-03	9 PDC
0.100E-03	10 PHE
0.000	11 PXB
0.100E-03	12 PSE

CLOSED LOOP EIGENVALUES, FILTER 1

0.333 180.	1 E13
25.1 180.	2 E01
0.111 180.	3 E02

RMS STATE EST ERROR, FILTER 1

2.03	1 X01
0.277	2 X02
0.000	3 X03
2.03	4 X06
0.107	5 X07
0.000	6 X08
0.171E-12	7 X09
0.000	8 X10
0.000	9 X11
0.000	10 X12
0.000	11 X13
0.000	12 X14

K12 GAIN MATRIX, FILTER

1 HD	2 Q	3 TH	4 DB	5 DC	6 HDI	7 HDE	8 ASI	9 ASE	
0.130E-06	-0.287E-07	-0.220E-04	0.000	0.000	-0.155E-12	0.134E-13	0.518E-11	-0.629E-08	1 E13
1.53	1.39	-259.	0.000	0.000	0.153E-03	0.156E-06	-0.508E-02	-0.120	2 E01
-24.7	4.41	0.417E+04	0.000	0.000	0.881E-05	-0.254E-05	-0.296E-03	1.18	3 E02

is acceptable although estimates of longitudinal gust and inertial velocity are not very accurate. The controller and closed-loop eigenvalues are the same because the K_{12} gain matrix coefficients of DB and DC are zero. (G_1 and G_2 are the same as in Table 17.)

In Table 23 we explore the effect of adding a noise-free normal acceleration measurement. The principal effects are to lower the filter order from third to second order, and to produce non-zero coefficients for DB and DC in the K_{12} filter gain matrix. This latter change means that controller eigenvalues will be a function of the regulator gains, and the controller eigenvalues will not necessarily be stable. We assert that non-zero coefficients of DB and DC in K_{12} arise because the noise-free measurement AZP is an explicit function of DB and DC in the measurement equations. The effect of the additional measurement in reducing rms state estimation error is almost nil except for the normal gust state which is halved.

In Table 24 we demonstrate the truth of the above assertion. Here we relocate the noise-free measurement of normal acceleration, AZP, from the pilot's station to instantaneous center of rotation for longitudinal cyclic pitch control inputs.* The latter location results in elimination of the explicit dependency of the AZP measurement equation upon DB since its coefficient ($Z_{\delta_B} - \ell_x M_{\delta_B}$) being zero defines ℓ_x for the instantaneous center location. The principal change with respect to the filter design of Table 23 is that the coefficients of DB are again zero in the K_{12} filter gain matrix.

*This location is frequently regarded as a desirable one for normal acceleration measurement in fixed-wing aircraft. This is so because the accelerometer measurement is then very nearly proportional to angle of attack which, in turn, is ideal for augmentation of short-period dynamic characteristics (Ref. 10, pp. 446-453).

TABLE 23. EFFECT OF NOISE-FREE a_Z' MEASUREMENT ON FILTER DESIGN, UH-1H, 100 KT

Q MATRIX DIAGONAL, FILTER 1

4.24	1 PUG
2.92	2 PVG
1.00	3 PHC
10.0	4 P U
0.100E-01	5 P W
0.100E-03	6 P Q
0.100E-05	7 PTH
0.100E-03	8 PDB
0.100E-03	9 PDC
0.100E-03	10 PHE
0.100E-03	11 PXB
0.100E-03	12 PSE

CLOSED LOOP EIGENVALUES, FILTER 1

0.423 180.	1 E01
0.101 180.	2 E02

RMS STATE EST ERROR, FILTER 1

1.98	1 X01
0.131	2 X02
0.117E-07	3 X03
1.98	4 X04
0.104	5 X07
0.994E-08	6 X08
0.829E-10	7 X09
0.191E-11	8 X10
0.719E-11	9 X11
0.000	10 X12
0.115E-01	11 X13
0.000	12 X14

K12 GAIN MATRIX, FILTER

1 HD	2 Q	3 TH	4 DB	5 DC	6 HDI	7 HDE	8 ASI	9 ASE	10 AZP	
1.99	1.72	-336.	0.371	-0.759	-0.116E-03	-0.109E-06	-0.487E-02	-0.141	-0.595E-01	1 E01
-1.01	0.259	170.	-6.64	13.6	-0.100E-04	0.549E-07	-0.265E-03	-0.435E-02	1.05	2 E02

TABLE 24. EFFECT OF SENSOR LOCATION FOR NOISE-FREE a_Z' MEASUREMENT ON FILTER DESIGN, UH-1H, 100 KT

Q MATRIX DIAGONAL, FILTER 1

4.24	1 PUG
2.92	2 PWG
1.00	3 PHC
10.0	4 P U
0.100E-01	5 P W
0.100E-03	6 P Q
0.100E-05	7 PTH
0.100E-03	8 PDB
0.100E-03	9 PDC
0.100E-03	10 PHE
0.100E-03	11 PX3
0.100E-03	12 PSE

CLOSED LOOP EIGENVALUES, FILTER 1

0.587	1
100.	E13
[illegible]	2
100.	E01

RMS STATE EST ERROR, FILTER 1

2.00	1 X01
0.106	2 X02
0.747E-08	3 X03
2.00	4 X04
0.106	5 X07
0.731E-13	6 X08
0.000	7 X09
0.000	8 X10
0.483E-13	9 X11
0.000	10 X12
0.104E-01	11 X13
0.000	12 X14

K12 GAIN MATRIX, FILTER

1 HD	2 Q	3 TH	4 DB	5 DC	6 HDI	7 HDE	8 ASI	9 ASE	10 AZP	
-0.444E-01	-0.106	7.50	0.000	0.392E-03	-0.587E-07	-0.261E-08	0.492E-06	0.215E-02	0.284E-04	1 E13
1.40	-3.84	-236.	0.000	-0.642	-0.150E-03	0.841E-07	0.125E-02	-0.103	-0.456E-01	2 E01

Data in Table 25 show the effect of using a noisy measurement of normal acceleration. The differences by comparison with Table 23 are that the filter order is increased from second to third order, and the coefficients of DB and DC in the K_{12} filter gain matrix are again zero. Consequently, the controller eigenvalues are stable and are the same as the closed-loop filter eigenvalues. Notice that for the first time the K_{11} filter gain matrix has a number of columns greater than zero. The rms state estimation error is not much affected by the normal acceleration measurement noise.

Table 26 explores the effect of adding noise-free measurement of longitudinal-acceleration-independent-of-pitch, AXP, to the baseline measurement set. It is interesting to explore using this additional quantity because of its traditional use in flight control technology to provide smoothed, broadband airspeed feedback signals via complementary filtering. The principal effects are to again reduce the filter order from third to second order, and to produce non-zero coefficients of DB and DC in the K_{12} filter gain matrix. Somewhat to our surprise, there is a small reduction in rms estimation error for normal gust velocity and almost no reduction for all other states.

In Table 27 we explore the effects of adding noise-free measurements of both normal acceleration and longitudinal-acceleration-independent-of-pitch to the baseline measurement set. The principal effect is that the filter is first order. Coefficients of DB and DC in the K_{12} filter gain matrix are non-zero. The rms state estimation error is not changed significantly with respect to values obtained when either acceleration measurement was used separately (refer to Tables 23 and 26).

7. Re-Emphasis of Key Points in Filter-Observer Synthesis

To conclude the design synthesis of the filter-observer, we emphasize again the three ways the filter-observer affects the final controller design:

TABLE 25. EFFECT OF a_z' MEASUREMENT NOISE ON FILTER DESIGN, UH-1H, 100 KT

Q MATRIX DIAGONAL, FILTER 1

4.24	1 PUG
2.92	2 PWG
1.00	3 PHC
10.0	4 P U
0.100E-01	5 P W
0.100E-03	6 P Q
0.100E-05	7 PTH
0.100E-03	8 PDB
0.100E-03	9 PDC
0.100E-03	10 PHE
0.100E-03	11 PXB
0.100E-03	12 PSE

R MATRIX DIAGONAL, FILTER 1

0.100E-03	1 AZP
0.000	2 HD
0.000	3 Q
0.000	4 TH
0.000	5 DB
0.000	6 DC
0.000	7 HDI
0.000	8 HDE
0.000	9 ASI
0.000	10 ASE

CLOSED LOOP EIGENVALUES, FILTER 1

120.	1
180.	E13
0.422	2
180.	E01
0.103	3
180.	E02

RMS STATE EST ERROR, FILTER 1

2.01	1 X01
0.177	2 X02
0.000	3 X03
2.01	4 X05
0.105	5 X07
0.000	6 X09
0.169E-12	7 X09
0.000	8 X10
0.000	9 X11
0.000	10 X12
0.115E-01	11 X13
0.000	12 X14

K11 GAIN MATRIX, FILTER 1

AZP	
0.666E-01	1 E13
-6.04	2 E01
124.	3 E02

K12 GAIN MATRIX, FILTER

1 HD	2 Q	3 TH	4 DB	5 DC	6 HDI	7 HDE	8 ASI	9 ASE	
0.166E-01	-0.288	-2.80	0.000	0.000	-0.135E-07	0.340E-09	0.485E-06	-0.798E-03	1 E13
1.20	1.41	-202.	0.000	0.000	0.150E-03	0.341E-07	-0.499E-02	-0.104	2 E01
-0.987	2.89	167.	0.000	0.000	0.834E-05	-0.239E-07	-0.278E-03	0.421E-01	3 E02

TABLE 26. EFFECT OF NOISE-FREE ($a_x - g \sin \Theta$) MEASUREMENT ON FILTER DESIGN, UH-1H, 100 KT

Q MATRIX DIAGONAL, FILTER 1

4.24	1 PUG
2.92	2 PWG
1.00	3 PHG
10.0	4 P U
0.100E-01	5 P W
0.100E-03	6 P Q
0.100E-05	7 PTH
0.100E-03	8 PDB
0.100E-03	9 PDC
0.100E-03	10 PHE
0.100E-03	11 PXB
0.100E-03	12 PSE

CLOSED LOOP EIGENVALUES, FILTER 1

1.03	1
180.	E01
0.110	2
180.	E02

RMS STATE EST ERROR, FILTER 1

2.02	1 X01
0.121	2 X02
0.724E-08	3 X03
2.02	4 X06
0.107	5 X07
0.105E-09	6 X08
0.225E-09	7 X09
0.331E-11	8 X10
0.112E-10	9 X11
0.000	10 X12
0.853E-02	11 X13
0.000	12 X14

K12 GAIN MATRIX, FILTER

1 HD	2 Q	3 TH	4 DB	5 DC	6 HDI	7 HDE	8 ASI	9 ASE	10 AXP	
0.857	-2.79	-126.	-0.317	-0.648	-0.415E-03	-0.250E-07	-0.750E-02	-0.521E-01	0.569	1 E01
-1.32	17.5	-107.	5.71	11.7	-0.249E-04	-0.765E-07	-0.410E-03	-0.397	-10.3	2 E02

TABLE 27. EFFECT OF NOISE-FREE ($a_x - g \sin \Theta$) AND a_z' MEASUREMENTS ON FILTER DESIGN, UH-1H, 100 KT

Q MATRIX DIAGONAL, FILTER 1

4.24	1 PUG
2.92	2 PNG
1.00	3 PHC
10.0	4 P U
0.100E-01	5 P W
0.100E-03	6 P Q
0.100E-05	7 PTH
0.100E-03	8 PDB
0.100E-03	9 PDC
0.100E-03	10 PHE
0.100E-03	11 PXB
0.100E-03	12 PSE

CLOSED LOOP EIGENVALUES, FILTER 1

0.997E-01	1
100.	EG1

RMS STATE EST ERROR, FILTER 1

1.97	1 XG1
0.104	2 XG2
0.734E-08	3 XG3
1.97	4 XG6
0.104	5 XG7
0.242E-08	6 XG8
0.130E-09	7 XG9
0.236E-13	8 X10
0.236E-12	9 X11
0.000	10 X12
0.698E-08	11 X13
0.000	12 X14

K12 GAIN MATRIX, FILTER 1

1 HD	2 Q	3 TH	4 DB	5 DC	6 HDI	7 HDE	8 ASI	9 ASE	10 AZP	11 AXP	
2.10	-0.503	-344.	0.183E-03	-0.706	-0.288E-03	0.163E-05	0.124E-02	-0.134	-0.272E-01	0.309	1 EG1

- The filter-observer synthesis process provides a means for choosing the best sensor complex from among many candidates. As a result, the quality of the complex is also quantified.

- The filter-observer provides the best estimates of the total state vector, given the desired measurements, to use as the regulator input.

- The filter-observer provides the only direct means for the noise and disturbances to affect closed-loop system behavior. If the matrix $[G_1 - K_{12}G_2]$ is null, then the controller and closed-loop filter poles are identical. The controller poles are then also guaranteed to be stable.

The above considerations lead to the recommendation that filter-observer synthesis precede regulator synthesis. Because these are completely separable design processes, the filter-observer design can be set aside once satisfactory performance is achieved, and work then proceeds with the regulator. This is the topic of the next subsection.

C. REGULATOR SYNTHESIS

The steps involved in synthesis of the regulator portion of the controller are summarized in Table 28. Although ten steps are listed, Steps 3 through 8 are repeated until all bandwidth design goals have been addressed in any given application. These ten steps are elaborated in the following paragraphs where required, and are illustrated by examples.

1. Cost Function Control Weightings

One element of the cost function diagonal control weighting matrix, R_R, should be set initially to unity. This is permissible since one coefficient in the cost function may be an arbitrary positive number. The remainder of the diagonal elements are chosen in ratios to the first, such that limitations of the physical controls, or upon their use, are taken into account. These limitations may be the result of rate, authority, or power limits or possibly the result of flying qualities constraints, e.g., avoid "throttle thrash." Specifically, the remainder

TABLE 28. REGULATOR SYNTHESIS

1. Set R_R to accommodate limitations upon controls or their use.

2. Order key variable bandwidth requirements in decreasing order.

3. Identify highest bandwidth requirement not yet addressed, ω_c.

4. Compute transfer functions

   Output: Variable subject to ω_c requirement

   Inputs: Variables satisfying prior ω_c requirements which may serve as surrogate controls

   All loops satisfying prior ω_c requirements must be closed

5. Approximate above transfer functions at $s = j\omega_c$ by K/s^{n+1}.

6. Calculate $(2^n\omega_c^2)^{n+1}\, r/K^2$ for each approximation (r is cost function weighting on input variable).

7. Set smallest $(2^n\omega_c^2)^{n+1}\, r/K^2$ value equal to cost function weighting, q_R, for variable subject to ω_c requirement.

8. Compute regulator solution with additional cost function weighting, q_R.

9. Repeat from Step 3 until all bandwidth requirements are addressed.

10. Change R_R to affect relative use of the available control points; maintain ratios of Q_R and R_R elements supporting related control objectives.

of the diagonal elements is the ratio of the square of the limit on the element having the unity coefficient to the square of the limit on the control variable being weighted.

A particularly desirable alternative is to use the R_R values resulting from a previously completed solution at a nearby flight condition. The R_R values used at this stage of design are ultimately modified in the last step.

2. Order Key Variable Bandwidth Requirements

Designation of key variables and their associated control bandwidth requirements define the primary design goals for regulator synthesis as explained in Section II. The ordering of these key variables and their control bandwidth requirements according to decreasing bandwidth provides a rational basis for systematic synthesis. This approach results in satisfaction of the more stringent, high gain, inner loop, high bandwidth requirements first; the next most stringent, and so on. Proceeding in this manner assures that the more stringent of either all prior bandwidth requirements or the minimum system augmentation necessary to support the immediate bandwidth requirement is met at each stage of design. It is also interesting to note the similarity of this procedure to the one described on page 664 of Ref. 10 for synthesis via frequency response methods.

3. Computation of Transfer Functions

Each bandwidth requirement is addressed in turn, starting with the highest. Consider the highest bandwidth requirement not yet addressed. (We shall designate this bandwidth by ω_c since it is approximately equal to crossover frequency, as demonstrated in Section II.) Transfer functions are computed for the variable which is subject to the bandwidth requirement. The input variables for these transfer functions are selected by the designer from among the controls and all variables satisfying prior bandwidth requirements. (The latter variables may be thought of as surrogate controls.) If the designer is unfamiliar with

the conventional bases for selection (e.g., airspeed is controlled with pitch attitude in cruising flight), all of the above named variables may be included. Later steps will result in an optimal selection. All loops satisfying prior bandwidth requirements must be closed when computing these transfer functions.

4. Approximation of Transfer Functions

Approximations to the computed transfer functions are required for the frequency region near ω_c. The form of the approximations required is K/s^{n+1}. There are two viable ways for obtaining these approximations. The first, and easiest, method is to simply approximate the transfer function by its magnitude asymptote at $s = j\omega_c$. The appropriate phase approximation is carried in the sign of the gain for the approximation and the value of n + 1. The second method involves finding the tangent to the Bode plot at $s = j\omega_c$. The phase approximation is again carried in the sign of the gain for the approximation and the value of n + 1. Either method results in a pair of values for K and n for each transfer function. The values are somewhat dependent upon the approximation method used, but the effects of this dependency are minimized by the manner in which K and n are ultimately used. It is our recommendation that one approximation method be used throughout the regulator synthesis, however.

5. Obtaining the Cost Function Coefficient

The cost function coefficient, q_R, for the variable subject to the current bandwidth requirement is determined next. (q_R denotes an element of the diagonal matrix, Q_R.) The quantity

$$(2^n \omega_c^2)^{n+1} r/K^2$$

is calculated using the K and n values for each transfer function approximation. r in the above quantity represents the cost function weighting coefficient for the control or surrogate control variable corresponding

to the particular transfer function. This may be an element of the diagonal R_R matrix or an element of Q_R determined in a previous step.

q_R for the current bandwidth requirement is set equal to the smallest calculated value for the above quantity.

This step contains the key to understanding of this approach to regulator synthesis. The quantity being calculated is an evaluation of the effectiveness of each control or surrogate control variable for achieving the specified bandwidth. Large values for q_R indicate low effectiveness and vice versa. The lowest value for q_R is picked so as to insure that the most effective control (or surrogate control) variable is used to achieve the specified bandwidth.

6. Continuing the Regulator Synthesis

The next step is computation of the regulator solution using the additional cost function weighting coefficient, q_R. At this point the designer is ready to address the next bandwidth requirement and so returns once again to the step for computation of the appropriate transfer functions. The sequence of steps from that point repeats (at least in principle) until all bandwidth requirements have been addressed.

As experience is gained with the controlled element and the series of regulator design steps, the designer may find that several, or all, bandwidth requirements can be addressed simultaneously. The reasons for this are that uncoupled or weakly coupled or serial subsystems within the controlled element often present situations wherein the effects of loop closures satisfying prior bandwidth requirements upon the various transfer functions are known or easily estimated without recalculating transfer functions. This is especially the case when the effect of one (or more) prior loop closures is nil, or if one (or more) prior loop closures is at very high gain. In the latter case, ratios of transfer function numerators of higher kinds give close approximations to the actual closed-loop transfer functions (refer to Ref. 10, pp. 163-177, and Ref. 11, pp. 63-70).

Techniques using numerators of higher kinds (that is to say, multivariable system transmission zeros) are the core of a regulator synthesis technique recently advanced by Harvey and Stein (Ref. 4). Their technique is based upon a single parameter relaxation from a singular regulator problem solution. The particular singular regulator solution selected for the relaxation starting point is derived from the modal properties desired for the finite modulus poles of the singular system.

7. Adjustment of the Diagonal R_R Matrix

After all bandwidth requirements have been addressed, it may turn out that the relative use of control points is inappropriate. For example, the main rotor collective pitch control may be more active in terms of zero crossings per second than the longitudinal cyclic pitch control in level cruising flight. (Main rotor collective should be a trim control in this situation.) Inappropriate control use (required authority, required rate or activity too high) is rectified by increasing the cost function weighting coefficients in R_R for those controls. In order that bandwidth requirements continue to be satisfied, it is necessary to increase by the same factor all those elements in Q_R which have a ratio relationship to each element of R_R being increased. (This ratio relationship arises from successive applications of $q_R = \min [(2^n\omega_c^2)^{n+1} r/K]$.) Adjustments made in this manner assure simultaneous satisfaction of bandwidth and control use requirements.

8. Regulator Synthesis Examples

This subsection illustrates application of the ten regulator design steps in Table 28. Application is to longitudinal dynamics of the UH-1H for the hover flight condition. Regulator design function and bandwidth requirements are listed in Table 29.

Step 1. The control weighting cost function coefficient arbitrarily selected to be unity is that weighting longitudinal cyclic pitch rate, DBD.

$$R_R(1) = 1.0$$

TABLE 29

UH-1H LONGITUDINAL FLIGHT SYSTEM FUNCTION AND BANDWIDTH REQUIREMENTS

Flight Condition:	
Hover	
Functions:	
Rate-of-climb command	
Groundspeed hold	
Bandwidths:	(Rad/Sec)
Cyclic (DB)	25.7
Collective (DC)	25.7
Pitch (TH)	2.0
Rate-of-climb error (HDE)	1.0
Integral of HDE (HDI)	0.82
Groundspeed error (XD)	0.5
Integral of XD (XDI)	0.1

Our expressed desire is to have maximum collective pitch rate, DCD, be significantly less than maximum longitudinal cyclic pitch rate to satisfy flying qualities requirements. A ratio of $\sqrt{10}$ to 1 is selected on the basis of flying qualities engineering judgment. Consequently, the cost function coefficient weighting collective pitch rate is:

$$R_R(2) = \left(\frac{\sqrt{10}}{1}\right)^2 = 10.$$

Step 2. The key variable bandwidth requirements are already in order of decreasing bandwidth in Table 29.

Step 3. Refer to Table 29. The highest bandwidth requirement not yet addressed is for the longitudinal cyclic pitch actuator output, DB. (The bandwidth requirement for the collective pitch actuator output, DC, is equal to that for DB. When this occurs it is immaterial which requirement is addressed first. Indeed, since the UH-1H has no unstable roots, and the two actuators are completely independent, both requirements can be addressed simultaneously.)

Step 4. Compute transfer functions. The output variable subject to the bandwidth requirement of 25.7 rad/sec is DB. The input variables which may serve as controls are DBD and DCD. (There is no possibility for surrogate controls because no prior bandwidth requirements have been satisfied. Consequently, there are no prior loop closures to incorporate.) The candidate transfer functions are:

$$\frac{DB}{DBD} = \frac{1}{s} \qquad \frac{DB}{DCD} = 0$$

That this is so is readily determined from inspection of the plant equations (Table 10). Similar considerations lead to transfer functions for collective pitch, DC.

$$\frac{DC}{DCD} = \frac{1}{s} \qquad \frac{DC}{DCD} = 0 \qquad \frac{DC}{DB} = 0$$

The third transfer function for collective pitch arises from the possbility that DC, which "satisfies a prior bandwidth requirement," may be considered a surrogate control for DB. The uncoupled nature of the two actuators and stability of the open-loop plant result in DB having no effect upon DC even when the loops satisfying the bandwidth requirement for DB are closed.

Step 5. Approximate the transfer functions. No approximation is required in this case since the transfer functions are already in the form K/s^{n+1}. The values for K and n are:

Transfer Function	K	n
$\delta_B/\dot{\delta}_B$ (DB/DBD)	1.0	0
$\delta_C/\dot{\delta}_C$ (DC/DCD)	1.0	0

The zero valued transfer functions need not be considered.

Step 6. Calculation of $(2^n \omega_c^2)^{n+1} r/K^2$. For the DB requirement the value is:

$$[2^0 (25.7)^2]^1 R_R(1)/(1.0)^2 = 662.$$

For the DC requirement the value is:

$$[2^0 (25.7)^2]^1 R_R(2)/(1.0)^2 = 6620.$$

Step 7. Selection of the cost function coefficient. There is only one finite value of $(2^n \omega_c^2)^{n+1} r/K^2$ for the DB bandwidth requirement. It is therefore the smallest value and is set equal to the corresponding cost function weighting for DB, $Q_R(4)$.

$$Q_R(4) = 662.$$

The situation for the DC bandwidth requirement is similar. The cost function weighting for DC is $Q_R(5)$.

$$Q_R(5) = 6620.$$

Step 8. Compute the regulator solution with the additional cost weighting. The computed regulator gain matrix, K_R, for $Q_R(4) = 662.$ and $Q_R(5) = 6620.$ is a 2×12 matrix of zeros except for two elements:

$$K_R(1,4) = 25.7 \text{ rad/sec}$$

$$K_R(2,5) = 25.7 \text{ rad/sec}$$

Step 9. Repeat the design process until all bandwidth requirements are addressed. All requirements are not addressed; therefore return to Step 3.

Step 3. Refer to Table 29. The highest bandwidth requirement not yet addressed is for pitch attitude, $\omega_{c_{TH}} = 2.0$ rad/sec.

Step 4. Compute transfer functions. The output variable subject to the bandwidth requirement is pitch attitude, TH. The candidate controls and surrogate controls are DBD, DCD, DB and DC. We will restrict our attention to the surrogate controls DB and DC for the purpose of illustration. These transfer functions may be obtained from the appropriate ratios of numerators for the open-loop controlled element transfer functions in Table 30. (A flight controls engineer would ordinarily reject collective pitch, DC, as a candidate for controlling pitch attitude. We shall continue to include it here in order to show that the design process automatically rejects use of collective pitch for pitch attitude control.) These transfer functions and the corresponding Bode plots are given in Figs. 14a and 14b. (The two actuator loops satisfying the prior bandwidth requirements are closed, but this does not happen to affect the transfer functions in this particular case.)

Step 5. Approximate the transfer functions. Two methods for approximating transfer functions are illustrated in Fig. 16a for the TH/DB transfer function. The solid amplitude ratio curve in Fig. 16a is $|G(j\omega)|_{dB}$ and the dashed curve is composed of the asymptotes for $|G(j\omega)|_{dB}$. In the vicinity of the pitch attitude bandwidth requirement, $\omega_{c_{TH}} = 2.0$ rad/sec, the asymptote is given by $-0.169/s^2$. (This can also be computed readily from the factored transfer function itself. It is accomplished by making low-frequency approximations to the factors with root modulus greater than 2.0 rad/sec, and high-frequency approximations to the factors with root modulus less than 2.0 rad/sec. Multiplying out the result gives an answer directly in the form K/s^{n+1}).

Approximation of the actual amplitude ratio curve requires the Bode plot of Fig. 16a to expedite approximation. A tangent to the curve is drawn at $\omega = \omega_{c_{TH}} = 2.0$ rad/sec. $|K|_{dB}$ is determined by the intersection

TABLE 30. OPEN-LOOP CONTROLLED ELEMENT TRANSFER FUNCTIONS

CASE: UH1H HOVER 122LONG 31-JAN-79 CONTROLLED ELEMENT TF'S

DENOMINATOR:

```
 1.0000
( .00000    ) ( .00000    ) ( .00000    ) ( .00000    )
( .38494    )
(( .10339    , .18934    , .19576E-01, .18833    ))
(( .26279    , .92717    , .24365    , .89459    ))
< .11863E-01>
```

NUMERATOR: TH/DBD

```
-.16910
( .00000    ) ( .00000    ) ( .00000    ) (-.79065E-02)
( .33300    ) ( .39184    )
< .17445E-03>
```

NUMERATOR: TH/DCD

```
-.33000E-02
( .00000    ) ( .00000    ) ( .00000    ) ( .10854E-01)
( .33300    ) (-11.270    )
< .13442E-03>
```

NUMERATOR: HDE/DBD

```
 .24729
( .00000    ) ( .00000    ) ( .00000    ) ( .33300    )
(-1.4789    )
(( .35965    , 1.3542    , .48705    , 1.2636    ))
<-.22334    >
```

NUMERATOR: HDE/DCD

```
-9.7980
( .00000    ) ( .00000    ) ( .00000    )
(( .18545    , .14356    , .26623E-01, .14107    ))
(( .25760    , .93210    , .24011    , .90064    ))
<-.17544    >
```

NUMERATOR: HDI/DCD

```
-9.7980
( .00000    ) ( .00000    )
(( .18545    , .14356    , .26623E-01, .14107    ))
(( .25760    , .93210    , .24011    , .90064    ))
<-.17544    >
```

NUMERATOR: XD/DBD

```
 1.0606
( .00000    ) ( .00000    ) ( .00000    ) ( .33300    )
( .38296    )
(( .19712E-01, 2.2663    , .44674E-01, 2.2659    ))
< .69473    >
```

NUMERATOR: XDI/DBD

```
 1.0606
( .00000    ) ( .00000    ) ( .33300    ) ( .38296    )
(( .19712E-01, 2.2663    , .44674E-01, 2.2659    ))
< .69473    >
```

K/s^{n+1} APPROXIMATION	$(2^n \omega_{c_{TH}}^{\zeta})^{n+1} Q_{DB}/(K_{DB}^{TH})^2$
Asymptotic $K = -0.169$, $n = 1.0$	1,484,183
$G(j\omega)$ $K = -0.316$, $n = 1.5$	2,851,632

$$\frac{\theta}{\delta_B} = \frac{-.1691(s-.0079)(s+.333)(s+.39184)}{(s+.38494)[s^2+2(.16339)(.18934)s+(.18934)^2]} \times [s^2+2(.26279)(.92717)s+(.92717)^2]$$

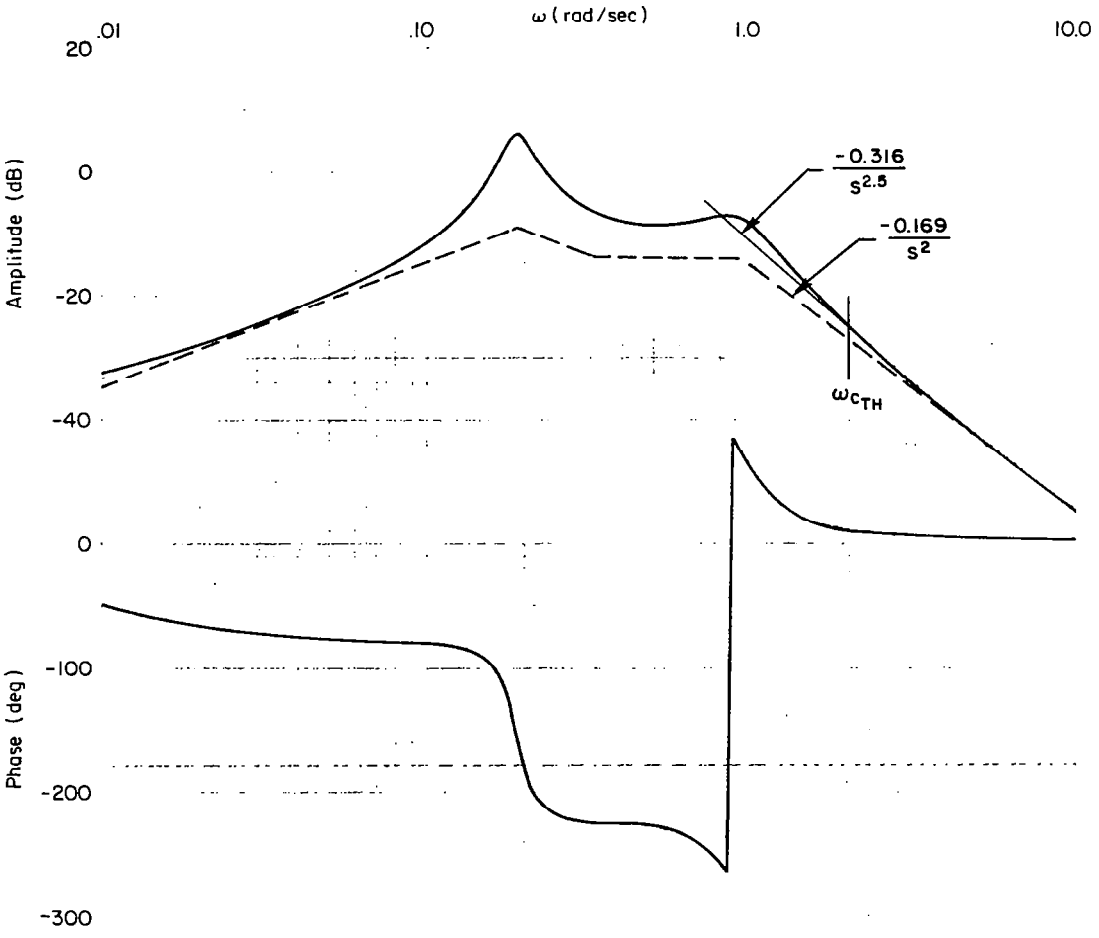

Figure 16a. Transfer Functions for Selecting $Q_R(3)$ Value for Pitch Attitude Control Bandwidth Requirement

K/s^{n+1} APPROXIMATION	$(2^n \omega_{c_{TH}}^2)^{n+1} Q_{DC}/(K_{DC}^{TH})^2$
Asymptotic K = 0.0372, n = 2.0	19,604,468,000

$$\frac{\theta}{\delta_e} = \frac{-.0033(s + .010854)(s + .333)(s + 11.27)}{(s + .38494)[s^2 + 2(.16339)(.18934)s + (.18934)^2]} \times [s + 2(.26279)(.92717)s + (.92717)^2]$$

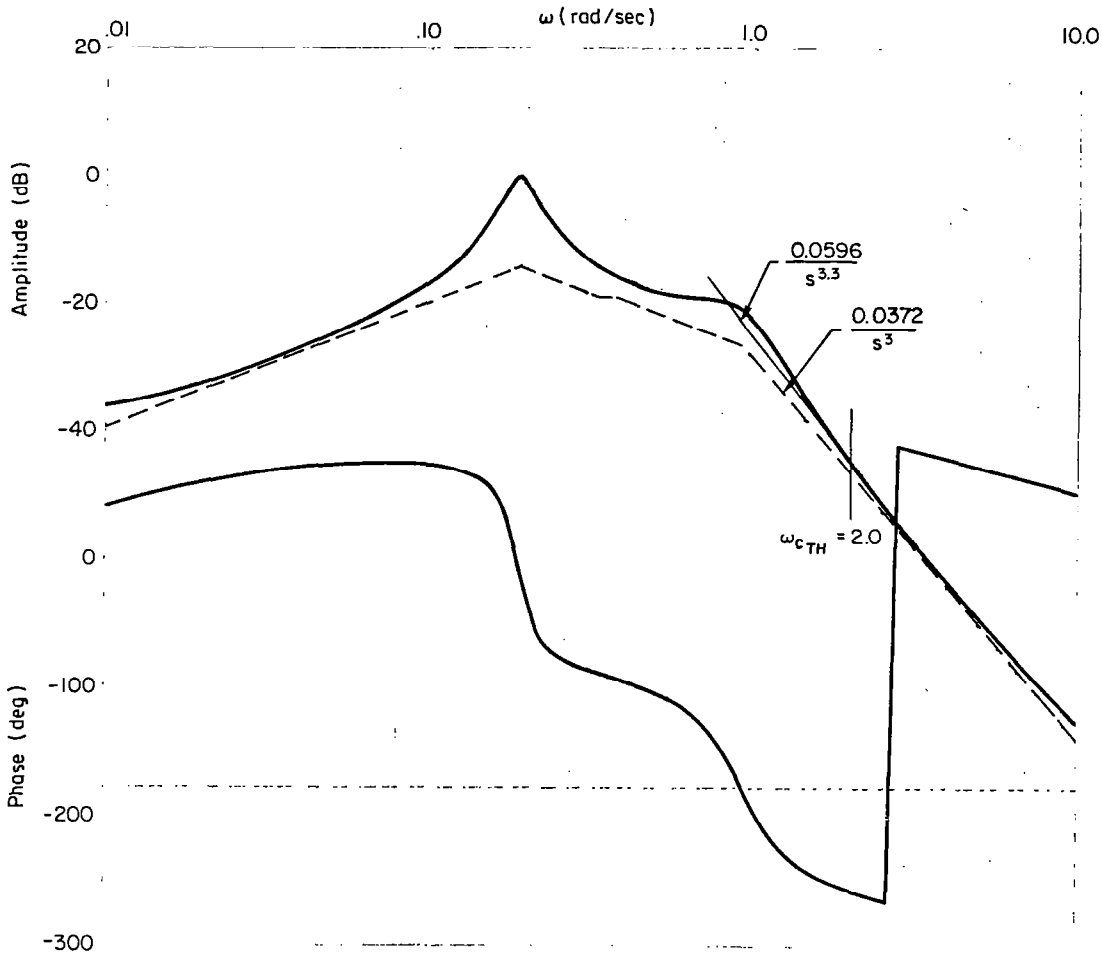

Figure 16b. Transfer Functions for Selecting $Q_R(3)$ Value for Pitch Attitude Control Bandwidth Requirement

of the tangent with $\omega = 1.0$ rad/sec, and $-(n+1)$ is the slope of the tangent in 20's of dB's per decade.

Either method of approximation may be used, but one method should be used exclusively throughout. We shall continue using the asymptotic approximation which, for the TH/DC transfer function, is $0.0372/s^3$ as shown in Fig. 16b. The asymptotic approximations are summarized below.

Transfer Function	K	n
θ/δ_B (TH/DB)	−0.169	1
θ/δ_c (TH/DC)	0.0372	2

Step 6. Calculation of $(2^n \omega_c^2)^{n+1} r/K^2$.

For the DB control:

$$(2^n \omega_{c_{TH}}^2)^{n+1} Q_R(4)/(K_{DB}^{TH})^2 = [2^1 (2.)^2]^2 662./(-0.169)^2$$

$$= 1,484,183.$$

For the DC control:

$$(2^n \omega_{c_{TH}}^2)^{n+1} Q_R(5)/(K_{DC}^{TH})^2 = [2^2 (2.)^2]^3 6620./(0.0372)^2$$

$$= 19,604,468,000.$$

Step 7. Selection of the cost function coefficient. The smallest value of $(2^n \omega_c^2)^{n+1} r/K^2$ is set equal to the cost function weighting for pitch attitude, $Q_R(3)$.

$$Q_R(3) = 1,484,183.$$

From here, all steps are very similar up to the point where all bandwidth requirements have been addressed. The regulator solution that

results is for the "completed" design. Table 31 summarizes this regulator solution. The cost function weightings, closed-loop eigenvalues and regulator gain matrix are given in this table.

We are now in a position to consider how R_R might be modified in Step 10. This requires knowledge of the relationships among the control and output variables that were operative in determining the cost function coefficients. These relationships are summarized in Table 32. This table has the following interpretation. Consider either of the last two columns, DBD or DCD. The bottom-most Q_R entry indicates the outer-loop variable which is the ultimate object of control. (The variable name is read in the left-most column.) The Q_R entry immediately above indicates the control (or surrogate control) variable for the column entry below. This interpretation applies on up the column to each Q_R or R_R entry in turn. It also applies (individually) for each column. Thus, $\int \dot{x}\, dt$ has as a surrogate control $\dot{x}$ which, in turn, has the surrogate control θ. Similarly, $\int \dot{h}_e\, dt$ is preceded in the control chain by $\dot{h}_e$, which is controlled by δ_c, which is effected finally by $\dot{\delta}_c$, the "actual" control.

The "Control Variable Association" differentiation directly reflects the origin of the smaller Q_R cost weighting at each bandwidth step. Thus, $Q_R(3)$, which is the weighting for pitch attitude, θ, derived from the 1.48×10^6 found for DB as opposed to the 1.96×10^{10} for DC.

If every entry in any one column is multiplied by a common factor, the design bandwidths will tend to be unchanged. (Exceptions will occur only if the multiplying factor is such that one or more Q_R's would change columns if the formal procedures of Steps 3 through 9 were followed.)

Because the longitudinal speed and pitch degrees of freedom are nearly uncoupled from the vertical speed degree of freedom, it is not terribly interesting to illustrate the impact of multiplying every entry in one column by a constant factor for a hover flight condition and vice versa (but to a lesser extent). On the other hand, the 100 kt cruise condition is interesting because longitudinal speed, pitch and vertical speed couplings are strong. The relationships among control and output variables and cost function coefficients for this 100 kt flight condition are summarized in Table 33. The cost function coefficients related

Q MATRIX DIAGONAL, REGULATOR
1

0.000	1 HD
0.000	2 Q
0.148E+07	3 TH
662.	4 DB
0.662E+04	5 DC
69.0	6 HDE
46.6	7 HDI
357.	8 XD
3.57	9 XDI
0.000	10 AOA
0.000	11 ASE

R MATRIX DIAGONAL, REGULATOR
1

1.00	1 DBD
10.0	2 DCD

CLOSED LOOP EIGENVALUES, REGULATOR
1

25.7 180.	1 X01
25.7 180.	2 X02
2.77 -132.	3 X03
2.77 132.	4 X06
0.907 -157.	5 X07
0.907 157.	6 X08
0.505 180.	7 X09
0.102 180.	8 X10
0.336 180.	9 X11
0.117E-02 180.	10 X12
0.269E-02 180.	11 X13
0.100 180.	12 X14

TABLE 31

REGULATOR SYNTHESIS SUMMARY,
UH-1H, HOVER

REGULATOR GAIN MATRIX

1 X01	2 X02	3 X03	4 X06	5 X07	6 X08	7 X09	8 X10	9 X11	10 X12	11 X13	12 X14	
0.254	0.523	0.717	22.8	1.98	-537.	-0.152E+04	29.9	-0.518E-01	0.252	28.9	1.89	1 DBD
-0.264	-1.07	-4.16	0.819	-3.37	-0.846	-0.936	-0.517E-02	27.0	-2.16	-0.122	0.221E-01	2 DCD

TABLE 32

RELATIONSHIPS AMONG CONTROL AND OUTPUT VARIABLES
AND COST FUNCTION COEFFICIENTS — HOVER

Output Variable	Bandwidth Requirement (rad/sec)	Control Variable Association	
		DBD	DCD
		$R_R(1) = 1.00$	$R_R(2) = 10.0$
δ_B (DB)	25.7	$Q_R(4) = 662.$	
δ_c (DC)	25.7		$Q_R(5) = 6620.$
θ (TH)	2.0	$Q_R(3) = 1.48 \times 10^6$	
$\dot{h}_e$ (HDE)	1.0		$Q_R(6) = 69.0$
$\int \dot{h}_e \, dt$ (HDI)	0.82		$Q_R(7) = 46.6$
$\dot{x}$ (XD)	0.50	$Q_R(8) = 357.$	
$\int \dot{x} \, dt$ (XDI)	0.10	$Q_R(9) = 3.57$	

TABLE 33

RELATIONSHIPS AMONG CONTROL AND OUTPUT VARIABLES
AND COST FUNCTION COEFFICIENTS — 100 KT

Output Variable	Bandwidth Requirement (rad/sec)	Control Variable Association	
		DBD	DCD
		$R_R(1) = 1.00$	$R_R(2) = 1.00f$
δ_B (DB)	25.7	$Q_R(4) = 662.$	
δ_c (DC)	25.7		$Q_R(5) = 662.\, f$
θ (TH)	1.5	$Q_R(3) = 3.55 \times 10^5$	
$\dot{h}_e$ (HDE)	0.70		$Q_R(8) = 5.95\, f$
$\int \dot{h}_e \, dt$	0.32		$Q_R(6) = 4.77\, f$

f = 1.00, 10.0, 100.

to height control (the right-most column of Table 33) are multiplied by f = 1.00, 10.0 and 100.

Summaries of the resulting regulator designs are given for Tables 34, 35, and 36 for f = 1.00, 10.0 and 100., respectively. These summaries include the cost function coefficients, closed-loop regulator eigenvalues, regulator gain matrix, and rms responses for states, outputs and controls. The gains based on control deflections for the three values of f are summarized as:

$$\begin{bmatrix} \frac{s}{27.7}+1 \\ \frac{s}{28.6}+1 \\ \frac{s}{31.1}+1 \end{bmatrix} \delta_B = \begin{bmatrix} -.012 \\ .005 \\ .022 \end{bmatrix} u_g + \begin{bmatrix} -.013 \\ -.108 \\ -.209 \end{bmatrix} w_g + \begin{bmatrix} -.069 \\ -.315 \\ -.923 \end{bmatrix} \dot{h}_c + \begin{bmatrix} .008 \\ .009 \\ .026 \end{bmatrix} u + \begin{bmatrix} -.053 \\ -.206 \\ -.727 \end{bmatrix} w + \begin{bmatrix} 9.63 \\ 9.86 \\ 7.49 \end{bmatrix} q \tag{47}$$

$$+ \begin{bmatrix} 28.3 \\ 62.6 \\ 161.4 \end{bmatrix} \theta + \begin{bmatrix} .018 \\ .093 \\ .334 \end{bmatrix} \delta_c + \begin{bmatrix} -.031 \\ -.181 \\ -.666 \end{bmatrix} \int \dot{h}_e \, dt + \begin{bmatrix} -.718 \\ -.867 \\ -.965 \end{bmatrix} \int u_{ASe} \, dt \quad \begin{matrix} , & f = 1. \\ , & f = 10. \\ , & f = 100. \end{matrix}$$

$$\begin{bmatrix} \frac{s}{26.8}+1 \\ \frac{s}{26.5}+1 \\ \frac{s}{26.1}+1 \end{bmatrix} \delta_c = \begin{bmatrix} -.008 \\ -.004 \\ -.001 \end{bmatrix} u_g + \begin{bmatrix} .053 \\ .026 \\ .006 \end{bmatrix} w_g + \begin{bmatrix} .132 \\ .082 \\ .034 \end{bmatrix} \dot{h}_c + \begin{bmatrix} -.001 \\ -.001 \\ -.001 \end{bmatrix} u + \begin{bmatrix} .079 \\ .057 \\ .028 \end{bmatrix} w + \begin{bmatrix} -.664 \\ .01 \\ .139 \end{bmatrix} q \tag{48}$$

$$+ \begin{bmatrix} -17.9 \\ -12.2 \\ -5.44 \end{bmatrix} \theta + \begin{bmatrix} .019 \\ .01 \\ .004 \end{bmatrix} \delta_B + \begin{bmatrix} .075 \\ .054 \\ .026 \end{bmatrix} \int \dot{h}_e \, dt + \begin{bmatrix} .163 \\ .049 \\ .01 \end{bmatrix} \int u_{ASe} \, dt \quad \begin{matrix} , & f = 1. \\ , & f = 10. \\ , & f = 100. \end{matrix}$$

TABLE 34. REGULATOR SYNTHESIS SUMMARY (f = 1.0)

Q MATRIX DIAGONAL, REGULATOR

1	
0.000	1 HD
0.000	2 Q
0.355E+06	3 TH
662.	4 DB
662.	5 DC
4.77	6 HDI
0.000	7 AZP
5.95	8 HDE
0.000	9 XD
0.000	10 AOA

R MATRIX DIAGONAL, REGULATOR

1	
1.00	1 DBD
1.00	2 DCD

CLOSED LOOP EIGENVALUES, REGULATOR

1	
25.7	1
180.	X01
25.7	2
180.	X02
2.20	3
-124.	X03
2.20	4
124.	X06
1.55	5
180.	X07
0.792	6
180.	X08
0.309	7
180.	X09
0.431E-01	8
180.	X10
0.116	9
180.	X11
0.269	10
180.	X12
0.100	11
180.	X13

RMS, TOTAL

1	
2.06	1 X01
1.71	2 X02
1.00	3 X03
1.39	4 X06
0.960	5 X07
0.238E-02	6 X08
0.373E-02	7 X09
0.491E-01	8 X10
0.122	9 X11
0.385	10 X12
0.116E-01	11 X13
1.19	12 E06
7.25	13 E01
1.78	14 E02

RMS, OUTPUT+CONTROLS

1	
1.01	1 HD
0.238E-02	2 Q
0.373E-02	3 TH
0.491E-01	4 DB
0.122	5 DC
0.385	6 HDI
0.519	7 AZP
0.263	8 HDE
1.40	9 XD
0.886E-02	10 AOA
0.129	11 DBD
0.331	12 DCD

REGULATOR GAIN MATRIX

1 X01	2 X02	3 X03	4 X06	5 X07	6 X08	7 X09	8 X10	9 X11	10 X12	11 X13	
0.325	0.359	1.92	-0.211	1.47	-267.	-784.	27.7	-0.501	0.853	19.9	1 DBD
0.218	-1.41	-3.55	0.296E-01	-2.11	17.8	479.	-0.501	26.8	-2.01	-4.36	2 DCD

TABLE 35. REGULATOR SYNTHESIS SUMMARY (f = 10.0)

Q MATRIX DIAGONAL, REGULATOR

1	
0.000	HD
0.000	Q
0.355E+06	TH
662.	DB
0.662E+04	DC
47.7	HDI
0.000	AZP
59.5	HDE
0.000	XD
0.000	AOA

CLOSED LOOP EIGENVALUES, REGULATOR

1	
25.7 180.	X01
25.7 180.	X02
2.52 180.	X03
2.21 -117.	X05
2.21 117.	X07
0.875 180.	X08
0.326 180.	X09
0.425E-01 180.	X10
0.116 180.	X11
0.269 180.	X12
0.100 180.	X13

RMS, TOTAL

1	
2.06	X01
1.71	X02
1.00	X03
3.10	X06
1.44	X07
0.756E-02	X08
0.899E-02	X09
0.101	X10
0.455E-01	X11
0.254	X12
0.306E-01	X13
3.06	E06
7.29	E01
1.81	E02

RMS, OUTPUT+CONTROLS

1	
1.02	HD
0.756E-02	Q
0.899E-02	TH
0.101	DB
0.455E-01	DC
0.254	HDI
0.575	AZP
0.253	HDE
3.11	XD
0.669E-02	AOA
0.757	DBD
0.181	DCD

R MATRIX DIAGONAL, REGULATOR

1	
1.00	DBD
10.0	DCD

REGULATOR GAIN MATRIX

1 X01	2 X02	3 X03	4 X06	5 X07	6 X08	7 X09	8 X10	9 X11	10 X12	11 X13	
-0.138	3.10	9.02	-0.246	5.90	-282.	-0.179E+04	28.6	-2.67	5.18	24.8	1 DBD
0.115	-0.696	-2.17	0.259E-01	-1.50	-0.265	324.	-0.267	26.5	-1.44	-1.31	2 DCD

TABLE 36. REGULATOR SYNTHESIS SUMMARY (f = 100.)

Q MATRIX DIAGONAL, REGULATOR

1	
0.000	1 HD
0.000	2 Q
0.355E+06	3 TH
662.	4 DB
0.662E+05	5 DC
477.	6 HDI
0.000	7 AZP
595.	8 HDE
0.000	9 XD
0.000	10 AOA

R MATRIX DIAGONAL, REGULATOR

1	
1.00	1 DBD
100.	2 DCD

CLOSED LOOP EIGENVALUES, REGULATOR

1	
25.2 180.	1 X01
25.7 180.	2 X02
5.71 180.	3 X03
2.46 -106.	4 X06
2.46 106.	5 X07
0.893 180.	6 X08
0.423E-01 180.	7 X09
0.332 180.	8 X10
0.116 180.	9 X11
0.269 180.	10 X12
0.100 100.	11 X13

RMS, TOTAL

1	
2.06	1 X01
1.71	2 X02
1.00	3 X03
3.83	4 X06
1.86	5 X07
0.141E-01	6 X08
0.119E-01	7 X09
0.208	8 X10
0.948E-02	9 X11
0.112	10 X12
0.436E-01	11 X13
3.82	12 E06
7.23	13 E01
1.94	14 E02

RMS, OUTPUT+CONTROLS

1	
1.01	1 HD
0.141E-01	2 Q
0.119E-01	3 TH
0.208	4 DB
0.948E-02	5 DC
0.112	6 HDI
0.875	7 AZP
0.175	8 HDE
3.84	9 XD
0.765E-02	10 AOA
2.01	11 DBD
0.599E-01	12 DCD

REGULATOR GAIN MATRIX

1 X01	2 X02	3 X03	4 X06	5 X07	6 X08	7 X09	8 X10	9 X11	10 X12	11 X13	
-0.688	6.49	28.7	-0.823	22.6	-233.	-0.502E+04	31.1	-10.4	20.7	30.0	1 DBD
0.267E-01	-0.165	-0.877	0.243E-01	-0.729	-3.64	142.	-0.104	25.1	-0.684	-0.261	2 DCD

Recall that the equation relating the controls to the states for the regulator is $u = -Cx$. In Eqs. 47 and 48 we have moved the state variables δ_B and δ_C to the left-hand side of the equations for $\dot{\delta}_B$ and $\dot{\delta}_C$, respectively. This is because the state variables δ_B and δ_C always remain integrals of the control variables $\dot{\delta}_B$ and $\dot{\delta}_C$.

The gains across the three values for f, for several variables in each equation, are plotted vs. f in Fig. 17. The most noticeable effect, and one which is wholly expected, is that the gains in the δ_B equation (Eq. 47) increase and the gains in the δ_C equation (Eq. 48) decrease as f increases. This is so because increasing f effectively increases the penalty on use of δ_C as a control point. Thus, the regulator is forced to rely more heavily on the longitudinal cyclic control point.

Figure 17 also illustrates, for the variables plotted, that a sort of power law might be appropriate for the effect of increasing the δ_C cost function weighting on the regulator gains. To the extent that such a relationship exists, it might be exploited in further refining the method for computing desired cost function weightings.

The highest frequency eigenvalues representing the inner-loop bandwidths associated with the actuators are changed only slightly as f is varied. This is to be expected since a relative change in emphasis between collective and cyclic controls should not affect the highest frequency modes. Similarly, the three lowest frequency eigenvalues, 0.100, 0.116, and 0.269, related to the shaping filters u_g, w_g, and $\dot{h}_c$, respectively, do not vary with f at all. This too is to be expected, because the shaping filter modes are not controllable. They are used only to shape the white process noise.

A comparative summary of rms response and control activity is given in Table 37. Just as with the gain shifts of Eqs. 47 and 48, this performance summary shows a very marked shift from use of collective pitch to control altitude to use of longitudinal cyclic pitch and pitch rate to control altitude as f is increased. (Consider the rms values for DCD and DC vis a vis the rms values for DBD, DB and Q for the three values of f.) Yet outer-loop performance is not changed that significantly. (Consider the rms values for HDE and TH.) As f is increased, one real

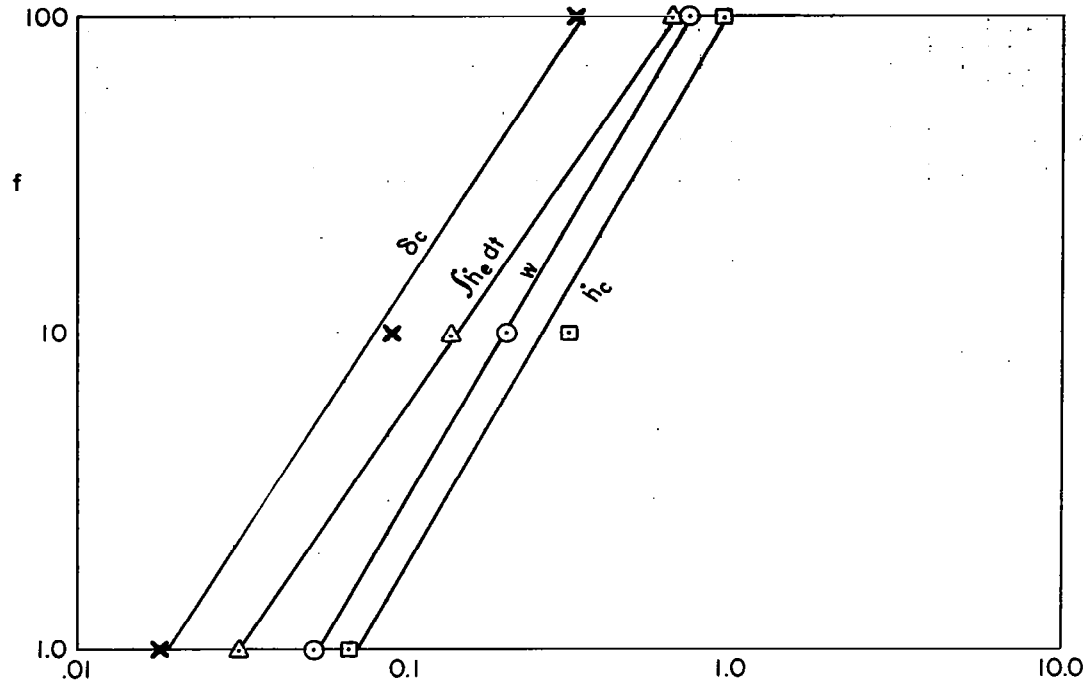

Figure 17a. Selected Gains in δ_B Equation (Eq. 47) vs. f

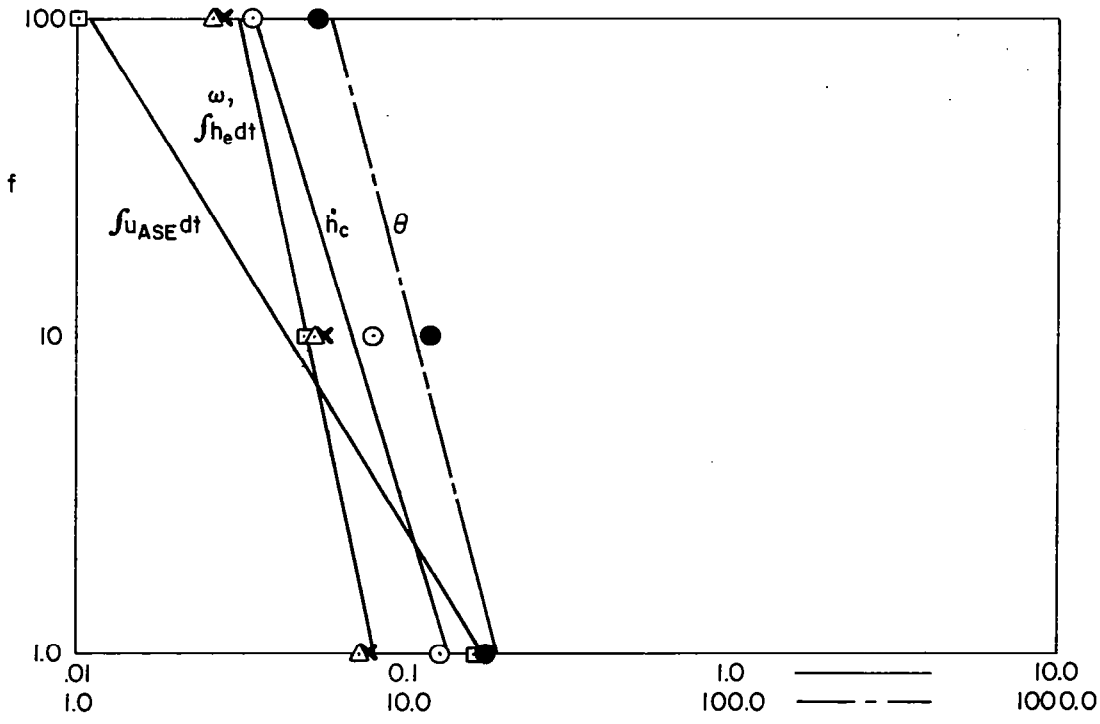

Figure 17b. Selected Gains in δ_C Equation (Eq. 48) vs. f

TABLE 37

COMPARATIVE PERFORMANCE SUMMARY

(For Closed-Loop System Including Filter Observer)

	Multiplying Factor, f		
Variable	1.00	10.0	100.
$\dot{h}$ (HD)	1.01	1.02	1.01
q (Q)	0.238E-02	0.756E-02	0.141E-01
θ (TH)	0.373E-02	0.899E-02	0.119E-01
δ_B (DB)	0.491E-01	0.101	0.208
δ_C (DC)	0.122	0.455E-01	0.948E-02
HDI ($\int \dot{h}_e \, dt$)	0.385	0.254	0.112
a_z' (AZP)	0.519	0.575	0.875
$\dot{h}_e$ (HDE)	0.263	0.253	0.175
$\dot{x}$ (XD)	1.40	3.11	3.84
α (AOA)	0.886E-02	0.669E-02	0.766E-02
$\dot{\delta}_B$ (DBD)	0.129	0.757	2.01
$\dot{\delta}_C$ (DCD)	0.331	0.181	0.599E-01
DB control activity[a]	0.418	1.19	1.54
DC control activity[a]	0.432	0.633	1.01

[a] x control activity = $\sigma_{\dot{x}}/(2\pi\sigma_x)$. This is the expected number of positive-going zero crossings per unit time.

root increases in modulus by a factor of 3.7 and the closed-loop short-period damping ratio decreases from 0.56 to 0.28. This shift in relative use of controls is accompanied by an increase in control activity for both controls. As seen from the bottom of Table 37, there is an almost fourfold increase in positive-going zero crossing rate for the δ_B control, as f is increased by two orders of magnitude. Notice also that this particular control activity measure also illustrates the dramatic shift in the control burden from δ_C to δ_B as the penalty on δ_C is increased in the cost function.

Figure 18 shows the rms response of several variables and the two control activities plotted as functions of the three values of f. First, notice that the slope of the line depends on the control point associated with the particular variable; the δ_C variables show a negative slope, while the δ_B variables have positive slope. This same feature was observed in Fig. 17. We might also infer, as before, that some power law

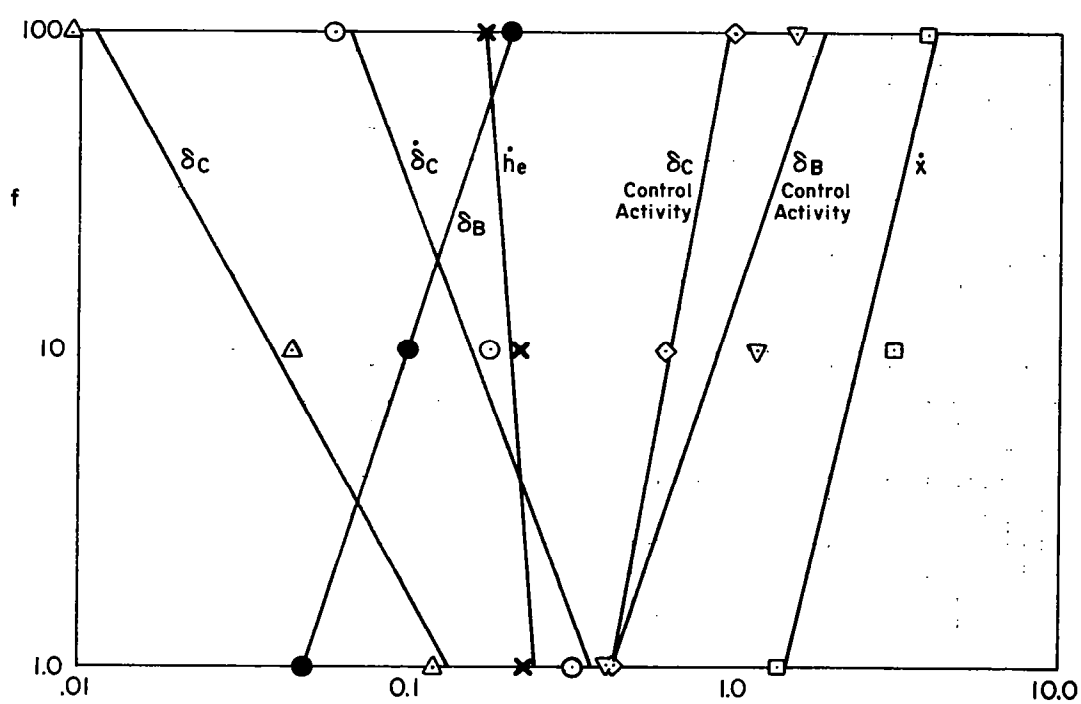

Figure 18. Selected Values of RMS Responses vs. f

exists which approximately defines the effect of increasing the δ_C control point weighting upon the various rms response levels. Since such a relationship does not hold for variables not plotted in Fig. 18, we cannot draw any conclusions here.

Flying qualities dictate that collective pitch be used as a trim control in cruising flight. Hence, the rms values of DC and DCD should be small. f = 10. seems to produce reasonably small rms values for DC and DCD, while the DC control activity is only modestly increased.

Another example case is summarized below for the 100 kt cruise flight condition. This example differs from the previous one in that airspeed control replaces pitch attitude control as one of the ultimate outer-loop goals. Relationships among the control and output variables and cost function coefficients are summarized in Table 38. Table 39 is a summary of the resulting regulator design.

TABLE 38

RELATIONSHIPS AMONG CONTROL AND OUTPUT VARIABLES AND COST FUNCTION COEFFICIENTS

Output Variable	Bandwidth Requirement (rad/sec)	Control Variable Association	
		DBD	DCD
		$R_R(1) = 1.00$	$R_R(2) = 10.0$
δ_B (DB)	25.7	$Q_R(4) = 662.$	
δ (DC)	25.7		$Q_R(5) = 6620.$
θ (TH)	1.5	$Q_R(3) = 354,742.$	
$\dot{h}_e$ (HDE)	0.70	(See note)	(See note)
$\int \dot{h}_e dt$ (HDI)	0.32		$Q_R(6) = 2.84$
u_{AS_e} (ASE)	0.10	$Q_R(9) = 3.44$	
$\int u_{AS_e} dt$ (ASI)	0.02	$Q_R(8) = 1.37 \times 10^{-3}$	

Note: Bandwidth requirement is satisfied without additional feedback. This is indicated by HDE/DC = 7.3 (n = −1), and HDE/TH = 169. (n = −1).

TABLE 39. REGULATOR SYNTHESIS SUMMARY, UH-1H, 100 KT

Q MATRIX DIAGONAL, REGULATOR

1	
0.000	1 HD
0.000	2 Q
0.355E+06	3 TH
662.	4 DB
0.662E+04	5 DC
2.84	6 HDI
0.000	7 HDE
0.137E-02	8 ASI
3.44	9 ASE
0.000	10 XD
0.000	11 AOA

R MATRIX DIAGONAL, REGULATOR

1	
1.00	1 DBD
10.0	2 DCD

CLOSED LOOP EIGENVALUES, REGULATOR

1	
25.7 180.	1 X01
25.7 180.	2 X02
2.20 -124.	3 X03
2.20 124.	4 X06
0.728 -174.	5 X07
0.728 174.	6 X08
0.335 180.	7 X09
0.627E-01 180.	8 X10
0.156E-01 180.	9 X11
0.116 180.	10 X12
0.269 180.	11 X13
0.100 180.	12 X14

REGULATOR GAIN MATRIX

1 X01	2 X02	3 X03	4 X06	5 X07	6 X08	7 X09	8 X10	9 X11	10 X12	11 X13	12 X14	
-0.217	1.18	2.99	0.682	1.80	-277.	-895.	27.9	-0.627	1.34	23.9	0.225E-01	1 DBD
-0.852E-02	-0.496	-0.981	0.335	-0.243	3.82	61.9	-0.627E-01	25.9	-0.324	-0.934	0.930E-02	2 DCD

An interesting feature in this 100 kt cruise example is that bandwidth requirements on HDE are met as the result of imposing prior bandwidth requirements on TH, DB and DC. This is indicated by the fact that the asymptotic approximations to the transfer functions (obtained in Steps 4 and 5) for HDE/TH and for HDE/DC are pure gains. Thus,

$$\frac{HDE}{TH} = -169. \qquad \begin{cases} K = -169. \\ n = -1 \end{cases}$$

$$\frac{HDE}{DC} = 7.30 \qquad \begin{cases} K = 7.30 \\ n = -1 \end{cases}$$

$n = -1$ indicates a pure gain transfer function approximation. When this occurs, no cost function weighting (i.e., a value of zero) should be used on the variable under consideration.

Generally, $n < 0$ indicates either that the bandwidth requirement is met ($n = -1$), or that a prior bandwidth requirement has, in effect, used the current variable under consideration as an inner-loop feedback ($n < -1$).

D. CONTROLLER SOLUTION

Synthesis activities to this point have generated all the data required for the controller solution. The data merely need to be combined in the appropriate way.

The structure of the controller is shown in Fig. 14. Equations for the coefficient matrices (A_F, B_F, C_F and D_F) are given on page 67. The "controller solution" is simply an evaluation of these four coefficient matrices. These matrices, together with the controller equations in Fig. 14, enable a circuit designer or software specialist to implement the controller.

Controller coefficient matrices for the longitudinal UH-1H are given in Table 40 for the hover flight condition and in Table 41 for the

TABLE 40. CONTROLLER COEFFICIENT MATRICES, UH-1H, HOVER

$$\dot{\hat{y}} = A_F\hat{y} + B_Fz$$

$$u = C_F\hat{y} + D_Fz$$

AF MATRIX

1 E13	2 E01	3 E02	
-0.333	0.906E-09	0.363E-08	1 E13
-34.3	-0.922	-2.37	2 E01
-1.60	-3.76	-15.0	3 E02

BF MATRIX

1 HD	2 Q	3 TH	4 DB	5 DC	6 HDE	7 HDI	8 XD	9 XDI	
-0.146E-06	4.97	0.310E-06	0.142E-09	-0.922E-07	0.452E-15	0.000	-0.104E-08	0.000	1 E13
95.6	-29.1	788.	-34.3	59.7	-0.295E-06	0.000	-9.13	0.000	2 E01
592.	-76.5	-0.123E+04	-1.60	381.	-0.183E-05	0.000	1.36	0.000	3 E02

CF MATRIX

1 E13	2 E01	3 E02	
-28.9	-0.254	-0.523	1 DBD
0.122	0.264	1.07	2 DCD

DF MATRIX

1 HD	2 Q	3 TH	4 DB	5 DC	6 HDE	7 HDI	8 XD	9 XDI	
21.5	538.	0.149E+04	-29.9	0.518E-01	-0.717	-0.252	-26.6	-1.89	1 DBD
-42.5	1.30	79.8	0.517E-02	-27.0	4.16	2.16	-0.436	-0.221E-01	2 DCD

TABLE 41. CONTROLLER COEFFICIENT MATRICES, UH-1H, 100 KT

$$\dot{\hat{y}} = A_F\hat{y} + B_Fz$$

$$u = C_F\hat{y} + D_Fz$$

AF MATRIX

1 E13	2 E01	3 E02	
-0.333	-0.614E-08	0.130E-06	1 E13
8.06	-0.183	1.52	2 E01
-125.	1.17	-25.0	3 E02

BF MATRIX

1 HD	2 Q	3 TH	4 DB	5 DC	6 HDI	7 HDE	8 ASI	9 ASE	
-0.314E-05	4.97	0.530E-03	0.657E-06	-0.171E-05	0.263E-12	-0.180E-12	-0.908E-11	0.162E-06	1 E13
-36.3	261.	0.613E+04	8.06	-20.1	-0.145E-04	-0.157E-03	0.478E-03	1.87	2 E01
594.	-0.419E+04	-0.100E+06	-125.	325.	-0.422E-04	0.546E-04	0.147E-02	-30.6	3 E02

CF MATRIX

1 E13	2 E01	3 E02	
-23.9	-0.558	-1.22	1 DBD
0.934	-0.313	0.479	2 DCD

DF MATRIX

1 HD	2 Q	3 TH	4 DB	5 DC	6 HDI	7 HDE	8 ASI	9 ASE	
28.1	271.	-0.434E+04	-27.9	0.627	-1.34	-2.99	-0.193E-01	-2.15	1 DBD
-11.6	-2.14	0.206E+04	0.627E-01	-25.9	0.324	0.981	-0.786E-02	0.281	2 DCD

100 kt cruise flight condition. It must be appreciated that the controller function is different in one respect for each flight condition (groundspeed control in hover in distinction to airspeed control in 100 kt cruise). At each flight condition only one controller function (flight control system mode) is addressed. Other controller functions would be developed in similar form by similar methods. Different measurements may be used for different controller functions as in the case of the two example functions given (proportional-plus-integral groundspeed error in distinction to proportional-plus-integral airspeed error).

Controller transfer functions are summarized in Table 42 for the hover flight condition and in Table 43 for the 100 kt cruise flight condition. The characteristic polynomial roots are the same as the closed-loop filter-observer roots for these special cases (refer to Tables 17 and 22). This is for the reason that the $[G_1 - K_{12}G_2]$ matrix is null for these cases as was explained earlier.

The numerators of these transfer functions are not particularly remarkable in most respects. However, they are not exactly what a conventional frequency response design approach would lead to either. This is particularly so with respect to the non-minimum phase zeros at low frequencies (e.g., the DCD/TH numerator in Table 42) and at mid frequencies (e.g., the DBD/TH numerator in Table 43). The non-minimum phase zeros at high frequencies do not really affect the design because of low loop gain at those frequencies.

Another observation is that every measurement is fed back to every control. This results in eighteen controller transfer functions. While there are some controller transfer function paths for which the gain is negligible at all frequencies (e.g., the DCD/XDI numerator in Table 42), not many have this property. This is in contrast to the eight to ten non-zero controller transfer functions an experienced conventional frequency response designer would use. More will be said in the next chapter concerning controller simplification.

The controller transfer functions are third order (not counting integrals of errors). This order is certainly acceptable as a practical

TABLE 42. CONTROLLER TRANSFER FUNCTIONS, UH-1H, HOVER

CASE: UH1H HOVER I22LONG 2-FEB-79 CONTROLLER TRANSFER FUNCTIONS

DENOMINATOR:

1.0000
(.31507) (.33300) (15.614)
< 1.6383 >

NUMERATOR: DBD/ HD

21.541
(.11140) (.31682) (.33300)
< .25317 >

NUMERATOR: DBD/ Q

538.16
(15.694)
((.29748 , .24420 , .19475 , .14734))
< 503.67 >

NUMERATOR: DBD/ TH

1486.9
(.24018) (.33300) (15.988)
< 1901.3 >

NUMERATOR: DBD/ DB

-29.879
(.18186) (.33300) (15.428)
<-27.917 >

NUMERATOR: DBD/ DC

.51781E-01
(.29977) (.33300) (-4127.1)
<-21.332 >

NUMERATOR: DBD/HDE

-.71669
(.31507) (.33300) (15.614-)
<-1.1741 >

NUMERATOR: DBD/HDI

-.25178
(.31507) (.33300) (15.614)
<-.41249 >

NUMERATOR: DBD/ XD

-26.641
(.27441) (.33300) (15.595)
<-37.964 >

NUMERATOR: DBD/XDI

-1.8892
(.31507) (.33300) (15.614)
<-3.0950 >

NUMERATOR: DCD/ HD

-42.506
(.11509) (.31500) (.33300)
<-.51672 >

NUMERATOR: DCD/ Q

1.3819
(-.28691E-01) (1.2724) (-53.279)
< 2.5324 >

NUMERATOR: DCD/ TH

79.797
(.33300) (-.45581) (2.4905)
<-30.165 >

NUMERATOR: DCD/ DB

.51744E-02
(-.11656) (.33300) (-2054.8)
< .41471 >
PC=036035

NUMERATOR: DCD/ DC

-27.008
(-.94888E-01) (.33300) (.33773)
< .28821 >

NUMERATOR: DCD/HDE

4.1570
(.31507) (.33300) (15.614)
< 6.8103 >

NUMERATOR: DCD/HDI

2.1563
(.31507) (.33300) (15.614)
< 3.5326 >

NUMERATOR: DCD/ XD

-.43622
(.15039) (.33300) (17.982)
<-.39283 >

NUMERATOR: DCD/XDI

-.22059E-01
(.31507) (.33300) (15.614)
<-.36139E-01>

TABLE 43. CONTROLLER TRANSFER FUNCTIONS, UH-1H, 100 KT

CASE: UH1H 100KT 128LONG 2-FEB-79 CONTROLLER TRANSFER FUNCTIONS

DENOMINATOR:

1.0000
(.11136) (.33300) (25.074)
< .92977 >

NUMERATOR: DBD/ HD

28.057
(-.81761E-01) (.12973) (.33300)
<-.99096E-01>

NUMERATOR: DCD/ HD

-11.590
(.10443) (.33300) (-.47364)
< .19091 >

NUMERATOR: DBD/ Q

273.94
(.57922E-01) (.19074) (43.160)
< 129.19 >

NUMERATOR: DCD/ Q

-2.1404
(.14888) (.40243) (998.36)
<-128.03 >

NUMERATOR: DBD/ TH

-4344.4
(.11516) (.33300) (-2.3193)
< 386.40 >

NUMERATOR: DCD/ TH

2059.9
(.12469) (.33300) (.80143)
< 68.566 >

NUMERATOR: DBD/ DB

-27.876
(.12362) (.33300) (19.767)
<-22.684 >

NUMERATOR: DCD/ DB

.62709E-01
(.16364) (.33300) (-967.21)
<-3.3050 >

NUMERATOR: DBD/ DC

.62710
(.10160) (.33300) (-589.14)
<-12.500 >

NUMERATOR: DCD/ DC

-25.870
(.10784) (.33300) (18.819)
<-17.484 >

NUMERATOR: DBD/HDE

-2.9885
(.11133) (.33300) (25.074)
<-2.7778 >

NUMERATOR: DCD/HDE

.98066
(.11140) (.33300) (25.074)
< .91216 >

NUMERATOR: DBD/HDI

-1.3402
(.11135) (.33300) (25.074)
<-1.2460 >

NUMERATOR: DCD/HDI

.32357
(.11137) (.33300) (25.074)
< .32089 >

NUMERATOR: DBD/ASE

-2.1499
(.11284) (.33300) (8.2305)
<-.66249 >

NUMERATOR: DCD/ASE

.28138
(.11284) (.33300) (-29.069)
<-.30735 >

NUMERATOR: DBD/ASI

-.19271E-01
(.12935) (.33300) (25.162)
<-.20987E-01>

NUMERATOR: DCD/ASI

-.78565E-02
(.13233) (.33300) (24.982)
<-.86490E-02>

matter for flight control system implementation. It is estimated that an experienced conventional frequency response designer would use two first-order filters.

This completes explanation of the controller synthesis procedures and examples. The next section explains and illustrates procedures for examining more of the system and controller properties and for conducting the controller design assessment. These key activities are necessary to better understand what the optimal synthesis hath wrought, as well as to assure that other quantitative requirements and qualitative requirements, which we are not able to incorporate directly into the problem formulation and solution procedure, are satisfied.

SECTION V

DESIGN ASSESSMENT

At this stage of the design process a controller has been synthesized that consists of a filter-observer and a regulator. This section discusses the next step in the design process — examination and expansion of the synthesis results into a composite, total picture of system properties, behavior, and design margins. The goal here is to present the techniques needed to evaluate a preliminary FCS design. By exercising these techniques, the analyst will be able to:

- Determine whether design goals have been met.
- Define quantitatively all the important properties of the system, e.g.,
  - expand the scope of the results (e.g., to include transient characteristics).
  - highlight the system's dominant properties.
  - reveal the sensitivity of dominant properties to uncertainties.
- Broaden the understanding of the optimal synthesis design results, for example:
  - relative importance of the various terms in the control laws.
  - factors which contribute to particular control behavior (e.g., see Section IV discussion of results when $G_1 - K_{12}G_2 \approx 0$).
  - implications for future design strategy.
- Explore simplifications of the design which may lead to a simpler, more practical, controller.
- Investigate the implications of controller architecture on results.
- Generalize design for other applications.

A marriage of evaluation techniques from classical and optimal control theory will provide the basis for the design analysis.

Table 44 presents a more specific outline of the system and controller properties that are examined in this chapter. All of the assessment goals listed above are addressed by one or more of the table entries, although there is not always a direct correspondence between the two. The design goal list addresses rather fundamental questions, whereas the table (and the remainder of this section) presents a systematic checklist-like method for answering these questions while simultaneously defining and evaluating a given FCS design.

To this end, notice that the topics addressed are divided into two major categories: properties of the system, and properties of the controller. Within each category a definite hierarchy exists, so that the evaluation proceeds from the simple and qualitative to the detailed and quantitative. Along the way, certain features may be deemed unimportant or uninteresting and are thus excluded from more thorough examination. In this way, the need for microscopic analysis of each aspect of the design is eliminated, and the number of assessment steps is correspondingly decreased.

The remainder of this chapter is devoted to a close look at many of the techniques for design evaluation listed in Table 44. We begin with an exploration of the stability characteristics of the system; stability is typically the most fundamental consideration in any feedback system. Certain metrics from classical control theory such as gain and phase margins are computed. These provide a quantitative rank-ordering of all variables in terms of their tendency toward instability. Then, for each variable, the mode which is the first to become unstable as the closed-loop gain increases is identified as the crucial mode.

Next, the response characteristics of the system are assessed. This task is divided into three areas: response of the primary variables, response of the secondary variables, and response of the controls. Certain behavior is expected in a variable with satisfactory response: the transient response to commands must be smooth and well-behaved; the response to disturbances should be minimal; the control activity must be within reasonable physical limits; and command following should be

TABLE 44. DESIGN ASSESSMENT

FEATURE	PROPERTY	ASSESSMENT DATA/TECHNIQUES	CONSIDERATIONS
SYSTEM PROPERTIES			
Stability			
Nominal modal dampings	Closed-loop characteristic equations	Closed-loop eigenvalues	
Margins for key loops	Phase and gain margins for key open-loop characteristics	Open-loop frequency responses	
Crucial mode(s)	First mode to go unstable as loop gain(s) are varied	s-plane/Bode root loci	Can be both high and low gains in conditionally stable situation
Response			
Primary controlled variables			
Specified command-response relationships	Rapid, well-damped, minimum-tailed time histories for specified transient inputs	Indicial, ramp-input responses	Defines time character
		s-plane/Bode root loci	Defines dominant modes
	Good output/command following for specified random inputs	RMS response ratios (covariance matrix)	
Disturbance/noise inputs	Indifference/suppression of effects of unwanted inputs	Bandwidths (frequency responses)	Also relates to command-response accuracy
		RMS values (covariances)	
Secondary variables			
Specified command-response relationships	Desirable phasing and amplitude relative to primary variable	Indicial responses to commands	Defines time character
	Motion harmony, coupling of variables	s-plane root loci with closed-loop modal response ratios	Defines dominant modes for secondary variables
		RMS values	
Control activity	Control rates, positions; limiting potential, favorable or negligible cross-coupling	Indicial responses	Also defines reasonable authority limits
		RMS values, exceedances	

(concluded on following page)

TABLE 44. (Concluded)

FEATURE	PROPERTY	ASSESSMENT DATA/TECHNIQUES	CONSIDERATIONS
SYSTEM PROPERTIES (CONCLUDED)			
Sensitivity			
Sensitivity of key response modes Crucial Dominant primary Dominant secondary	Sensitivity to off-nominal conditions, component tolerances/ variations, uncertainties, etc.	First-order gain or parameter sensitivities	
Sensitivity to parasitic nonlinearities Threshold Effects	Different thresholds in various loops	Comparison of pertinent open-loop frequency responses	Effects of zero gains on various outer/inner loops
Graceful Degradation Conventional loop structure	No gross instability problems with various loop failures	Use stability analysis techniques on system where one or more loops has failed	
Integrated sensor structure, adaptive filter-observer	No gross instability problems with various loop failures	Use stability analysis techniques on system where one or more sensors has failed	Will increase order of filter-observer, and increase rms state estimation error
CONTROLLER PROPERTIES			
Gain Levels			
Control saturation	Level of input state which saturates control	RMS values, controller gains	Indicates outer extent of control space
Minimum increment of control	Level of input state which corresponds to minimum control output	Controller gains	Indicates inner extent of control space; effective threshold of variable fed to control; dynamic range information; permits elimination of low gain, low effectiveness feedbacks
Sensor Complex			
Equalization economy	Minimum structure controller	Structure, architecture	Sensor/computational tradeoff Eliminate low gain, low effectiveness feedbacks
Commonality of elements/ gain settings for different operational modes	Common controller elements for each operational mode	Controller gains over many operational modes	

good. For both the primary and secondary variables the modes that dominate the response character are identified.

The final consideration within the system properties category is the sensitivity of the design. Here, too, there are three areas of interest. The first is the sensitivity of the key response modes (i.e., the crucial and dominant modes) to off-nominal conditions, which is quantified with the use of first-order gain and parameter sensitivities. The second is the system sensitivity to parasitic nonlinearities such as different thresholds for the various feedbacks. Here, open-loop frequency response plots provide the data for assessment. Finally, the ability of the design to degrade gracefully is evaluated, based on its stability and response characteristics when loops are systematically opened.

Consideration of properties peculiar to the controller follows. There are two major considerations: the gain levels and the sensor complex. Questions concerning control saturation and minimum increment of control are addressed within the context of gain levels. Under the heading of sensor complex fall many concerns which affect the controller mechanization. These include: equalization economy, which refers to the desire for minimum sensor/signal compensation/control channel features in the system implementation; and commonality of elements, a desire for the minimum number of gain and/or element changes over the range of operating modes. Both economy of equalization and commonality of elements are evaluated via variation of system architecture.

Limited design assessments were undertaken during the course of the filter-observer and the regulator synthesis. Those aspects will be only briefly referred to at the appropriate points as the discussion winds its way through Table 44. Certain other features which are enumerated in the table are beyond the scope of this report; these too will be discussed only briefly, without benefit of examples. In all other cases, however, the discussion of the evaluation techniques will be accompanied by examples from the UH-1H hover FCS design, presented in full in Appendix C.

A. STABILITY

As stated previously, an understanding of the stability characteristics of a system is probably the most fundamental of all design assessment aspects. Interest lies not only in determining whether or not a given system is stable, but also in what causes the system to be stable and what modes of the system are most likely to become unstable when differences appear between the actual and analytical systems. Such information is needed to define management safety and to evaluate the performance of a design in off-nominal conditions.

The most obvious place to begin the stability assessment is with the closed-loop system denominator. All closed-loop roots should lie in the left-half complex plane and indeed this is guaranteed for an LQG optimal controller if the open-loop plant is detectable and stabilizable and if a positive definite performance index was used in controller synthesis. In fact, these conditions assure uniform asymptotic stability (i.e., $\hat{x}(t) \rightarrow 0$ as $t \rightarrow \infty$, see Ref. 24). One measure of the degree of stability is the damping of the closed-loop roots. Table 45 contains an example closed-loop transfer function (θ/θ_c). Notice that not only are the denominator roots all stable, as assured because the uniform asymptotic stability criteria are obeyed here, but that the minimum damping ratio present is 0.674.

Some additional observations can be made as to the system's dynamic behavior by further examination of the θ/θ_c transfer function. Many of the poles cancel exactly (or nearly so) with zeros for this transfer function. These modes will, therefore, not appear in θ response to θ_c commands. The resulting approximation to θ/θ_c shown at the bottom of Table 45 reflects the closed-loop actuator characteristics (at 25.73) and the well-damped short-period mode represented by the quadratic.

At this point, one might be tempted to conclude the stability assessment, by correctly observing that the closed-loop denominator has permitted identification of all the important aspects of stability. Yet there is still much which needs to be said about a system's stability beyond simple closed-loop root considerations. In particular, we are

TABLE 45

CLOSED-LOOP θ/θ_c TRANSFER FUNCTION

CASE: UH1H HOVER ALL LOOPS CLOSED

DENOMINATOR:

```
 1.0000
( .10195    ) ( .31507    ) ( .33300    ) ( .33595    )
( .50520    ) ( 15.614    ) ( 25.716    ) ( 25.726    )
(( .92313    , .90723    , .83748    , .34882    ))
(( .67380    , 2.7741    , 1.8692    , 2.0498    ))
< 118.79    >
```

NUMERATOR: TH/VTH FILE NAME? THVTH.2CL
OLD FILE

```
-251.70
( .00000    ) ( .51016E-03) ( .24046    ) ( .33300    )
( .33300    ) ( 15.968    ) ( 25.716    )
(( .92283    , .90699    , .83699    , .34939    ))
<-1.1565    >
```

$$\frac{\theta}{\theta_c} = \frac{-251.7(s)(s+.00051)(s+.24)(s+.333)^2(s+15.968)(s+25.72)[s^2+2(.923)(.91)s+(91)^2]}{(s+.102)(s+.315)(s+.333)(s+.336)(s+.5)(s+15.614)(s+25.72)(s+25.73)}$$

$$\times [s^2+2(.923)(.91)s+(.91)^2][s^2+2(.674)(2.77)s+(2.77)^2]$$

$$\doteq \frac{-251.7(s)(s+.00051)(s+.24)}{(s+.102)(s+.315)(s+.5)(s+25.73)[s^2+2(.674)(2.77)s+(2.77)^2]}$$

interested in two things: general margins and the modes that would be the first to go unstable as likely system parameters are changed.

The first concern is the particular margins of stability for each loop. There are two common margins: the gain margin, which is the difference between the gain at the crossover frequency and the gain at the −180 deg phase point; and the phase margin, which is the difference between the phase at crossover and −180 deg. Figure 19 is an open-loop frequency response plot for θ/θ_c, where $\dot{x}$, $\int \dot{x}\,dt$, and θ loops are open. The gain margin of 21 dB and phase margin of 56 deg reveal the excellent stability margins for this loop.

In addition, it is instructive to convert the phase margin, φ_M, to an equivalent τ in a pure time delay, $e^{-j\omega\tau}$. In physical terms this delay, if added to the system, would be just sufficient to destabilize the system. The delay itself can be thought of as the low-frequency measure of a large number of high-frequency leads and lags which are not accounted for in our system model. If these are given by

$$\tau = \sum \tau_i - \sum T_i$$

then

$$G_{hi}(s) = \frac{\prod_i^n (T_i s + 1)}{\prod_i^m (\tau_i s + 1)}$$

That is, the delay τ is the sum of the high-frequency lags minus the sum of the high-frequency leads. For the θ/θ_c loop presented in Fig. 19 the allowable τ is computed as

$$\tau = \frac{\varphi_M}{\omega_c} = \frac{56/57.3}{2.3}$$

$$= 0.425 \text{ sec}$$

This can be considered a delay or lag margin.

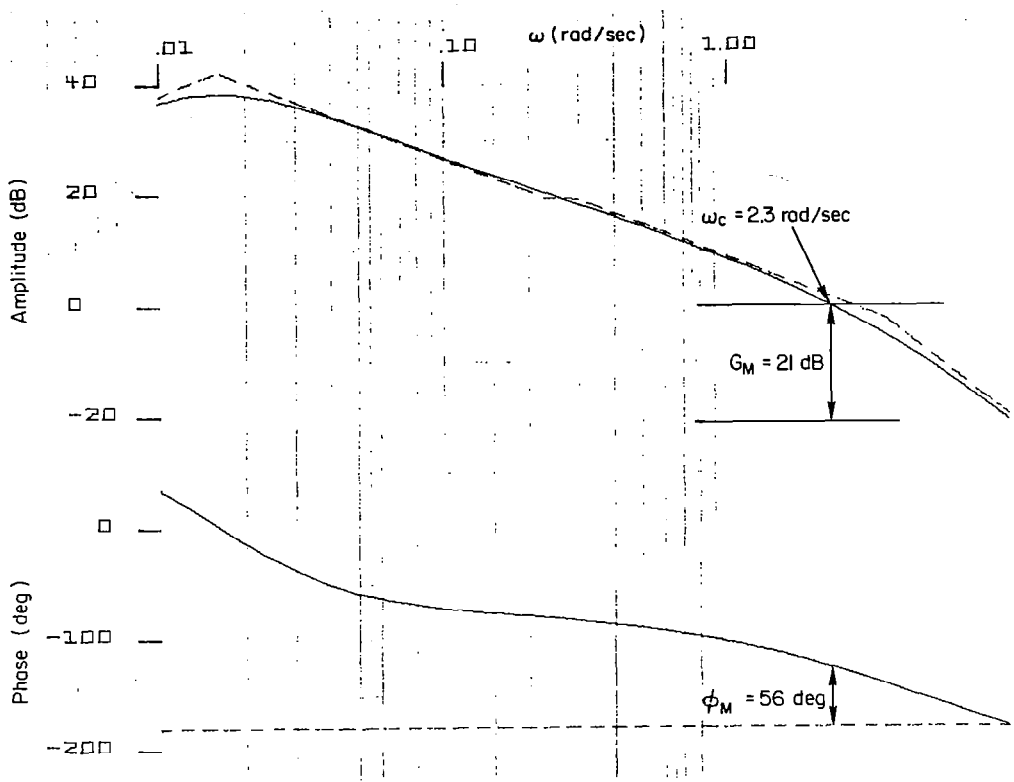


```
CASE:  UH1H HOVER                    XD,XDI AND TH LOOPS OPENED

DENOMINATOR:

  1.0000
( .00000    ) ( .30483    ) ( .33300    ) ( .33863    )
( 3.5187    ) ( 15.568    ) ( 25.714    ) ( 26.577    )
(( .77420    , .16484E-01, .12762E-01, .10433E-01))
(( .92994    , .90422    , .84086    , .33250    ))
< .28587    >


NUMERATOR:   TH/VTH   FILE NAME?  THVTH
 NEW FILE

 -251.70
( .00000    ) (-.89352E-04) ( .23999    ) ( .33300    )
( .33300    ) ( 15.961    ) ( 25.721    )
(( .92498    , .90635    , .83836    , .34442    ))
< .20183    >
```

$$\left.\frac{\theta}{\theta_c}\right|_{OL} \doteq \frac{-251.7(s-.00009)(s+.24)(s+.333)(s+15.961)(s+25.721)[s^2+2(.925)(.91)s+(.91)^2]}{(s+.305)(s+.339)(s+3.52)(s+15.568)(s+25.714)(s+26.577)} \times [s^2+2(.77)(.0165)s+(.0165)^2][s^2+2(.93)(.90)s+(.90)^2]$$

$$\doteq \frac{-251.7(s+.24)}{(s+.305)(s+3.52)(s+26.577)[s^2+2(.77)(.0165)s+(.0165)^2]}$$

Figure 19. Frequency Response for Open-Loop θ/θ_c

Consider now the second concern; namely, given the gain and phase margins for a loop, which mode will become unstable first as the gain margin approaches zero or added lags create a time delay which approaches τ? This question can be answered with the use of an s-plane root locus plot or a Bode root locus plot. Both are shown for the θ/θ_c example in Fig. 20. The root locus is a plot of the open-loop poles and zeros (symbols ✕ and ⊡, respectively), and the locus of closed-loop roots. In Fig. 20a we see the short-period root locus heading for the right-half plane as the closed-loop gain increases. Thus, it is the short-period mode which will become unstable first when the gain margin is zero. This is confirmed by the Bode root locus plot of Fig. 20b. Here the Bode plot and root locus plot are combined. The important open-loop poles and zeros are called out, as well as the closed-loop roots (the solid rectangular symbols). The crosses which depict the second-order closed-loop roots are shown moving into the right-half plane (at $\omega \doteq 10$ rad/sec) for the short-period mode, thus identifying it as the "crucial" mode for the θ/θ_c loop.

This completes the stability assessment for the θ/θ_c loop. The same procedure should be followed for every other loop in the design. That is, examine the closed-loop roots, compute the stability margins, and identify the crucial modes. The results of this process for the $\dot{h}/\dot{h}_c$, $\int \dot{h}_e\, dt/\dot{h}_c$, $\dot{x}/\dot{x}_c$, $\int \dot{x}\, dt/\dot{x}_c$ loops are presented in Appendix C, Figs. C-8, C-9, C-10, and C-11, respectively. Notice that the $\dot{h}/\dot{h}_c$ loop has a gain margin $G_M = \infty$. As a practical matter, this is an impossibility and simply indicates that one or more modes (and, indeed, one which is the crucial mode) has been neglected. Although the crucial mode for this loop cannot be identified, it is always possible to compute an effective τ from phase margin and crossover frequency which represents a crucial value for the high-frequency leads and lags.

Many other techniques are available in the literature for stability assessment, for example the Routh and Hurwitz tests (Ref. 26) and the Nyquist stability criterion (Ref. 27). The methods used here have been selected to give the best mixture of meaningful results from a combined optimal/conventional standpoint.

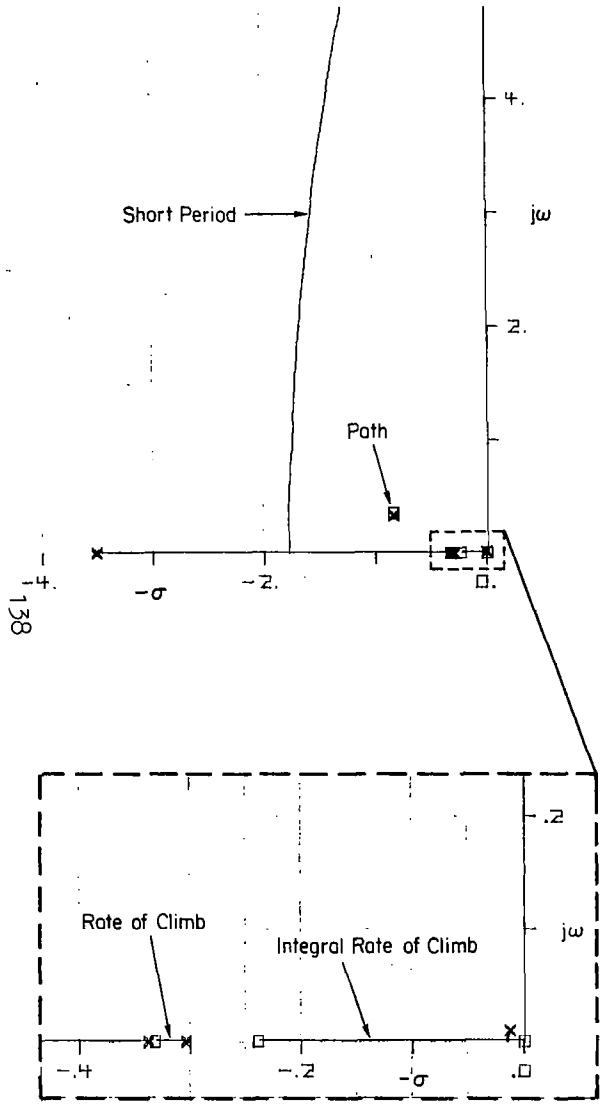

a) s-plane Root Locus

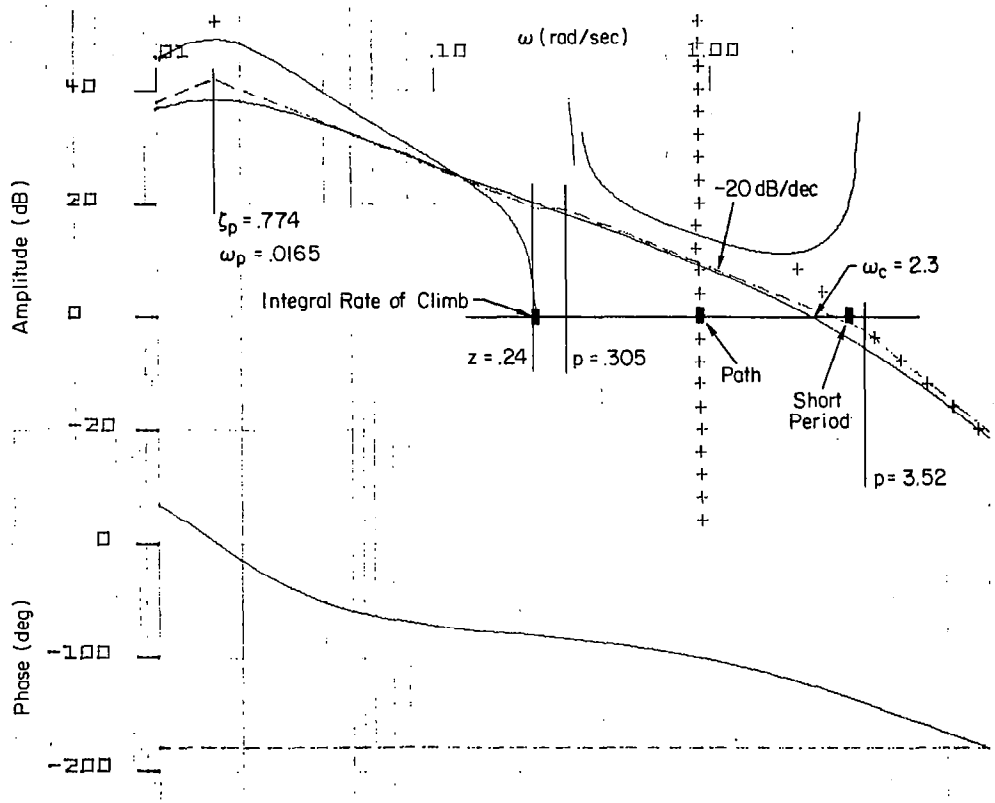

b) Bode Root Locus

Figure 20. System Survey for $\theta/\theta_c\big|_{\theta,\ \dot{x},\ \int \dot{x}\,dt}$ opened

B. RESPONSE

Turn attention now to the system's response characteristics. For this aspect of assessment the system's output variables are divided into three classes:

- Primary controlled variables perform the explicit commanded functions of the FCS. For the UH-1H hover example these functions are rate-of-climb command and groundspeed hold, so the primary variables are $\dot{h}$ and $\dot{x}$ as outputs or $\dot{h}_e$ and $\dot{x}_e$ as error quantities.

- Secondary variables are those vehicle output variables which remain after identifying primary variables. The UH-1H hover secondary variables include θ, q, α, and u_{AS_e}.

- Controls, δ_B and δ_C, for example, comprise the final category.

The next three sections discuss the assessment of response characteristics for each category of variables.

1. Primary Controlled Variables

The most fundamental single indication of controlled variable response behavior is the response/command bandwidth. Among other things, the bandwidth:

- Indicates the range of command frequencies over which feedback acts to provide good command following and error suppression.

- Indicates the frequency range over which disturbances are suppressed.

- Specifies the speed of response, since the bandwidth is inversely proportional to the indicial response rise time.

Because bandwidth properties play such an important role, appropriate bandwidth values were made the key design requirements. Further, the output variables (to be included in the regulator cost function) were chosen to insure desirable low-pass properties and particular time response behavior (e.g., including $\int \dot{h}_e \, dt$ guarantees that the indicial

response in $\dot{h}$ is such that $\dot{h}_e$ approaches zero in the steady state). Thus, "bandwidth" will have its traditional meaning in a low-pass filter context.

To be certain that bandwidth goals were met, we examine opened-loop frequency response plots such as presented in Fig. 19. Here, for the θ/θ_c loop, the goal was a bandwidth of 2.0 rad/sec. The stretch of -20 dB/decade slope on either side of the 0 dB crossover frequency (ω_c) permits us to approximate the bandwidth by ω_c. Similar bandwidth assessment is indicated in Figs. C-8 through C-11 for the primary variables.

We have previously emphasized that the bandwidth numbers partition the response into regions of action — regions where feedback is useful in improving the response and regions where feedback effects are nil. The details of the system behavior in these regions are most conveniently addressed in the frequency domain, with the closed-loop response/command and error/command characteristics being of particular interest. For example, Figs. 21 and 22 present closed-loop Bode plots for the $\dot{h}/\dot{h}_c$ and $\dot{h}_e/\dot{h}_c$ transfer functions, respectively.

Several essential aspects of the $\dot{h}/\dot{h}_c$ response are apparent from Fig. 21. There is good following of command input magnitudes at all frequencies below the bandwidth of approximately 1.4 rad/sec, as evidenced by the unity gain. Beyond that, the response to commands is smoothed and attenuated (integrated once) out to 25.7 rad/sec, and even more attenuated (integrated twice) thereafter (not shown). In addition, the phase shift up to the bandwidth is nearly linear with frequency. This closed-loop system response is dominated by only one lead and one quadratic lag out to 26 rad/sec. In fact, the response can be approximated by $1.4/(.7s + 1)$ for all frequencies below 26 rad/sec. Thus, the response character of what at first glance seems to be a rather complicated transfer function can be reduced to the simple form $K/(T_1 s + 1)$.

Similarly, Fig. 22 provides much information regarding the nature of the $\dot{h}_e$ response to $\dot{h}_c$. Here again the frequency response has three distinct regions: for $\omega < 0.1146$ rad/sec it behaves as a zero position error system; for 0.1146 rad/sec $< \omega < 0.91$ rad/sec it behaves as a zero

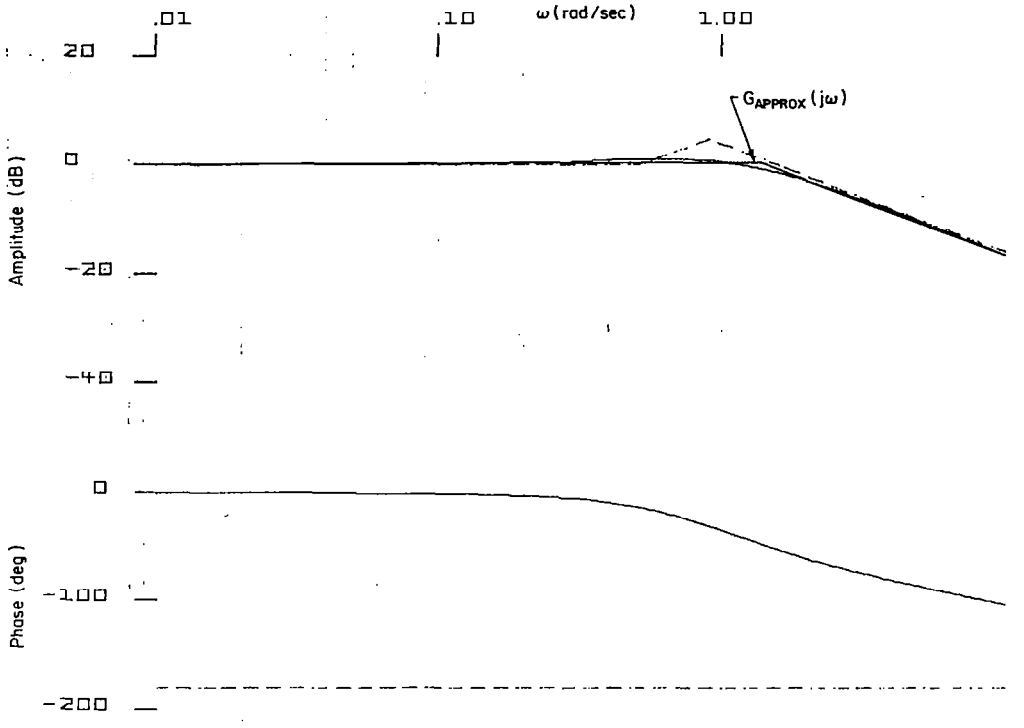


```
CASE:  UH1H HOVER                    ALL LOOPS CLOSED

DENOMINATOR:

   1.0000
 ( .10195     ) ( .31507     ) ( .33300     ) ( .33595     )
 ( .50520     ) ( 15.614     ) ( 25.714     ) ( 25.726     )
 (( .92313    , .90723     , .83748     , .34882     ))
 (( .67380    , 2.7741     , 1.8692     , 2.0498     ))
 < 118.79

NUMERATOR:   HD/HDC    FILE NAME?  HDHDC.2CL
 NEW FILE

   40.908
 ( .10195     ) ( .31507     ) ( .33300     ) ( .33601     )
 ( .50240     ) ( .52197     ) ( 15.614     ) ( 25.726     )
 (( .67251    , 2.7694     , 1.8625     , 2.0496     ))
   118.79
```

$$\frac{\dot{h}}{\dot{h}_c} \doteq \frac{40.908(s+.52197)}{[s^2+2(.923)(.907)s+(.907)^2](s+25.7)} \doteq \frac{35.98}{(s+1.4)(s+25.7)}$$

$$G_{approx}(j\omega) = \frac{1.4}{(.7s+1)} \quad \text{(accurate out to 25.7 rad/sec)}$$

Figure 21. $\dot{h}/\dot{h}_c$ Closed-Loop Frequency Response

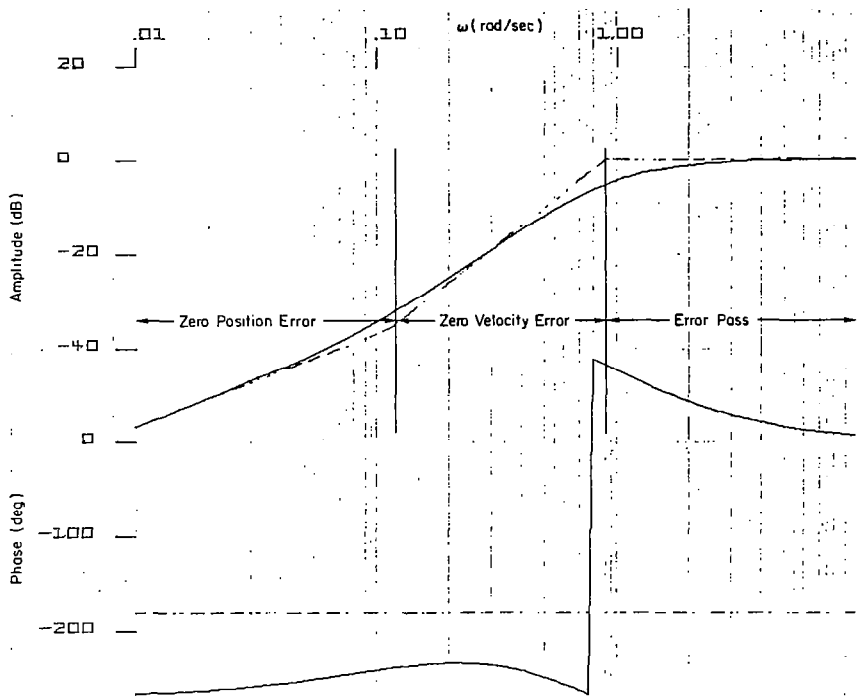

CASE: UH1H HOVER ALL LOOPS CLOSED

DENOMINATOR:

```
 1.0000
( .10195    ) ( .31507    ) ( .33300    ) ( .33595    )
( .50520    ) ( 15.614    ) ( 25.716    ) ( 25.726    )
(( .92313    , .90723    , .83748    , .34882    ))
(( .67380    , 2.7741    , 1.8692    , 2.0498    ))
< 118.79    >
```

```
NUMERATOR:  HDE/HDC   FILE NAME?  HDEHDC.2CL
 OLD FILE

 1.0000
( .00000    ) ( .10199    ) ( .11459    ) ( .31507    )
( .33300    ) ( .33575    ) ( .50556    ) ( 15.614    )
( 25.726    ) ( 27.282    )
(( .67087    , 2.7736    , 1.8663    , 2.0518    ))
< 17.547    >
```

$$\frac{\dot{h}_e}{\dot{h}_c} \doteq \frac{s(s + .1146)}{[s^2 + 2(.923)(.907)s + (.907)^2]}$$

Figure 22. $\dot{h}_e/\dot{h}_c$ Closed-Loop Frequency Response

velocity error system; and beyond the bandwidth of approximately 1.4 rad/sec there is no error suppression ($|\dot{h}_e/\dot{h}_c| = 1$).

Both the $\dot{h}/\dot{h}_c$ and $\dot{h}_e/\dot{h}_c$ Bode plots lead us to suspect that the mode that dominates the $\dot{h}$ response is, not surprisingly, the path mode ($\zeta = 0.923$, $\omega = 0.907$). It is this mode that provides the general shape for both plots. Indeed, Fig. 23 confirms this suspicion with a Bode root locus plot of $\dot{h}/\dot{h}_c$, where the $\dot{h}_e$ and $\int \dot{h}_e\, dt$ loops have been opened. The dominant mode is closest to the point of crossover, which approximates the bandwidth due to the stretch of −20 dB/decade slope.

The discovery of the dominant mode for the $\dot{h}$ response leads naturally to an examination of the transient time response behavior of this variable. Plots of both the indicial and ramp responses of $\dot{h}$ to $\dot{h}_c$ input are shown in Fig. 24. The path mode does, of course, dominate the response, as it did in the frequency response plots of Figs. 21 and 22. However, the initial part of the indicial response is quite first-order-like, even though the path mode is second-order. This is not surprising, since the almost-critical damping of this second-order mode ($\zeta = 0.923$) allowed us to approximate the frequency response by $1.4/(.7s + 1)$ out to 26 rad/sec. The transfer function for $\dot{h}/\dot{h}_c$ contains a lead term (the path mode) as well as the quadratic lag, and the lead part of the combination provides the overshoot in the indicial response shape. Thus, initially the response is first order, with a time constant near T_1; then, after the first 0.4 sec the response is that of the heavily damped path mode, with the 12 percent overshoot attributed to the lead at 0.53 rad/sec. These time domain characteristics reflect the dominant features of the frequency response (Fig. 21).

A similar comparison can be drawn between the $\dot{h}_e/\dot{h}_c$ frequency response plot of Fig. 22 and the $\dot{h}$ time response to an $\dot{h}_c$ ramp input shown in Fig. 24. Remember the three frequency regions which were present in Fig. 22 — a region of zero position error, a region of zero velocity error, and a region where the error was passed with unity gain. Those same divisions can be made for the ramp response in Fig. 24. The $\dot{h}$ response at low frequencies looks like that of an equivalent first-order

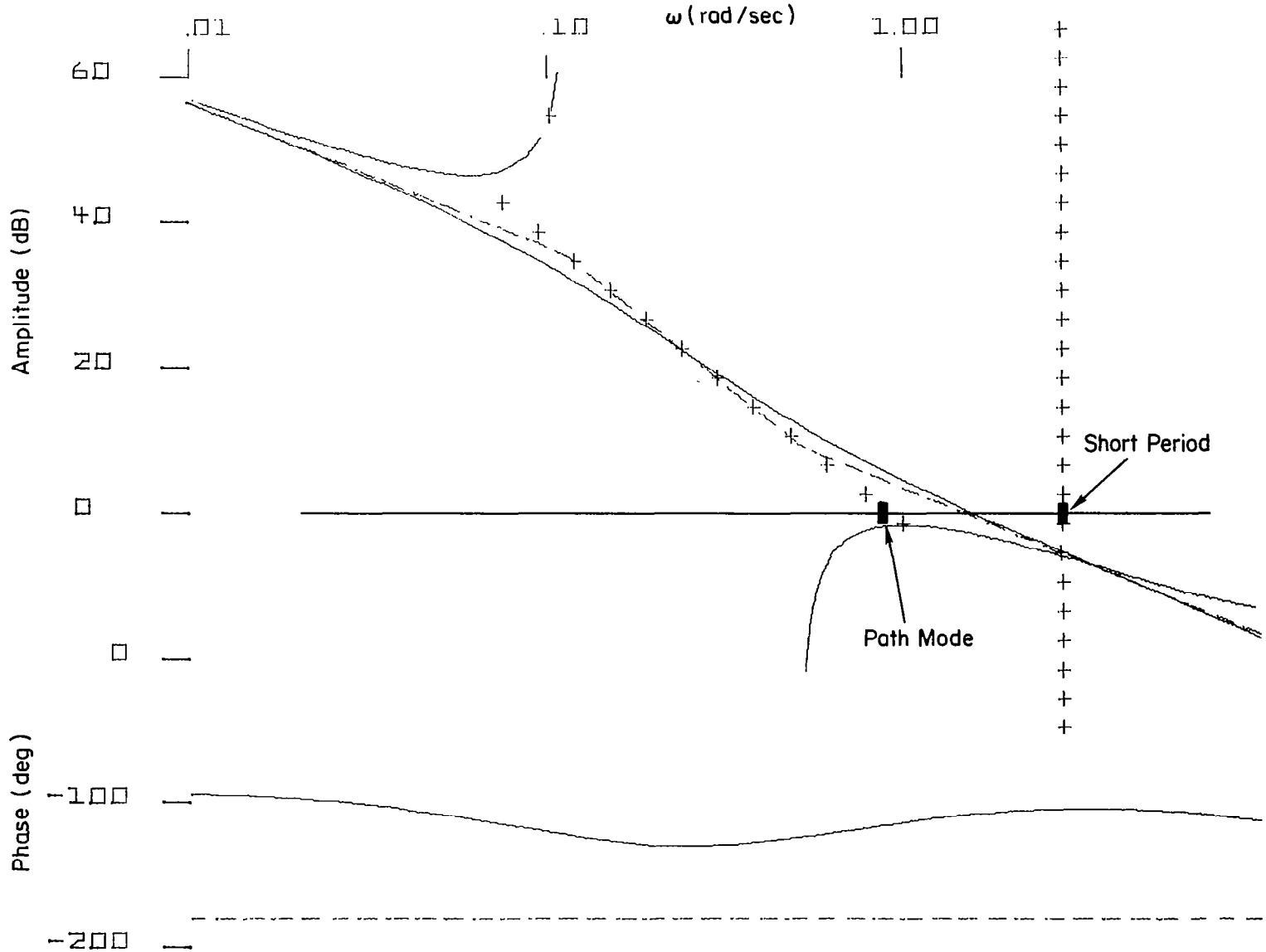

Figure 23. Bode Root Locus for $\dot{h}/\dot{h}_c\big|_{\dot{h}_e,\ \int \dot{h}_e\, dt}$ opened

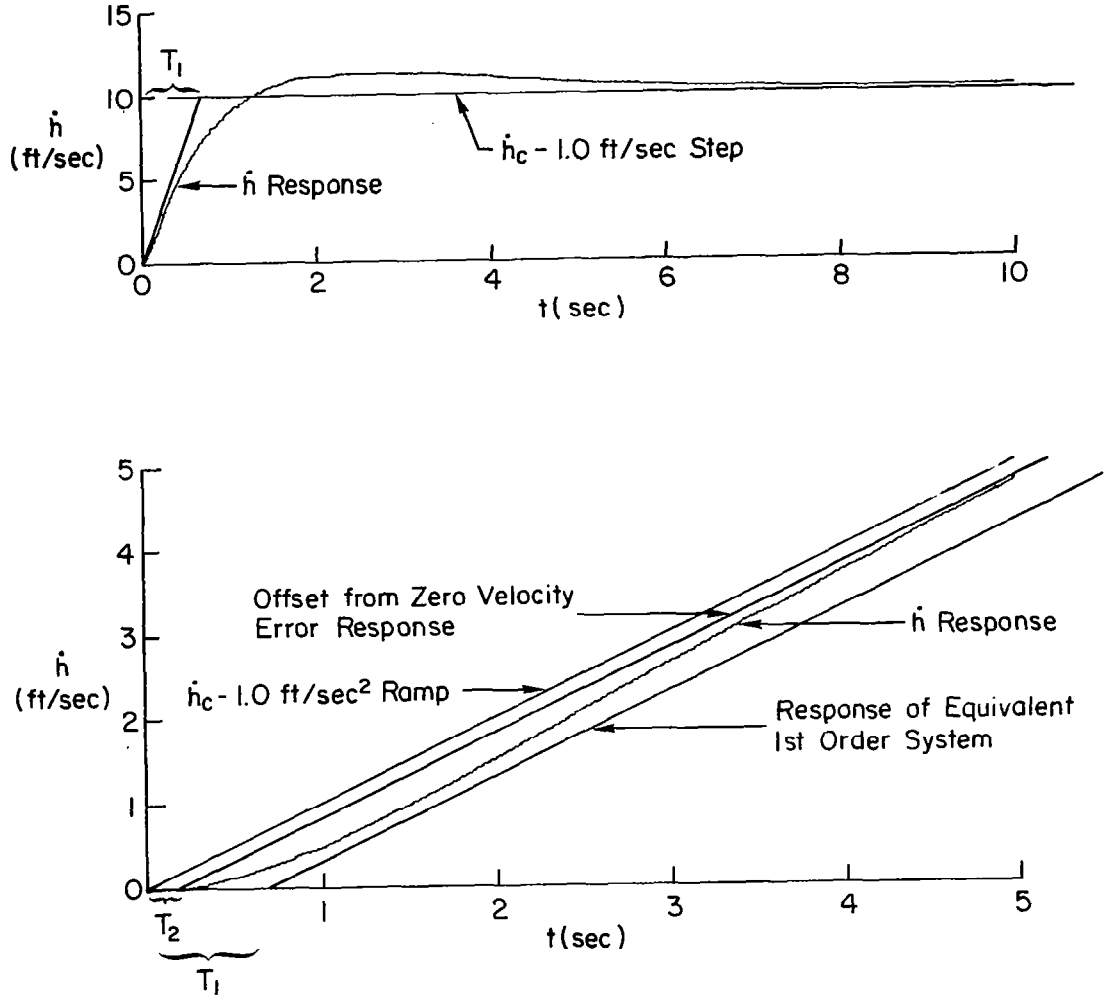

Figure 24. Closed-Loop $\dot{h}/\dot{h}_e$ Time Responses

system, $1.4(T_1 s + 1)$, where $T_1 = 0.7$ sec. At mid frequencies the response exhibits the characteristics of a zero velocity error system, and begins to approach the $\dot{h}_c$ input ramp. But the response never quite reaches the command because the zero velocity error behavior is only active in mid frequencies. Thus, there is ultimately a non-zero offset of the response from the command. This is illustrated by the ramp delayed by T_2 seconds. Again, the characteristics of the $\dot{h}/\dot{h}_c$ ramp response are consistent with those we would predict from the $\dot{h}_e/\dot{h}_c$ frequency in the frequency domain.

The command-following properties of the primary variables can also be examined using the rms levels of the states, outputs and controls in response to process and measurement noise. These are presented in Table 46. Notice, for example, that the rms levels of $\dot{h}_c$ and $\dot{h}$ are approximately equal ($\dot{h}_c = 1.0$ ft/sec, $\dot{h} = 1.01$ ft/sec), which corroborates the command following behavior gleaned from both the frequency domain (Fig. 21) and the time domain (Fig. 24). The ability of this system to suppress error can also be illustrated by comparing the rms level of $\dot{h}_c$ and $\dot{h}_e$ ($\dot{h}_c = 1.0$ ft/sec), $\dot{h}_e = 0.259$ ft/sec). The rms level of error is approximately one-fourth of the rms command input, which is expected in light of our previous observations regarding $\dot{h}_e/\dot{h}_c$ in the frequency domain.

Considerations of the error suppression character of the rate-of-climb loop lead naturally to an investigation of the system response to gust disturbances. As a general rule of thumb the design should be indifferent to gust disturbances, in order for the control system to perform satisfactorily in actual flight. As stated at the outset, the behavior of the system in the presence of disturbances is fundamentally a function of the bandwidth. As such, the gust suppression question has already been addressed in principle. An example of the $\dot{h}$ behavior in response to longitudinal and normal gusts is presented in Fig. 25. Gust suppression for this particular variable is excellent.

This concludes a detailed example evaluation of the primary variable response. The example used for the rate-of-climb variable showed it to have satisfactory response characteristics in every response. To complete the story, a parallel evaluation of the groundspeed ($\dot{x}$) variable

TABLE 46

RMS RESPONSES TO MEASUREMENT AND PROCESS NOISE

RMS, TOTAL 1			
	1		
2.06	X01	u_g	
	2		
1.71	X02	w_g	
	3		
1.00	X03	$\dot{h}_c$	
	4		
0.742E-01	X06	u	
	5		
1.01	X07	w	
	6		
0.315E-03	X08	q	
	7		
0.153E-02	X09	θ	
	8		
0.494E-01	X10	δ_B	
	9		
0.921E-01	X11	δ_C	
	10		
0.293	X12	$\int \dot{h}_e \, dt$	
	11		
0.186E-02	X13	x_{BAR}	
	12		
0.477E-01	X14	$\int \dot{x}_e \, dt$	
	13		
0.186E-02	E13		Filter States
	14		
6.37	E01		
	15		
39.3	E02		

RMS, OUTPUT+CONTROLS 1			
	1		
1.01	HD	$\dot{h}$	
	2		
0.315E-03	Q	q	
	3		
0.153E-02	TH	θ	
	4		
0.494E-01	DB	δ_B	
	5		
0.921E-01	DC	δ_C	
	6		
0.259	HDE	$\dot{h}_e$	
	7		
0.293	HDI	$\int \dot{h}_e \, dt$	
	8		
0.530E-02	XD	$\dot{x}_e$	
	9		
0.477E-01	XDI	$\int \dot{x}_e \, dt$	
	10		
1.17	AOA	α	
	11		
2.05	ASE	u_{AS_e}	
	12		
0.466E-01	DBD	$\dot{\delta}_B$	
	13		
0.255	DCD	$\dot{\delta}_C$	

```
    CASE:  UH1H HOVER 122LONG 31-JAN-79 ALL LOOPS CLOSED
FLOATING UNDERFLOW       PC=036035

  DENOMINATOR:

     1.0000
    ( .10195     ) ( .31507     ) ( .33300     ) ( .33595     )
    ( .50520     ) ( 15.614     ) ( 25.716     ) ( 25.726     )
    (( .92313     , .90723     , .83748     , .34882     ))
    (( .67390     , 2.7741     , 1.8692     , 2.0498     ))
    < 119.79     >
FLOATING UNDERFLOW       PC=036035


  NUMERATOR:   HD/ UG   FILE NAME?  HDUG.2CL
   NEW FILE

    -.98613E-01
    ( .00000     ) ( .16125     ) ( .32805     ) ( .33300     )
    ( .48787     ) ( 25.726     ) ( 42.847     )
    (( .60809     , .40520E-01, .24640E-01, .32167E-01))
    (( .69689     , 2.7215     , 1.8966     , 1.9519     ))
    <-.71329E-02>

   EXCESS OR INCORRECT ROOT FOUND
```

Transient Response to -10.0 ft/sec u_g Step Input

$$\frac{\dot{h}}{u_g} = \frac{-.1s(s+42.8)[s^2+2(.61)(.04)s+(.04)^2]}{(s+.336)(s+15.6)(s+25.72)[s^2+2(.923)(.91)s+(.91)^2]}$$

```
    CASE:  UH1H HOVER 122LONG 31-JAN-79 ALL LOOPS CLOSED
FLOATING UNDERFLOW       PC=036035

  DENOMINATOR:

     1.0000
    ( .10175     ) ( .31507     ) ( .33300     ) ( .33595     )
    ( .50520     ) ( 15.614     ) ( 25.716     ) ( 25.726     )
    (( .92313     , .90723     , .83748     , .34882     ))
    (( .67390     , 2.7741     , 1.8692     , 2.0498     ))
    < 119.79     >
FLOATING UNDERFLOW       PC=036035


  NUMERATOR:   HD/ WG   FILE NAME?  HDWG.2CL
   NEW FILE

    -.38580
    ( .00000     ) ( .15158E-01) ( .10198     ) ( .32014     )
    ( .33300     ) ( .33892     ) ( .51520     ) ( 25.726     )
    ( 42.790     )
    (( .63102     , 2.8085     , 1.7722     , 2.1787     ))
    <-.96398E-01>
```

Transient Response to -1.0 ft/sec w_g Step Input

$$\frac{\dot{h}}{w_g} = \frac{-.4s(s+.015)(s+42.79)}{(s+15.6)(s+25.72)[s^2+2(.923)(.91)s+(.91)^2]}$$

Figure 25. Time Responses of $\dot{h}$ to Gust Disturbances

is necessary. Such an investigation was performed, and some of the results appear in Appendix C. Again, satisfactory response was observed, and the groundspeed mode at 0.505 rad/sec provides the dominant behavior.

In the process of these examinations much has been learned about the details of the optimal design. Also, the evaluation has shown that no iterations are needed as far as primary responses are concerned.

2. Secondary Variables

Techniques that were appropriate for the assessment of primary variable responses are again called upon at this stage. The bandwidth is still the single most revealing measure of the secondary variable responses. Referring back to Fig. 19, which depicts the open-loop frequency response for θ/θ_c, we see that the bandwidth (equal to about ω_c, due to the stretch of -20 dB/decade slope) is 2.3 rad/sec, quite close to the design goal of 2.0 rad/sec. While secondary variable bandwidth can be used to divide the frequency response into regions of feedback effectiveness and ineffectiveness (similar to the primary variable assessment), the expected forms for response/command and error/command frequency responses are changed. This is because the secondary variables are usually inner loops and do not have explicit command input points. For example, in the hover FCS we cannot command pitch attitude (θ); the closed-loop design requires us to command groundspeed ($\dot{x}$) instead. If, however, the groundspeed loop should fail (due to component degradation, say) it would then be imperative that θ/θ_c exhibit good command following, error and gust suppression and transient response behavior, since the system would <u>have</u> to be commanded by θ_c. This θ_c system is also a possibility as a primary system in its own right. We will have occasion to discuss both these events in more detail later.

For now, we will rely on the Bode root locus plot of Fig. 20 to show that the short-period mode, which is closest to ω_c, dominates the θ response. This is hardly unexpected, since the θ and q closures provided the improved damping and stiffening for the short-period mode ($\zeta_{sp}|_{OL} = 0.26279$, $\omega_{sp}|_{OL} = 0.92797$; $\zeta_{sp}|_{CL} = 0.6738$, $\omega_{sp}|_{CL} = 2.7741$). Reference 10, pages 80-87 also indicates a graphical method for determining the dominant mode by plotting the modal response coefficients as time vectors.

With the dominant mode exposed, we proceed to an investigation of the transient response characteristics. Again, the absence of an explicit closed-loop θ_c command point makes indicial and ramp responses to commands meaningless. The real concern in the evaluation of secondary variable time responses is for motion harmony and favorable (or negligible) coupling between primary and secondary variables. For this reason, Fig. 26 presents the responses of $\dot{h}$, δ_C, θ, $\dot{x}$, and δ_B to a 1.0 ft/sec $\dot{h}_c$ step input. It is clear that θ and $\dot{h}$ are almost totally uncoupled, since an $\dot{h}_c$ input elicits very little response from θ and a quite noticeable response from $\dot{h}$. This phenomenon can actually be explained on the basis of control activity. Since δ_B mainly controls θ while δ_C primarily controls $\dot{h}$, and the controls are almost uncoupled, we expect the θ and $\dot{h}$ responses to be essentially uncoupled as well. This point is addressed in the next subsection.

The same uncoupled behavior of h and θ can be seen in their respective rms responses to process and measurement noise. Table 46 gives the rms θ responses as less than 0.1 deg for a 1.0 ft/sec rms $\dot{h}_c$ level. This further confirms the high degree of h-θ decoupling.

There is also interest in the response of secondary variables to gust inputs. Figure 27 reveals that the θ inner loop is quite indifferent to gust disturbances. This is desirable, although not really imperative, again because θ is not a controlled variable. But if the $\dot{x}$ loop should fail or be switched out, it is reassuring to know that this inner loop exhibits good gust suppression.

The secondary variable θ has demonstrated satisfactory response character during the several stages of its assessment. One important difference in the methods used to evaluate primary and secondary variable responses arose in connection with command following and error suppression. Unlike the primary variables, the secondary variables have no meaningful command points. We must therefore depend on open-loop transfer function characteristics to divulge the dominant mode(s). In addition, the concerns in the time domain center around motion harmony and the extent of inter-variable coupling (or decoupling) rather than rapid and accurate response to commands.

$$\frac{\dot{h}}{\dot{h}_c} \doteq \frac{40.908(s+.52)}{(s+25.72)[s^2+2(.923)(.91)s+(.91)^2]}$$

$$\frac{\delta_c}{\dot{h}_c} \doteq \frac{4.157(s+.38)(s+.47)(s+.55)}{(s+.51)(s+25.72)[s^2+2(.923)(.91)s+(.91)^2]}$$

$$\frac{\theta}{\dot{h}_c} \doteq \frac{-.0007(s+.37)[s^2+2(.58)(.1)s+.1^2]}{\times\,[s^2+2(.9)(6.9)s+(6.9)^2][s^2+2(.999)(16.3)s+(16.3)^2]} \times [s^2+2(.923)(.91)s+(.91)^2][s^2+2(.67)(2.77)s+(2.77)^2]$$

$$\frac{\dot{x}}{\dot{h}_c} = \frac{-.8s(s+.39)(s-.577)[s^2+2(.59)(1.8)s+(1.8)^2]}{(s+.1)(s+.51)(s+25.72)} \times [s^2+2(.923)(.91)s+(.91)^2][s^2+2(.67)(2.77)s+(2.77)^2]$$

$$\frac{\delta_B}{\dot{h}_c} = \frac{-.72(s-2.2)[s^2+2(.96)(.5)s+(.5)^2]}{\times\,[s^2+2(.74)(2.0)s+(2.0)^2]} \times [s^2+2(.67)(2.77)s+(2.77)^2]$$

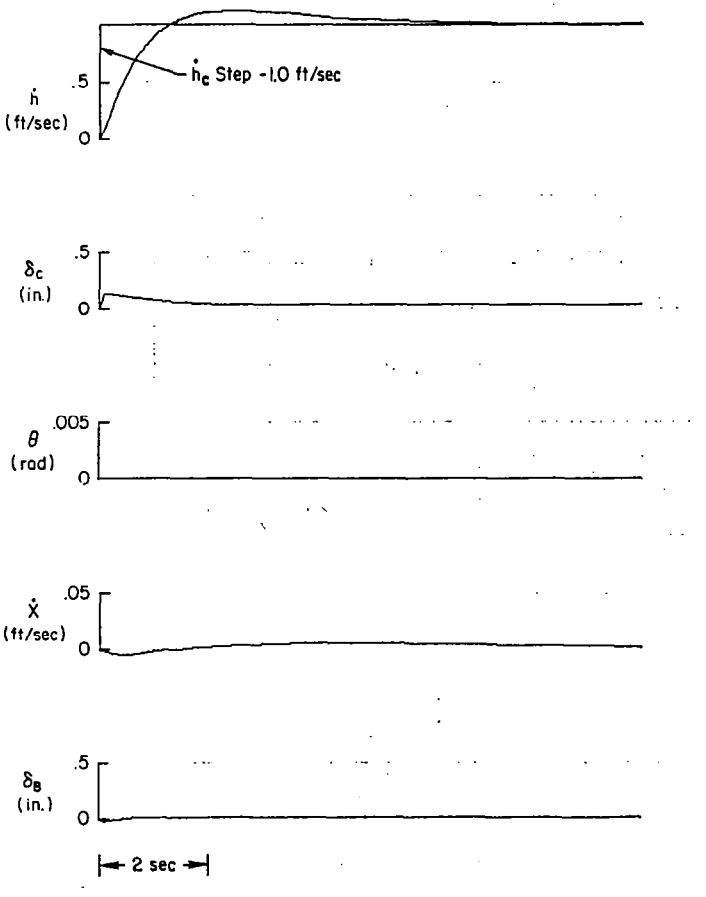

Figure 26. Transient Responses of Several Variables to $\dot{h}_c$ Step Input

```
CASE:  UH1H HOVER 122LONG 31-JAN-79 ALL LOOPS CLOSED

DENOMINATOR:

   1.0000
 ( .10195     ) ( .31507     ) ( .33300     ) ( .33595     )
 ( .50520     ) ( 15.614     ) ( 25.716     ) ( 25.726     )
 (( .92313     , .90723     , .83748     , .34882     ))
 (( .67390     , 2.7741     , 1.8692     , 2.0498     ))
 < 119.79     >

NUMERATOR:   TH/ WG   FILE NAME?  THWG.2CL
 NEW FILE

   .38000E-02
 ( .10290     ) ( .33300     ) ( .33300     ) ( 25.726     )
 (( .99403     , .34557     , .34351     , .37710E-01))
 (( .92188     , .91517     , .84369     , .35460     ))
 (( .77874     , 28.439     , 22.302     , 17.966     ))
 < .91509E-01>
```

Transient Response to -1.0 ft/sec w_g Step Input

$$\frac{\theta}{w_g} \doteq \frac{.004[s^2 + 2(.78)(28.6)s + (28.6)^2]}{(s + .315)(s + .51)(s + 15.6)(s + 25.7)[s^2 + 2(.67)(2.77)s + (2.77)^2]}$$

```
CASE:  UH1H HOVER 122LONG 31-JAN-79 ALL LOOPS CLOSED

DENOMINATOR:

   1.0000
 ( .10195     ) ( .31507     ) ( .33300     ) ( .33595     )
 ( .50520     ) ( 15.614     ) ( 25.716     ) ( 25.726     )
 (( .92313     , .90723     , .83748     , .34882     ))
 (( .67390     , 2.7741     , 1.8692     , 2.0498     ))
   119.79

NUMERATOR:   TH/ UG   FILE NAME?  THUG.2CL
 NEW FILE

  -.19000E-02
 ( .89119E-01) ( .33300     ) ( .33300     ) ( 7.5257     )
 ( 25.724     ) ( 38.150     )
 (( .50519     , .24630     , .12442     , .21256     ))
 (( .92523     , .39866     , .83146     , .34096     ))
  -.67934E-02>
```

Transient Response to -10.0 ft/sec u_g Step Input

$$\frac{\theta}{u_g} \doteq \frac{-.002(s + 7.5)(s + 38.)[s^2 + 2(.51)(.25)s + (.25)^2]}{(s + .315)(s + .51)(s + 15.6)(s + 25.7)[s^2 + 2(.67)(2.77)s + 2.77)^2]}$$

Figure 27. Closed-Loop Transient Response of θ to Gust Inputs

3. Control Activity

The third area of response assessment has an emphasis different from the first two areas. Since the control actuation bandwidths are at high frequency (25.7 rad/sec for the UH-1H example), the command following, error suppression and time history characteristics are fairly uninteresting. Instead, the evaluation of control activity centers around the following two considerations: the level of control activity required by the controller and the extent of control cross-coupling.

The question of appropriate control activity levels was first addressed during the regulator synthesis. As the final step, a measure of control activity (positive zero-crossing rate) was used to ascertain whether or not the cost function weights on $\dot{\delta}_B$ and $\dot{\delta}_C$ in R_R were appropriate. As it turned out, the main rotor collective control point was too active, and thus the cost function weighting on $\dot{\delta}_C$ was increased by an order of magnitude. This 10:1 ratio of $\dot{\delta}_C$:$\dot{\delta}_B$ discourages use of the δ_C control point in the regulator synthesis, and positive-going zero crossing rate for δ_C showed the desired decrease.

There are several other measures of control activity level which can be used at this point in the response assessment. These are illustrated in Table 47. The first two measures are the rms levels of the control position and control rate. These values can be compared to the limiting control capabilities of the particular aircraft. For example, the UH-1H longitudinal cyclic has a 13.0 in. maximum travel, while the main rotor collective maximum travel is 10.7 in. We can see that the rms levels of δ_B and δ_C are well below the corresponding maximum capabilities. Thus, if the assumed inputs are realistic estimates the actual control activity should be moderate.

Table 47 also shows the number of axis crossings per second (N_O), the number of positive-going axis crossings per second [$N_L(0)$], and the number of positive exceedances of 10 percent full travel per second [$2N_L(.1th)$]. The first two indicate the level of monitoring activity required of the pilot in supervisory or, for that matter, the manual activity needed if the pilot were to take over from the automatic system. These are

TABLE 47. CONTROL ACTIVITY

Axis crossings per second $N_o = \frac{1}{\pi} \frac{\sigma_{\dot{x}}}{\sigma_x}$

Positive exceedance of x per second $N_L(x) = \frac{N_o}{2} e^{-x^2/2\sigma_x}$

$\sigma_{\dot{x}}$ = rms of control rate

σ_x = rms of control position

	Longitudinal Cyclic, DB	Main Rotor Collective, DC
σ_x (in.)	0.0494	0.0921
$\sigma_{\dot{x}}$ (in./sec)	0.0466	0.255
N_o (1/sec)	0.300	0.881
$N_L(0)$ (1/sec)	0.150	0.441
$N_L(.1th)$[a] (1/sec)	5.6×10^{-9}	8.8×10^{-4}

[a]Positive exceedance of 10 percent full travel per second (for DB, 10 percent full travel = 1.30 in., for DC, 10 percent full travel = 1.07 in.)

considerations which come under the heading of "handling qualities." The $N_L(.1th)$ measure can be used in a probabilistic sense to determine the average time between exceedances of 10 percent full travel $[1/2N_L(.1th)]$.

Up to this point, the investigation of control response has not addressed the extent of control cross-coupling. Decoupled controls are desirable in that they permit control of variables from a single control point. This simplifies the controller both from an implementation and a performance standpoint. There are many quantities that reveal the nature of control cross-coupling; two will be presented here. The controller transfer functions that involve control position and rate are given in Table 48. The transfer function approximations are divided into low, mid and high frequency regions. It will be recalled that DB and DC are the measurement vector components corresponding to best estimates of δ_B and δ_C. As such, they are <u>not</u> the integrals of the control variables $\dot{\delta}_B$ (DBD) and $\dot{\delta}_C$ (DCD). Accordingly, to avoid confusion, the controller transfer functions in Table 48 are referred to as DBD/DB, etc.

The low, mid and high frequency approximations for DBD/DB, and the mid and high frequency approximations for DCD/DC are essentially pure gains.

This is the expected result of designing the actuators as high gain inner loops. The low frequency washout present in DCD/DC [i.e., $27s/(s+15.6)$ in Table 48] is undesirable in a physical installation (e.g., for actuator rigidity considerations) and may be considered an anomaly of the optimal design process.

The cross-coupled transfer functions, $\dot{\delta}_B/\delta_C$ and $\dot{\delta}_C/\delta_B$, illustrate a second point, i.e., that the controls are essentially decoupled for the frequency region above 100 rad/sec. In this frequency band, both transfer functions revert to low gain quantities which may be neglected. In an upcoming section we will discuss the advantage of this control decoupling, namely, it provides a means of simplifying controller implementation.

A further confirmation of the cross-coupled control characteristics is found by referring back to the indicial transient response plots in Fig. 26. The time responses of five variables to a 1.0 ft/sec $\dot{h}_c$ step input were first used to examine the harmony of the primary and secondary variables. These time responses also illustrate the degree of control decoupling. For a step $\dot{h}_c$ we see a corresponding δ_C response, in the positive direction. Meanwhile, no δ_B response is evident. From this we can conclude that δ_C provides the $\dot{h}$ control, and that δ_B and δ_C are essentially uncoupled. Similar time responses to, say, an $\dot{x}_c$ would show corresponding responses for $\dot{x}$, θ and δ_B, illustrating that δ_B is used in $\dot{x}$ and θ control and again that δ_B and δ_C are not significantly cross-coupled.

This concludes our discussion of the design's response character. We have divided the preceding discussion into three areas: primary controlled variable responses, secondary variable responses and control responses. The primary variables were characterized by good command following, error suppression, indifference to gusts, and smooth, well-damped, minimum-tailed transient responses. For each primary variable we identified the mode that dominates that variable's response. The assessment of the secondary variable's responses was mainly concerned with motion harmony and coupling among the primary and secondary variables, and identifying that mode for each variable which dominates the response. Finally, the evaluation of the control activity centered on the levels of control activity and the extent of control cross-coupling.

TABLE 48. CONTROLLER TRANSFER FUNCTIONS AND APPROXIMATIONS

CASE: UH1H HOVER 122LONG 2-FEB-79 CONTROLLER TRANSFER FUNCTIONS

DENOMINATOR:

1.0000
(.31537) (.33300) (15.614)
< 1.6383 >

NUMERATOR: DBD/ DB

-29.879
(.18186) (.33300) (15.428)
<-27.917 >

NUMERATOR: DCD/ DB

.51744E-02
(-.11656) (.33300) (-2064.8)
< .41471 >

NUMERATOR: DBD/ DC

.51781E-01
(.29977) (.33300) (-4127.1)
<-21.332 >

NUMERATOR: DCD/ DC

-27.008
(-.94888E-01) (.33300) (.33773)
< .28821 >

	LOW FREQUENCY APPROXIMATION ($0.34 \leq \omega \leq 15.6$ rad/sec)	MID FREQUENCY APPROXIMATION ($15.6 \leq \omega \leq 2064.$ rad/sec)	HIGH FREQUENCY APPROXIMATION ($2064. \leq \omega$)
$\frac{DBD}{DB}$	$\frac{-29.879(s+15.43)}{(s+15.6)}$		
$\doteq$	-29.553	-29.879	-29.874
$\frac{DBD}{DC}$	$\frac{.052(s-4127.1)}{(s+15.6)}$	$\frac{.052(s-4127.1)}{s}$	
$\doteq$	-13.757	$-214.6/s$	$.052$
$\frac{DCD}{DB}$	$\frac{.0052(s-2064.8)}{(s+15.6)}$	$\frac{.0052(s-2064.8)}{s}$	
$\doteq$	$-.685$	$-10.74/s$	$.0052$
$\frac{DCD}{DC}$	$\frac{-27.008.5}{(s+15.6)}$		
$\doteq$	$-1.73s$	27.008	27.008

C. SENSITIVITY

The design assessment, in addressing questions of stability and response, has exposed performance characteristics only for the system as modeled and only within the intended operating environment. It is equally important, however, to analyze the effectiveness of the design in various off-nominal situations. Thus, we wish to examine the system's sensitivity to airframe variations, sensor thresholds, major component failure and the like. Following Table 44, these examinations are divided into three areas:

- Sensitivity of key response modes.
- Sensitivity to parasitic nonlinearities.
- Graceful degradation.

The next sections discuss each area in turn.

1. Key Response Modes

The assessment of system stability and response led to identification of some key response modes for each variable: the crucial mode, which becomes unstable first; and the dominant mode, which shapes most of a variable's response. These may or may not be the same mode. Here we are concerned with the sensitivity of these key modes to off-nominal conditions, component tolerances and variations, and state equation uncertainties, nonlinearities and simplifications. It is possible, of course, to perform a sensitivity analysis on all modes of each variable. But the very fact that we are able to identify key modes means that other modes are less important and also less sensitive. Thus, their assessment may be deferred until a detailed design evaluation is undertaken.

Because "tolerances," "variations," "off-nominal conditions," etc., all tend to be small, we can enlist first-order gain and parameter sensitivities, which derive from small perturbation considerations, to quantify the key response mode sensitivities. First-order gain sensitivities compute incremental changes in closed-loop pole locations due to incremental changes in open-loop gains. This gain sensitivity is equal to the

negative of the modal response coefficient for the particular closed-loop root, and is a measure of the slope along a root locus. As such, it is meaningful to plot the sensitivities on a root locus, as shown in Fig. 28. Here the first-order sensitivity of the short-period mode to incremental K_θ changes is plotted on the θ/θ_c root locus. Remember that the short-period mode is the critical mode for the θ loop. Also listed at the bottom of Fig. 28 are the modal response coefficients for every other root of θ/θ_c. In general, the incremental gain sensitivities for these other roots are quite small, reinforcing our assertion that only the key response modes have significant sensitivities.

First-order gain sensitivities are useful in evaluating the effect of changing the closed-loop gain upon the location of the closed-loop roots. If, however, we wish to assess the effect of changing parameters of the controlled element upon the root locations, we can use parameter sensitivities. The software (Ref. 23) can be used to compute the sensitivity of each regulator eigenvalue to incremental changes in the F, G and C matrices. This reflects the sensitivity of the closed-loop roots to any uncertainties in the various stability derivatives, for example. Figure 27 illustrates the parameter sensitivity of the path mode for the $\dot{h}$ variable. The lower portion of the table is the entire matrix of sensitivities of the path mode (the dominant mode for $\dot{h}$) to changes in the components of the F matrix. These sensitivities are normalized by the path mode eigenvalue, and are expressed as a magnitude and phase (in degrees). We can plot element F(6,5) (outlined in the sensitivity matrix) on a root locus for $\dot{h}_e/\dot{h}_c$, to indicate the direction in which the path mode would move for an incremental change in the M_w stability derivative. (Table B-2 in Appendix B shows that the element F(6,5) is the M_w derivative.) Each non-zero element in this sensitivity matrix could be plotted as a vector on the root plot in the complex plane to produce a graphical representation of the parameter sensitivities of the system design. This provides a means to account for undertain specification of the controlled element, and the effect of this uncertainty upon the closed-loop roots.

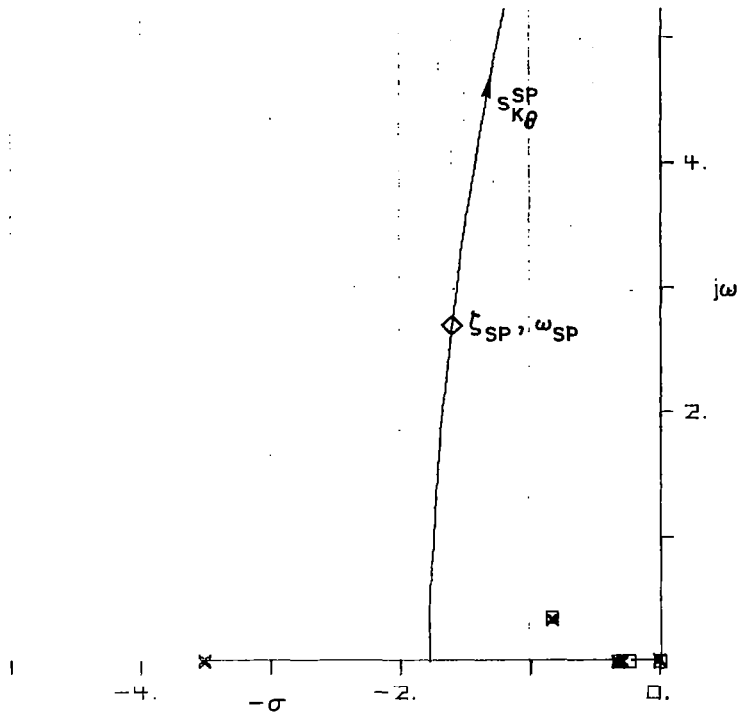

First-Order Closed-Loop Poles	Modal Response Coefficients = $-S_K$
.00000000E+00	.00000000E+00
.36771000E-04	-.12465728E-03
.23483000E+00	.54222716E-02
.33283000E+00	.12629187E-02
.33300000E+00	-.52225129E-03
.15611000E+02	.38109978E-01
.25716000E+02	.16554270E-02
.26961000E+02	.37335695E+00

	Second-Order Closed-Loop Roots			Modal Response Coefficients			First-Order Gain Sensitivities	
	ζ	ω	Re	Im	Mod	∠	Mod	∠
SP	.50867E+00	.31452E+01	-.21192E+00	-.18526E+01	.18647E+01	263.474	1.8647	83.47
Path	.92365E+00	.90563E+00	.26192E-02	.30844E-02	.40464E-02	49.663	0.00405	229.66

Figure 28. First-Order Gain Sensitivities for θ Loop

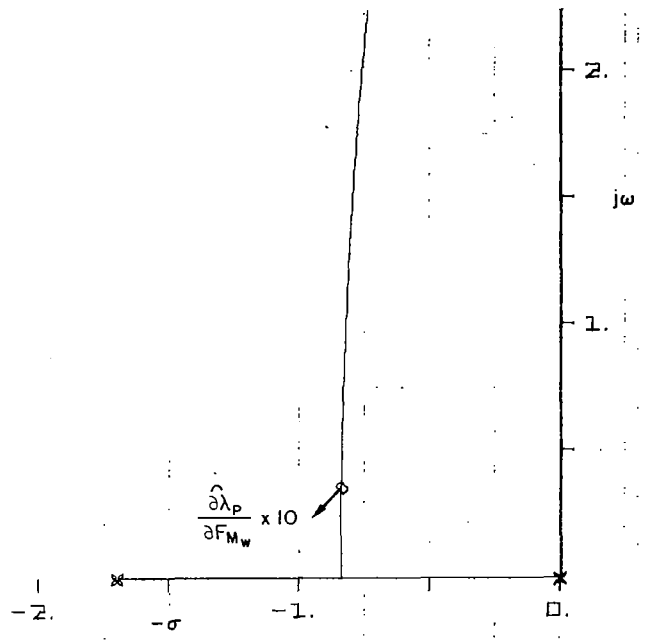

NORMALIZED F MATRIX SENSITIVITY TO EIGENVALUE : -0.837 0.349

1 X01	2 X02	3 X03	4 X06	5 X07	6 X08	7 X09	8 X10	9 X11	10 X12	11 X13	12 X14	
0.0000 90.0	0.0000 90.0	0.0000 90.0	0.0000 90.0	0.0000 90.0	0.0000 90.0	0.0000 90.0	0.0000 90.0	0.0000 90.0	0.0000 90.0	0.0000 90.0	0.0000 90.0	1 X01
0.0000 90.0	0.0000 90.0	0.0000 90.0	0.0000 90.0	0.0000 90.0	0.0000 90.0	0.0000 90.0	0.0000 90.0	0.0000 90.0	0.0000 90.0	0.0000 90.0	0.0000 90.0	2 X02
0.0000 90.0	0.0000 90.0	0.0000 90.0	0.0000 90.0	0.0000 90.0	0.0000 90.0	0.0000 90.0	0.0000 90.0	0.0000 90.0	0.0000 90.0	0.0000 90.0	0.0000 90.0	3 X03
0.0000 90.0	0.0000 90.0	0.0000 90.0	0.154E-02 -16.3	0.496E-02 167.	0.298E-01 -51.2	0.749 -3.57	1.03 -94.8	0.629E-02 161.	0.0000 90.0	0.131 -178.	0.0000 90.0	4 X06
0.0000 90.0	0.0000 90.0	0.0000 90.0	0.654E-02 -129.	0.117E-01 -126.	0.191E-01 -164.	0.793E-02 -116.	0.476E-01 152.	0.135E-01 -131.	0.0000 90.0	0.603E-02 69.2	0.0000 90.0	5 X07
0.0000 90.0	0.0000 90.0	0.0000 90.0	0.182E-01 51.4	0.154E-01 -124.	0.258 18.4	0.0000 90.0	3.65 -25.2	0.662E-03 -129.	0.0000 90.0	0.462 -108.	0.0000 90.0	6 X08
0.0000 90.0	0.0000 90.0	0.0000 90.0	0.0000 90.0	0.0000 90.0	3.81 138.	0.0000 90.0	0.0000 90.0	0.0000 90.0	0.0000 90.0	0.0000 90.0	0.0000 90.0	7 X09
0.0000 90.0	0.0000 90.0	0.0000 90.0	0.0000 90.0	0.0000 90.0	0.0000 90.0	0.0000 90.0	0.0000 90.0	0.0000 90.0	0.0000 90.0	0.0000 90.0	0.0000 90.0	8 X10
0.0000 90.0	0.0000 90.0	0.0000 90.0	0.0000 90.0	0.0000 90.0	0.0000 90.0	0.0000 90.0	0.0000 90.0	0.0000 90.0	0.0000 90.0	0.0000 90.0	0.0000 90.0	9 X11
0.0000 90.0	0.0000 90.0	0.0000 90.0	0.484E-02 -120.	0.308E-01 62.7	0.0000 90.0	0.614E-02 -108.	0.0000 90.0	0.0000 90.0	0.0000 90.0	0.0000 90.0	0.0000 90.0	10 X12
0.0000 90.0	0.0000 90.0	0.0000 90.0	0.0000 90.0	0.0000 90.0	0.425E-01 19.4	0.0000 90.0	0.0000 90.0	0.0000 90.0	0.0000 90.0	0.553E-02 72.6	0.0000 90.0	11 X13
0.0000 90.0	0.0000 90.0	0.0000 90.0	0.365E-01 161.	0.116E-02 164.	0.0000 90.0	0.0000 90.0	0.0000 90.0	0.0000 90.0	0.0000 90.0	0.0000 90.0	0.0000 90.0	12 X14

Figure 29. Parameter Sensitivity of Path Mode to Changes in M_w, for h

We have discussed some possible techniques for evaluating first-order sensitivities in order to assess the behavior of the key response modes due to various off-nominal conditions. In particular, gain sensitivities are useful in computing incremental changes in closed-loop root location due to changes in closed-loop gains, while parameter sensitivities reveal the effect of controlled element parameter variations upon closed-loop root location. Only two key modes were presented as examples; in the course of the assessment it is necessary to examine the sensitivity characteristics of all key modes.

2. Parasitic Nonlinearities

In constructing a linear set of state and output equations for optimal controller synthesis, various nonlinearities were neglected. The assessment of key response mode sensitivity can be useful to quantify the first-order effects of some of these neglected nonlinearities. In a detailed design evaluation, however, it is necessary to have a more complete understanding of these parasitic nonlinearities and their effect upon system performance. Because this is a detailed design task, we will give only an outline of the assessment procedure here.

One basic problem arises when certain types of nonlinearities produce limit cycle behavior. The most common types of parasitic nonlinearities are threshold-like phenomena in the sensor and actuation/load elements. These can cause problems in two ways:

- If one of the control points has a higher threshold than the others, then for some small region in the control space the feedback to that control point is not active. For the UH-1H, suppose that the threshold for δ_B is larger than that for δ_C. Then for some input levels, only the δ_C control is active.

- If each of the sensors has a different threshold, then in some region of the control space certain sensors will not be sending useful signals. Thus, although all control points may be active, several of the sensors may have outputs equal to zero and the system is simply incomplete, possibly even unstable in the threshold region.

As an example, suppose that the $\dot{h}_e$ and $\int \dot{h}_e \, dt$ sensors have higher thresholds than all other UH-1H sensors. Examining the root locus and transfer function for the θ closure (Fig. 30), we see that, for some gain values, the θ closure has right-half plane roots when the $\dot{h}_e$ and $\int \dot{h}_e \, dt$ loops are open due to thresholds. This would lead to low-amplitude limit cycle behavior.

It is therefore imperative to examine possible combinations of open and closed loops in order to identify those which exhibit oscillatory behavior. The use of Bode plots in conjunction with describing function techniques (Ref. 26) serves to estimate the resulting limit cycle amplitudes. Of course, the details of the limit cycle itself are dependent on the nature of the nonlinearity. We have given an example of the problems that occur due to differential control point or sensor thresholds. There are two additional categories of parasitic nonlinearities that should also be considered in practical flight control systems: hysteresis, due to cable/pushrod-Coulumb friction interations; and valve friction operation within the actuator's closed loops. These are discussed in greater detail in Ref. 28.

3. Graceful Degradation

Above we have examined the problem of design sensitivity on a small scale (that is, the sensitivity to relatively small effects such as off-nominal conditions and parasitic nonlinearities). Here we consider major component failure, to ascertain whether the system performance will degrade gracefully. This is a major concern in the operating environment, and should be a consideration even within the preliminary design phase.

As one might expect, the techniques used for assessing graceful degradation depend on the controller architecture. Here we consider two possible controller mechanizations, which comprise two limiting cases. The first is a single thread system, wherein the controller gains are fixed and satisfactory performance is obtained only when all elements are working correctly. These are typical of the majority of flight control systems today. However, when fail-safe or fail-operational requirements are

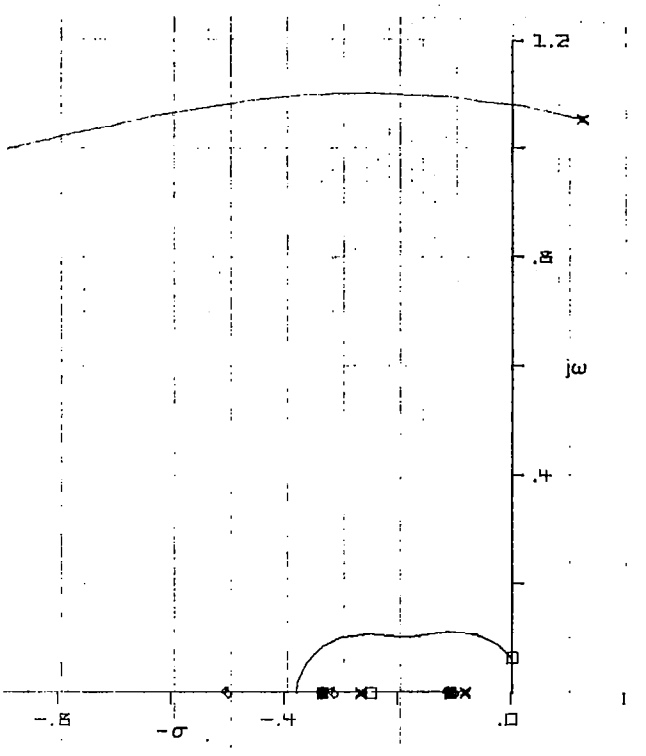

CASE: UH1H HOVER 122LONG 2-FEB-79 HDE,HDI,THE OPENED LOOP

DENOMINATOR:

```
  1.0000
( .00000    ) ( .81179E-01) ( .10995    ) ( .26561    )
( .33300    ) ( .33312    ) ( 5.0735    ) ( 15.563    )
( 25.269    ) ( 27.286    )
((-.11902    , 1.0633    ,-.12656    , 1.0558    ))
< 16.189    >
```

NUMERATOR: TH/VTH

```
  -251.70
( .00000    ) ( .10900    ) ( .24838    ) ( .33300    )
( .33300    ) ( 15.943    ) ( 27.302    )
((-.32679E-01, .64265E-01,-.21001E-02, .64230E-01))
<-1.3584    >
```

$$\frac{\theta}{V_\theta} \doteq \frac{-251.7[s^2 + 2(-.033)(.064)s + (.064)^2]}{(s + .08)(s + 5.07)(s + 25.27)[s^2 + 2(-.12)(1.06)s + (1.06)^2]}$$

Figure 30. Locus of Roots for θ Closure with $\dot{h}_e$ and $\int \dot{h}_e\, dt$ Loops Opened

present, modern FCS mechanizations use two-, three-, or four-fold ("threads") redundancy.

Considerations for a single-thread design's graceful degradation are quite straightforward, and in fact very similar to techniques used in determining the design's sensitivity to parasitic nonlinearities. We noted that for some small regions in the control space certain control points or sensors could be inoperative due to differential trehsolds. In an extension of this idea, we can identify some large regions of the control space wherein control points or sensors are imperative due to component failure. Thus, the evaluation of the effects of differential thresholds and component failure in single-thread installations can be conducted in parallel. For the former, the differential thresholds and the control region affected are usually small, whereas for the latter the differential thresholds are infinite and the control region affected is quite large. The analysis is identical, however.

The real drawback in assessing a single-thread architecture is the enormity of the task. It is necessary to make an exhaustive catalog of likely failure possibilities and examine each in detail. For a multiply-redundant system, the necessary work is far greater still, if fail-operative performance is to be guaranteed.

At the other extreme from the single-thread system is a system employing an adaptive filter-observer controller architecture. Such a controller is automatically reconfigured by an onboard computer if one or more components should fail. It is the computer's job to detect the failure and recompute the necessary controller gains, similar to the controller synthesis discussed in Chapter IV. For this type of mechanization the workload in analyzing graceful degradation is substantially reduced. The system is easily assessed using the software developed in this work; the task consists of systematically deleting sensors and control points, and using the optimal controller software to synthesize the resulting controller gains. Each of these "degraded" designs must be subjected to stability and response assessment, in order to quantify the effects of degradation. This approach does not take into account the software and

hardware which must detect failures and recompute controller gains, nor does it account for transients in the process. The method will, however, provide an upper bound on degraded system performance. The matter of system behavior in the transient region during the controller recomputation is perhaps best evaluated using the actual controller.

4. Concluding Remarks on System Property Assessment

The assessment of system properties illustrated here has been organized so that a logical progression exists from simple to complex, preliminary design to detailed design, qualitative to quantitative. In the process a much clearer understanding of the essential nature and behavior of the optimal controller has been gained. In fact, there has been a quantum increase in our understanding of the optimal controller synthesized in Chapter IV; there we had only four matrices that provided information about the design (A_F, B_F, C_F and D_F). Now we are equipped with much more insight into the stability, response and sensitivity characteristics of the system. The remainder of this chapter is devoted to assessing certain properties that are peculiar to the controller.

In the following sections we hope to better define and improve our understanding of the optimal controller itself. Attention will be focused first on the gain levels produced by the design. Our concern here lies both with too high and too low gain values — with control saturation as well as minimum increment of control. These extremes, taken together, provide measures of how well the controller uses the available dynamic range of a channel. The second property to be considered relates to the sensor array. In this connection we desire to exercise hardware and software economy in the sensor/equalization complex and to evolve a controller that will perform satisfactorily over a wide range of operating environments. The discussion of these issues is not meant to be exhaustive, but it does cover those controller properties that should be evaluated in the preliminary design phase.

D. GAIN LEVELS

The controller gain levels provide some important insight into the behavior of the FCS. Obviously, we are interested in both limiting cases:

- What is the magnitude of each output that corresponds to saturation of each control point?
- What is the magnitude of each output that corresponds to the minimum increment of control for each control point?

Saturation levels permit us to identify boundaries in the control space which separate the space into regions where control can be exerted to modify the basic vehicle dynamics. Outside of these regions, the dynamic performance characteristics are those of the vehicle alone. On the other hand, the minimum increment of control establishes the control precision. The levels of the output variables which correspond to the minimum increment define an inner region of the control space wherein control is effectively not present. Inside this region the system dynamics are, again, those of the vehicle alone.

The assessment of gain levels involves a tradeoff between too high gains, which cause the control boundaries to be reached with small inputs (bang-bang control) and too low gains which require large inputs to even force entry into the available control space. The level required to saturate a control also depends on the type of actuators; full authority parallel servos generally saturate at a larger percentage of maximum travel than restricted authority series servos. Regardless, the first step in determining the effective control space boundaries consists of defining the control point saturation levels. For the UH-1H, with its full authority parallel servos, the maximum longitudinal cyclic travel is 13.0 inches, while the maximum main rotor collective travel is 10.7 inches.

Next we turn to the D_F matrix, shown in Table 49, which contains the gains between each output and both control points. The units are also indicated. Since the elements of the control vector are control rates, and the saturation levels are control positions, it is necessary to divide

TABLE 49. GAIN LEVEL ASSESSMENT

DF MATRIX

1 HD	2 Q	3 TH	4 DB	5 DC	6 HDE	7 HDI	8 XD	9 XDI	
21.5	538.	0.149E+04	-29.9	0.518E-01	-0.717	-0.252	-26.6	-1.89	1 DBD
-42.5	1.30	79.8	0.517E-02	-27.0	4.16	2.16	-0.435	-0.221E-01	2 DCD
$\frac{in./sec}{ft/sec}$	$\frac{in./sec}{rad/sec}$	$\frac{in./sec}{rad}$	$\frac{in./sec}{in.}$	$\frac{in./sec}{in.}$	$\frac{in./sec}{ft/sec}$	$\frac{in./sec}{ft}$	$\frac{in./sec}{ft/sec}$	$\frac{in./sec}{ft}$	

	CONTROL GAINS (K_z^u)		MAGNITUDE CORRESPONDING TO CONTROL SATURATION (u_{max}/K_z^u) [a]		MAGNITUDE CORRESPONDING TO MINIMUM INCREMENT OF CONTROL (u_{min}/K_z^u) [b]	
	$K_z^{\delta B}$	$K_z^{\delta C}$	$z_{max}^{\delta B}$	$z_{max}^{\delta C}$	$z_{min}^{\delta B}$	$z_{min}^{\delta C}$
$\dot{h}$	$\frac{.72 \text{ in.}}{\text{ft/sec}}$	$\frac{1.57 \text{ in.}}{\text{ft/sec}}$	18.1 ft/sec	6.8 ft/sec	.087 ft/sec	.04 ft/sec
q	$\frac{.314 \text{ in.}}{\text{deg/sec}}$	$\frac{.0008 \text{ in.}}{\text{deg/sec}}$	41.4 deg/sec	13375 deg/sec	.199 deg/sec	78 deg/sec
θ	$\frac{.87 \text{ in.}}{\text{deg}}$	$\frac{.052 \text{ in.}}{\text{deg}}$	14.9 deg	206 deg	.072 deg	1.2 deg
$\dot{h}_e$	$\frac{.024 \text{ in.}}{\text{ft/sec}}$	$\frac{.154 \text{ in.}}{\text{ft/sec}}$	542 ft/sec	69.5 ft/sec	2.6 ft/sec	.41 ft/sec
$\int \dot{h}_e dt$	$\frac{.00848 \text{ in.}}{\text{ft}}$	$\frac{.08 \text{ in.}}{\text{ft}}$	1542 ft	134 ft	7.37 ft	.78 ft
$\dot{x}$	$\frac{.89 \text{ in.}}{\text{ft/sec}}$	$\frac{.016 \text{ in.}}{\text{ft/sec}}$	14.6 ft/sec	669 ft/sec	.07 ft/sec	3.91 ft/sec
$\int \dot{x} dt$	$\frac{.063 \text{ in.}}{\text{ft}}$	$\frac{.0008 \text{ in.}}{\text{ft}}$	206 ft	13375 ft	.992 ft	78 ft

[a] $\delta_{B_{max}} = 13$ in., $\delta_{C_{max}} = 10.7$ in.

[b] $\delta_{B_{min}} = \delta_{C_{min}} = 1/16$ in.

each element of the D_F matrix by the appropriate gain between the control position and rate. For example, each gain between the outputs and $\dot{\delta}_B$ is divided by 29.9, the gain between δ_B and $\dot{\delta}_B$. The gains are thus expressed as inches of control per units of output. These normalized gains are listed in Table 49.

Dividing the saturation levels by the normalized gains gives the magnitude of each output which corresponds to saturation of the δ_B or δ_C control point. The smaller of the two numbers for each output defines the control space boundaries within which linear control can be exerted to modify vehicle dynamics. These quantities may also be used to eliminate the ineffective gains from the D_F matrix.

We can also compute the output magnitude that corresponds to the minimum increment of control, by dividing the minimum increment of control by the normalized gains. The term "minimum increment of control" refers to the smallest amount a control effector or surface will move, regardless of input level. The minimum increment of control exists because of friction and other thresholds, and defines the precision with which a given control surface can be positioned. A typical power amplifier-actuator-load combination has a dynamic range of 100-300; thus, we have chosen to use 1/16 in. as the minimum increment of control for the computations in Table 49.

The resulting output variable magnitudes that correspond to the minimum increments of control define the inner boundary of the linear control space. They can also be used to eliminate ineffective controller gains. For example, we see that using δ_B to control the pitching velocity, q, provides an accuracy of approximately 0.2 deg/sec. If δ_C were used, the accuracy is 78 deg/sec! The main rotor collective is obviously not useful in commanding pitching velocity and thus the gain $K_q^{\delta C}$ could be eliminated.

Using the above reasoning, we can eliminate about half of the controller gains, which results in the simplified controller of Fig. 31. One should be certain to determine that this simplified structure does not differ significantly from the one synthesized in Section IV by comparing the stability, response and sensitivity characteristics of the two designs. The desire for a simple system leads naturally into the sensor array assessment of the next section.

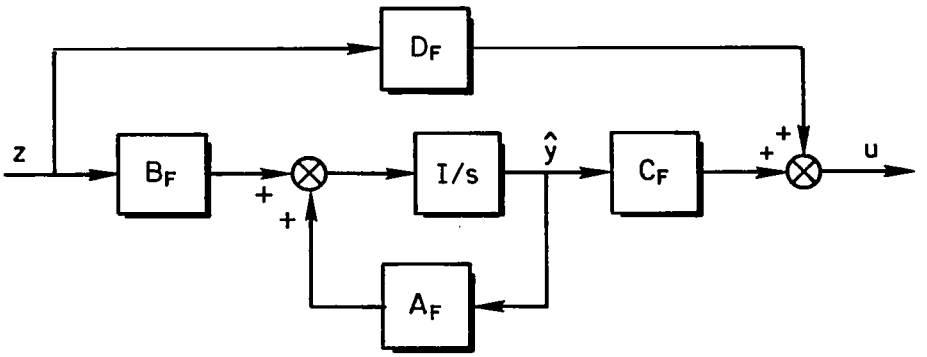

$$A_F = \begin{matrix} \\ \hat{y}_1 \\ \hat{y}_2 \\ \hat{y}_3 \end{matrix} \begin{matrix} \begin{matrix} \hat{y}_1 & \hat{y}_2 & \hat{y}_3 \end{matrix} \\ \begin{bmatrix} -0.333 & 0. & 0. \\ -34.3 & -0.922 & -2.37 \\ -1.6 & -3.76 & -15.0 \end{bmatrix} \end{matrix}$$

$$B_F = \begin{matrix} \\ \hat{y}_1 \\ \hat{y}_2 \\ \hat{y}_3 \end{matrix} \begin{matrix} \begin{matrix} \dot{h} & q & \theta & \delta_B & \delta_C & \dot{h}_e & \int \dot{h}_e & \dot{x} & \int \dot{x} \end{matrix} \\ \begin{bmatrix} 0. & 4.97 & 0. & 0. & 0. & 0. & 0. & 0. & 0. \\ 95.6 & 29.1 & -788. & -34.3 & 59.7 & 0. & 0. & -9.13 & 0. \\ 592. & -76.5 & -1230. & -1.6 & 381. & 0. & 0. & 1.36 & 0. \end{bmatrix} \end{matrix}$$

$$C_F = \begin{matrix} \\ \dot{\delta}_B \\ \dot{\delta}_C \end{matrix} \begin{matrix} \begin{matrix} \hat{y}_1 & \hat{y}_2 & \hat{y}_3 \end{matrix} \\ \begin{bmatrix} -28.9 & -0.254 & -0.523 \\ 0.122 & 0.264 & 1.07 \end{bmatrix} \end{matrix}$$

$$D_F = \begin{matrix} \\ \dot{\delta}_B \\ \dot{\delta}_C \end{matrix} \begin{matrix} \begin{matrix} \dot{h} & q & \theta & \delta_B & \delta_C & \dot{h}_e & \int \dot{h}_e & \dot{x} & \int \dot{x} \end{matrix} \\ \begin{bmatrix} 21.5 & 538. & 1490. & -29.9 & 0. & 0. & 0. & 26.6 & -1.89 \\ 42.5 & 0. & 0. & 0. & -27.0 & 4.16 & 2.16 & 0. & 0. \end{bmatrix} \end{matrix}$$

Figure 31. Simplified Controller Gains

E. SENSOR/EQUALIZATION COMPLEX

This is the third look at assessment of the sensor complex. It was first considered back in the filter-observer synthesis, when the rms state estimation error was compared to the desired error budget. If the budget was exceeded, the sensor array was clearly not able to provide an accurate estimation of the states. Alternately, if the estimation error was well within the budget, sensors might be deleted in the name of cost effectiveness and other such considerations.

The second pass at assessing the sensor array occurred during evaluation of the controller gain levels. Here it was seen that many ineffective controller gains could be eliminated, with no discernible performance degradation. The result was a further simplified controller.

Now we turn to two further considerations for the sensor complex. The first is sensor/equalization economy, which refers to the desire for minimum compensation of the vehicle dynamics and a minimum array of sensor and equalization computation to achieve performance goals. This desire arises out of considerations such as cost, reliability, maintenance, and the like. Referring back to Fig. 31, note that certain small gains in the A_F and B_F matrices have been set to zero. This is based on control realities, but is also consistent with economy of equalization. The importance of re-evaluating the stability, response and sensitivity of this further simplified system has been emphasized because a design which does not meet performance standards is useless, regardless of how simple it may be.

Examination of certain eigenvalue sensitivities can divulge the effects of deleting some controller gains upon the closed-loop root locations. This was discussed previously regarding first-order parameter sensities of the eigenvalues to changes in the F and G matrices. Here we use first-order eigenvalue sensitivities to changes in the regulator matrix C. An example of the matrix sensitivities for the short-period mode eigenvalue is given in Table 50. The only significant sensitivities here indicate that the important controller gains are:

TABLE 50

SENSITIVITY OF SHORT-PERIOD MODE
TO C MATRIX CHANGES

NORMALIZED C MATRIX SENSITIVITY TO EIGENVALUE : -1.87 2.05

1 x01 u_g	2 x02 w_g	3 x03 $\dot{h}_c$	4 x06 u	5 x07 W	6 x08 q	7 x09 θ	8 x10 δ_B	9 x11 δ_C	10 x12 $\int \dot{h}_e dt$	11 x13 x	12 x14 $\int \dot{x}\, dt$	
0.000 90.0	0.000 90.0	0.000 90.0	0.316E-03 180.	0.190E-02 0.000	0.427E-02 0.000	0.471E-03 180.	0.380E-01 180.	0.127E-03 180.	0.939E-05 180.	0.450E-04 0.000	0.396E-05 180.	1 DBD
0.000 90.0	0.000 90.0	0.000 90.0	0.185E-03 0.000	0.528E-01 0.000	0.109E-03 180.	0.471E-05 0.000	0.107E-03 180.	1.08 180.	0.131E-02 180.	0.308E-05 0.000	0.752E-06 0.000	2 DCD

Indicates significant sensitivity

$$w,\ q,\ \delta_B \rightarrow \dot{\delta}_B$$

$$w,\ \delta_C,\ \int \dot{h}_e\, dt \rightarrow \dot{\delta}_C$$

Two observations can be made. First, we presumably could have picked in advance which sensitivities would be important based on the controller gains that were eliminated. We see that their presence has negligible effect on the location of the short-period mode, based on the sensitivity magnitudes of the corresponding deleted terms in the controller gain matrices.

The search for a practical optimal controller, which has guided our synthesis and assessment throughout, leads to one other goal for the design. This is the desire for satisfactory performance over a wide range of operating conditions. Suppose, for example, that it was necessary to store a redundant set of controller gains for ten different helicopter operating setpoints. The storage problems alone prevent such a design from ever being used in a real-world situation, not to mention the huge expense involved in assessing the performance of all ten designs. What we would prefer is a single design that is easily adapted to almost all operating modes.

The concerns here are guided by questions like:

> Suppose we wish to create a command attitude (θ_C) system from a rate-of-climb command ($\dot{h}_C$) design simply by opening the $\dot{h}$ loops. Does the resulting θ_C system exhibit satisfactory stability, response and sensitivity characteristics, and if not, how can they be improved?

It is obvious that the desire for commonality of elements/gain settings is closely related to the desire for graceful degradation. Thus, the scenario posed above can be examined in parallel with the behavior of the θ loop when the $\dot{h}$ loop has degraded. These kinds of considerations insure that the optimal controller that is ultimately implemented is as simple and universal as possible.

F. SUMMARY

In summary, we return to our original goals in assessing the design to see whether we have been successful.

- Determine whether design goals have been met. The primary design goals in this work are the variable bandwidths that are set using the regulator cost function. An examination of the frequency response plots for the closed-loop system and various open-loop transfer functions assured that these bandwidths were attained. In addition, a good stretch of −20 dB/decade slope on either side of the open-loop frequency response crossover points was also created. This allows the bandwidth to be approximated by the crossover frequency.

Many other secondary design goals were also attained. These include: a filter-observer that has an rms state estimation error within the error budget; zero steady-state response of the two primary error variables, accomplished by including the integrals of these variables in the regulator cost function; and a controller that provides control decoupling for the longitudinal degrees of freedom. Each design goal was produced by a specific synthesis step (e.g., computing the regulator cost function to obtain the desired bandwidths) and the assessment was used to verify the desired results (and sometimes to guide iterations).

- Define quantitatively all the important properties of the system. Three examples were cited to illustrate this goal. The first was to expand the scope of the results. When design synthesis was completed, the end product was a set of four controller gain matrices. It was practically impossible to predict system and controller properties and performances based only on looking at this rather compact collection of gains. Instead, the scope of the design was expanded to include frequency responses, transient responses to commands and disturbances, root loci, various stability criteria, sensitivity criteria and many statistical metrics. All were essential in obtaining a quantitative design assessment.

The second example given for this assessment goal was to highlight the system's dominant properties. In both the stability evaluation and the

response evaluation we were able to identify, for each variable, those modes that dominated the particular characteristics observed. In doing so, a fairly complicated transfer function was invariably reduced to a much simpler and more manageable one, making the stability and response behavior easier to comprehend. Often these dominant modes provided a convenient method for partitioning the response. The partitions correspond to certain well-known systems (such as zero position error, zero velocity error, etc.) and the behavior is thus more readily analyzed.

A third example was to reveal the sensitivity of dominant properties to uncertainties. Having identified the dominant modes in connection with stability and response characteristics, we were then able to predict the effect upon system behavior of changes in these dominant modes. These "changes" ran the gamut from off-nominal conditions, controlled element equation uncertainies and simplifications, through thresholds, hysteresis and other parasitic nonlinearities, to component failure. The goal, of course, was to assure satisfactory FCS performance in the face of any or all such uncertainties. The sensitivity is variously quantified using first-order gain and parameter sensitivities, describing function analysis, and failure simulation.

- Broaden the understanding of the optimal system design results.

This goal guided all of the techniques used. Too often, an optimal controller design is only a theoretical solution because the design results are not well understood. In the introduction we gave three examples of the breadth of understanding desired. The relative importance of the various controller partitions was illustrated in the controlled gain level considerations. On the basis of control saturation and minimum increment of control we were able to define control regions for each output variable. The effectiveness of each control point in regulating each output quantity was also evaluated.

Many aspects of the controller behavior could be attributed to specific factors in the controlled element as a result of the assessment. For instance, the steady-state error response characteristics for the primary (or outer) loops were established. Dominant modes in various responses were identified. Conditions under which control poles are independent of the regulator solution were identified.

Implications for future design strategy appeared at each assessment step. In the synthesis of the controller little attention was paid to questions of graceful degradation and commonality of elements. From our assessment of these design aspects it is apparent that more consideration should be given to systematic analysis of these features during design synthesis.

- Explore simplification of the design which may lead to a simpler, more practical controller. Throughout the assessment we have been concerned with design simplification. This began with identification of the dominant system properties and their sensitivity to uncertainty. Simplicity was also paramount in considerations of controller gain levels, sensor array, equalization economy and commonality of elements. Although simplicity was continually emphasized, it was also stressed that the simplified systems should be rigorously analyzed to insure that the simplification was not accompanied by a loss in performance.

- Investigate the implications of controller architecture on results. Such an investigation was conducted during assessment of graceful degradation. This particular aspect of the evaluation was dependent on the controller architecture. We examined only two candidates — a single thread, multiply-redundant controller and an adaptive filter-observer controller — and saw that these two mechanization strategies required quite different assessment techniques. The resulting performance implications were also different, as well as the implementation problems. From just two example architectures it was seen that the controller properties can be quite implementation-dependent.

- Generalized design for other applications. The imposing task that characterizes the assessment of a new FCS design makes it desirable to design a system that is useful over many vehicles and many operating modes. This aspect was touched upon when we looked at the suitability of a given design in several operating modes. Thus, it was desirable to permit an $\dot{h}_c$ system to become a θ_c system simply by opening the $\dot{h}$ loops. We could also examine the performance of a candidate FCS design in various aircraft, perhaps in a simulation environment.

So we see that the list of assessment tasks enumerated in Table 44 has allowed us to attain our assessment goals. Figure 32 depicts a flow chart that could be used in design assessment. If it is ever necessary to interrupt this flow, due to the need for redesign, the chart should be re-entered at the top. This is to insure that the design always meets all assessment goals.

In final conclusion, it cannot be emphasized too strongly that the fundamental purpose of design assessment is to provide an in-depth understanding of the candidate system properties and behavior. This enhanced comprehension is vital in an optimal controller design; without it, such designs will be overly complex and the total system behavior will be poorly appreciated.

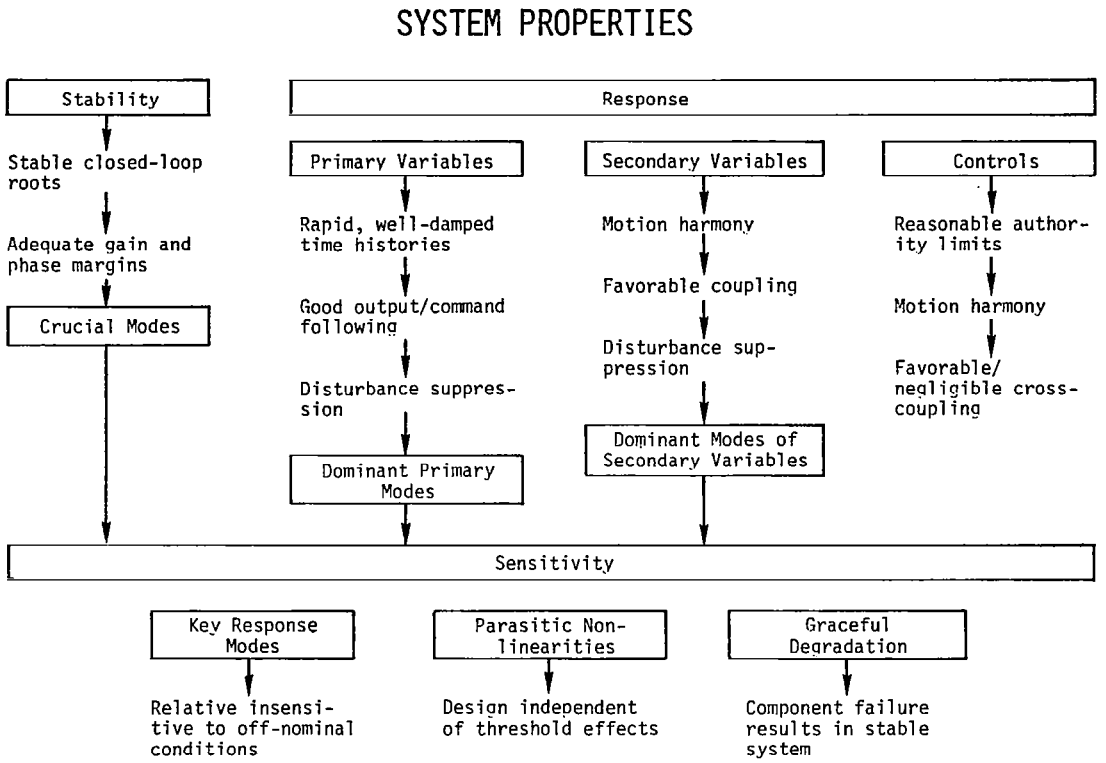

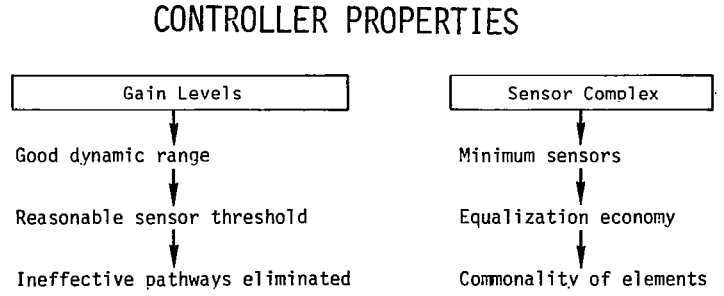

Figure 32. Assessment Flow Diagram

REFERENCES

1. Bryson, A. E., Jr., and Yu-Chi Ho, Applied Optimal Control, Blaisdell, Waltham, MA, 1969, pp. 168-175.

2. Murphy, R. D., and K. S. Narendra, "Design of Helicopter Stabilization Systems Using Optimal Control Theory," J. Aircraft, Vol. 6, No. 2, Mar.-Apr. 1969, pp. 129-136.

3. Hall, W. E. Jr., and A. E. Bryson, Jr., "Inclusion of Rotor Dynamics in Controller Design for Helicopters," J. Aircraft, Vol. 10, No. 4, Apr. 1973, pp. 200-206.

4. Harvey, C. A., and G. Stein, "Quadratic Weights for Asymptotic Regulator Properties," IEEE Trans. Automatic Control, Vol. AC-23, No. 3, June 1978, pp. 378-387.

5. Whitbeck, R. F., "A Frequency Domain Approach to Linear Optimal Control," J. Aircraft, Vol. 5, No. 4, July-Aug. 1968, pp. 395-401.

6. Bryson, A. E., Jr., "Applications of Optimal Control Theory in Aerospace Engineering," J. Spacecraft and Rockets, Vol. 4, No. 5, May 1967, pp. 545-553.

7. Athans, M., "The Role and Use of the Stochastic Linear-Quadratic-Gaussian Problem in Control System Design," IEEE Trans. Automatic Control, Vol. AC-16, No. 6, Dec. 1971, pp. 529-552.

8. Kwakernaak, H., and R. Sivan, Linear Optimal Control, Wiley-Interscience, New York, 1972.

9. D'Azzo, J. J., and C. H. Houpis, Feedback Control System Analysis and Synthesis, McGraw-Hill, New York, 1960.

10. McRuer, D. T., I. L. Ashkenas, and D. Graham, Aircraft Dynamics and Automatic Control, Princeton Univ. Press, Princeton, NJ, 1973, Chapt. 2 and 3.

11. Hofmann, L. G., G. L. Teper, and R. F. Whitbeck, "Application of Frequency Domain Multivariable Control Synthesis Techniques to an Illustrative Problem in Jet Engine Control," in Alternatives for Linear Multivariable Control, M. K. Sain, J. L. Peczkowski and J. L. Melsa (eds.), National Engineering Consortium, Chicago, 1978, pp. 51-70, Appendix.

12. McRuer, D. T. and E. S. Krendel, Mathematical Models of Human Pilot Behavior, AGARD-AG-188, Jan. 1974.

13. Hofmann, L. G., Topics on Practical Application of Optimal Control to Single and Multiple Control-Point Flight Control Problems, AFFDL-TR-70-52, Feb. 1971, pp. 102-105.

14. McRuer, D. T. and D. H. Weir, "Relationships Between Optimal and Conventional 'Good' Systems — A Simple Case Study," Aerospace Vehicle Flight Control Systems, Soc. Auto. Engrs., SP-358, May, 1970, pp. 1-7.

15. Chalk, C. R., T. P. Neal, T. M. Harris, F. E. Pritchard, and R. J. Woodcock, Background Information and User Guide for MIL-F-8785B (ASG), "Military Specification — Flying Qualities of Piloted Airplanes, AFFDL-TR-69-72, Aug. 1969.

16. Corliss, L. D., and P. D. Talbot, A Failure Effects Simulation of a Low Authority Flight Control Augmentation System on a UH-1H Helicopter, NASA TM-73,258, Aug. 1977, pp. 24-26.

17. Sinha, N. K. and Z. Elrazaz, "Sensitivity of the Eigenvalues of Aggregated Models," Proc. IEEE, Vol. 66, No. 7, July 1978, pp. 804-806.

18. Skira, C. A. and R. L. De Hoff, "A Practical Approach to Linear Model Analysis for Multivariable Turbine Engine Control Design," in Alternatives For Linear Multivariable Control, M. K. Sain, J. L. Peczkowski, and J. L. Melsa (eds.), National Engineering Consortium, Chicago, 1978, pp. 34-36.

19. Aoki, M., "Control of Large-Scale Dynamic Systems by Aggregation," IEEE Trans. on A.C., Vol. AC-13, No. 3, June 1968, pp. 246-253.

20. Pearce, B. F., Topics on Flexible Airplane Dynamics: Residual Stiffness Effects in Truncated Modal Analysis, ASD-TDR-63-334, Pt. I, July 1963.

21. Stapleford, R. L., L. G. Hofmann, J. J. Best, C. D. Wezeman, and W. A. Johnson, Transfer Function Approximations for Large Highly Coupled Elastic Boosters with Fuel Slosh, NASA CR-464, Apr. 1966.

22. Hofmann, L. G., W. F. Clement, D. Graham, G. L. Teper, B. L. Wiscons, D. L. Hemmel, and R. H. McFarland, ILS Glide Slope Standards: Part I, A Review of Flight Inspection Standards Affecting Landing Performance and Comparison with Limits Evolved from a System Analysis, FAA-RD-74-119-Pt-1, June 1975.

23. Riedel, S. A., Practical Optimal Control for Flight Control Application: Vol. II, Software User's Guide, NASA CR-152306, Mar. 1979.

24. Gelb, A. (ed.), Applied Optimal Estimation, The MIT Press, Cambridge, MA, 1974.

25. Kelly, R. J., "Time Reference Microwave Landing System Multipath Control Techniques," in Navigation: J. of Inst. Nav., Vol. 23, No. 1, Spring, 1976, pp. 42-58.

26. Graham, Dunstan, and Duane McRuer, Analysis of Nonlinear Control Systems, John Wiley and Sons, Inc., New York, 1961.

27. Methods of Analysis and Synthesis of Piloted Aircraft Flight Control Systems, BuAer Rept. AE 61-4, Vol. I, Mar. 1952.

28. McRuer, Duane T., and Donald E. Johnston, Flight Control Systems Properties and Problems — Vol. I, NASA CR-2500, Feb. 1975.

29. Bryson, Arthur E., Jr., and W. Earl Hall, Jr., Optimal Control and Filter Synthesis by Eigenvector Decomposition, Stanford University SUDAAR No. 436, Nov. 1971.

APPENDIX A

TRANSFORMATIONS FOR SINGULAR FILTER PROBLEMS ENABLING EIGENVECTOR DECOMPOSITION

This appendix documents a transformation of the Euler-Lagrange equations for the optimal state estimation or "filter" problem. This transformation is motivated by a desire to solve singular filter problems wherein some or all of the measurements are noise free. Attention is restricted to the steady-state solution for constant plants. Solution without transformation via existing computer codes (e.g., Ref. A-1 as modified by R. Bach and G. Slater) is not possible because the inverse of the measurement noise spectral density matrix is required. Transformation for continued use of these codes is recommended since the codes make use of the robust and efficient QR algorithm for eigenanalysis. Furthermore, this approach satisfies our research needs for a minimum of additional software development and risk of encountering numerical difficulties.

Consider the plant and measurement equations

$$\dot{x} = Fx + Gu + \Gamma w \quad , \quad x(0) = x_0$$

$$z_1 = H_1 x + v_1$$

$$z_2 = H_2 x + v_2$$

where

Vector	Dimension	Vector Name
x	n	State
u	p	Control
w	q	Process noise
z_1	m_1	Noisy measurements
z_2	m_2	Noise-free measurements
v_1	m_1	Measurement noise
v_2	m_2	Dummy measurement noise

G, Γ, H_1 and H_2 matrices are assumed to have full rank. Process and measurement noise are Gaussian with

$$E[w] = 0 \qquad E[v_1] = 0 \qquad E[v_2] = 0$$

$$E[w(t_1)w'(t_2)] = Q\delta(t_1 - t_2)$$

$$E[v_1(t_1)v'(t_2)] = R_1\delta(t_1 - t_2)$$

$$E[v_2(t_1)v_2'(t_2)] = \lim_{\epsilon \to 0^+} \epsilon R_2\delta(t_1 - t_2)$$

w, v_1 and v_2 are mutually statistically independent random processes. Their power spectral densities, Q, R_1 and R_2, are diagonal matrices having full rank.

It is always possible to order the measurements so that noisy measurements are in z_1 and noise-free measurements are in z_2 as reflected in the above equations.

Also, it is always possible to reorder the state vector elements by means of elementary transformations to obtain $H_2 = [H_{21} \quad H_{22}]$ wherein H_{22} full rank.

Furthermore, the transformation matrix, T, defined in Table A-1 can always be used to obtain H_2 in the form:

$$H_2 = [H_{21} \quad H_{22}] = [0 \quad I]$$

Next, consider Γ in partitioned form wherein Γ_2 has m_2 rows.

$$\Gamma = \begin{bmatrix} \Gamma_1 \\ \Gamma_2 \end{bmatrix}$$

Form $A^{-1} \triangleq \Gamma_2 Q \Gamma_2'$. Let the rank of A^{-1} be defined as r. Assume for the present that A^{-1} has full rank, $r = m_2$. This assumption is equivalent

TABLE A-1. TRANSFORMATION MATRIX

Given:

$$\dot{\bar{x}} = \bar{F}\bar{x} + \bar{G}\bar{u} + \bar{\Gamma}w \quad , \quad x(0) = x_o$$

$$z_1 = \bar{H}_1\bar{x} + v_1$$

$$z_2 = \bar{H}_2\bar{x} + v_2$$

$$\bar{H}_2 = [\bar{H}_{21} \quad \bar{H}_{22}]$$

and $\bar{H}_{22}$ is $m_2 \times m_2$ and nonsingular. The nonsingular transformation, T, $x = \Gamma\bar{x}$ where

$$T = \begin{bmatrix} I & 0 \\ \bar{H}_{21} & \bar{H}_{22} \end{bmatrix} \quad , \quad T^{-1} = \begin{bmatrix} I & 0 \\ -\bar{H}_{22}^{-1}\bar{H}_{21} & \bar{H}_{22}^{-1} \end{bmatrix}$$

results in

$$\begin{Bmatrix} x_1 \\ x_2 \end{Bmatrix} = \begin{Bmatrix} x_1 \\ z_2 \end{Bmatrix} = \begin{Bmatrix} \bar{x}_1 \\ \bar{H}_{21}\bar{x}_1 + \bar{H}_{22}\bar{x}_2 \end{Bmatrix}$$

$$F = T\bar{F}T^{-1} = \begin{bmatrix} F_{11} & F_{12} \\ F_{21} & F_{22} \end{bmatrix}$$

$$F_{11} = \bar{F}_{11} - \bar{F}_{12}\bar{H}_{22}^{-1}\bar{H}_{21} \qquad F_{12} = \bar{F}_{12}\bar{H}_{22}^{-1}$$

$$F_{21} = \bar{H}_{22}\bar{F}_{21} - \bar{H}_{22}\bar{F}_{22}\bar{H}_{22}^{-1}\bar{H}_{21} + \bar{H}_{21}\bar{F}_{11} - \bar{H}_{21}\bar{F}_{21}\bar{H}_{22}^{-1}\bar{H}_{21}$$

$$F_{22} = \bar{H}_{22}\bar{F}_{22}\bar{H}_{22}^{-1} + \bar{H}_{21}\bar{F}_{12}\bar{H}_{22}^{-1}$$

$$G = T\bar{G} = \begin{bmatrix} G_1 \\ G_2 \end{bmatrix} \quad , \quad G_1 = \bar{G}_1 \quad , \quad G_2 = \bar{H}_{21}\bar{G}_1 + \bar{H}_{22}\bar{G}_2$$

$$\Gamma = T\bar{\Gamma} = \begin{bmatrix} \Gamma_1 \\ \Gamma_2 \end{bmatrix} \quad , \quad \Gamma_1 = \bar{\Gamma}_1 \quad , \quad \Gamma_2 = \bar{H}_{21}\bar{\Gamma}_1 + \bar{H}_{22}\bar{\Gamma}_2$$

$$H = \bar{H}T^{-1} = \begin{bmatrix} H_{11} & H_{12} \\ H_{21} & H_{22} \end{bmatrix}$$

$$H_{11} = \bar{H}_{11} - \bar{H}_{12}\bar{H}_{22}^{-1}\bar{H}_{21} \quad , \quad H_{12} = \bar{H}_{12}\bar{H}_{22}^{-1}$$

$$H_{21} = 0 \quad , \quad H_{22} = I$$

to the requirement that the derivative of every noise-free measurement contain an independent white noise component. All subsequent developments either require this assumption be satisfied, or that a single parameter relaxation of this assumption be used (refer to Appendix B).

Euler-Lagrange equations for the filter problem are (e.g., Ref. A-2, pp. 395-396):

$$\begin{Bmatrix} \dot{x} \\ \dot{\lambda} \end{Bmatrix} = \begin{bmatrix} F & -\Gamma Q \Gamma' \\ -H_1' R_1^{-1} H_1 & -F' \end{bmatrix} \begin{Bmatrix} x \\ \lambda \end{Bmatrix} + \begin{bmatrix} G & 0 \\ 0 & H_1' R_1 \end{bmatrix} \begin{Bmatrix} u \\ z_1 \end{Bmatrix}$$

$$+ \begin{bmatrix} 0 \\ H_2' R_2^{-1} \end{bmatrix} (1/\epsilon)(z_2 - H_2 x)$$

These equations may be partitioned more finely and Laplace transformed.

$$\begin{bmatrix} (sI - F_{11}) & -F_{12} & \Gamma_1 Q \Gamma_1' & \Gamma_1 Q \Gamma_2' \\ -F_{21} & (sI - F_{22}) & \Gamma_2 Q \Gamma_1' & \Gamma_2 Q \Gamma_2' \\ H_{11}' R_1^{-1} H_{11} & H_{11}' R_1^{-1} H_{12} & (sI + F_{11}') & F_{21}' \\ \epsilon H_{12}' R_1^{-1} H_{11} & \epsilon H_{12}' R_1^{-1} H_{12} & \epsilon F_{12} & \epsilon(sI + F_{22}') \end{bmatrix} \begin{Bmatrix} x_1 \\ x_2 \\ \lambda_1 \\ \lambda_2 \end{Bmatrix}$$

$$= \begin{Bmatrix} x_{10} \\ x_{20} \\ \lambda_{10} \\ \epsilon\lambda_{20} \end{Bmatrix} + \begin{bmatrix} G_1 & 0 & 0 \\ G_2 & 0 & 0 \\ 0 & H_{11}' R_1^{-1} & 0 \\ 0 & \epsilon H_{12}' R_1^{-1} & I \end{bmatrix} \begin{Bmatrix} u \\ z_1 \\ R_2^{-1}(z_2 - x_2) \end{Bmatrix}$$

The last Euler-Lagrange equation has been multiplied through by the parameter ϵ. If ϵ is allowed to approach zero from above, the result is that $z_2 \equiv x_2$ since R_2 is diagonal and nonsingular by assumption. $z_2 \equiv x_2$ replaces the last Euler-Lagrange equation.

Let us examine this result from another viewpoint. Assume a solution for the optimal state estimate, $\hat{x}$, of the form (e.g., Ref. A-2, page 396):

$$\hat{x} = \begin{Bmatrix} \hat{x}_1 \\ \hat{x}_2 \end{Bmatrix} = \begin{Bmatrix} x_1 \\ x_2 \end{Bmatrix} + \begin{bmatrix} P & P_{12} \\ P_{12}' & P_{22} \end{bmatrix} \begin{Bmatrix} \lambda_1 \\ \lambda_2 \end{Bmatrix}$$

However, in order that the error in a log-likelihood cost function remain bounded for the noise-free measurements [recall these are weighted by $(1/\epsilon)R_2^{-1}$ in that cost function], $z_2 = x_2 = \hat{x}_2$ is required. Consider the assumed solution. Since λ_1 and λ_2 are not necessarily zero, P_{12} and P_{22} must be zero because P_{22}, the error covariance for the error in the estimate of x_2, is zero.

The second Euler-Lagrange equation may be solved for λ_2. Making use of $z_2 \equiv x_2$ and $A^{-1} \triangleq \Gamma_2 Q \Gamma_2'$, the result is:

$$\lambda_2 = A[F_{21}x_1 - (sI - F_{22})z_2 + z_{20} - \Gamma_2 Q \Gamma_1' \lambda_1 + G_2 u]$$

The first and third Euler-Lagrange equations can be rewritten as

$$\begin{bmatrix} (sI - F_{11} + \Gamma_1 Q \Gamma_2' A F_{21}) & (\Gamma_1 Q \Gamma_1' - \Gamma_1 Q \Gamma_2' A \Gamma_2 Q \Gamma_1') \\ (H_{11}' R_1^{-1} H_{11} + F_{21}' A F_{21}) & (sI + F_{11}' - F_{21}' A \Gamma_2 Q \Gamma_1') \end{bmatrix} \begin{Bmatrix} x_1 \\ \lambda_1 \end{Bmatrix}$$

$$= \begin{Bmatrix} (x_{10} - \Gamma_1 Q \Gamma_2' A z_{20}) \\ (\lambda_{10} - F_{21}' A z_{20}) \end{Bmatrix} \begin{bmatrix} (G_1 - \Gamma_1 Q \Gamma_2' A G_2) & 0 & (F_{12} + \Gamma_1 Q \Gamma_2' A[sI - F_{22}]) \\ (-F_{21}' A G_2) & (H_{11}' R_1^{-1}) & (-H_{11}' R_1^{-1} H_{12} + F_{21}' A[sI - F_{22}]) \end{bmatrix} \begin{Bmatrix} u \\ z_1 \\ z_2 \end{Bmatrix}$$

Specialization of the assumed solution for the optimal state estimate

$$\hat{x}_1 = x + P\lambda_1$$

$$\hat{x}_2 = x_2 = z_2$$

was justified previously. This assumed solution may be substituted in the first and third Euler-Lagrange equations to obtain them in terms of P, $\hat{x}_1$ and λ_1.

$$\begin{bmatrix} (sI - F_{11} + \Gamma_1 Q \Gamma_2' A F_{21} + P[H_{11}' R_1^{-1} H_{11} + F_{21}' A F_{21}]) & (\Gamma_1 Q \Gamma_1' - \Gamma_1 Q \Gamma_2' A \Gamma_2 Q \Gamma_1' + [F_{11} - \Gamma_1 Q \Gamma_2' A F_{21}]P \\ & + P[F_{11}' - F_{21}' A \Gamma_2 Q \Gamma_1'] - P[H_{11}' R_1^{-1} H_{11} + F_{21}' A F_{21}]P \\ (H_{11}' R_1^{-1} H_{11} + F_{21}' A F_{21}) & (sI + F_{11}' - F_{21}' A \Gamma_2 Q \Gamma_1' - [H_{11}' R_1^{-1} H_{11} + F_{21}' A F_{21}]P \end{bmatrix} \begin{Bmatrix} \hat{x}_1 \\ \lambda_1 \end{Bmatrix}$$

$$= \begin{Bmatrix} (x_{10} - \Gamma_1 Q \Gamma_2' A z_{20} + P[\lambda_{10} - F_{21}' A z_{20}]) \\ (\lambda_{10} - F_{21}' A z_{20}) \end{Bmatrix} \begin{bmatrix} (F_{12} + \Gamma_1 Q \Gamma_2' A(sI - F_{22}) + PF_{21}' A(sI - F_{22}) \\ - PH_{11}' R_1^{-1} H_{12}) \\ (F_{21}' A(sI - F_{22}) - H_{11}' R_1^{-1} H_{12}) \end{bmatrix} z_2$$

$$+ \begin{bmatrix} (G_1 - \Gamma_1 Q \Gamma_2' A G_2 - PF_{21} A G_2) \\ (-F_{21}' A G_2) \end{bmatrix} u + \begin{bmatrix} (PH_{11}' R_1^{-1}) \\ (H_{11}' R_1^{-1}) \end{bmatrix} z_1$$

Elimination of the costate-to-state coupling in the above equation results in an algebraic Riccati equation.

$$\Gamma_1 Q \Gamma_1' - \Gamma_1 Q \Gamma_2' A \Gamma_2 Q \Gamma_1' + [F_{11} - \Gamma_1 Q \Gamma_2' A F_{21}]P$$

$$+ P[F_{11}' - F_{21} A \Gamma_2 Q \Gamma_1'] - P[H_{11}' R_1^{-1} H_{11} + F_{21}' A F_{21}]P = 0$$

Assume the Riccati equation is satisfied, and rewrite the $\hat{x}_1$ equation in terms of the filter gain matrices

$$K_{11} = PH_{11}'R_1^{-1}$$

and

$$K_{12} = (PF_{21}' + \Gamma_1 Q \Gamma_2')A$$

This results in

$$(sI - F_{11} + K_{12}F_{21} + K_{11}H_{11})\hat{x}_1$$

$$= (\hat{x}_{10} - K_{12}z_{20}) + K_{11}z_1 + (F_{12} + K_{12}[sI - F_{22}] - K_{11}H_{12})z_2 + (G_1 - K_{12}G_2)u$$

Occurrence of $[s(\hat{x}_1 - K_{12}z_2) - (\hat{x}_{10} - K_{12}z_{20})]$ in the above equation suggests a more appropriate choice of filter state coordinates is the $(n - m_2)$ vector, $\hat{y}$.

$$\hat{y} \triangleq \hat{x}_1 - K_{12}\, z_2$$

Then the differential equation for the estimate becomes:

$$\dot{\hat{y}} = (F_{11} - K_{12}F - K_{11}H_{11})\hat{y} + ([F_{11} - K_{12}F_{21} - K_{11}H_{11}]K_{12}$$

$$+ F_{12} - K_{12}F_{22} - K_{11}H_{12})z_2 + K_{11}z_1 + (G_1 - K_{12}G_2)u$$

$$\hat{y}(0) = \hat{x}_{10} - K_{12}\, z_{20}$$

$\hat{x}_1$ is obtained from $\hat{y}$ by means of

$$\hat{x}_1 = \hat{y} + K_{12}\, z_2$$

Figure A-1 shows the structure of the resulting reduced order filter. Recall, however, that this solution is in terms of a transformation of the

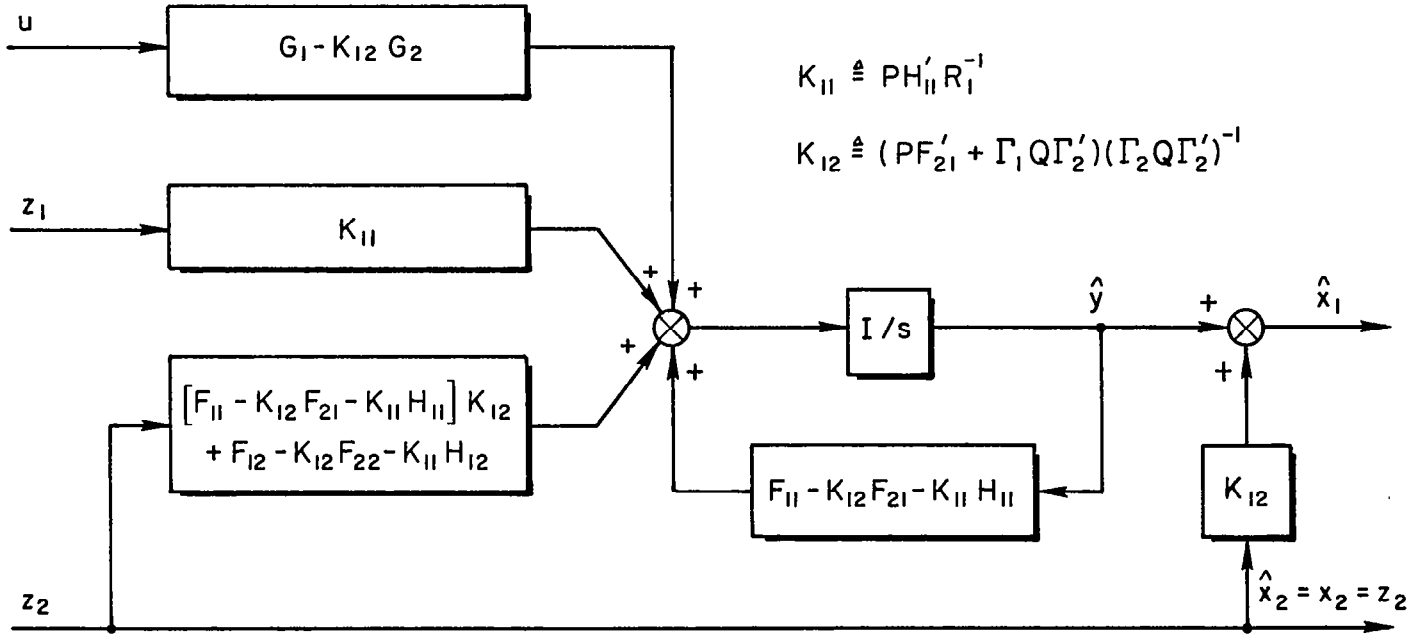

Figure A-1. Optimal Filter-Observer Structure ($\Gamma_2 Q \Gamma_2'$ Full Rank)

state vector for the original problem. Appropriate inverse transformation must be applied before interfacing this solution with the regulator portion of the optimal stochastic controller.

Consider the error in the estimate, $\hat{y}$. The quantity corresponding to $\hat{y}$ is y where:

$$y \triangleq x_1 - K_{12}z_2 = x_1 - K_{12}x_2$$

The differential equation for y is:

$$\dot{y} = (F_{11} - K_{12}F_{21} - K_{11}H_{11})y$$

$$+ ([F_{11} - K_{12}F_{21} - K_{11}H_{11}]K_{12} + F_{12} - K_{12}F_{22})z_2$$

$$+ K_{11}H_{11}x_1 + (G_1 - K_{12}G_2)u + (\Gamma_1 - K_{12}\Gamma_2)w$$

$$y(0) = x_{10} - K_{12}\, z_{20}$$

The differential equation for the error in the estimate, $\tilde{y}$, is:

$$\dot{\tilde{y}} \triangleq \dot{\hat{y}} - \dot{y} = (F_{11} - K_{12}F_{21} - K_{11}H_{11})\tilde{y}$$

$$- (\Gamma_1 - K_{12}\Gamma_2)w + K_{11}v_1$$

The error in $\hat{y}$ is also the error in $\hat{x}_1$ because

$$\tilde{y} = (\hat{x}_1 - K_{12}\, z_2) - (x_1 - K_{12}\, z_2) = \tilde{x}_1$$

Consider the properties of the covariance of $\tilde{x}_1$. The covariance of $\tilde{x}_1$ is denoted by X. X is the solution of the equation:

$$(F_{11} - K_{12}F_{21} - K_{11}H_{11})X + X(F_{11}' - F_{21}'K_{12}' - H_{11}'K_{11}')$$

$$+ (\Gamma_1 - K_{12}\Gamma_2)Q(\Gamma_1' - \Gamma_2'K_{12}') + K_{11}R_1K_{11}' = 0$$

Necessary and sufficient conditions for a minimum of the trace of X with respect to K_{12} and K_{22} are

$$K_{11}^* = XH_{11}'R_1^{-1}$$

$$K_{12}^* = (XF_{21}' + \Gamma_1Q\Gamma_2')(\Gamma_2Q\Gamma_2')^{-1}$$

provided R_1 and $(\Gamma_2Q\Gamma_2')$ are positive definite. R_1 and $(\Gamma_2Q\Gamma_2')$ are always positive definite here by definition and assumption.

Substitution of K_{11}^* and K_{12}^* into the covariance equation results in the Riccati equation obtained earlier with P replaced by X. This confirms the optimality of the singular filter solution and shows that P is the covariance for $\dot{x}_1$ and $\tilde{y}$.

Several concluding comments are in order.

The solution given here is a special case of the solution given in Ref. A-3, pages 327-332. It is a special case in that here we have transformed the state vector at the outset in order to avoid introducing $(n-m_2)^2$ parameters unnecessarily. (Those parameters are in the first $(n-m_2)$ columns of the T matrix in Ref. A-3, page 329.)

In view of the above, one might ask, "Why bother with this development if the results of Ref. A-3 may be specialized?" The answer has several points:

- The development in Ref. A-3 is a "heuristic" one, particularly with respect to incorporating the "free gain matrix, B_1."
- There is no demonstration that the Riccati equation in Ref. 2 results from the Euler-Lagrange equations or their equivalent. This is necessary in order that:

- The resulting filter be optimal.
- The eigenvalue decomposition method of solution be applicable.

- There is a desire to eliminate the unnecessary parameters in the Ref. A-3 formulation for the sake of simplicity.

REFERENCES FOR APPENDIX A

A-1. Bryson, Arthur E., Jr., and W. Earl Hall, Jr., Optimal Control and Filter Synthesis by Eigenvector Composition, Stanford Univ., SUDAAR No. 436, Nov. 1971.

A-2. Bryson, Arthur E., Jr., and Yu-Chi Ho, Applied Optimal Control, Blaisdell, Waltham, MA, 1969.

A-3. Gelb, Arthur, ed., Applied Optimal Estimation, MIT Press, Cambridge, MA, 1974.

APPENDIX B

UH-1H EQUATIONS OF MOTION AND ACTUATION SYSTEM

The first quantitative step in design is formulation of the equations of motion in state vector form:

$$\dot{x} = Fx + Gu + \Gamma w$$

$$z = Hx + v$$

$$y = H_R x$$

where

- x is the state vector, composed of shaping filter states (x_s) and controlled element states (x_c)
- u is the control vector
- w is the process noise vector
- z is the measurement vector
- v is the measurement noise vector
- y is the output vector, composed of the quantities being measured (Hx) and the other output quantities (y_o)

The specific selection of the vector components and their corresponding equations (kinematic, perturbation, shaping filter and auxiliary) is the subject of the next two subsections. The longitudinal vehicle dynamics are given first, then the dynamics of the shaping filters and, finally, the actuator model.

LONGITUDINAL EQUATIONS OF MOTION

For the longitudinal problem, the vector components indicated in Table B-1 are used. The equations of motion can be stated in terms of the variables comprising those vectors.

TABLE B-1. VECTOR COMPONENTS FOR LONGITUDINAL PROBLEM

Vector	Elements	Computer Mnemonic	Description
x_S	u_g	XO1[a]	Longitudinal gust velocity (ft/sec)
	w_g	XO2	Vertical gust velocity (ft/sec)
	$\dot{h}_c$	XO3	Commanded altitude rate (ft/sec)
x_C	u	XO6	Longitudinal velocity (ft/sec)
	w	XO7	Vertical velocity (ft/sec)
	q	XO8	Pitching velocity (rad/sec)
	θ	XO9	Pitch angle (rad)
	δ_B	X10	Longitudinal cyclic (in.)
	δ_C	X11	Main rotor collective (in.)
	$\int \dot{h}_e \, dt$	X12	Integral of altitude rate error (ft)
	x_{BAR}	X13	Horizontal stabilizer bar (ft)
	$\int u_{AS_e} dt$	X14	Integral of airspeed error (ft)[b]
	$\int \dot{x} \, dt$	X14	Integral of inertial speed error (ft)[c]
u	$\dot{\delta}_B$	DBD	Longitudinal cyclic rate (in./sec)
	$\dot{\delta}_C$	DCD	Main rotor collective rate (in./sec)
w	w_{u_g}	PNU	Longitudinal gust velocity process noise (ft/sec)
	w_{w_g}	PNW	Vertical gust velocity process noise (ft/sec)
	$w_{\dot{h}_c}$	PNC	Commanded altitude rate process noise (ft/sec)
z	$\dot{h}$	HD	Altitude rate (ft/sec)
	q	Q	Pitching velocity (rad/sec)
	θ	TH	Pitch angle (rad)
	δ_B	DB	Longitudinal cyclic (in.)
	δ_C	DC	Main rotor collective (in.)
	$\int \dot{h}_e \, dt$	HDI	Integral of altitude rate error (ft)
	$\dot{h}_e$	HDE	Altitude rate error (ft/sec)
	$\int u_{AS_e} dt$	ASI	Integral of airspeed error (ft)[b]
	u_{AS_e}	ASE	Airspeed error (ft/sec)[b]
	$\int \dot{x} \, dt$	XDI	Integral of inertial speed error (ft)[c]
	$\dot{x}$	XD	Inertial speed error (ft/sec)[c]
	a'_x	AXP	Longitudinal acceleration independent of pitch ($a_x - g \sin \theta$) (ft/sec^2)[d]
	a'_z	AZP	Vertical acceleration measured ℓ_x ft forward of c.g. (ft/sec^2)[d]
y_O	α	AOA	Angle of attack (rad)
	$\dot{x}$	XD	Inertial speed (ft/sec)[b]
	u_{AS_e}	ASE	Airspeed error (ft/sec)[c]

[a]State vector mnemonics are automatically generated by software.

[b]Used in 100 kt case. [c]Used in 1 kt (hover) case. [d]Not used in all cases.

Perturbation Equations of Motion

These equations are derived in Ref. B-1, with the exception of the x_{BAR} equation, derived in Fig. B-1.

$$\dot{u} = (-X_u)u_g + (-X_w)w_g + X_u u + X_w w + (X_q - W_o)q + (-g \cos \theta_o)\theta + X_{\delta_B}\delta_B + X_{\delta_C}\delta_C + X_{\delta_B x_{BAR}}$$

$$\dot{w} = (-Z_u)u_g + (-Z_w)w_g + Z_u u + Z_w w + (Z_q + U_o)q + (-g \sin \theta_o)\theta + Z_{\delta_B}\delta_B + Z_{\delta_C}\delta_C + Z_{\delta_B x_{BAR}}$$

$$\dot{q} = (-M_u)u_g + (-M_w)w_g + M_u u + M_w w + M_q q + M_{\delta_B}\delta_B + M_{\delta_C}\delta_C + M_{\delta_B x_{BAR}}$$

$$\dot{\theta} = q \qquad \dot{x}_{BAR} = -0.333\, x_{BAR} + 4.97\, q$$

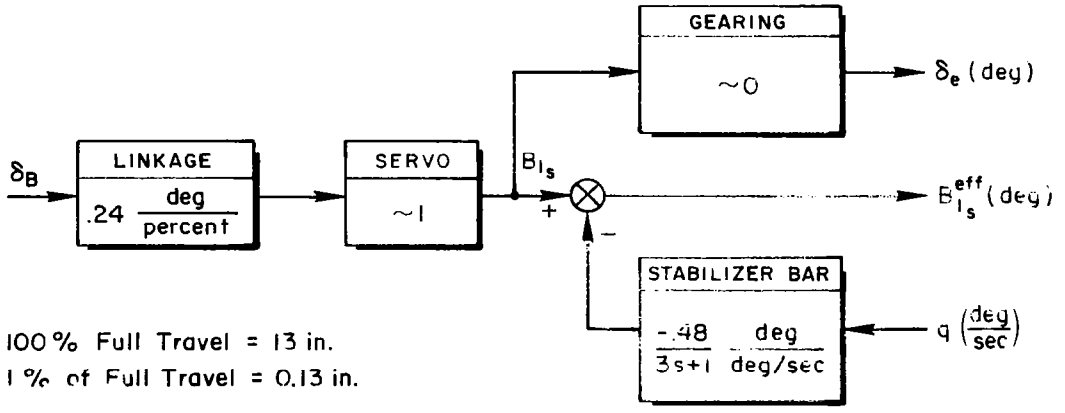

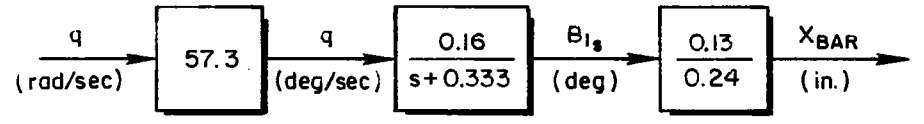

Figure B-1. Pitch Axis Stabilizer Bar (from Ref. B-2)

Kinematic Equations

These equations are derived in Ref. B-1.

$$(\int \dot{h}_e\, dt) = \dot{h}_c + (-\sin\theta_o)u + (\cos\theta_o)w + (-V_{T_o})\theta + (-\epsilon)\int \dot{h}_e\, dt$$

$$(\int u_{ASE}\, dt) = (-\cos\theta_o)u_g + (-\sin\theta_o)w + (\cos\theta_o)u + (\sin\theta_o)w + (-\epsilon)\int u_{ASE}\, dt$$

$$(\int \dot{x}\, dt) = (\cos\theta_o)u + (\sin\theta_o)w + (-\epsilon)\int \dot{x}\, dt$$

The ϵ factors are used to obtain bounded rms integral responses when integral loops are not yet closed. Otherwise, $\epsilon \equiv 0$.

Shaping Filter Equations

These equations are derived using a simplified version of the model for random turbulence. Gradient effects associated with the normal turbulence component are neglected. The random turbulence components have Gaussian probability density functions with zero means. The standard deviation σ_{u_g} should be chosen from a Rayleigh probability density function* having a characteristic speed of $\sigma_{\sigma_{u_g}}$ ft/sec. However, for the sake of simplicity, the mean value of σ_{u_g}, which is $\sigma_{\sigma_{u_g}}$, is used.

$$\sigma_{u_g} = \sigma_{\sigma_{u_g}} = 2.79 - 0.245 \log_{10} h \quad \text{ft/sec} \qquad h > 100 \text{ ft}$$

$$= 2.3 \text{ ft/sec} \qquad h \leq 100 \text{ ft}$$

The standard deviation σ_{w_g} is a function of σ_{u_g}. The frequency content of the random turbulence and $\sigma_{\sigma_{u_g}}$ are functions of altitude.

The power spectral densities for the longitudinal and normal random turbulence components at a given altitude are respectively:

*The Rayleigh probability density function is for u_g.

$$\Phi_{u_g} = \frac{\sigma_{u_g}^2 2V_{A_o}/L_u}{\omega^2 + (V_{A_o}/L_u)^2}$$

$$\Phi_{w_g} = \frac{\sigma_{w_g}^2 2(1.594V_{A_o}/L_w)}{\omega^2 + (1.594V_{A_o}/L_w)^2}$$

where

$$\sigma^2 = \frac{1}{2\pi}\int_{-\infty}^{\infty} \Phi \, d\omega$$

Φ_{w_g} is a lower-order approximation to the Dryden power spectral density such that the mean-square level and half-power frequency are preserved.

The differential equations for unit-white-noise shaping filters producing output variables u_g and w_g having power spectral densities Φ_{u_g} and Φ_{w_g} respectively are:

$$\dot{u}_g = -|V_{A_o}|/L_u u_g + \sigma_{u_g}\sqrt{2|V_{A_o}|/L_u}\, w_{u_g}$$

$$\dot{w}_g = -1.594|V_{A_o}|/L_w w_g + \sigma_{w_g}\sqrt{2(1.594)|V_{A_o}|/I_w}\, w_{w_g}$$

where w_{u_g} and w_{w_g} are independent, zero-mean, unit white noises. V_{A_o} is the trim airspeed.

The integral scale lengths L_u and L_w are given as functions of altitude h by

$$L_u = 145[h]^{1/3} \qquad 100 \leq h \leq 1750 \text{ ft}$$

$$= 145[100]^{1/3} = 673 \qquad h \leq 100 \text{ ft}$$

$$L_w = h \qquad h \leq 1750 \text{ ft}$$

The standard deviation for the normal turbulence component σ_{w_g} is related to the standard deviation for the longitudinal turbulence component σ_{u_g} through the integral scale lengths.

$$\sigma_{w_g} = \sqrt{L_w/L_u}\,\sigma_{u_g}$$

The rate-of-climb command equation is given by:

$$(\dot{h}_c) = \dot{h}_c\dot{h}_c + \sigma_{\dot{h}_c}\sqrt{2\omega_{\dot{h}_c}}\,w_{\dot{h}_c}$$

where $w_{\dot{h}_c}$ is an independent, zero-mean, unit white noise.

Auxiliary Equations

These are derived in Ref. B-1.

$$\dot{h} = (\sin\theta_o)u + (-\cos\theta_o)w + V_{T_o}\theta$$

$$\dot{h}_e = \dot{h}_c + (-\sin\theta_o)u + (\cos\theta_o)w + (-V_{T_o})\theta$$

$$u_{AS_e} = (-\cos\theta_o)u_g + (-\sin\theta_o)w_g + (\cos\theta_o)u + (\sin\theta_o)w$$

$$\dot{x} = (\cos\theta_o)u + (\sin\theta_o)w$$

$$a_x' = (-X_u)u_g + (-X_w)w_g + X_u u + X_w w + X_q q + (-g\cos\theta_o)\theta + X_{\delta_B}\delta_B + X_{\delta_C}\delta_C + X_{\delta_B}x_{BAR}$$

$$a_z' = -(Z_u - \ell_x M_u)u_g - (Z_w - \ell_x M_w)w_g + (Z_u - \ell_x M_u)u_g + (Z_w - \ell_x M_w)w + (Z_q - \ell_x M_q)q + (Z_{\delta_B} - \ell_x M_{\delta_B})\delta_B + (Z_{\delta_C} - \ell_x M_{\delta_C})\delta_C + (Z_{\delta_B} - \ell_x M_{\delta_B})x_{BAR}$$

$$\alpha = (-1/V_{T_o})w_g + (1/V_{T_o})w$$

Table B-2 presents the longitudinal matrix equations in literal form. Table B-3 lists values for the parameters found in the longitudinal state vector equations, for two key flight conditions. All parameter values are from Ref. B-2 except those for the shaping filter equations. These latter were derived above.

ACTUATION SYSTEM

The actuation system has identical dynamics for all four control axes. A first-order approximation to the third-order combination of series and boost actuators is used. The first-order model includes an approximation of the series actuator phase lag at low frequencies. Dynamics in the parallel trim actuator path are neglected. The bases for these approximations are explained elsewhere in this report.

Let DX represent the output displacement of any boost actuator (DX = DB, DC) and DXD represent d(DX)/dt. The differential equation included in the plant model for DX is:

$$\dot{DX} = DX$$

Unity gain feedback around the integration element of the actuator model is provided by the optimal regulator solution. The Q_R and R_R cost function weighting coefficients are selected to obtain each effective actuator break frequency, ω_A, which approximates the combination of the series and boost actuator dynamics. The method for selecting the cost function coefficients to accomplish this is described in Sections II and IV.

$$\omega_A \triangleq [1/\omega_{boost} + 2\zeta_{series}/\omega_{series}]^{-1} = 25.73 \text{ rad/sec}$$

$$\omega_{boost} = 50. \text{ rad/sec}$$

$$2\zeta_{series} = \sqrt{2} \qquad \text{(From Ref. B-3)}$$

$$\omega_{series} = 75. \text{ rad/sec}$$

TABLE B-2. LITERAL MATRICES FOR LONGITUDINAL INPUT DATA

$F =$

UG	WG	HDC	U	W	Q	TH	DB	DC	HDI	XBR	XDI[a]	ASI[a]	
$-\lvert V_{A_o}\rvert/L_u$	0	0	0	0	0	0	0	0	0	0	0	0	UG
0	$-1.594\lvert V_{A_o}\rvert/L_w$	0	0	0	0	0	0	0	0	0	0	0	WG
0	0	$-\omega_{hc}$	0	0	0	0	0	0	0	0	0	0	HDC
$-X_u$	$-X_w$	0	X_u	X_w	$X_q - W_o$	$-g\cos\theta_o$	X_{δ_B}	X_{δ_C}	0	X_{δ_B}	0	0	U
$-Z_u$	$-Z_w$	0	Z_u	Z_w	$Z_q + U_o$	$-g\sin\theta_o$	Z_{δ_B}	Z_{δ_C}	0	Z_{δ_B}	0	0	W
$-M_u$	$-M_w$	0	M_u	M_w	M_q	0	M_{δ_B}	M_{δ_C}	0	M_{δ_B}	0	0	Q
0	0	0	0	0	1.	0	0	0	0	0	0	0	TH
0	0	0	0	0	0	0	0	0	0	0	0	0	DB
0	0	0	0	0	0	0	0	0	0	0	0	0	DC
0	0	1.	$-\sin\theta_o$	$-\cos\theta_o$	0	$-V_{T_o}$	0	0	$-\epsilon$	0	0	0	HDI
0	0	0	0	0	4.97	0	0	0	0	-.333	0	0	XBR
0	0	0	$\cos\theta_o$	$\sin\theta_o$	0	0	0	0	0	0	$-\epsilon$	x	XDI[a]
$-\cos\theta_o$	$-\sin\theta_o$	0	$\cos\theta_o$	$\sin\theta_o$	0	0	0	0	0	0	x	$-\epsilon$	ASI[a]

$$F = \begin{bmatrix} F_s & 0 \\ C_c H_s & F_c \end{bmatrix} \qquad H_s = I$$

[a]XDI used in hover example;
ASI used in 100 kt example

(continued on following page)

TABLE B-2. (Continued)

$$
G = \begin{array}{c}
\begin{matrix} \text{DBD} & \text{DCD} \end{matrix} \\
\left[\begin{array}{cc}
0 & 0 \\ 0 & 0 \\ 0 & 0 \\ \hline 0 & 0 \\ 0 & 0 \\ 0 & 0 \\ 0 & 0 \\ 1. & 0 \\ 0 & 1. \\ 0 & 0 \\ 0 & 0 \\ 0 & 0 \\ 0 & 0
\end{array}\right]
\begin{array}{l}
\text{UG} \\ \text{WG} \\ \text{HDC} \\ \hline \text{U} \\ \text{W} \\ \text{Q} \\ \text{TH} \\ \text{DB} \\ \text{DC} \\ \text{HDI} \\ \text{XBR} \\ \text{XDI}^{a} \\ \text{ASI}^{a}
\end{array}
\end{array}
= \begin{bmatrix} 0 \\ G_C \end{bmatrix}
$$

$$
\Gamma = \begin{array}{c}
\begin{matrix} \text{PUG} & \text{PWG} & \text{PHC} & \text{PU} & \text{PW} & \text{PQ} & \text{PTH} & \text{PDB} & \text{PDC} & \text{PHI} & \text{PXB} & \text{PXI}^{a} & \text{PSE}^{a} \end{matrix} \\
\left[\begin{array}{ccccccccccccc}
\sqrt{2\lvert V_{T_0}\rvert/L_u} & 0 & 0 & 0 & 0 & 0 & 0 & 0 & 0 & 0 & 0 & 0 & 0 \\
0 & \sqrt{2\times 1.594\lvert V_{T_0}\rvert/L_u} & 0 & 0 & 0 & 0 & 0 & 0 & 0 & 0 & 0 & 0 & 0 \\
0 & 0 & \sqrt{2\omega_{n_c}} & 0 & 0 & 0 & 0 & 0 & 0 & 0 & 0 & 0 & 0 \\ \hline
0 & 0 & 0 & 1. & 0 & 0 & 0 & 0 & 0 & 0 & 0 & 0 & 0 \\
0 & 0 & 0 & 0 & 1. & 0 & 0 & 0 & 0 & 0 & 0 & 0 & 0 \\
0 & 0 & 0 & 0 & 0 & 1. & 0 & 0 & 0 & 0 & 0 & 0 & 0 \\
0 & 0 & 0 & 0 & 0 & 0 & 1. & 0 & 0 & 0 & 0 & 0 & 0 \\
0 & 0 & 0 & 0 & 0 & 0 & 0 & 1. & 0 & 0 & 0 & 0 & 0 \\
0 & 0 & 0 & 0 & 0 & 0 & 0 & 0 & 1. & 0 & 0 & 0 & 0 \\
0 & 0 & 0 & 0 & 0 & 0 & 0 & 0 & 0 & 1. & 0 & 0 & 0 \\
0 & 0 & 0 & 0 & 0 & 0 & 0 & 0 & 0 & 0 & 1. & 0 & 0 \\
0 & 0 & 0 & 0 & 0 & 0 & 0 & 0 & 0 & 0 & 0 & 1. & 0 \\
0 & 0 & 0 & 0 & 0 & 0 & 0 & 0 & 0 & 0 & 0 & 0 & 1.
\end{array}\right]
\begin{array}{l}
\text{UG} \\ \text{WG} \\ \text{HDC} \\ \hline \text{U} \\ \text{W} \\ \text{Q} \\ \text{TH} \\ \text{DB} \\ \text{DC} \\ \text{HDI} \\ \text{XBR} \\ \text{XDI}^{a} \\ \text{ASI}^{a}
\end{array}
\end{array}
= \begin{bmatrix} \Gamma_S \\ \Gamma_C \end{bmatrix}
$$

[a]XDI used in hover example; ASI used in 100 kt example.

(concluded on following page)

TABLE B-2. (Concluded)

UG	WG	HDC	U	W	Q	TH	DB	DC	HDI	XBR	XDI[a]	ASI[a]	
0	0	0	$\sin\theta_o$	$-\cos\theta_o$	0	V_{T_o}	0	0	0	0	0	0	HD
0	0	0	0	0	1.0	0	0	0	0	0	0	0	Q
0	0	0	0	0	0	1.0	0	0	0	0	0	0	TH
0	0	0	0	0	0	0	1.0	0	0	0	0	0	DB
0	0	0	0	0	0	0	0	1.0	0	0	0	0	DC
0	0	1.0	$-\sin\theta_o$	$\cos\theta_o$	0	$-V_{T_o}$	0	0	0	0	0	0	HDE
0	0	0	0	0	0	0	0	0	1.0	0	0	0	HDI
0	0	0	$\cos\theta_o$	$\sin\theta_o$	0	0	0	0	0	0	0	0	XD[b]
0	0	0	0	0	0	0	0	0	0	0	1.0	0	XDI[a]
0	0	0	0	0	0	0	0	0	0	0	0	1.0	ASI[a]
$-\cos\theta_o$	$-\sin\theta_o$	0	$\cos\theta_o$	$\sin\theta_o$	0	0	0	0	0	0	0	0	ASE[b]
$-X_u$	$-X_w$	0	X_u	X_w	X_q	$-g\cos\theta_o$	X_{δ_B}	X_{δ_C}	0	X_{δ_B}	0	0	AXP[c]
$-(Z_u - \ell_x M_u)$	$-(Z_w - \ell_x M_w)$	0	$Z_u - \ell_x M_u$	$Z_w - \ell_x M_w$	$Z_q - \ell_x M_q$	0	$Z_{\delta_B} - \ell_x M_{\delta_B}$	$Z_{\delta_C} - \ell_x M_{\delta_C}$	0	$Z_{\delta_B} - \ell_x M_{\delta_B}$	0	0	AZP[c]
0	$-1/V_{T_o}$	0	0	$1/V_{T_o}$	0	0	0	0	0	0	0	0	AOA

$$= H_R = \begin{bmatrix} F_M H_S & H_M \\ F_O H_S & H_O \end{bmatrix},$$

$$H_S = I$$

[a]XDI used in hover example; ASI used in 100 kt cruise.

[b]XD used as measurement in hover, output at 100 kt; ASE used as measurement at 100 kt, output in hover.

[c]Used to investigate acceleration measurements in 100 kt case.

TABLE B-3. VALUES FOR LONGITUDINAL EQUATIONS OF MOTION PARAMETERS

Parameter		100 kt (Case 128)	1 kt (Case 122)	Reference
V_A	kt	100.0	1.0	
$V_{T_o} = V_{A_o}$	ft/sec	168.78	1.69	
L_u	ft	1450.0	1450.0	
L_w	ft	1000.0	1000.0	
$\dot{\omega}_{h_c}$	rad/sec	0.1	0.1	
$\dot{\sigma}_{h_c}$	ft/sec	1.0	1.0	
σ_{u_g}	ft/sec	2.06	2.06	
σ_{w_g}	ft/sec	1.71	1.71	
h_o	ft	1000.0	1000.0	B-2
W_o	ft/sec	8.91	0.12	
U_o	ft/sec	168.54	1.68	
g	ft/sec^2	32.2	32.2	
θ_o	deg	3.02	4.04	
X_u	1/sec	−0.0451	−0.0034	
Z_u	1/sec	0.0888	−0.0991	
M_u	1/sec-ft	0.0050	0.0019	
X_w	1/sec	0.0950	0.0250	
Z_w	1/sec	−0.9963	−0.3850	
M_w	1/sec-ft	−0.0066	−0.0038	
X_q	ft/sec	1.7727	0.5797	
Z_q	ft/sec	−3.4493	0.2913	
M_q	1/sec	−0.7012	−0.1900	
X_{δ_B}	ft/in.-sec^2	0.5568	1.0406	
Z_{δ_B}	ft/in.-sec^2	5.0738	0.3214	
M_{δ_B}	1/in.-sec^2	−0.1728	−0.1691	
X_{δ_c}	ft/in.-sec^2	1.1402	0.6806	
Z_{δ_c}	ft/in.-sec^2	−13.1274	−9.7745	
M_{δ_c}	1/in.-sec^2	−0.0223	−0.0033	B-2
ℓ_x	ft	7.30	7.30	
h	ft	1000.0	1000.0	
$-\epsilon$	1/sec	→ 0	→ 0	

CONTROL AUTHORITY MODEL

The model for determining control displacement and rate requirements assumes mechanization in terms of series, parallel and boost actuators as shown below. Mechanization is the same for all control axes. Dynamics of the series and parallel servos are neglected. This block diagram enables us to write equations for the series actuator displacement

$$\dot{XS} = -K\,XS + (1 - K/\omega_A)\,DXD$$

$$DXS = XS + DXD/\omega_A$$

and the parallel actuator rate

$$DXPD = K\,DXS$$

where K is the gain in the integral path determined in the course of design.

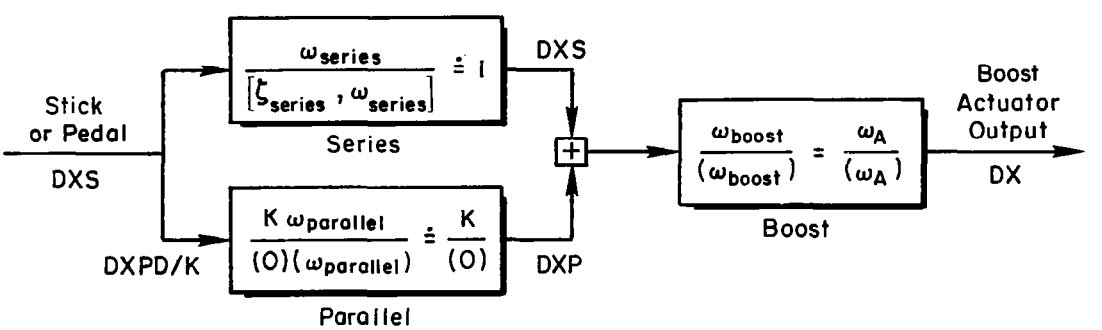

REFERENCES FOR APPENDIX B

B-1 McRuer, D. T., I. L. Ashkenas, and D. Graham, Aircraft Dynamics and Automatic Control, Princeton University Press, 1973.

B-2 Heffley, R. K., Wayne F. Jewell, John M. Lehman, and Richard A. Van Winkle, A Compilation and Analysis of Helicopter Handling Qualities Data, Vol. I: Data Compilation, STI TR-1087-1, Mar. 1979.

B-3 Corliss, L. D., and P. D. Talbot, A Failure Effects Simulation of a Low Authority Flight Control Augmentation System on a UH-1H Helicopter, NASA TM -73,258, Aug. 1977.

APPENDIX C

UH-1H, HOVER, EXAMPLE APPLICATION

This appendix presents the highlights of the synthesis and assessment procedures used in the design of a longitudinal flight control system for the UH-1H at hover. None of the design iteration steps are included, only the final results. Also, just a sampling of the assessment data is presented. The next several paragraphs describe the data which follow.

Table C-1 provides an overview of the primary design goals in this synthesis. They involve identifying the flight condition and the corresponding functions to be performed by the FCS, which in turn specify the bandwidths. The actuator bandwidths were computed using an approximation to the actual UH-1H hardware actuators (see Appendix B).

Tables C-2 and C-3 list the matrices used to define the problem. The shaping filter and controlled element equations are provided in Table C-2, while the measurement and output equations can be found in Table C-3.

Table C-4 contains the elements of the final filter-observer synthesis, discussed previously in Section IV (see Table 16).

Table C-5 begins the regulator synthesis portion of this example with a list of the relevant controlled element transfer functions. Figure C-1 presents an example of the portion of the regulator synthesis procedure that is concerned with making approximations to the transfer functions, computing the associated cost function weightings for each surrogate control, and choosing the most effective control point by selecting the smallest cost function weighting. The θ closure is computed here, using cyclic and collective as the candidate control points. Notice that for the TH/DB transfer function both the asymptotic and actual Bode plots are used in computing K and n. Compared to the cost function weighting when collective is used as the control point there is little difference between the asymptote and the actual transfer function approximations. Based on the cost function weightings, longitudinal cyclic is chosen as the most effective θ control point.

As was mentioned in Section IV, it is often possible in a particular application to predict the effect of various closures on subsequent closed-loop transfer functions and thereby eliminate the iterative section of the regulator synthesis by effectively closing all of the loops simultaneously. This was possible for the example at hand. Table C-6 presents the design of the regulator by indicating the process of choosing the most effective control point at each step. Notice that the cost function weighting on collective rate, R_{DCD}, is an order of magnitude larger than the cost function weighting on cyclic rate, R_{DBD}. This reflects the results of the 100 kt design study wherein collective activity was judged to be too severe when the cost function weightings on the actuator rates were equal (see Section IV).

Table C-7 presents the final regulator design for this example.

Once the filter-observer and regulator syntheses are complete, all that remains in the optimal controller design is to compute the controller coefficient matrices, shown in Table C-8, and the controller transfer functions, shown in Table C-9.

The design assessment begins in Fig. C-2 with closed-loop transfer functions and transient responses to step inputs of u_g, w_g, and $\dot{h}_c$. This provides information on the gust suppression characteristics of the design, as well as the response to command inputs.

Next we examine Bode plots of various closed-loop transfer functions to see if the design goals were attained. Figure C-3 shows the rate-of-climb response to rate-of-climb command; the -45 deg phase angle falls at approximately 1.2 rad/sec. Figure C-4 presents the error response for the same variable — the -3 dB point is at 1.0 rad/sec.

Figure C-5 is a Bode plot for the approximation of the θ/θ_c transfer function with all loops closed. Figures C-6 and C-7 plot the proportional plus integral and proportional plus integral error transfer functions, respectively, for the groundspeed loop. Again we see a close agreement between the design goals and the actual design.

The final steps presented here for assessing the design via classical control metrics make use of the I_M matrix (see Fig. 6) to compute

various open-loop transfer functions. These open-loop transfer functions provide a means for determining the effect of the outer-loop closures on the inner-loop bandwidths.

Figure C-8 is a plot of the rate-of-climb proportional-plus-integral transfer function with the proportional and integral loops opened. The crossover frequency is about 1.2 rad/sec. Figure C-9 examines the rate-of-climb integral bandwidth by plotting the HDI/VHI transfer function with the HDI loop opened. Figures C-10 and C-11 show similar plots for the proportional-plus-integral groundspeed loops. Figure C-12 plots a more inner loop, the θ loop, with the θ, $\dot{x}$, and $\int \dot{x}\,dt$ loops opened. Here we see a crossover frequency of approximately 2.3 rad/sec.

Finally, an assessment of this FCS design based on statistical metrics is presented in Table C-10. The process noise augmentation has been removed here. We can compare the rms response of the plant states and filter states to the combined process and measurement noise with any secondary design goals specified at the outset. We also have at hand the rms response of the outputs and controls, which enables us to compute measures of control activity such as the positive-going zero crossing rate, also shown in the table.

This appendix has presented just a sample of the design synthesis and assessment tools available. Increased familiarity with the design process will enable a designer to feel comfortable with this method and the resulting data analysis.

TABLE C-1

EXAMPLE APPLICATION

UH-1H Longitudinal Flight Control System

Flight Condition: Hover

Functions:

- Rate-of-climb command
- Groundspeed hold

Bandwidths:	(rad/sec)
Cyclic (DB):	25.73
Collective (DC):	25.73
Pitch (TH):	2.0
Rate-of-climb error (HDI):	1.0
Integral of HDE (HDI):	0.82
Groundspeed error (XD):	0.5
Integral of XD (XDI):	0.1

TABLE C-2. PLANT; CONTROLLED ELEMENT AND SHAPING FILTERS

$$\dot{x} = Fs + Gu + \Gamma w \quad , \quad x(0) = x_0$$

$$x' = \{ \underset{\text{Long. gust velocity}}{UG} \quad \underset{\text{Normal gust velocity}}{WG} \quad \underset{\text{R/C command}}{HDC} \mid \underset{\text{Longitudinal velocity}}{U} \quad \underset{\text{Normal velocity}}{W} \quad \underset{\text{Pitch rate}}{Q} \quad \underset{\text{Pitch attitude}}{TH} \quad \underset{\text{Longitudinal cyclic}}{DB} \quad \underset{\text{Main rotor collective}}{DC} \quad \underset{\text{Integral R/C error}}{HDI} \quad \underset{\text{Horizontal stab. bar}}{XBR} \quad \underset{\text{Integral long. speed}}{XDI} \}$$

F MATRIX

1 X01	2 X02	3 X03	4 X06	5 X07	6 X08	7 X09	8 X10	9 X11	10 X12	11 X13	12 X14	
-0.117E-02	0.000	0.000	0.000	0.000	0.000	0.000	0.000	0.000	0.000	0.000	0.000	1 X01
0.000	-0.269E-02	0.000	0.000	0.000	0.000	0.000	0.000	0.000	0.000	0.000	0.000	2 X02
0.000	0.000	-0.100	0.000	0.000	0.000	0.000	0.000	0.000	0.000	0.000	0.000	3 X03
0.340E-02	-0.250E-01	0.000	-0.340E-02	0.250E-01	0.460	-32.1	1.04	0.681	0.000	1.04	0.000	4 X06
0.991E-01	0.385	0.000	-0.991E-01	-0.385	1.97	-2.27	0.321	-9.77	0.000	0.321	0.000	5 X07
-0.190E-02	0.380E-02	0.000	0.190E-02	-0.380E-02	-0.190	0.000	-0.169	-0.330E-02	0.000	-0.169	0.000	6 X08
0.000	0.000	0.000	0.000	0.000	1.00	0.000	0.000	0.000	0.000	0.000	0.000	7 X09
0.000	0.000	0.000	0.000	0.000	0.000	0.000	0.000	0.000	0.000	0.000	0.000	8 X10
0.000	0.000	0.000	0.000	0.000	0.000	0.000	0.000	0.000	0.000	0.000	0.000	9 X11
0.000	0.000	1.00	-0.705E-01	0.998	0.000	-1.69	0.000	0.000	0.000	0.000	0.000	10 X12
0.000	0.000	0.000	0.000	0.000	4.97	0.000	0.000	0.000	0.000	-0.333	0.000	11 X13
0.000	0.000	0.000	0.998	0.705E-01	0.000	0.000	0.000	0.000	0.000	0.000	0.000	12 X14

(continued on following page)

TABLE C-2. (Continued)

Long. cyclic rate — Main rotor collective

u' = DBD DCD

G MATRIX

1 DBD	2 DCD	
0.000	0.000	1 X01
0.000	0.000	2 X02
0.000	0.000	3 X03
0.000	0.000	4 X06
0.000	0.000	5 X07
0.000	0.000	6 X08
0.000	0.000	7 X09
1.00	0.000	8 X10
0.000	1.00	9 X11
0.000	0.000	10 X12
0.000	0.000	11 X13
0.000	0.000	12 X14

(concluded on following page

TABLE C-2. (Concluded)

GAMMA MATRIX

1 PUG	2 PWG	3 PHC	4 P U	5 P W	6 P Q	7 PTH	8 PDB	9 PDC	10 PHD	11 PXB	12 PXD	
0.483E-01	0.000	0.000	0.000	0.000	0.000	0.000	0.000	0.000	0.000	0.000	0.000	1 X01
0.000	0.734E-01	0.000	0.000	0.000	0.000	0.000	0.000	0.000	0.000	0.000	0.000	2 X02
0.000	0.000	0.447	0.000	0.000	0.000	0.000	0.000	0.000	0.000	0.000	0.000	3 X03
0.000	0.000	0.000	1.00	0.000	0.000	0.000	0.000	0.000	0.000	0.000	0.000	4 X06
0.000	0.000	0.000	0.000	1.00	0.000	0.000	0.000	0.000	0.000	0.000	0.000	5 X07
0.000	0.000	0.000	0.000	0.000	1.00	0.000	0.000	0.000	0.000	0.000	0.000	6 X08
0.000	0.000	0.000	0.000	0.000	0.000	1.00	0.000	0.000	0.000	0.000	0.000	7 X09
0.000	0.000	0.000	0.000	0.000	0.000	0.000	1.00	0.000	0.000	0.000	0.000	8 X10
0.000	0.000	0.000	0.000	0.000	0.000	0.000	0.000	1.00	0.000	0.000	0.000	9 X11
0.000	0.000	0.000	0.000	0.000	0.000	0.000	0.000	0.000	1.00	0.000	0.000	10 X12
0.000	0.000	0.000	0.000	0.000	0.000	0.000	0.000	0.000	0.000	1.00	0.000	11 X13
0.000	0.000	0.000	0.000	0.000	0.000	0.000	0.000	0.000	0.000	0.000	1.00	12 X14

TABLE C-3. PLANT; OUTPUT AND MEASUREMENT EQUATIONS

$$y = H_R x \qquad H_R = \left[- - H - - \right]$$

$$z = Hx + v$$

$$z' = \{ HD \quad Q \quad TH \quad DB \quad DC \quad HDE \quad HDI \quad XD \quad XDI \}$$

(HD: Rate of climb; Q: Pitch rate; TH: Pitch attitude; DB: Longitud. cyclic; DC: Main rotor collective; HDE: R/C error; HDI: Integral of R/C error; XD: Longitud. speed; XDI: Integral of long. speed)

HR MATRIX

1 X01	2 X02	3 X03	4 X06	5 X07	6 X08	7 X09	8 X10	9 X11	10 X12	11 X13	12 X14	
0.000	0.000	0.000	0.705E-01	-0.998	0.000	1.69	0.000	0.000	0.000	0.000	0.000	1 HD
0.000	0.000	0.000	0.000	0.000	1.00	0.000	0.000	0.000	0.000	0.000	0.000	2 Q
0.000	0.000	0.000	0.000	0.000	0.000	1.00	0.000	0.000	0.000	0.000	0.000	3 TH
0.000	0.000	0.000	0.000	0.000	0.000	0.000	1.00	0.000	0.000	0.000	0.000	4 DB
0.000	0.000	0.000	0.000	0.000	0.000	0.000	0.000	1.00	0.000	0.000	0.000	5 DC
0.000	0.000	1.00	-0.705E-01	0.998	0.000	-1.69	0.000	0.000	0.000	0.000	0.000	6 HDE
0.000	0.000	0.000	0.000	0.000	0.000	0.000	0.000	0.000	1.00	0.000	0.000	7 HDI
0.000	0.000	0.000	0.998	0.705E-01	0.000	0.000	0.000	0.000	0.000	0.000	0.000	8 XD
0.000	0.000	0.000	0.000	0.000	0.000	0.000	0.000	0.000	0.000	0.000	1.00	9 XDI
0.000	-0.592	0.000	0.000	0.592	0.000	0.000	0.000	0.000	0.000	0.000	0.000	10 AOA
-0.998	-0.705E-01	0.000	0.998	0.705E-01	0.000	0.000	0.000	0.000	0.000	0.000	0.000	11 ASE

TABLE C-4. FILTER-OBSERVER SYNTHESIS

Q MATRIX DIAGONAL, FILTER 1

4.24	1 PUG
2.92	2 PWG
1.00	3 PHC
0.100E-04	4 P U
0.100E-04	5 P W
0.100E-04	6 P Q
0.100E-05	7 PTH
0.100E-04	8 PDB
0.100E-04	9 PDC
0.100E-04	10 PHD
0.000	11 PXB
0.100E-04	12 PXD

R MATRIX DIAGONAL, FILTER 1

0.000	1 HD
0.000	2 Q
0.000	3 TH
0.000	4 DB
0.000	5 DC
0.000	6 HDE
0.000	7 HDI
0.000	8 XD
0.000	9 XDI

CLOSED LOOP EIGENVALUES, FILTER 1

0.333 180.	1 E13
15.6 180.	2 E01
0.315 180.	3 E02

RMS STATE EST ERROR, FILTER 1

0.173	1 X01
0.541E-01	2 X02
0.000	3 X03
0.000	4 X06
0.000	5 X07
0.000	6 X08
0.000	7 X09
0.000	8 X10
0.000	9 X11
0.000	10 X12
0.000	11 X13
0.000	12 X14

K12 GAIN MATRIX, FILTER

1 HD	2 Q	3 TH	4 DB	5 DC	6 HDE	7 HDI	8 XD	9 XDI	
0.941E-08	-0.679E-09	-0.159E-07	0.000	0.000	-0.286E-16	0.000	0.195E-08	0.000	1 E13
-6.07	-8.57	10.3	0.000	0.000	0.184E-07	0.000	29.5	0.000	2 E01
-38.9	2.54	65.8	0.000	0.000	0.118E-06	0.000	-7.16	0.000	3 E02

TABLE C-5. CONTROLLED ELEMENT TRANSFER FUNCTIONS

CASE: UH1H HOVER 122LONG 31-JAN-79 CONTROLLED ELEMENT TF'S

DENOMINATOR:

```
 1.0000
( .00000    ) ( .00000    ) ( .00000    ) ( .00000    )
( .38494    )
(( .10339    , .18934    , .19576E-01, .18833    ))
(( .26279    , .92717    , .24365    , .89459    ))
< .11863E-01>
```

NUMERATOR: TH/DBD

```
-.16910
( .00000    ), ( .00000    ) ( .00000    ) (-.79065E-02)
( .33300    ) ( .39184    )
< .17445E-03>
```

NUMERATOR: TH/DCD

```
-.33000E-02
( .00000    ) ( .00000    ) ( .00000    ) ( .10854E-01)
( .33300    ) (-11.270    )
< .13442E-03>
```

NUMERATOR: HDE/DBD

```
 .24729
( .00000    ) ( .00000    ) ( .00000    ) ( .33300    )
(-1.4789    )
(( .35965    , 1.3542    , .48705    , 1.2636    ))
<-.22334    >
```

NUMERATOR: HDE/DCD

```
-9.7980
( .00000    ) ( .00000    ) ( .00000    )
(( .18545    , .14356    , .26623E-01, .14107    ))
(( .25760    , .93210    , .24011    , .90064    ))
<-.17544    >
```

NUMERATOR: HDI/DCD

```
-9.7980
( .00000    ) ( .00000    )
(( .18545    , .14356    , .26623E-01, .14107    ))
(( .25760    , .93210    , .24011    , .90064    ))
<-.17544    >
```

NUMERATOR: XD/DBD

```
 1.0606
( .00000    ) ( .00000    ) ( .00000    ) ( .33300    )
( .38296    )
(( .19712E-01, 2.2663    , .44674E-01, 2.2659    ))
< .69473    >
```

NUMERATOR: XDI/DBD

```
 1.0606
( .00000    ) ( .00000    ) ( .33300    ) ( .38296    )
(( .19712E-01, 2.2663    , .44674E-01, 2.2659    ))
< .69473    >
```

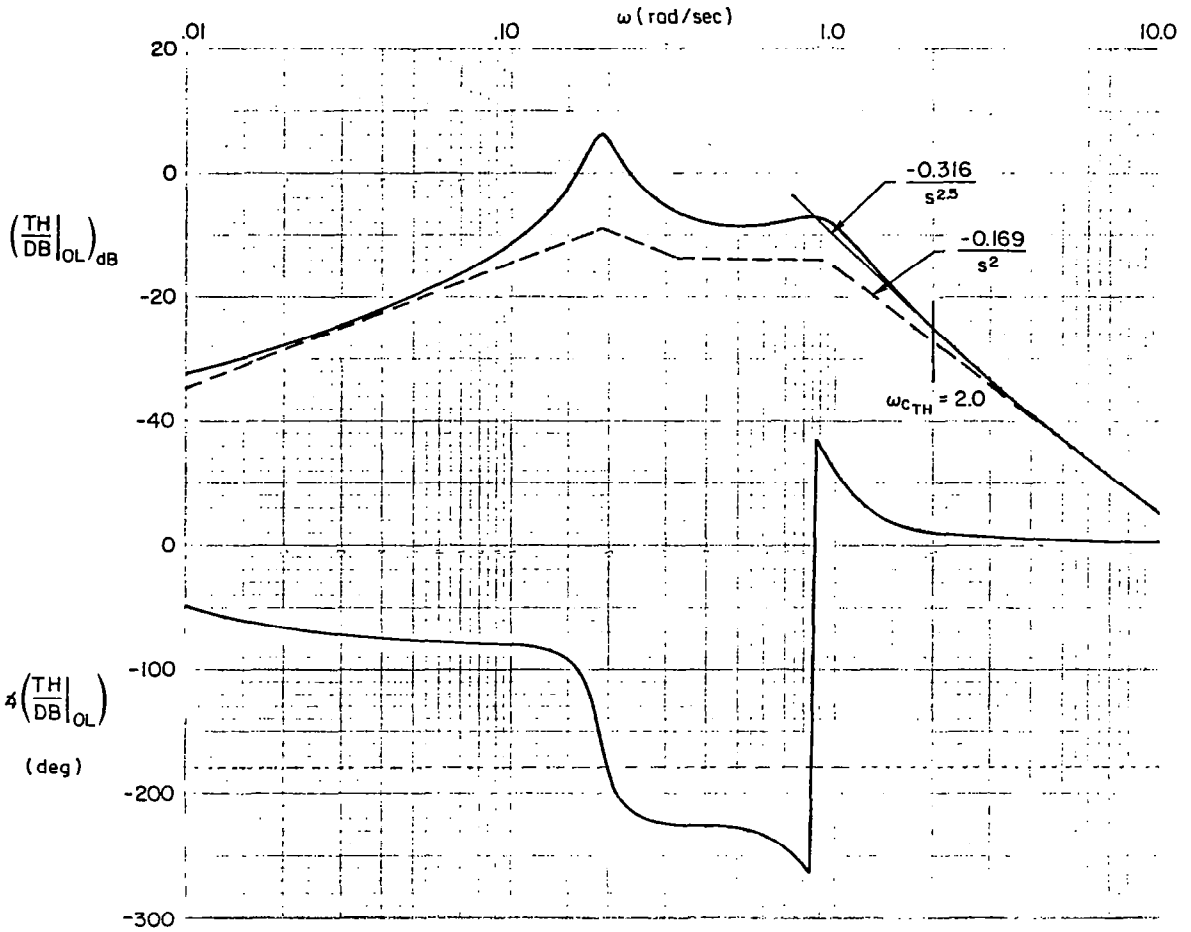

K/s^{n+1} APPROXIMATION	$\frac{(2^n \omega_{c_{TH}}^2)^{n+1} Q_{DB}}{\left(K_{DB}^{TH}\right)^2}$
Asymptotic K = 0.169, n = 1.0	1,484,183
G(jω) K = 0.316, n = 1.5	2,851,632

Figure C-1. Approximating Transfer Functions — Selecting Value for Q_R

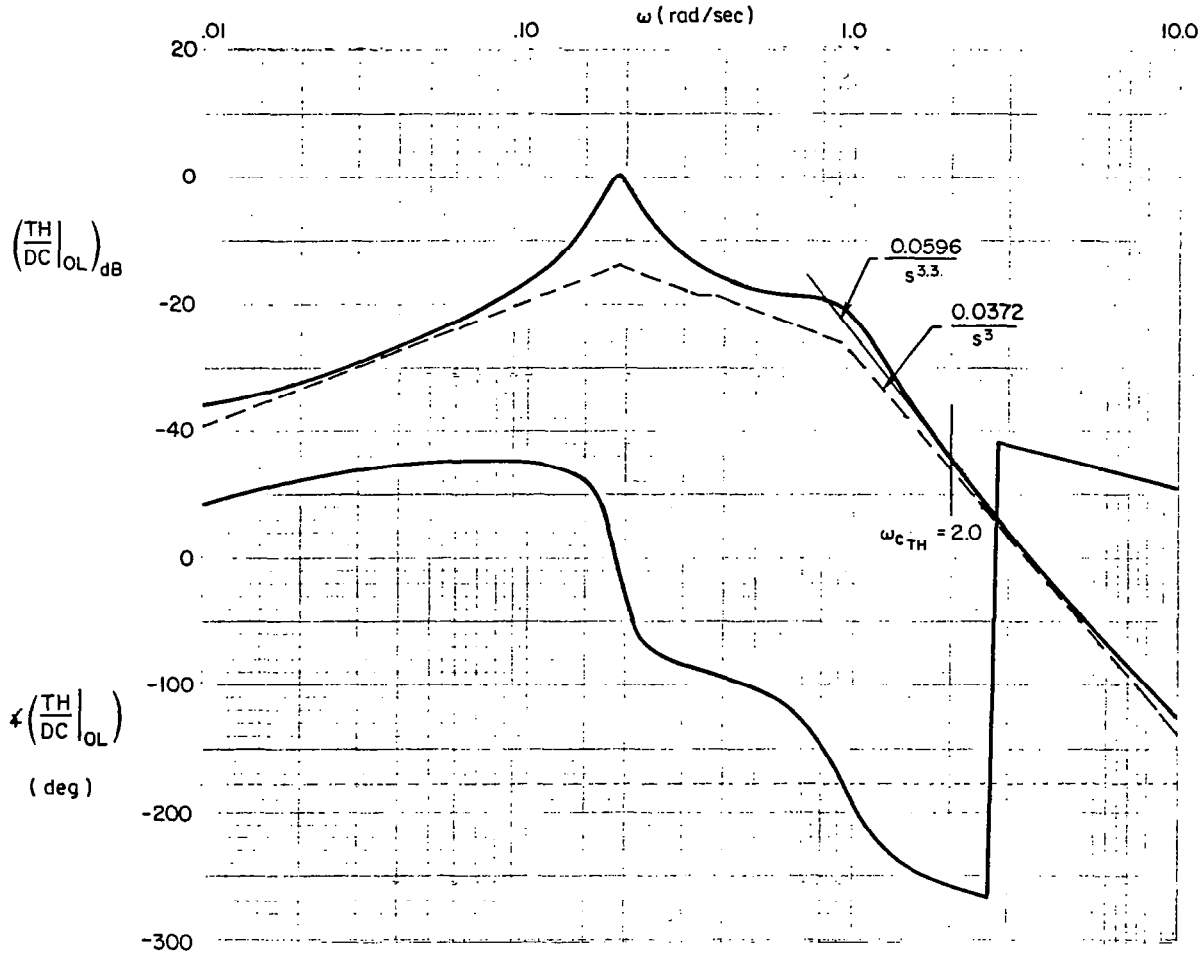

K/s^{n+1} APPROXIMATION	$\frac{(2^n \omega_{c_{TH}}^2)^{n+1} Q_{DC}}{\left(K_{DC}^{TH}\right)^2}$
Asymptotic K = 0.0372, n = 2.0	19,604,468,000

Figure C-1. (Concluded)

TABLE C-6. SUMMARY OF Q_R AND R_R SELECTION

	ω_c		$R_{DBD} = 1.0$		$R_{DCD} = 10.0$		
Longitudinal Cyclic Actuator	25.7	$\left.\frac{DB}{DBD}\right\|_{\omega_c} = \frac{1}{s}$	K = 1.0 n = 0	$Q_{DB} = 662.34$	$\left.\frac{DB}{DCD}\right\|_{\omega_c} = 0$		
Main Rotor Collective Actuator	25.7	$\frac{DC}{DBD} = 0$			$\left.\frac{DC}{DCD}\right\|_{\omega_c} = \frac{1}{s}$	K = 1.0 n = 0	$Q_{DC} = 6623.4$
Pitch Attitude	2.0	$\left.\frac{TH}{DB}\right\|_{\omega_c} = \frac{.169}{s^2}$	K = 0.169 n = 1	$Q_{TH} = 1,482,428$	$\left.\frac{TH}{DC}\right\|_{\omega_c} = \frac{.0372}{s^2}$	K = 0.0372 n = 1	$Q_{TH} = 19,604,468,000$
Rate-of-Climb Error, Proportional	1.0	$\left.\frac{HDE}{DB}\right\|_{\omega_c} = \frac{.1866}{s}$	K = 0.1866 n = 0	$Q_{HDE} = 19022.0$	$\left.\frac{HDE}{DC}\right\|_{\omega_c} = \frac{-9.798}{s}$	K = -9.798 n = 0	$Q_{HDE} = 69.0$
Rate-of-Climb Error, Integral	0.82				$\left.\frac{HDI}{HDE}\right\|_{\omega_c} = \frac{1}{s}$	K = 1.0 n = 0	$Q_{HDI} = 46.6$
Groundspeed Error, Proportional	0.5	$\left.\frac{XD}{TH}\right\|_{\omega_c} = \frac{-32.2}{s}$	K = -32.2 n = 0	$Q_{XD} = 357.33$	$\left.\frac{XD}{HDE}\right\|_{\omega_c} = -3.22$		
Groundspeed Error, Integral	0.1	$\left.\frac{XDI}{XD}\right\|_{\varphi_c} = \frac{1}{s}$	K = 1.0 n = 0	$Q_{XDI} = 3.57$			

Q MATRIX DIAGONAL, REGULATOR

1	
0.000	1 HD
0.000	2 Q
0.148E+07	3 TH
662.	4 DB
0.662E+04	5 DC
69.0	6 HDE
46.6	7 HDI
357.	8 XD
3.57	9 XDI
0.000	10 AOA
0.000	11 ASE

R MATRIX DIAGONAL, REGULATOR

1	
1.00	1 DBD
10.0	2 DCD

CLOSED LOOP EIGENVALUES, REGULATOR

1	
25.7 180.	1 X01
25.7 180.	2 X02
2.77 -132.	3 X03
2.77 132.	4 X06
0.907 -157.	5 X07
0.907 157.	6 X08
0.505 180.	7 X09
0.102 180.	8 X10
0.336 180.	9 X11
0.117E-02 180.	10 X12
0.269E-02 180.	11 X13
0.100 180.	12 X14

TABLE C-7. REGULATOR SYNTHESIS

REGULATOR GAIN MATRIX

1 X01	2 X02	3 X03	4 X06	5 X07	6 X08	7 X09	8 X10	9 X11	10 X12	11 X13	12 X14	
0.254	0.523	0.717	22.8	1.98	-537.	-0.152E+04	29.9	-0.518E-01	0.252	28.9	1.89	1 DBD
-0.264	-1.07	-4.16	0.819	-3.37	-0.846	-0.936	-0.517E-02	27.0	-2.16	-0.122	0.221E-01	2 DCD

TABLE C-8. CONTROLLER COEFFICIENT MATRICES

AF MATRIX

1 E13	2 E01	3 E02	
-0.333	0.906E-09	0.363E-08	1 E13
-34.3	-0.922	-2.37	2 E01
-1.60	-3.76	-15.0	3 E02

$$\dot{\hat{y}} = A_F \hat{y} + B_F z$$

$$u = C_F \hat{y} + D_F z$$

BF MATRIX

1 HD	2 Q	3 TH	4 DB	5 DC	6 HDE	7 HDI	8 XD	9 XDI	
-0.146E-06	4.97	0.310E-06	0.142E-09	-0.922E-07	0.452E-15	0.000	-0.104E-08	0.000	1 E13
95.6	-29.1	788.	-34.3	59.7	-0.295E-06	0.000	-9.13	0.000	2 E01
592.	-76.5	-0.123E+04	-1.60	381.	-0.183E-05	0.000	1.36	0.000	3 E02

CF MATRIX

1 E13	2 E01	3 E02	
-28.9	-0.254	-0.523	1 DBD
0.122	0.264	1.07	2 DCD

DF MATRIX

1 HD	2 Q	3 TH	4 DB	5 DC	6 HDE	7 HDI	8 XD	9 XDI	
21.5	538.	0.149E+04	-29.9	0.518E-01	-0.717	-0.252	-26.6	-1.89	1 DBD
-42.5	1.30	79.8	0.517E-02	-27.0	4.16	2.16	-0.436	-0.221E-01	2 DCD

TABLE C-9. CONTROLLER TRANSFER FUNCTIONS

CASE: UH1H HOVER 122LONG 2-FEB-79 CONTROLLER TRANSFER FUNCTIONS

DENOMINATOR:

```
  1.0000
( .31507    ) ( .33300    ) ( 15.614    )
< 1.6383    >
```

NUMERATOR: DBD/ HD

```
  21.541
( .11140    ) ( .31682    ) ( .33300    )
< .25317    >
```

NUMERATOR: DBD/ Q

```
  538.16
( 15.694    )
(( .79748    , .24420    , .19475    , .14734    ))
< 503.67    >
```

NUMERATOR: DBD/ TH

```
  1486.9
( .24018    ) ( .33300    ) ( 15.988    )
< 1901.3    >
```

NUMERATOR: DBD/ DB

```
  -29.879
( .18186    ) ( .33300    ) ( 15.428    )
<-27.917    >
```

NUMERATOR: DBD/ DC

```
  .51781E-01
( .29977    ) ( .33300    ) (-4127.1    )
<-21.332    >
```

NUMERATOR: DBD/HDE

```
  -.71659
( .31507    ) ( .33300    ) ( 15.614    )
<-1.1741    >
```

NUMERATOR: DBD/HDI

```
  -.25178
( .31507    ) ( .33300    ) ( 15.614    )
<-.41249    >
```

NUMERATOR: DBD/ XD

```
  -26.641
( .27441    ) ( .33300    ) ( 15.595    )
<-37.964    >
```

NUMERATOR: DBD/XDI

```
  -1.8892
( .31507    ) ( .33300    ) ( 15.614    )
<-3.0950    >
```

NUMERATOR: DCD/ HD

```
  -42.506
( .11589    ) ( .31500    ) ( .33300    )
<-.51672    >
```

NUMERATOR: DCD/ Q

```
  1.3019
(-.28691E-01) ( 1.2724    ) (-53.279    )
< 2.5324    >
```

NUMERATOR: DCD/ TH

```
  79.797
( .33300    ) (-.45581    ) ( 2.4905    )
<-30.165    >
FLOATING UNDERFLOW      PC=036035
```

NUMERATOR: DCD/ DB

```
  .51744E-02
(-.11656    ) ( .33300    ) (-2064.8    )
< .41471    >
FLOATING UNDERFLOW      PC=036035
```

NUMERATOR: DCD/ DC

```
  -27.008
(-.94888E-01) ( .33300    ) ( .33773    )
< .28821    >
```

NUMERATOR: DCD/HDE

```
  4.1570
( .31507    ) ( .33300    ) ( 15.614    )
< 6.8103    >
```

NUMERATOR: DCD/HDI

```
  2.1563
( .31507    ) ( .33300    ) ( 15.614    )
< 3.5326    >
```

NUMERATOR: DCD/ XD

```
  -.43622
( .15039    ) ( .33300    ) ( 17.982    )
<-.39283    >
```

NUMERATOR: DCD/XDI

```
  -.22059E-01
( .31507    ) ( .33300    ) ( 15.614    )
<-.36139E-01>
```

Longitudinal Gust Transfer Functions

```
   CASE:  UH1H HOVER 122LONG 31-JAN-79 ALL LOOPS CLOSED
FLOATING UNDERFLOW       PC=036035

 DENOMINATOR:

    1.0000
   ( .10195     )  ( .31507     )  ( .33300     )  ( .33595     )
   ( .50520     )  ( 15.614     )  ( 25.716     )  ( 25.726     )
   (( .92313     , .90723     , .83748     , .34882     ))
   (( .67380     , 2.7741     , 1.8692     , 2.0498     ))
     118.79     >


 NUMERATOR:   HD/ UG   FILE NAME?  HDUG.2CL
  NEW FILE

   -.93613E-01
   ( .00000     )  ( .10125     )  ( .32805     )  ( .33300     )
   ( .48797     )  ( 25.726     )  ( 42.847     )
   (( .60809     , .40520E-01, .24640E-01, .32167E-01))
   (( .69689     , 2.7215     , 1.8966     , 1.9518     ))
   <-.71328E-02>


 NUMERATOR:   DB/ UG   FILE NAME?  DBUG.2CL
  NEW FILE

   -3.4937
   ( .10140     )  ( .33300     )  ( .69651     )  ( 2.3403     )
   ( 3.7979     )  ( 25.724     )
   (( .86433     , .29608     , .28552     , .78370E-01))
   (( .89856     , .90773     , .81564     , .39936     ))
   <-1.3571     >


 NUMERATOR:   TH/ UG   FILE NAME?  THUG.2CL
  NEW FILE

   -.19090E-02
   ( .89119E-01)  ( .33300     )  ( .33300     )  ( 7.5257     )
   ( 25.724     )  ( 38.150     )
   (( .50519     , .24630     , .12442     , .21256     ))
   (( .92523     , .09866     , .83146     , .31096     ))
    -.67934E-02.


 NUMERATOR:   XD/ UG   FILE NAME?  XDUG.2CL
  NEW FILE

    .10373E-01
   ( .00000     )  ( .26728E-02)  ( .33300     )  ( .33300     )
   ( 6.8075     )  ( 25.724     )  ( 39.714     )
   (( .94505     , .91380     , .85445     , .32395     ))
   ((-.10977     , 1.8327     ,-.34779     , 1.7994     ))
     .59972E-01.


 NUMERATOR:   DC/ UG   FILE NAME?  DCUG.2CL
  NEW FILE

    1.5946
   ( .10116     )  ( .32513     )  ( .33300     )  ( .34094     )
   ( .48284     )  ( 25.726     )
   (( .20974     , .04304     , .75938     , .36614     ))
   (( .57499     , 2.7655     , 1.8867     , 2.0404     ))
    1.1618     >
```

Transient Response to -10.0 ft/sec u_g Step Input

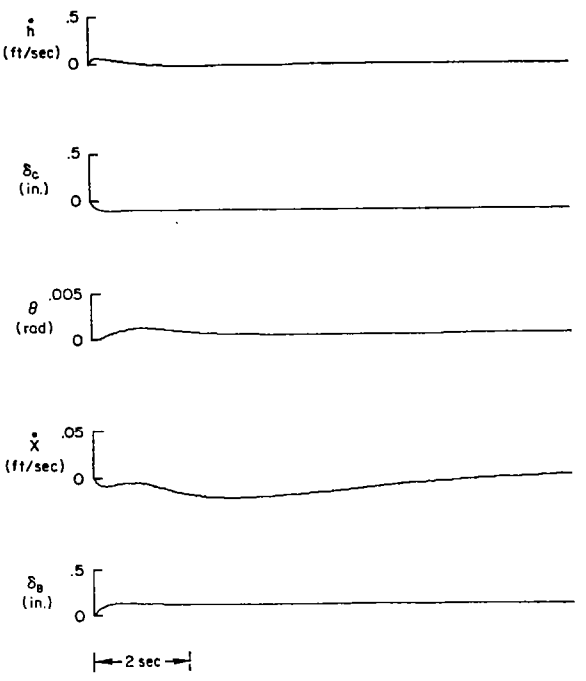

(continued on following page)

Figure C-2. Closed-Loop System Transfer Functions, Transient Response to Commands, Transient Response to Disturbances

Normal Gust Transfer Functions

```
CASE:  UH1H HOVER 122LONG 31-JAN-79 ALL LOOPS CLOSED
ATING UNDERFLOW       PC=036035

ENOMINATOR:

  1.0000
( .10195     ) ( .31507     ) ( .33300     ) ( .33595     )
( .50520     ) ( 15.614     ) ( 25.716     ) ( 25.726     )
(( .92313    , .90723     , .83748     , .34882     ))
(( .57380    , 2.7741     , 1.8692     , 2.0498     ))
< 119.79     >
ATING UNDERFLOW       PC=036035


UMERATOR:   HD/ WG   FILE NAME?  HDWG.2CL
NEW FILE

 -.38580
( .00000     ) ( .15150E-01) ( .10198     ) ( .32014     )
( .33300     ) ( .33892     ) ( .51520     ) ( 25.726     )
( 42.790     )
(( .63102    , 2.8085     , 1.7722     , 2.1787     ))
<-.96398E-01>


UMERATOR:   DR/ WG   FILE NAME?  DRWG.2CL
NEW FILE

 -6.6091
( .10211     ) ( .33300     ) (-6.7123     ) ( 25.726     )
(( .99748    , .33096     , .33013     , .23482E-01))
(( .95584    , .72377     , .69182     , .21270     ))
(( .90318    , 1.0757     , .97155     , .46175     ))
< 2.5732     >


UMERATOR:   TH/ WG   FILE NAME?  THWG.2CL
NEW FILE

  .38000E-02
( .10290     ) ( .33300     ) ( .33300     ) ( 25.726     )
(( .99403    , .34557     , .34351     , .37710E-01))
(( .92188    , .91517     , .84369     , .35460     ))
(( .77874    , 28.639     , 22.302     , 17.966     ))
< .91509E-01>


NUMERATOR:  XD/ WG   FILE NAME?  XDWG.2CL
NEW FILE

  .21957E-02
( .00000     ) ( .14808E-01) ( .27605     ) ( .33300     )
( .33468     ) (-7.0035     ) ( 25.726     ) (-28.403     )
( 81.909     )
(( .90770    , .90729     , .82355     , .38073     ))
< .34358     >


NUMERATOR:  DC/ WG   FILE NAME?  DCWG.2CL
NEW FILE

  18.007
( .10188     ) ( .31464     ) ( .33300     ) ( .33590     )
( .51001     ) ( 25.726     )
(( .91175    , .84947     , .77468     , .34855     ))
(( .67067    , 2.7835     , 1.8668     , 2.0647     ))
< 4.7364     >
```

Transient Response to -1.0 ft/sec w_g Step Input

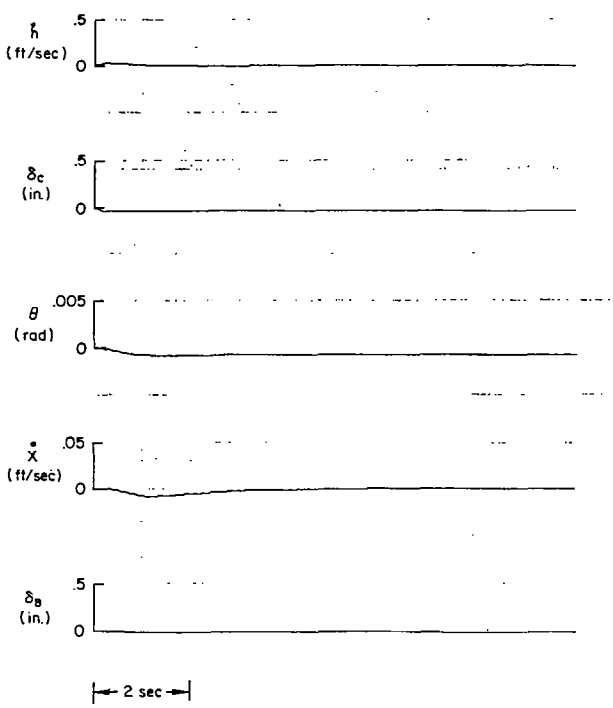

(concluded on following page)

Figure C-2. (Continued)

Rate-of-Climb Command Transfer Functions

CASE: UH1H HOVER 122LONG 31-JAN-79 ALL LOOPS CLOSED

DENOMINATOR:

```
  1.0000
( .10195    ) ( .31507    ) ( .33300    ) ( .33595    )
( .50520    ) ( 15.614    ) ( 25.716    ) ( 25.726    )
(( .92313    , .90723    , .83748    , .34882    ))
(( .67380    , 2.7741    , 1.8692    , 2.0498    ))
< 118.79    >
```

NUMERATOR: HD/HDC FILE NAME? HDHDC.2CL
NEW FILE

```
  40.908
( .10195    ) ( .31507    ) ( .33300    ) ( .33601    )
( .50240    ) ( .52197    ) ( 15.614    ) ( 25.726    )
(( .67251    , 2.7694    , 1.8625    , 2.0496    ))
< 118.79    >
```

NUMERATOR: DB/HDC FILE NAME? DBHDC.2CL
NEW FILE

```
 -.71669
( .10135    ) ( .31506    ) ( .33300    ) ( .39446    )
(-2.2043    ) ( 15.615    ) ( 25.741    )
(( .99877    , .49323    , .47290    , .14017    ))
(( .73782    , 2.0271    , 1.4956    , 1.3683    ))
< 2.6625    >
```

NUMERATOR: TH/HDC FILE NAME? THHDC.2CL
NEW FILE XDHDC.2CL

```
 -.71391E-03
( .31506    ) ( .33300    ) ( .33300    ) ( .37296    )
(( .58193    , .10137    , .58992E-01, .82440E-01))
(( .89789    , 6.9191    , 6.2125    , 3.0459    ))
(( .99988    , 16.332    , 16.330    , .25708    ))
<-.12207E-02>
```

NUMERATOR: XD/HDC FILE NAME? XDHDC.2CL
NEW FILE

```
 -.80053
( .00000    ) ( .31503    ) ( .31968    ) ( .33300    )
( .38773    ) (-.57722    ) ( 15.614    ) ( 25.741    )
(( .58773    , 1.7890    , 1.0514    , 1.4474    ))
< 7.7291    >
```

NUMERATOR: DC/HDC FILE NAME? DCHDC.2CL
NEW FILE

```
  4.1570
( .10235    ) ( .31507    ) ( .33300    ) ( .33684    )
( .38238    ) ( .47218    ) ( .55313    ) ( 15.614    )
( 25.726    )
(( .67330    , 2.7743    , 1.8680    , 2.0513    ))
< 4.6428    >
```

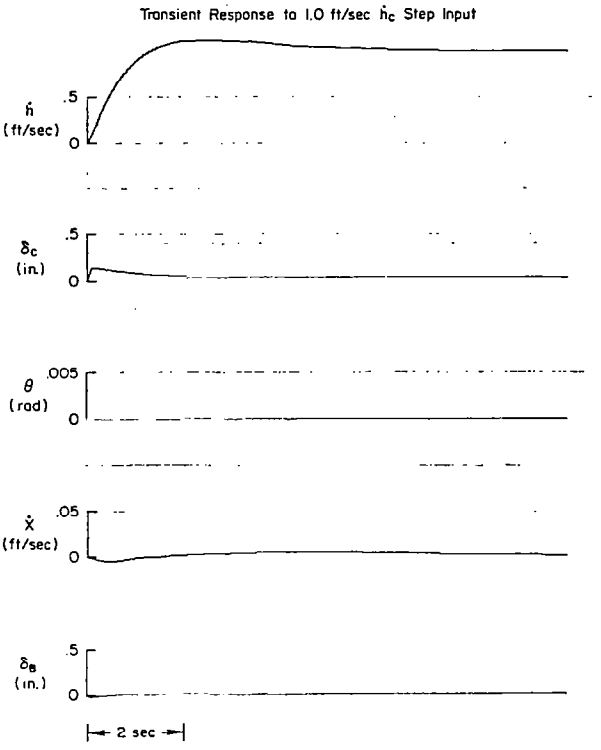

Figure C-2. (Concluded)

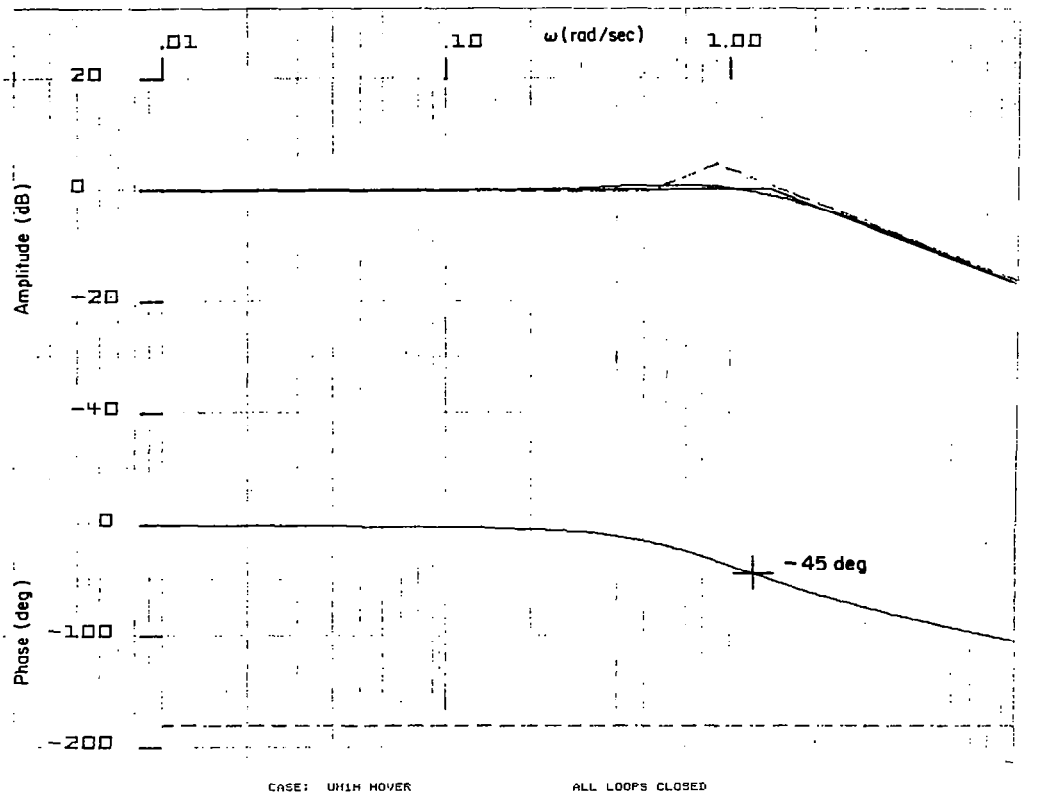

DENOMINATOR:

1.0000
(.10195) (.31507) (.33300) (.33595)
(.50520) (15.614) (25.716) (25.726)
((.92313 , .90723 , .83748 , .34882))
((.67390 , 2.7741 , 1.8692 , 2.0498))
< 118.79 >

NUMERATOR: HD/HDC FILE NAME? HDHDC.2CL
NEW FILE

40.908
(.10195) (.31507) (.33300) (.33601)
(.50240) (.52197) (15.614) (25.726)
((.67251 , 2.7694 , 1.8625 , 2.0496))
< 118.79 >

$$\frac{\dot{h}}{\dot{h}_c} \doteq \frac{41.0(s+.522)}{(s+25.7)[s^2+2(.923)(.91)s+(.91)^2]}$$

Figure C-3. Closed-Loop Frequency Response: $\dot{h}/\dot{h}_c$

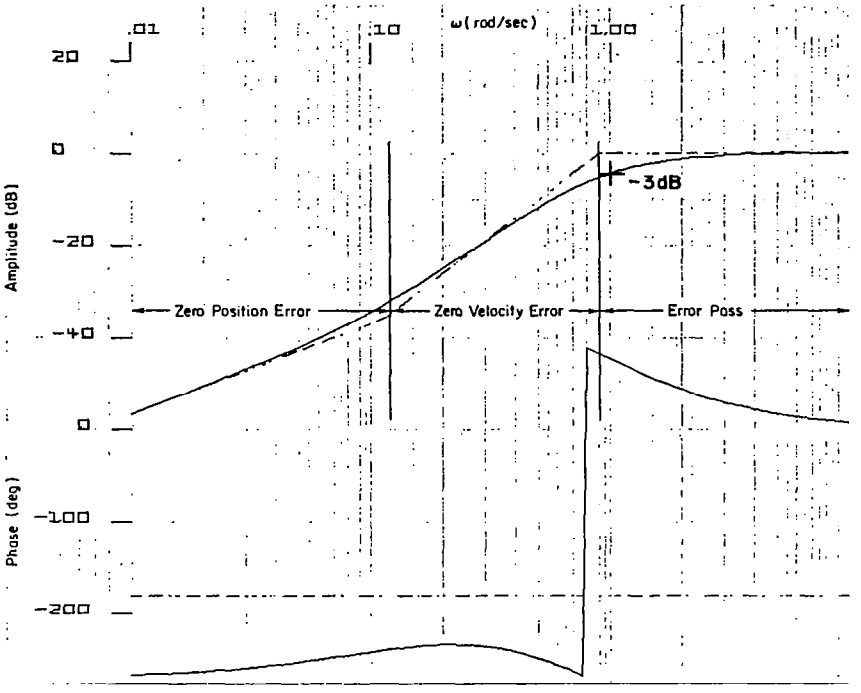

CASE: UH1H HOVER 122LONG 31-JAN-79 ALL LOOPS CLOSED

DENOMINATOR:

```
  1.0000
( .10195    ) ( .31507    ) ( .33300    ) ( .33595    )
( .50520    ) ( 15.614    ) ( 25.716    ) ( 25.726    )
(( .92313    , .90723    , .83748    , .34882    ))
(( .67380    , 2.7741    , 1.8692    , 2.0498    ))
< 118.79    >
```

NUMERATOR: HDE/HDC FILE NAME? HDEHDC.2CL
OLD FILE

```
  1.0000
( .00000    ) ( .10199    ) ( .11459    ) ( .31507    )
( .33300    ) ( .33575    ) ( .50554    ) ( 15.614    )
( 25.726    ) ( 27.282    )
(( .67297    , 2.7736    , 1.8663    , 2.0518    ))
< 17.547    >
```

$$\frac{\dot{h}_e}{\dot{h}_c} \triangleq \frac{s(s+.115)}{[s^2+2(.923)(.91)s+(.91)^2]}$$

Figure C-4. Closed-Loop Frequency Response: $\dot{h}_e/\dot{h}_c$

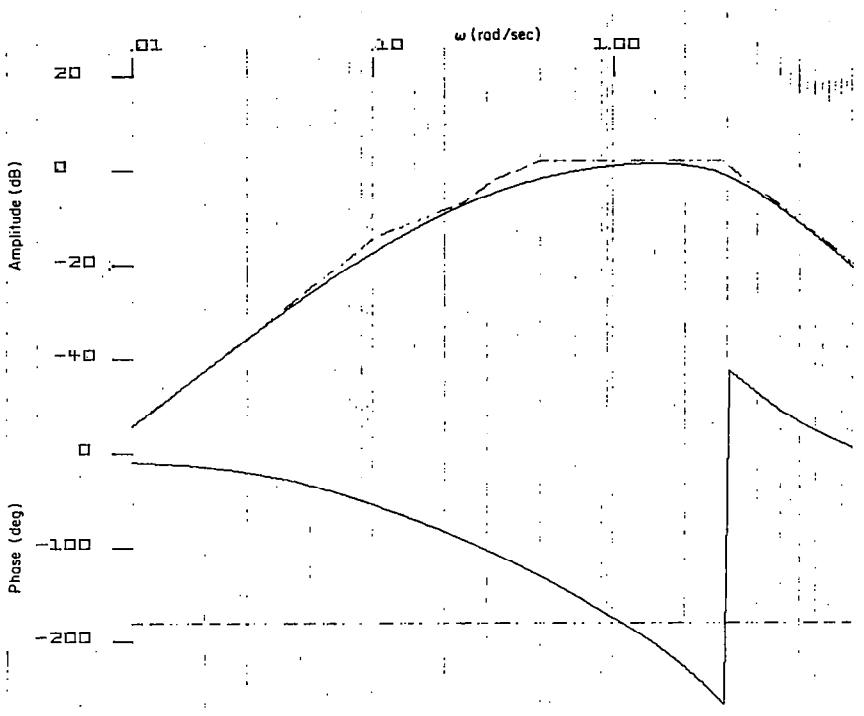


```
CASE:  UH1H HOVER 122LONG 31-JAN-79 ALL LOOPS CLOSED

DENOMINATOR:

   1.0000
  ( .10195     ) ( .31507     ) ( .33300     ) ( .33595     )
  ( .50520     ) ( 15.614     ) ( 25.716     ) ( 25.726     )
  (( .92313    , .90723     , .83748     , .34882     ))
  (( .67380    , 2.7741     , 1.8692     , 2.0498     ))
  < 118.79     >


NUMERATOR:   TH/VTH   FILE NAME?  THVTH.2CL
 OLD FILE

  -251.70
  ( .00000     ) ( .51016E-03) ( .24046     ) ( .33300     )
  ( .33300     ) ( 15.968     ) ( 25.716     )
  (( .92283    , .90699     , .83699     , .34939     ))
  <-1.1565     >
```

$$\frac{\theta}{\theta_c} = \frac{-251.7s^2}{(s+.1)(s+.51)(s+25.7)[s^2+2(.67)(2.77)s+(2.77)^2]}$$

Figure C-5. Closed-Loop Frequency Response: $\theta/v_\theta \doteq \theta/\theta_c$

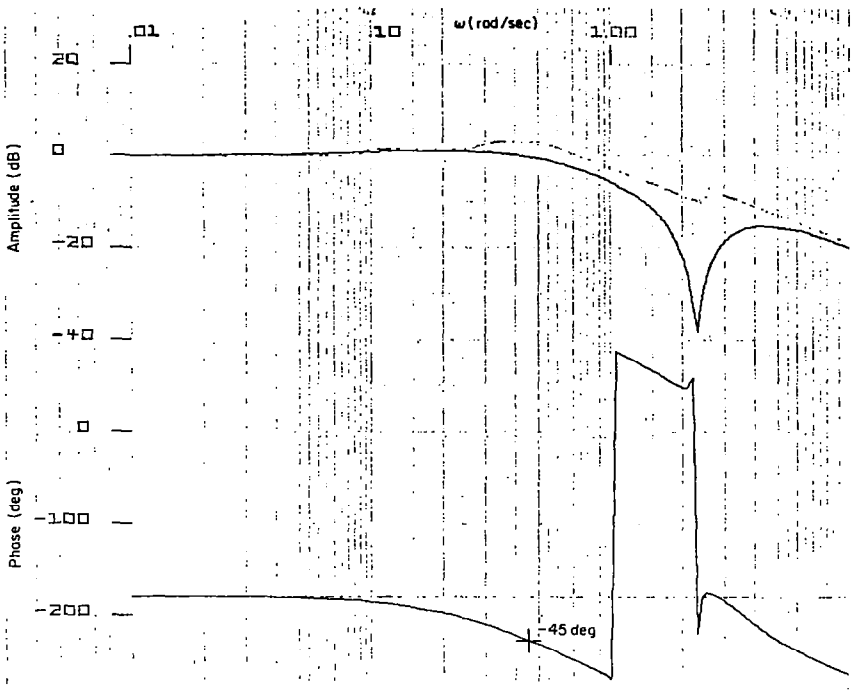

CASE: UH1H HOVER 122LONG 31-JAN-79 ALL LOOPS CLOSED

DENOMINATOR:

```
  1.0000
( .10195    ) ( .31507    ) ( .33300    ) ( .33595    )
( .50520    ) ( 15.614    ) ( 25.716    ) ( 25.726    )
(( .92313   , .90723    , .83748    , .34882    ))
(( .67380   , 2.7741    , 1.8692    , 2.0498    ))
< 118.79    >
```

NUMERATOR: XD/VXD

```
 -28.252
( .00000    ) ( .27433    ) ( .33296    ) ( .33300    )
( 15.594    ) ( 25.716    )
(( .92390   , .90551    , .83660    , .34648    ))
(( .20097E-01, 2.2706   , .45632E-01, 2.2702    ))
<-1456.9    >
```

NUMERATOR: XDI/VXI

```
 -2.0036
( .31507    ) ( .33295    ) ( .33300    ) ( 15.614    )
( 25.716    )
(( .92325   , .90595    , .83642    , .34806    ))
(( .20122E-01, 2.2693   , .45663E-01, 2.2689    ))
<-118.79    >
```

$$\frac{\dot{x}}{\dot{x}_c} \doteq \frac{-28.3[s^2 + 2(.02)(2.27)s + (2.27)^2]}{(s + .51)(s + 25.7)[s^2 + 2(.67)(2.77)s + (2.77)^2]}$$

Figure C-6. Closed-Loop Frequency Response: $(\dot{x}/v_{\dot{x}}) + (\int \dot{x}\,dt/v_{\int \dot{x}\,dt}) \doteq \dot{x}/\dot{x}_c$

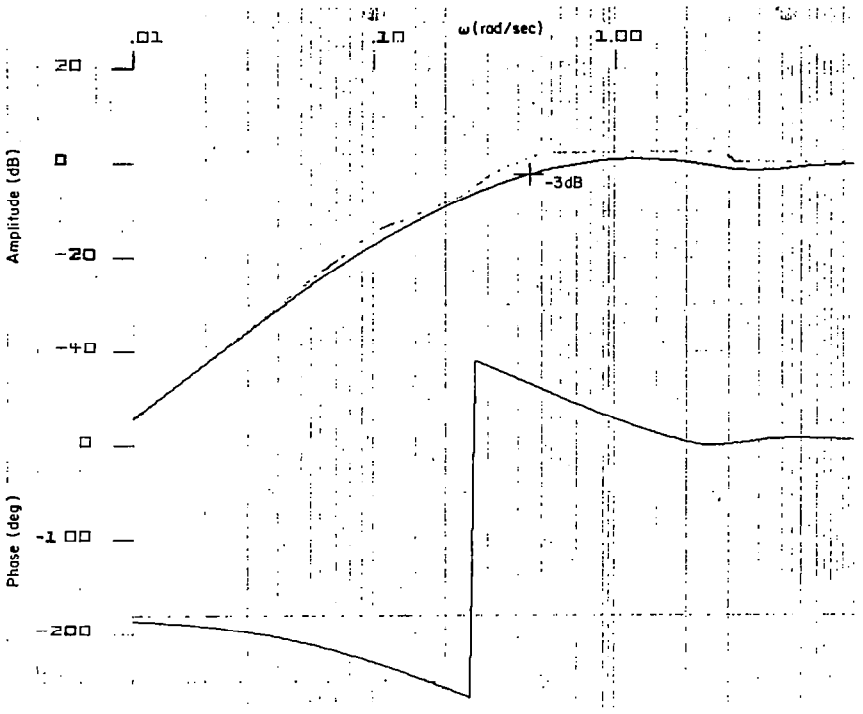

CASE: UH1H HOVER 122LONG 31-JAN-79 ALL LOOPS CLOSED

DENOMINATOR:

```
  1.0000
( .10195    ) ( .31507    ) ( .33300    ) ( .33595    )
( .50520    ) ( 15.614    ) ( 25.716    ) ( 25.726    )
(( .92313   , .90723    , .83748    , .34882    ))
(( .67380   , 2.7741    , 1.8692    , 2.0498    ))
< 118.79    >
```

NUMERATOR: XD/VXD

```
-28.252
( .00000    ) ( .27433    ) ( .33296    ) ( .33300    )
( 15.594    ) ( 25.716    )
(( .92390   , .90551    , .83660    , .34648    ))
(( .20097E-01, 2.2706   , .45632E-01, 2.2702    ))
<-1456.9    >
```

NUMERATOR: XDI/VXI

```
-2.0036
( .31507    ) ( .33295    ) ( .33300    ) ( 15.614    )
( 25.716    )
(( .92325   , .90595    , .83642    , .34806    ))
(( .20122E-01, 2.2693   , .45663E-01, 2.2689    ))
<-118.79    >
```

$$\frac{\dot{x}_e}{\dot{x}_c} \doteq \frac{(s-.001)(s+.001)}{(s+1)(s+.51)}$$

Figure C-7. Closed-Loop Frequency Response: $(\dot{x}/v_{\dot{x}}) + (\int \dot{x}\,dt/v_{\int \dot{x}\,dt} + 1) \doteq \dot{x}_e/\dot{x}_c$

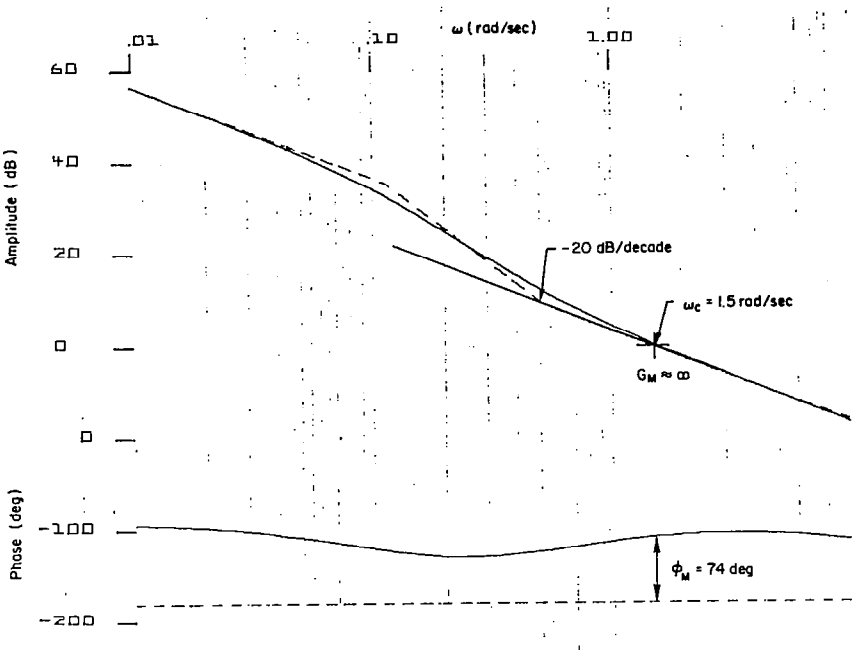

CASE: UH1H HOVER 122LONG 2-FEB-79 HDE AND HDI OPENED LOOP

DENOMINATOR:

```
  1.0000
( .00000 ) ( .10199 ) ( .11459 ) ( .31507 )
( .33300 ) ( .33575 ) ( .50556 ) ( 15.614 )
( 25.726 ) ( 27.282 )
(( .67287 , 2.7736 , 1.8663 , 2.0518 ))
< 17.547 >
```

NUMERATOR: HDE/VHE

```
-40.908
( .00000 ) ( .10195 ) ( .31507 ) ( .33300 )
( .33609 ) ( .50585 ) ( 15.614 ) ( 25.726 )
(( .67265 , 2.7692 , 1.8627 , 2.0491 ))
<-229.16 >
```

NUMERATOR: HDI/VHI

```
-21.190
( .10195 ) ( .31507 ) ( .33300 ) ( .33506 )
( .50574 ) ( 15.614 ) ( 25.726 )
(( .67328 , 2.7706 , 1.8654 , 2.0485 ))
<-118.79 >
```

$$\left.\frac{\dot{h}}{\dot{h}_c}\right|_{OL} \doteq \frac{-40.91(s+.51)}{s(s+.115)(s+27.3)}$$

Figure C-8. Open-Loop Frequency Response: $\dot{h}/\dot{h}_c\big|_{\dot{h}_e,\ \int \dot{h}_e\, dt\ \text{open}}$

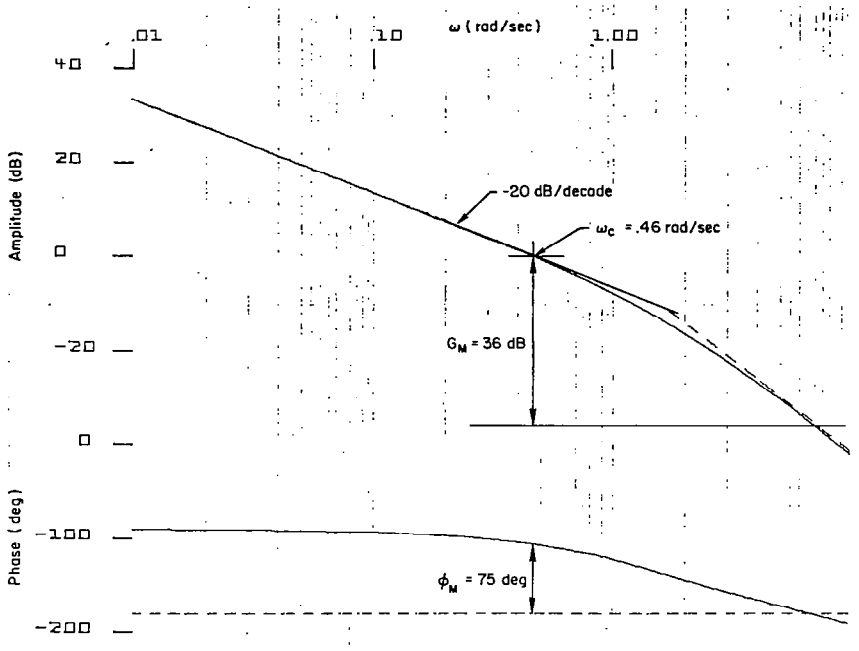

CASE: UH1H HOVER 122LONG 2-FEB-79 HDE AND HDI OPENED LOOP

DENOMINATOR:

```
  1.0000
( .00000    ) ( .10199    ) ( .11459    ) ( .31507    )
( .33300    ) ( .33575    ) ( .50556    ) ( 15.614    )
( 25.726    ) ( 27.282    )
(( .67287    , 2.7736     , 1.8663     , 2.0518     ))
< 17.547    >
```

NUMERATOR: HDI/VHI

```
-21.190
( .10195    ) ( .31507    ) ( .33300    ) ( .33606    )
( .50574    ) ( 15.614    ) ( 25.726    )
(( .67328    , 2.7706     , 1.8654     , 2.0485     ))
<-118.79    >
```

$$\left.\frac{\int \dot{h}_e \, dt}{\dot{h}_e}\right|_{OL} \doteq \frac{-21.2}{s(s+.51)(s+25.7)}$$

Figure C-9. Open-Loop Frequency Response: $\left.\int \dot{h}_e \, dt/\dot{h}_c\right|_{\int \dot{h}_e \, dt \text{ open}}$

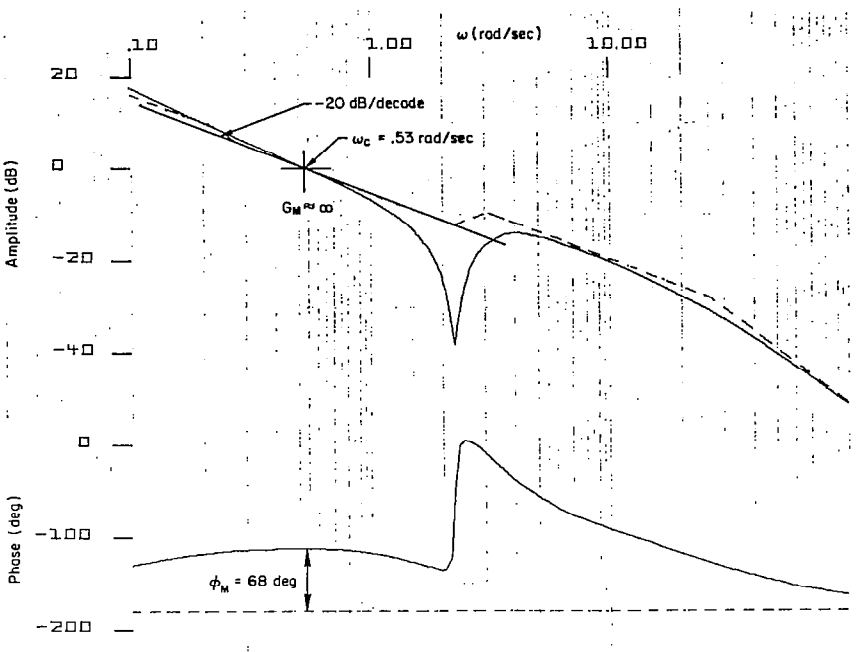

CASE: UH1H HOVER 122LONG 2-FEB-79 XD AND XDI OPENED LOOP

DENOMINATOR:

```
  1.0000
( .00000    ) ( .36768E-04) ( .23482    ) ( .33283    )
( .33300    ) ( 15.611    ) ( 25.716    ) ( 26.961    )
(( .92365   , .90563    , .83649    , .34707    ))
(( .50866   , 3.1452    , 1.5999    , 2.7079    ))
< .84033E-01>
```

NUMERATOR: XD/VXD

```
  -28.252
( .00000    ) ( .27433    ) ( .33296    ) ( .33300    )
( 15.594    ) ( 25.716    )
(( .92390   , .90551    , .83650    , .34648    ))
(( .20097E-01, 2.2706   , .45632E-01, 2.2702    ))
<-1456.9    >
```

NUMERATOR: XDI/VXI

```
  -2.0036
( .31507    ) ( .33295    ) ( .33300    ) ( 15.614    )
( 25.716    )
(( .92325   , .90595    , .83642    , .34806    ))
(( .20122E-01, 2.2693   , .45663E-01, 2.2689    ))
<-118.79    >
```

$$\left.\frac{\dot{x}}{\dot{x}_c}\right|_{OL} = \frac{-28.3[s^2 + 2(.02)(2.27)s + (2.27)^2]}{s(s + 27.0)[s^2 + 2(.51)(3.1)s + (3.1)^2]}$$

Figure C-10. Open-Loop Frequency Response: $\dot{x}/\dot{x}_c\big|_{\dot{x},\ \int \dot{x}\,dt\ \text{open}}$

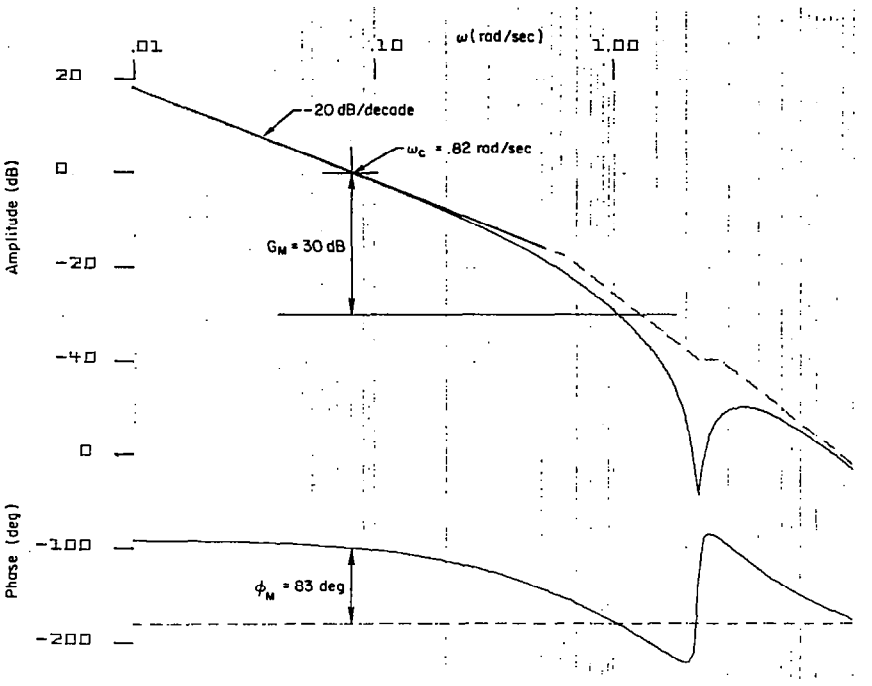


```
CASE:  UHIH HOVER 122LONG 31-JAN-79 XDI OPENED LOOP
DENOMINATOR:

  1.0000
( .00000    ) ( .31507    ) ( .33300    ) ( .33412    )
( .64743    ) ( 15.614    ) ( 25.716    ) ( 25.723    )
(( .92324    , .90740    , .83776    , .34864    ))
(( .67391    , 2.7474    , 1.8515    , 2.0298    ))
< 1456.9    >


NUMERATOR:  XDI/VXI   FILE NAME?  XDIVXI
 NEW FILE

 -2.0036
( .31507    ) ( .33295    ) ( .33300    ) ( 15.614    )
( 25.716    )
(( .92325    , .90595    , .83642    , .34806    ))
(( .20122E-01, 2.2693    , .45663E-01, 2.2689    ))
<-118.79    >
```

$$\left.\frac{\int \dot{x}\,dt}{\dot{x}_c}\right|_{OL} \doteq \frac{-2.0[s^2 + 2(.02)(2.27)s + (2.27)^2]}{s(s+.65)(s+25.7)[s^2 + 2(.67)(2.75)s + (2.75)^2]}$$

Figure C-11. Open-Loop Frequency Response: $\left.\int \dot{x}\,dt/\dot{x}_c\right|_{\int \dot{x}\,dt \text{ open}}$

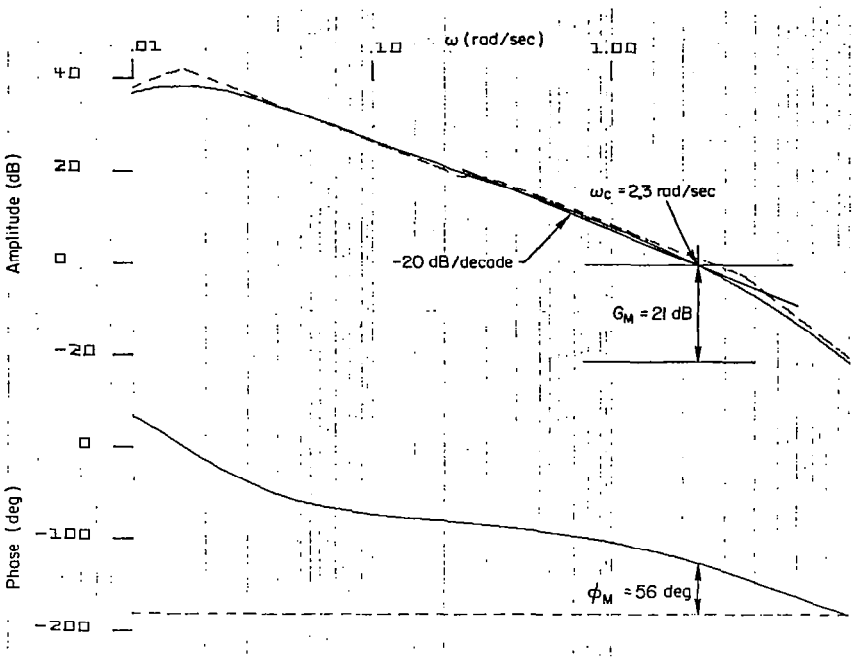

CASE: UH1H HOVER 122LONG 5-FEB-79 XD,XDI AND TH LOOPS OPENED

DENOMINATOR:

```
  1.0000
( .00000    ) ( .30483    ) ( .33300    ) ( .33863    )
( 3.5187    ) ( 15.568    ) ( 25.714    ) ( 26.577    )
(( .77420    , .16484E-01, .12762E-01, .10433E-01))
(( .92994    , .90422    , .84086    , .33250    ))
< .28587    >
```

NUMERATOR: TH/VTH FILE NAME? THVTH
NEW FILE

```
 -251.70
( .00000    ) (-.89352E-04) ( .23999    ) ( .33300    )
( .33300    ) ( 15.961    ) ( 25.721    )
(( .92498    , .90635    , .83836    , .34442    ))
< .20183    >
```

$$\frac{\theta}{\theta_c} \doteq \frac{-251.7\,s}{(s+3.52)(s+26.6)[s^2+2(.77)(.016)s+(.016)^2]}$$

Figure C-12. Open-Loop Frequency Response: $\theta/\theta_c|_{\dot{x},\ \int \dot{x}\,dt,\ \theta\ \text{open}}$

TABLE C-10. CLOSED-LOOP SYSTEM RMS PERFORMANCE
(PROCESS NOISE AUGMENTATION REMOVED)

RMS, TOTAL
1

2.06	1 X01
1.71	2 X02
1.00	3 X03
0.742E-01	4 X06
1.01	5 X07
0.315E-03	6 X08
0.153E-02	7 X09
0.494E-01	8 X10
0.921E-01	9 X11
0.293	10 X12
0.186E-02	11 X13
0.477E-01	12 X14
0.186E-02	13 E13
6.37	14 E01
39.3	15 E02

RMS, OUTPUT+CONTROLS
1

1.01	1 HD
0.315E-03	2 Q
0.153E-02	3 TH
0.494E-01	4 DB
0.921E-01	5 DC
0.259	6 HDE
0.293	7 HDI
0.530E-02	8 XD
0.477E-01	9 XDI
1.17	10 AOA
2.05	11 ASE
0.466E-01	12 DBD
0.255	13 DCD

CONTROL ACTIVITY	
CONTROL	POSITIVE-GOING ZERO-CROSSING RATE, $(1/2\pi)(\sigma_{\dot{x}}/\sigma_x)$
DB	0.150 (1/sec)
DC	0.441 (1/sec)

APPENDIX D

UH-1H, 100 KT, EXAMPLE APPLICATION

This appendix provides an overview of the design synthesis and assessment of a longitudinal flight control system for the UH-1H at cruise (100 kt). No design iteration steps are included; just the final design data are given. Only a small sample of the design assessment data is included. The next paragraphs explain the data which follow.

Table D-1 lists the primary design goals for this application. These design goals are the various bandwidths, which are determined from the functions intended to be accomplished by this FCS.

Tables D-2 and D-3 present the input data used to define the system. The shaping filter and controlled element state equations are given in Table D-2, and the measurement and output equations follow in Table D-3.

Table D-4 lists the elements of the final filter-observer design.

Table D-5 lists the various controlled element transfer functions of interest, while Table D-6 presents the procedure used to meet the bandwidth requirements by choosing the elements of Q_R and R_R for the regulator. As in the hover example, we were able to make use of the relatively uncoupled nature of this problem to design all of the loop closures simultaneously. Table D-7 provides a summary of the final regulator design.

With the filter-observer and the regulator synthesized, the software is used to obtain the controller gain matrices and the controller transfer functions, given in Tables D-8 and D-9, respectively.

Design assessment begins with the closed-loop transfer functions, shown in Fig. D-1, and the corresponding transient responses to u_g, w_g and $\dot{h}_c$ step inputs, also shown in Fig. D-1. These transient response plots enable us to determine the behavior of the closed-loop system in the presence of gust disturbances, as well as the behavior in response to command inputs.

Subsequent figures provide data on the frequency response characteristics of the closed-loop system. Figure D-2 presents the rate-of-climb error response to rate-of-climb command. Figure D-3 plots the pitch attitude response to pitch attitude command. The frequency response of longitudinal velocity to a longitudinal gust disturbance input is plotted in Fig. D-4, while the Bode plot of airspeed error to longitudinal gust disturbance is shown in Fig. D-5. These are only a few of the many interesting frequency response plots for this design.

An example of the statistical data available in the design assessment stage is shown in Table D-10. Here the process noise augmentation has been removed and we can examine the rms response of the plant and filter states to the combined process and measurement noise. We can also look at the rms response of the outputs and controls. These rms values are used to determine control activity levels, including positive-going zero crossing rate, which is shown to the right of the rms data. The control activity data are used in determining whether appropriate cost function weightings were chosen for the control rates (the R_R matrix) in the regulator design.

TABLE D-1

EXAMPLE APPLICATION

UH-1H Longitudinal Flight Control System

Flight Condition: 100 kt (Cruise)

Functions:

- Rate-of-climb command
- Airspeed hold

Bandwidths:	(rad/sec)
Cyclic (DB):	25.73
Collective (DC):	25.73
Pitch (TH):	1.5
Rate-of-climb error (HDE):	0.7
Integral HDE (HDI):	0.32
Airspeed Error (ASE):	0.1
Integral ASE (ASI):	0.02

TABLE D-2. PLANT; CONTROLLED ELEMENT AND SHAPING FILTERS

$$\dot{x} = Fs + Gu + \Gamma w \quad , \quad x(0) = x_o$$

$$x' = \{ \underset{\text{Long. gust velocity}}{UG} \quad \underset{\text{Normal gust velocity}}{WG} \quad \underset{\text{R/C command}}{HDC} \mid \underset{\text{Longitudinal velocity}}{U} \quad \underset{\text{Normal velocity}}{W} \quad \underset{\text{Pitch rate}}{Q} \quad \underset{\text{Pitch attitude}}{TH} \quad \underset{\text{Longitudinal cyclic}}{DB} \quad \underset{\text{Main rotor collective}}{DC} \quad \underset{\text{Integral R/C error}}{HDI} \quad \underset{\text{Horizontal stab. bar}}{XBR} \quad \underset{\text{Integral long. speed}}{XDI} \}$$

F MATRIX

1 X01	2 X02	3 X03	4 X05	5 X07	6 X08	7 X09	8 X10	9 X11	10 X12	11 X13	12 X14	
-0.116	0.000	0.000	0.000	0.000	0.000	0.000	0.000	0.000	0.000	0.000	0.000	1 X01
0.000	-0.269	0.000	0.000	0.000	0.000	0.000	0.000	0.000	0.000	0.000	0.000	2 X02
0.000	0.000	-0.100	0.000	0.000	0.000	0.000	0.000	0.000	0.000	0.000	0.000	3 X03
0.451E-01	-0.925E-01	0.000	-0.451E-01	0.925E-01	-7.14	-32.1	0.557	1.14	0.000	0.557	0.000	4 X06
-0.888E-01	0.996	0.000	0.888E-01	-0.996	165.	-1.69	5.07	-13.1	0.000	5.07	0.000	5 X07
-0.500E-02	0.560E-02	0.000	0.500E-02	-0.660E-02	-0.701	0.000	-0.173	-0.223E-01	0.000	-0.173	0.000	6 X08
0.000	0.000	0.000	0.000	0.000	1.00	0.000	0.000	0.000	0.000	0.000	0.000	7 X09
0.000	0.000	0.000	0.000	0.000	0.000	0.000	0.000	0.000	0.000	0.000	0.000	8 X10
0.000	0.000	0.000	0.000	0.000	0.000	0.000	0.000	0.000	0.000	0.000	0.000	9 X11
0.000	0.000	1.00	-0.527E-01	0.999	0.000	-169.	0.000	0.000	0.000	0.000	0.000	10 X12
0.000	0.000	0.000	0.000	0.000	4.97	0.000	0.000	0.000	0.000	-0.333	0.000	11 X13
-0.999	-0.527E-01	0.000	0.999	0.527E-01	0.000	0.000	0.000	0.000	0.000	0.000	-0.100E-02	12 X14

(continued on following page)

TABLE D-2. (Continued)

Long. cyclic rate

Main rotor collective

$$u' = \{ \text{DBD} \quad \text{DCD} \}$$

G MATRIX

	1 DBD	2 DCD
1 X01	0.000	0.000
2 X02	0.000	0.000
3 X03	0.000	0.000
4 X06	0.000	0.000
5 X07	0.000	0.000
6 X08	0.000	0.000
7 X09	0.000	0.000
8 X10	1.00	0.000
9 X11	0.000	1.00
10 X12	0.000	0.000
11 X13	0.000	0.000
12 X14	0.000	0.000

(concluded on following page

TABLE D-2. (Concluded)

GAMMA MATRIX

1 PUG	2 PWG	3 PHC	4 P U	5 P W	6 P Q	7 PTH	8 PDB	9 PDC	10 PHE	11 PXB	12 PSE	
0.482	0.000	0.000	0.000	0.000	0.000	0.000	0.000	0.000	0.000	0.000	0.000	1 X01
0.000	0.734	0.000	0.000	0.000	0.000	0.000	0.000	0.000	0.000	0.000	0.000	2 X02
0.000	0.000	0.447	0.000	0.000	0.000	0.000	0.000	0.000	0.000	0.000	0.000	3 X03
0.000	0.000	0.000	1.00	0.000	0.000	0.000	0.000	0.000	0.000	0.000	0.000	4 X06
0.000	0.000	0.000	0.000	1.00	0.000	0.000	0.000	0.000	0.000	0.000	0.000	5 X07
0.000	0.000	0.000	0.000	0.000	1.00	0.000	0.000	0.000	0.000	0.000	0.000	6 X08
0.000	0.000	0.000	0.000	0.000	0.000	1.00	0.000	0.000	0.000	0.000	0.000	7 X09
0.000	0.000	0.000	0.000	0.000	0.000	0.000	1.00	0.000	0.000	0.000	0.000	8 X10
0.000	0.000	0.000	0.000	0.000	0.000	0.000	0.000	1.00	0.000	0.000	0.000	9 X11
0.000	0.000	0.000	0.000	0.000	0.000	0.000	0.000	0.000	1.00	0.000	0.000	10 X12
0.000	0.000	0.000	0.000	0.000	0.000	0.000	0.000	0.000	0.000	1.00	0.000	11 X13
0.000	0.000	0.000	0.000	0.000	0.000	0.000	0.000	0.000	0.000	0.000	1.00	12 X14

TABLE D-3. PLANT; OUTPUT AND MEASUREMENT EQUATIONS

$$y = H_R x \qquad H_R = \left[- \; - \; H \; - \; - \right]$$

$$z = Hx + v$$

$$z' = \{ \underset{\text{Rate of climb}}{HD} \quad \underset{\text{Pitch rate}}{Q} \quad \underset{\text{Pitch attitude}}{TH} \quad \underset{\text{Longitud. cyclic}}{DB} \quad \underset{\text{Main rotor collective}}{DC} \quad \underset{\text{R/C error}}{HDE} \quad \underset{\text{Integral R/C error}}{HDI} \quad \underset{\text{Longitud. speed}}{XD} \quad \underset{\text{Integral long. speed}}{XDI} \}$$

HR MATRIX

1 X01	2 X02	3 X03	4 X06	5 X07	6 X08	7 X09	8 X10	9 X11	10 X12	11 X13	12 X14	
0.000	0.000	0.000	0.527E-01	-0.999	0.000	169.	0.000	0.000	0.000	0.000	0.000	1 HD
0.000	0.000	0.000	0.000	0.000	1.00	0.000	0.000	0.000	0.000	0.000	0.000	2 Q
0.000	0.000	0.000	0.000	0.000	0.000	1.00	0.000	0.000	0.000	0.000	0.000	3 TH
0.000	0.000	0.000	0.000	0.000	0.000	0.000	1.00	0.000	0.000	0.000	0.000	4 DB
0.000	0.000	0.000	0.000	0.000	0.000	0.000	0.000	1.00	0.000	0.000	0.000	5 DC
0.000	0.000	0.000	0.000	0.000	0.000	0.000	0.000	0.000	1.00	0.000	0.000	6 HDI
0.000	0.000	1.00	-0.527E-01	0.999	0.000	-169.	0.000	0.000	0.000	0.000	0.000	7 HDE
0.000	0.000	0.000	0.000	0.000	0.000	0.000	0.000	0.000	0.000	0.000	1.00	8 ASI
-0.999	-0.527E-01	0.000	0.999	0.527E-01	0.000	0.000	0.000	0.000	0.000	-0.000	0.000	9 ASE
0.000	0.000	0.000	0.999	0.527E-01	0.000	0.000	0.000	0.000	0.000	0.000	0.000	10 XD
0.000	-0.593E-02	0.000	0.000	0.593E-02	0.000	0.000	0.000	0.000	0.000	0.000	0.000	11 AOA

TABLE D-4. FILTER-OBSERVER SYNTHESIS

Q MATRIX DIAGONAL, FILTER 1

4.24	1 PUG
2.92	2 PWG
1.00	3 PHC
10.0	4 P U
0.000	5 P W
0.100E-03	6 P Q
0.100E-05	7 PTH
0.100E-03	8 PDB
0.100E-03	9 PDC
0.100E-03	10 PHE
0.000	11 PXB
0.100E-03	12 PSE

R MATRIX DIAGONAL, FILTER 1

0.000	1 HD
0.000	2 Q
0.000	3 TH
0.000	4 DB
0.000	5 DC
0.000	6 HDI
0.000	7 HDE
0.000	8 ASI
0.000	9 ASE

CLOSED LOOP EIGENVALUES, FILTER 1

0.333 180.	1 E13
25.1 180.	2 E01
0.111 180.	3 E02

RMS STATE EST ERROR, FILTER 1

2.03	1 X01
0.277	2 X02
0.000	3 X03
2.03	4 X06
0.107	5 X07
0.000	6 X08
0.171E-12	7 X09
0.000	8 X10
0.000	9 X11
0.000	10 X12
0.000	11 X13
0.000	12 X14

K12 GAIN MATRIX, FILTER

1 HD	2 Q	3 TH	4 DB	5 DC	6 HDI	7 HDE	8 ASI	9 ASE	
0.130E-06	-0.207E-07	-0.220E-04	0.000	0.000	-0.155E-12	0.134E-13	0.518E-11	-0.629E-08	1 E13
1.53	1.39	-259.	0.000	0.000	0.153E-03	0.156E-06	-0.503E-02	-0.120	2 E01
-24.7	4.41	0.417E+04	0.000	0.000	0.881E-05	-0.254E-05	-0.296E-03	1.18	3 E02

TABLE D-5. CONTROLLED ELEMENT TRANSFER FUNCTIONS

CASE: UH1H 100KT 128LONG 30-JAN-79 CONTROLLED ELEMENT TF'S

DENOMINATOR:

```
 1.0000
( .00000    ) ( .00000    ) ( .00000    ) ( .00000    )
( .69142    )
(( .22354    , .17435    , .38973E-01, .16993    ))
(( .43625    , 1.4971    , .65312    , 1.3472    ))
< .47106E-01>
```

NUMERATOR: TH/DBD

```
-.17280
( .00000    ) ( .00000    ) ( .00000    ) ( .14710E-01)
( .33300    ) ( 1.2044    )
<-.10194E-02>
```

NUMERATOR: TH/DCD

```
-.22300E-01
( .00000    ) ( .00000    ) ( .00000    ) ( .29081E-01)
( .33300    ) (-3.1286    )
< .67562E-03>
```

NUMERATOR: HDE/DBD

```
 5.0374
( .00000    ) ( .00000    ) ( .00000    ) ( .42303E-01)
( .33300    )
(( .15642    , 2.6370    , .41248    , 2.6046    ))
< .49346    >
```

NUMERATOR: HDE/DCD

```
-13.169
( .00000    ) ( .00000    ) ( .00000    )
(( .70493    , .17927    , .12637    , .12715    ))
(( .30308    , 1.3401    , .40618    , 1.2771    ))
<-.76012    >
```

NUMERATOR: HDI/DCD

```
-13.169
( .00000    ) ( .00000    )
(( .70493    , .17927    , .12637    , .12715    ))
(( .30308    , 1.3401    , .40618    , 1.2771    ))
<-.76012    >
```

NUMERATOR: ASE/DBD

```
 .82341
( .00000    ) ( .00000    ) ( .00000    ) ( .33300    )
( 1.2596    )
(( .73104E-01, 2.5391    , .18562    , 2.5323    ))
< 2.2266    >
```

NUMERATOR: ASI/DBD

```
 .82341
( .00000 -  ) ( .00000    ) ( .33300    ) ( 1.2596    )
(( .73104E-01, 2.5391    , .18562    , 2.5323    ))
< 2.2266    >
```

TABLE D-6. SUMMARY OF Q_R AND R_R SELECTION

	ω_c		$R_{DBD} = 1.0$		$R_{DCD} = 10.0$		
Longitudinal Cyclic Actuator	25.7	$\frac{DB}{DBD}\Big\|_{\omega_c} = \frac{1}{s}$	K = 1.0 n = 0	$Q_{DB} = 662.34$	$\frac{DB}{DCD}\Big\|_{\omega_c} = 0$		
Main Rotor Collective Actuator	25.7	$\frac{DC}{DBD} = 0$			$\frac{DC}{DCD}\Big\|_{\omega_c} = \frac{1}{s}$	K = 1.0 n = 0	$Q_{DC} = 6623.4$
Pitch Attitude	1.5	$\frac{TH}{DB}\Big\|_{\omega_c} = \frac{-0.2}{s^2}$	K = 0.2 n = 1	$Q_{TH} = 354,742$	$\frac{TH}{DC}\Big\|_{\omega_c} = \frac{0.07}{s^2}$	K = 0.07 n = 1	$Q_{TH} = 27,372,$ 214.3
Rate-of-Climb Error, Proportional	0.7	$\frac{HDE}{DB}\Big\|_{\omega_c} = \frac{15.63}{s}$	K = 15.63 n = 0	$Q_{HDE} = 1.33$	$\frac{HDE}{DC}\Big\|_{\omega_c} = 7.3$	n < 0	$Q_{HDE} = 0$
Rate-of-Climb Error, Integral	0.32				$\frac{HDI}{DC}\Big\|_{\omega_c} = \frac{15.3}{s}$	K = 15.3 n = 0	$Q_{HDI} = 2.84$
Airspeed Error, Proportional	0.1	$\frac{ASE}{TH}\Big\|_{\omega_c} = \frac{-32.13}{s}$	K = 32.13 n = 0	$Q_{ASE} = 3.44$	$\frac{ASE}{HDE}\Big\|_{\omega_c} = \frac{.206}{s}$	K = .206 n = 0	$Q_{ASE} = 83,594.6$
Airspeed Error, Integral	0.02	$\frac{ASI}{ASE}\Big\|_{\varphi_c} = \frac{1}{s}$	K = 1.0 n = 0	$Q_{ASI} = .00137$			

TABLE D-7. REGULATOR SYNTHESIS

Q MATRIX DIAGONAL, REGULATOR
1

0.000	1 HD
0.000	2 Q
0.355E+06	3 TH
662.	4 DB
0.662E+04	5 DC
2.84	6 HDI
0.000	7 HDE
0.137E-02	8 ASI
3.44	9 ASE
0.000	10 XD
0.000	11 AOA

R MATRIX DIAGONAL, REGULATOR
1

1.00	1 DBD
10.0	2 DCD

CLOSED LOOP EIGENVALUES, REGULATOR
1

25.7 180.	1 X01
25.7 180.	2 X02
2.20 -124.	3 X03
2.20 124.	4 X06
0.728 -174.	5 X07
0.728 174.	6 X08
0.335 180.	7 X09
0.627E-01 180.	8 X10
0.156E-01 180.	9 X11
0.116 180.	10 X12
0.269 180.	11 X13
0.100 180.	12 X14

REGULATOR GAIN MATRIX

1 X01	2 X02	3 X03	4 X06	5 X07	6 X08	7 X09	8 X10	9 X11	10 X12	11 X13	12 X14	
-0.217	1.18	2.99	0.682	1.80	-277.	-895.	27.9	-0.627	1.34	23.9	0.225E-01	1 DBD
-0.852E-02	-0.496	-0.981	0.335	-0.243	3.82	61.9	-0.627E-01	25.9	-0.324	-0.934	0.930E-02	2 DCD

TABLE D-8. CONTROLLER COEFFICIENT MATRICES

AF MATRIX

1 E13	2 E01	3 E02	
-0.333	-0.614E-08	0.130E-06	1 E13
8.06	-0.183	1.52	2 E01
-125.	1.17	-25.0	3 E02

BF MATRIX

1 HD	2 Q	3 TH	4 DB	5 DC	6 HDI	7 HDE	8 ASI	9 ASE	
-0.314E-05	4.97	0.530E-03	0.657E-06	-0.171E-05	0.263E-12	-0.180E-12	-0.908E-11	0.162E-06	1 E13
-36.3	261.	0.613E+04	8.06	-20.1	-0.145E-04	-0.157E-03	0.478E-03	1.87	2 E01
594.	-0.419E+04	-0.100E+06	-125.	325.	-0.422E-04	0.546E-04	0.147E-02	-30.6	3 E02

CF MATRIX

1 E13	2 E01	3 E02	
-23.9	-0.558	-1.22	1 DBD
0.934	-0.313	0.479	2 DCD

DF MATRIX

1 HD	2 Q	3 TH	4 DB	5 DC	6 HDI	7 HDE	8 ASI	9 ASE	
28.1	271.	-0.434E+04	-27.9	0.627	-1.34	-2.99	-0.193E-01	-2.15	1 DBD
-11.6	-2.14	0.206E+04	0.627E-01	-25.9	0.324	0.981	-0.786E-02	0.281	2 DCD

TABLE D-9. CONTROLLER TRANSFER FUNCTIONS

CASE: UH1H 100KT 128LONG 2-FEB-79 CONTROLLER TRANSFER FUNCTIONS

DENOMINATOR:

1.0000
(.11136) (.33300) (25.074)
< .92977 >

NUMERATOR: DBD/ HD

28.057
(-.81761E-01) (.12973) (.33300)
<-.99096E-01>

NUMERATOR: DCD/ HD

-11.590
(.10443) (.33300) (-.47364)
< .19091 >

NUMERATOR: DBD/ Q

270.94
(.57922E-01) (.19074) (43.160)
< 129.19 >

NUMERATOR: DCD/ Q

-2.1404
(.14888) (.40243) (998.36)
<-128.03 >

NUMERATOR: DBD/ TH

-4344.4
(.11516) (.33300) (-2.3193)
< 386.40 >

NUMERATOR: DCD/ TH

2059.9
(.12469) (.33300) (.80143)
< 68.566 >

NUMERATOR: DBD/ DB

-27.876
(.12362) (.33300) (19.767)
<-22.684 >

NUMERATOR: DCD/ DB

.62709E-01
(.16364) (.33300) (-967.21)
<-3.3050 >

NUMERATOR: DBD/ DC

.62710
(.10150) (.33300) (-589.14)
<-12.500 >

NUMERATOR: DCD/ DC

-25.870
(.10784) (.33300) (18.819)
<-17.484 >

NUMERATOR: DBD/HDE

-2.9885
(.11133) (.33300) (25.074)
<-2.7778 >

NUMERATOR: DCD/HDE

.98066
(.11140) (.33300) (25.074)
< .91216 >

NUMERATOR: DBD/HDI

-1.3402
(.11135) (.33300) (25.074)
<-1.2460 >

NUMERATOR: DCD/HDI

.32357
(.11137) (.33300) (25.074)
< .30089 >

NUMERATOR: DBD/ASE

-2.1499
(.11284) (.33300) (8.2005)
<-.66249 >

NUMERATOR: DCD/ASE

.28138
(.11284) (.33300) (-29.069)
<-.30735 >

NUMERATOR: DBD/ASI

-.19271E-01
(.12935) (.33300) (25.162)
<-.20887E-01>

NUMERATOR: DCD/ASI

-.78565E-02
(.13233) (.33300) (24.982)
<-.86490E-02>

```
  CASE:  UH1H 100KT 128LONG 31-JAN-79 ALL LOOPS CLOSED

DENOMINATOR:

   1.0000
  ( .15598E-01)  ( .62689E-01)  ( .11136    )  ( .33300    )
  ( .33514    )  ( 25.074     )  ( 25.736    )  ( 25.736    )
  (( .99458    , .72781     , .72387     , .75547E-01))
  (( .56441    , 2.2044     , 1.2442     , 1.8197     ))
  < .51948    >


NUMERATOR:   HD/ UG   FILE NAME?  HDUG.CL
 NEW FILE

   .91052E-01
  ( .00000    )  ( .18569E-01)  ( .11341    )  ( .33300    )
  ( .35737    )  ( 4.3024     )  (-10.043    )  ( 25.736    )
  (-99.898    )
  ((-.96687    , .10688     ,-.10334     , .27281E-01))
  < .28955E-01>


NUMERATOR:   TH/ UG   FILE NAME?  THUG.CL
 NEW FILE

  -.50000E-02
  ( .93651E-03)  ( .14365E-01)  ( .11334    )  ( .33300    )
  ( .33300    )  ( .48343     )  ( 1.0059    )  ( 12.441    )
  ( 25.736    )  ( 112.96     )
  <-.15663E-04>


NUMERATOR:   DB/ UG   FILE NAME?  DBUG.CL
 NEW FILE

   2.1469
  ( .11239    )  ( .33300    )  ( .47520    )  ( .61244    )
  (-1.3468    )  ( 9.9236    )  ( 25.736    )
  ((-.68707    , .90384E-02,-.62100E-02, .65672E-02))
  (( .64328    , 1.0345     , .66549     , .79207     ))
  <-.70321E-03>


NUMERATOR:   DC/ UG   FILE NAME?  DCUG.CL
 NEW FILE

  -.28098
  (-.11589E-01)  ( .26059E-01)  ( .11454    )  ( .33300    )
  ( .34735    )  (-25.709     )  ( 25.736    )
  (( .95211    , .78672     , .74905     , .24054     ))
  (( .57373    , 2.1627     , 1.2408     , 1.7713     ))
  <-.21531E-02>


NUMERATOR:  ASE/ UG   FILE NAME?  ASEUG.CL
 NEW FILE

  -.99960
  ( .00000    )  (-.64568E-02)  ( .11254    )  ( .33300    )
  ( .33490    )  ( .65545     )  ( .79111    )  ( 24.383    )
  ( 25.736    )  ( 26.458     )
  (( .55909      2.2381       1.2513     , 1.8556     ))
  < 3.4897    >
```

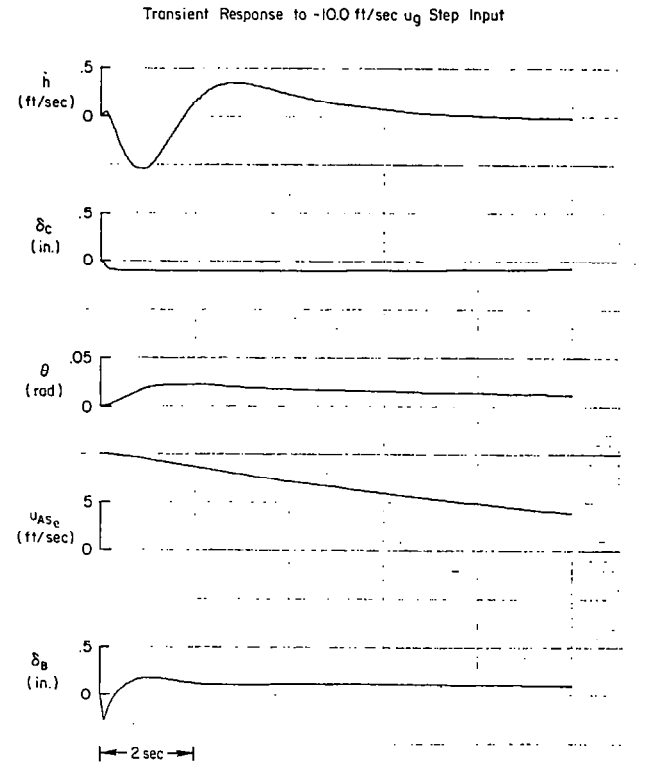

Figure D-1. Closed-Loop System Transfer Functions, Transient Response to Commands, Transient Response to Disturbances

Normal Gust Transfer Functions

```
CASE:  UH1H 100KT 128LONG 31-JAN-79 ALL LOOPS CLOSED

DENOMINATOR:

   1.0000
  ( .15598E-01)  ( .62689E-01)  ( .11136    )  ( .33300    )
  ( .33514    )  ( 25.074     )  ( 25.736    )  ( 25.736    )
  (( .99458    , .72781     , .72387     , .75547E-01))
  (( .56441    , 2.2044     , 1.2442     , 1.8197     ))
  < .51948    >


NUMERATOR:   HD/ WG   FILE NAME?  HDWG.CL
 NEW FILE

  -.99978
  ( .00000    )  ( .16914E-01)  ( .83964E-01)  ( .11385    )
  ( .30605    )  ( .33300    )  ( 1.4103    )  ( 25.736    )
  ( 44.274    )
  (( .94989    , 4.6358     , 4.4035     , 1.4491     ))
  <-.54865    >


NUMERATOR:   TH/ WG   FILE NAME?  THWG.CL
 NEW FILE

   .66000E-02
  ( .10956    )  ( .33300    )  ( .33300    )  ( 25.736    )
  (( .89644    , .11871E-01, .10542E-01, .52608E-02))
  (( .94942    , .86231     , .81870     , .27077     ))
  (( .65437    , 37.048     , 24.243     , 28.015     ))
  < .29579E-03>


NUMERATOR:   DB/ WG   FILE NAME?  DBWG.CL
 NEW FILE

   .11330
  (-.20270E-01)  ( .11004    )  ( .33300    )  ( .65235    )
  ( 1.0251    )  ( 25.736    )  (-248.88    )
  ((-.12448    , .16735     ,-.20832E-01, .16504     ))
  (( .85853E-01, 1.1490     , .98642E-01, 1.1447     ))
  < .13325E-01>


NUMERATOR:   DC/ WG   FILE NAME?  DCWG.CL
 NEW FILE

  -.14829E-01
  ( .22833E-01)  ( .10152    )  ( .15506    )  ( .29478    )
  ( .33300    )  ( 25.736    )  (-875.79    )
  (( .97056    , .83268     , .80817     , .20055     ))
  (( .55588    , 2.2338     , 1.2417     , 1.8569     ))
  < .40799E-01>


NUMERATOR:  ASE/ WG   FILE NAME?  ASEWG.CL
 NEW FILE

  -.52700E-01
  ( .00000    )  ( .10940    )  ( .33300    )  ( .33355    )
  ( 3.1080    )  ( 20.768    )  ( 25.736    )  ( 29.272    )
  (( .92354    , .91497     , .84510     , .35067     ))
  (( .23440    , 1.5927     , .37333     , 1.5483     ))
  <-66.127    >
```

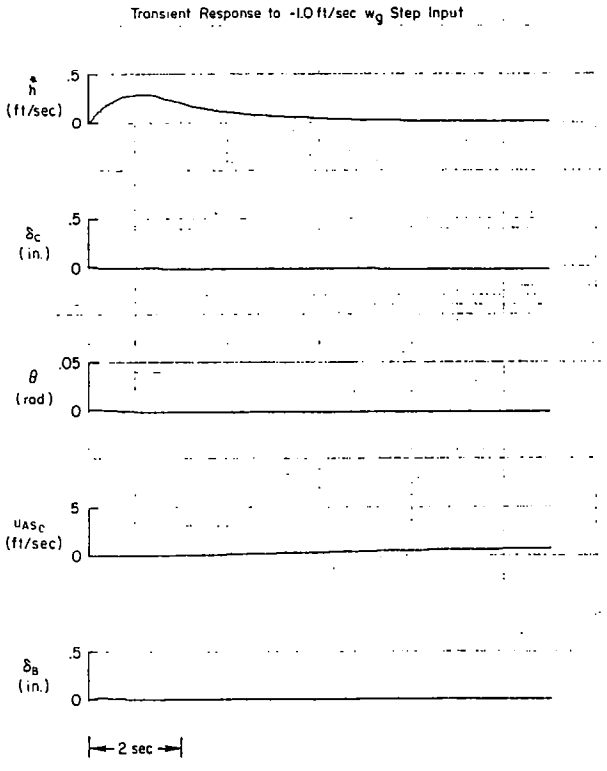

(continued on following page)

Figure D-1. (Continued)

Rate-of-Climb Command Transfer Functions

CASE: UH1H 100KT 128LONG 31-JAN-79 ALL LOOPS CLOSED

DENOMINATOR:

```
  1.0000
( .15598E-01)  ( .62689E-01)  ( .11136    )  ( .33300    )
( .33514    )  ( 25.074    )  ( 25.736    )  ( 25.736    )
(( .99458    , .72781    , .72387    , .75547E-01))
(( .56441    , 2.2044    , 1.2442    , 1.8197    ))
< .51948    >
```

NUMERATOR: HD/HDC FILE NAME? HDHDC.CL
NEW FILE

```
  27.968
( .15617E-01)  ( .63541E-01)  ( .11136    )  ( .32788    )
( .33300    )  ( .40471    )  ( 25.074    )  ( 25.736    )
(( .32561    , 2.4279    , .79056    , 2.2956    ))
< .51948    >
```

EXCESS OR INCORRECT ROOT FOUND

NUMERATOR: TH/HDC FILE NAME? THHDC.CL
NEW FILE

```
  .49448
( .11135    )  ( .33300    )  ( .33300    )  ( .39405    )
( 1.3004    )  ( 25.074    )  ( 25.732    )
(( .89777    , .12159E-01, .10916E-01, .53558E-02))
< .29846E-03>
```

NUMERATOR: DB/HDC FILE NAME? DBHDC.CL
NEW FILE

```
  -2.9885
(-.26572E-01)  ( .11136    )  ( .33300    )  ( .38836    )
( .63001    )  ( 25.074    )  ( 25.736    )
((-.17394    , .11043    ,-.19209E-01, .10875    ))
(( .48953    , 1.5212    , .74959    , 1.3352    ))
< .13345E-01>
```

NUMERATOR: DC/HDC FILE NAME? DCHDC.CL
NEW FILE

```
  .99066
( .22109E-01)  ( .11135    )  ( .11600    )  ( .31741    )
( .33300    )  ( .43851    )  ( .98720    )  ( 25.074    )
( 25.736    )
(( .55628    , 2.2228    , 1.2365    , 1.8471    ))
< .40857E-01>
```

NUMERATOR: ASE/HDC FILE NAME? ASEHDC.CL
NEW FILE

```
  -2.0226
( .00000    )  ( .11136    )  ( .33300    )  ( .33354    )
( .39154    )  ( 1.3953    )  ( 25.074    )  ( 25.736    )
(( .16643E-01, 2.6149    , .43519E-01, 2.6145    ))
<-59.894    >
```

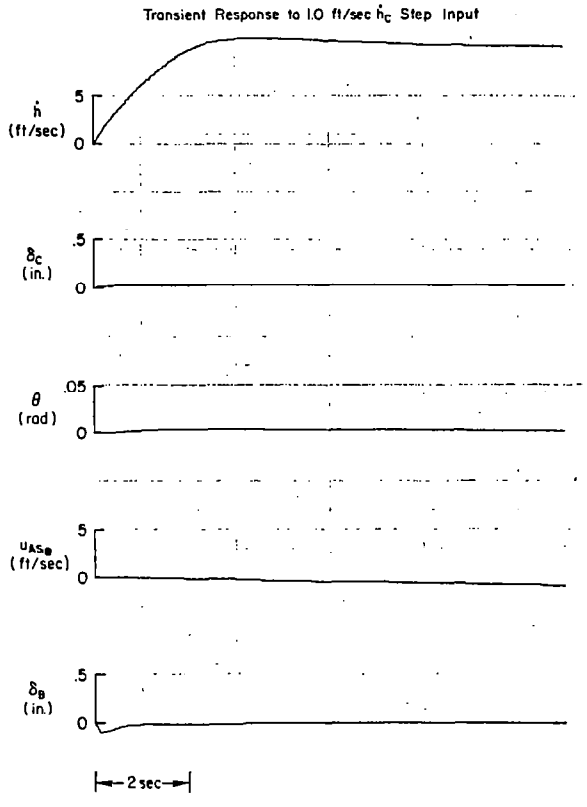

Figure D-1. (Concluded)

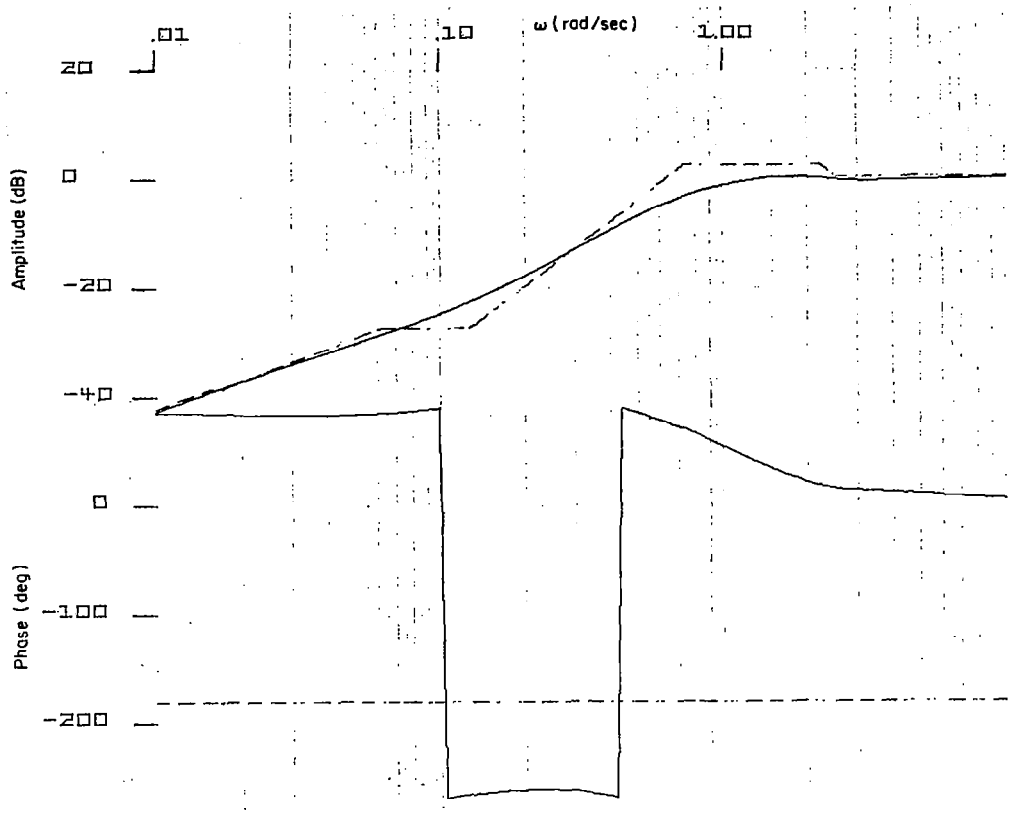

CASE: UH1H 100KT 128LONG 31-JAN-79 ALL LOOPS CLOSED

DENOMINATOR:

```
 1.0000
( .15598E-01)  ( .62689E-01)  ( .11136    )  ( .33300    )
( .33514    )  ( 25.074    )  ( 25.736    )  ( 25.736    )
(( .99458    , .72781    , .72387    , .75647E-01))
(( .56441    , 2.2044    , 1.2442    , 1.8197    ))
< .51948    >
```

NUMERATOR: HDE/HDC

```
 1.0000
( .00000    )  ( .17300E-01)  ( .11135    )  ( .33300    )
( .34523    )  ( 25.074    )  ( 25.736    )  ( 26.861    )
(( .99660    , .12917    , .12873    , .10644E-01))
(( .51985    , 2.5050    , 1.3022    , 2.1399    ))
< .40192    >
```

$$\frac{\dot{h}_e}{\dot{h}_c} \doteq \frac{s[s^2 + (.997)(.13)s + (.13)^2]}{(s + .06)[s^2 + 2(.995)(.73)s + (.73)^2]}$$

Figure D-2. Closed-Loop Frequency Response: $\dot{h}_e/\dot{h}_c$

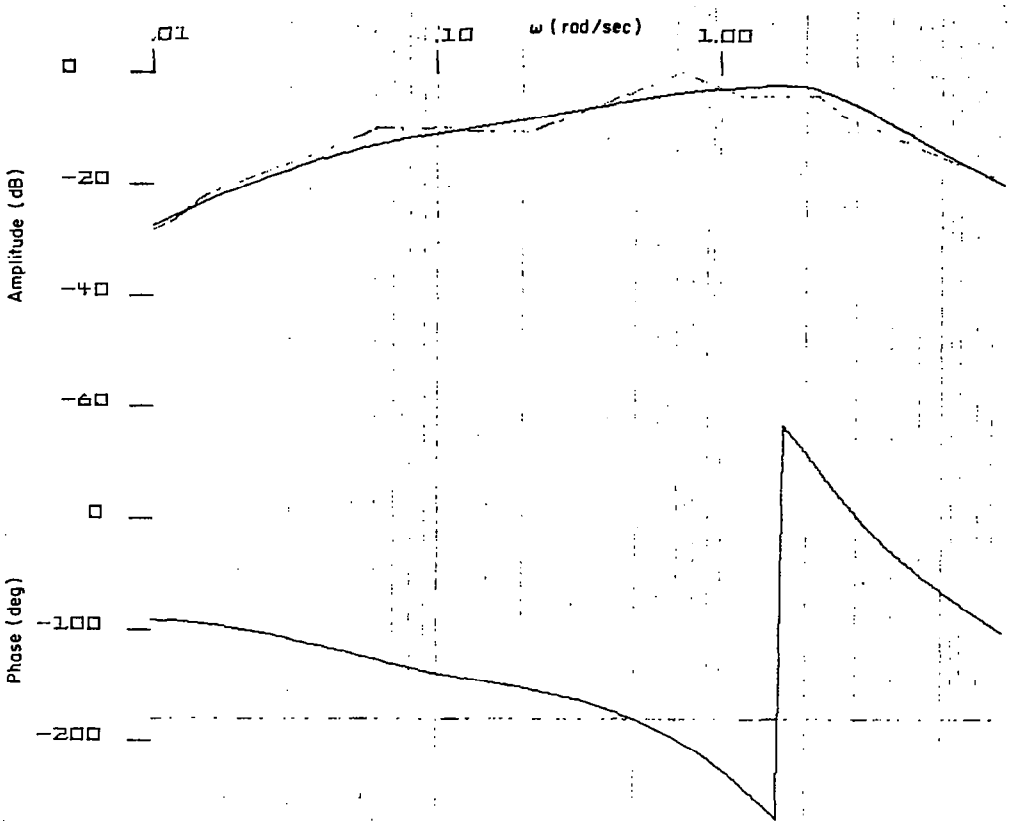


```
  CASE:  UH1H 100KT 128LONG 31-JAN-79 ALL LOOPS CLOSED
DENOMINATOR:

   1.0000
  ( .15598E-01)  ( .62689E-01)  ( .11135    )  ( .33300    )
  ( .33514    )  ( 25.074    )  ( 25.736    )  ( 25.736    )
  (( .99458    , .72781    , .72387    , .75647E-01))
  (( .56441    , 2.2044    , 1.2442    , 1.8197    ))
  < .51948    >


NUMERATOR:   TH/VTH   FILE NAME?  THVTH.CL
 NEW FILE

   704.78
  ( .00000    )  ( .11816E-01)  ( .12216    )  ( .21162    )
  ( .33300    )  ( .33300    )  ( 1.2135    )  (-2.7713    )
  ( 25.736    )
  <-2.0661    >
```

$$\frac{\theta}{\theta_c} \doteq \frac{705.0s(s+.212)(s+1.2)(s-2.77)}{(s+.063)(s+25.1)(s+25.7)[s^2+2(.99)(.73)s+(.73)^2][s^2+2(.56)(2.2)s+(2.2)^2]}$$

Figure D-3. Closed-Loop Frequency Response: $\theta/v_\theta \doteq \theta/\theta_c$

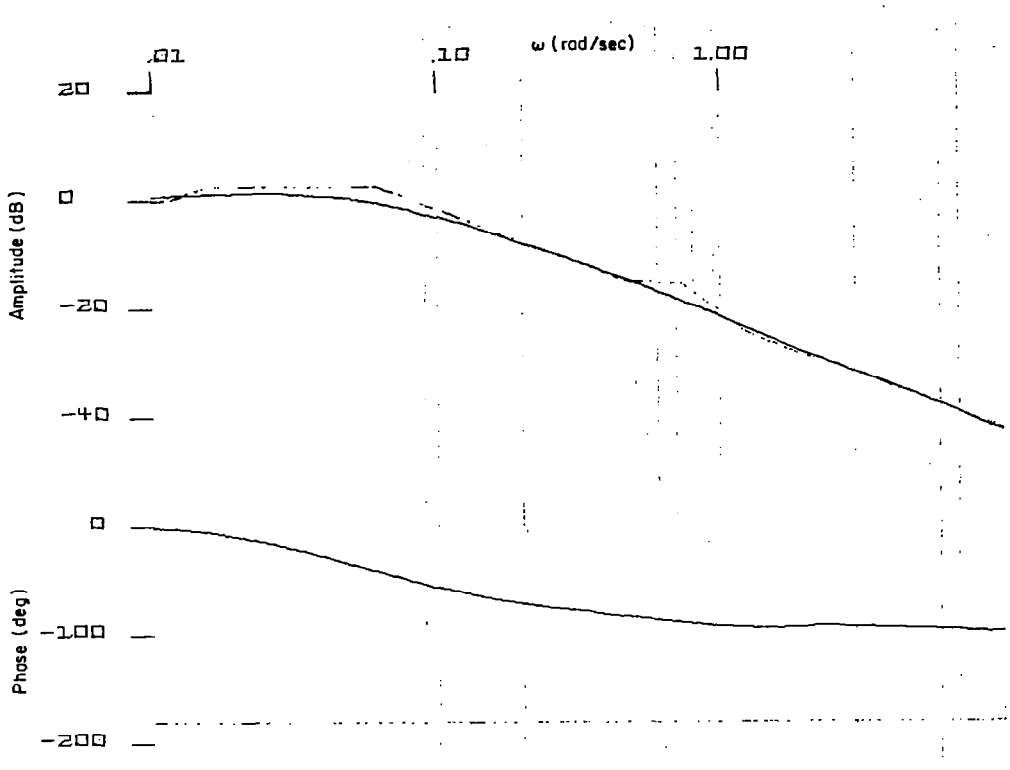


```
  CASE:  UH1H 100KT 128LONG 31-JAN-79 ALL LOOPS CLOSED

DENOMINATOR:

   1.0000
 ( .15598E-01)  ( .62689E-01)  ( .11136    )  ( .33300    )
 ( .33514    )  ( 25.074    )  ( 25.736    )  ( 25.736    )
 (( .99458    , .72781    , .72387    , .75647E-01))
 (( .56441    , 2.2044    , 1.2442    , 1.8197    ))
 < .51948    >


NUMERATOR:  X06/ UG   FILE NAME?  UUG.CL
 NEW FILE

   .45100E-01
 ( .11484E-01)  ( .11322    )  ( .33297    )  ( .33301    )
 ( .48113    )  ( 1.2669    )  ( 23.801    )  ( 25.732    )
 ( 46.923    )
 (( .54154    , 2.1330    , 1.1551    , 1.7931    ))
 < .51818    >
```

$$\frac{u}{u_g} \doteq \frac{.045(s+.48)(s+1.3)}{(s+.063)[s^2+2(.99)(.73)s+(.73)^2]}$$

Figure D-4. Closed-Loop Frequency Response: u/u_g

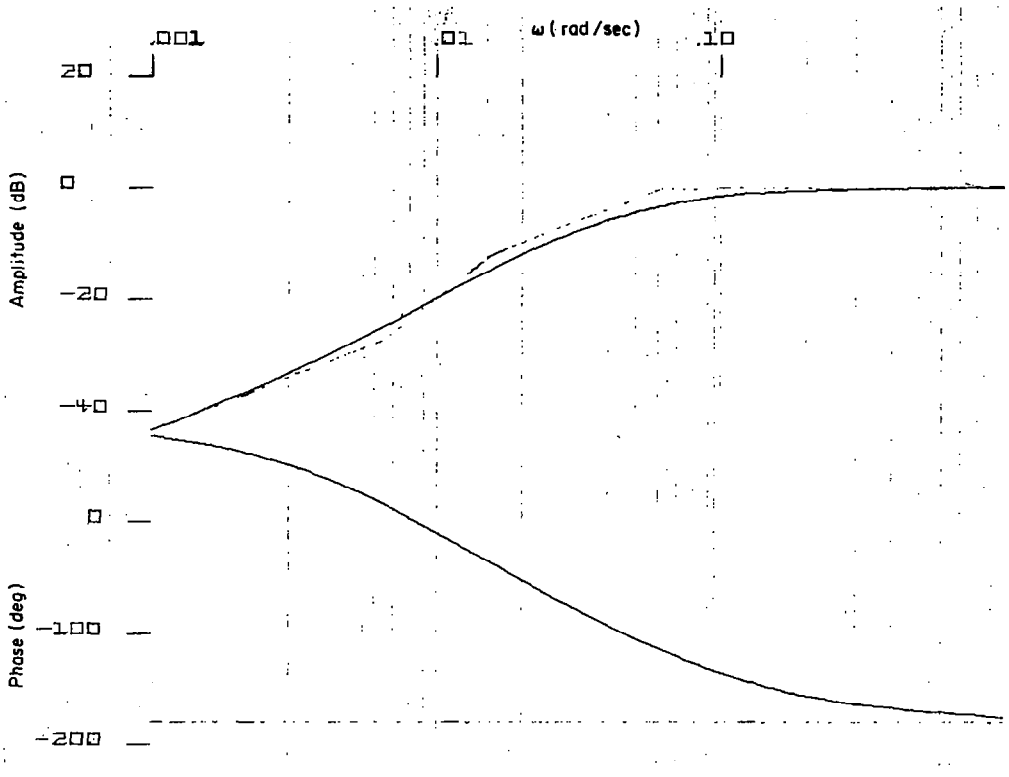

CASE: UH1H 100KT 128LONG 31-JAN-79 ALL LOOPS CLOSED

DENOMINATOR:

```
 1.0000
( .15598E-01)  ( .62689E-01)  ( .11136    )  ( .33300    )
( .33514    )  ( 25.074    )  ( 25.736    )  ( 25.736    )
(( .99458    , .72781    , .72387    , .75647E-01))
(( .56441    , 2.2044    , 1.2442    , 1.8197    ))
< .51948    >
```

NUMERATOR: ASE/ UG FILE NAME? ASEUG.CL
NEW FILE

```
-.99860
( .00000    )  (-.64568E-02)  ( .11254    )  ( .33300    )
( .33490    )  ( .65545    )  ( .79111    )  ( 24.383    )
( 25.736    )  ( 26.458    )
(( .55909    , 2.2381    , 1.2513    , 1.8556    ))
< 3.4897    >
```

$$\frac{u_{AS_e}}{u_g} \doteq \frac{-1.0s(s+.655)(s+.79)}{(s+.02)[s^2+2(.99)(.73)s+(.73)^2]}$$

Figure D-5. Closed-Loop Frequency Response: u_{AS_e}/u_g

TABLE D-10. CLOSED-LOOP SYSTEM RMS PERFORMANCE
(PROCESS NOISE AUGMENTATION REMOVED)

RMS, TOTAL

1	
2.06	X01
1.71	X02
1.00	X03
2.17	X06
1.48	X07
0.454E-02	X08
0.722E-02	X09
0.449E-01	X10
0.779E-01	X11
1.36	X12
0.233E-01	X13
63.6	X14
0.233E-01	E13
2.35	E01
36.1	E02

RMS, OUTPUT+CONTROLS

1	
1.06	HD
0.454E-02	Q
0.722E-02	TH
0.449E-01	DB
0.779E-01	DC
1.36	HDI
0.503	HDE
63.6	ASI
2.30	ASE
2.18	XD
0.812E-02	AOA
0.318	DBD
0.963E-01	DCD

CONTROL ACTIVITY	
CONTROL	POSITIVE-GOING ZERO-CROSSING RATE, $(1/2\pi)(\sigma_{\dot{x}}/\sigma_x)$
DB	1.13 (1/sec)
DC	0.197 (1/sec)

APPENDIX E

METHOD EXTENSION WHEN $(\Gamma_2 Q \Gamma_2')$ IS SINGULAR

APPROACH

Augment the Γ_S and Γ_C matrices so that the rank of Γ_2 is n_{w_2}

$$\Gamma = \begin{bmatrix} \Gamma_S \\ \Gamma_C \end{bmatrix} = T^{-1} \begin{bmatrix} \Gamma_1 \\ \Gamma_2 \end{bmatrix}$$

and the first n_{w_1} columns of Γ represent the process noise effects which are actually part of the first principles plant model. The remaining $n_w - n_{w_1} = n_{w_2}$ components of process noise are added for convenience in obtaining alternative limiting forms for the singular filter. The intensities of these n_{w_2} components are allowed to approach zero according to some externally specified ratio relationship chosen by the designer. (This is akin to the arbitrariness in selection of observer poles by the designer.)

This means that the diagonal Q matrix has the form

$$Q = \text{diag}\left\{ q_1, \cdots q_{n_{w_1}}, \mu, \mu q_{n_{w_1+2}}, \cdots \mu q_{n_w} \right\}$$

where $q_{n_{w_1+1}} = 1$ and μ approaches zero from above. Notice that there is also some arbitrariness in the elements of the n_{w_2} columns used to augment the Γ_S and Γ_C matrices. The effective maximum number of parameters which may be arbitrarily selected is $(nn_{w_2} - 1)$. The only restriction on parameter choices is that $(\Gamma_2 Q \Gamma_2')$ have full rank, $r = m_2$, for $\mu > 0$. Notice also that the columns augmenting Γ_1 may be identically zero by choice. This in turn results in Λ_{11} and Λ_{12} (see below) being null matrices.

The terms involved in the Euler-Lagrange equations for the optimal filter are $\Gamma_1 Q \Gamma_1'$, $\Gamma_1 Q \Gamma_2'$ and $(\Gamma_2 Q \Gamma_2')^{-1}$.

Separate the terms $\Gamma_1 Q \Gamma_1'$, $\Gamma_1 Q \Gamma_2'$ and $(\Gamma_2 Q \Gamma_2')^{-1}$ into components which are independent of and dependent on μ. That is, let

$$\Gamma_1 Q \Gamma_1' = \Xi_{11} + \mu \Lambda_{11}$$

$$\Gamma_1 Q \Gamma_2' = \Xi_{12} + \mu \Lambda_{12} = (\Gamma_2 Q \Gamma_1')'$$

$$\Gamma_2 Q \Gamma_2' = \Xi_{22} + \mu \Lambda_{22} \triangleq A^{-1}$$

Next, consider the behavior of various factors occurring in the Euler-Lagrange equations in the limit as μ approaches zero from above.

$$\lim_{\mu \xrightarrow{+} 0} \Gamma_1 Q \Gamma_1' = \Xi_{11}$$

$$\lim_{\mu \xrightarrow{+} 0} (\Gamma_2 Q \Gamma_2')^{-1} = \lim_{\mu \xrightarrow{+} \infty} (A^{(1)} + A^{(2)}/\mu)$$

$$\lim_{\mu \xrightarrow{+} 0} \Gamma_1 Q \Gamma_2' (\Gamma_2 Q \Gamma_2')^{-1} = \lim_{\epsilon \to 0} \left(\Xi_{12} A^{(1)} + \Lambda_{12} A^{(2)} + \Xi_{12} A^{(2)}/\mu \right)$$

$$\lim_{\mu \xrightarrow{+} 0} \Gamma_1 Q \Gamma_2' (\Gamma_2 Q \Gamma_2')^{-1} \Gamma_2 Q \Gamma_1'$$

$$= \lim_{\mu \xrightarrow{+} 0} \left(\Xi_{12} A^{(1)} \Xi_{12}' + \Lambda_{12} A^{(2)} \Xi_{12}' + \Xi_{12} A^{(2)} \Lambda_{12}' + \Xi_{12} A^{(2)} \Xi_{12}'/\mu \right)$$

The procedure continues by substituting the separated quantities into the Euler-Lagrange equation:

$$\begin{bmatrix} (sI-F_{11}) & \Gamma_1 Q \Gamma_1' \\ H_{11}' R_1^{-1} H_{11} & (sI+F_{11}') \end{bmatrix} \begin{Bmatrix} x_1 \\ \lambda_1 \end{Bmatrix}$$

$$= \begin{Bmatrix} x_{10} \\ \lambda_{10} \end{Bmatrix} + \begin{bmatrix} G_1 & 0 & F_{12} \\ 0 & H_{11}' R_1^{-1} & -H_{11}' R_1^{-1} H_{12} \end{bmatrix} \begin{Bmatrix} u \\ z_1 \\ z_2 \end{Bmatrix}$$

$$- \begin{bmatrix} \Gamma_1 Q \Gamma_2' (\Gamma_2 Q \Gamma_2')^{-1} F_{21} & -\Gamma_1 Q \Gamma_2' (\Gamma_2 Q \Gamma_2')^{-1} \Gamma_2 Q \Gamma_1' \\ F_{21}' (\Gamma_2 Q \Gamma_2')^{-1} F_{21} & -F_{21}' (\Gamma_2 Q \Gamma_2')^{-1} \Gamma_2 Q \Gamma_1' \end{bmatrix} \begin{Bmatrix} x_1 \\ \lambda_1 \end{Bmatrix} + \begin{bmatrix} \Gamma_1 Q \Gamma_2' (\Gamma_2 Q \Gamma_2')^{-1} \\ F_{21}' (\Gamma_2 Q \Gamma_2')^{-1} \end{bmatrix} z_{20}$$

$$- \begin{bmatrix} \Gamma_1 Q \Gamma_2' (\Gamma_2 Q \Gamma_2')^{-1} G_2 & 0 & -\Gamma_1 Q \Gamma_2' (\Gamma_2 Q \Gamma_2')^{-1} (sI - F_{22}) \\ F_{21}' (\Gamma_2 Q \Gamma_2')^{-1} G_2 & 0 & -F_{21}' (\Gamma_2 Q \Gamma_2')^{-1} (sI - F_{22}) \end{bmatrix} \begin{Bmatrix} u \\ z_1 \\ z_2 \end{Bmatrix}$$

The result is:

$$\begin{bmatrix} (sI - F_{11} + [\Xi_{12} A^{(1)} + \Lambda_{12} A^{(2)} + \Xi_{12} A^{(2)}/\mu] F_{21}) & (\Xi_{11} - [\Xi_{12} A^{(1)} \Xi_{12}' + \Lambda_{12} A^{(2)} \Xi_{12}' + \Xi_{12} A^{(2)} \Lambda_{12}' + \Xi_{12} A^{(2)} \Xi_{12}'/\mu]) \\ (H_{11}' R_1^{-1} H_{11} + F_{21}' [A^{(1)} + A^{(2)}/\mu] F_{21}) & (sI + F_{11}' - F_{21}' [A^{(1)} \Xi_{12}' + A^{(2)} \Lambda_{12}' + A^{(2)} \Xi_{12}'/\mu]) \end{bmatrix} \begin{Bmatrix} x_1 \\ \lambda_1 \end{Bmatrix}$$

$$= \begin{Bmatrix} x_{10} \\ \lambda_{10} \end{Bmatrix} \begin{bmatrix} (\Xi_{12} A^{(1)} + \Lambda_{12} A^{(2)} + \Xi_{12} A^{(2)}/\mu) \\ F_{21}' [A^{(1)} + A^{(2)}/\mu] \end{bmatrix} z_{20}$$

$$+ \begin{bmatrix} (G_1 - [\Xi_{12} A^{(1)} + \Lambda_{12} A^{(2)} + \Xi_{12} A^{(2)}/\mu] G_2 & 0 & (F_{12} + [\Xi_{12} A^{(1)} + \Lambda_{12} A^{(2)} + \Xi_{12} A^{(2)}/\mu](sI - F_{22})) \\ -F_{21}' [A^{(1)} + A^{(2)}/\mu] G_2 & H_{11} R_1^{-1} & (-H_{11}' R_1^{-1} H_{12} + F_{21}' [A^{(1)} + A^{(2)}/\mu][sI - F_{22}]) \end{bmatrix} \begin{Bmatrix} u \\ z_1 \\ z_2 \end{Bmatrix}$$

The revised steps in solution are as follows.

- Evaluate each element of each matrix in terms of numerical coefficient values for s^0, s^1, s^0/μ and s^1/μ in each matrix.

- Examine the resulting matrix equations via inspection of the numerical coefficients. If any equation has one or more non-zero coefficients for s^0/μ and/or s/μ, then multiply that equation through by μ and let $\mu \rightarrow 0$. (This is equivalent to simply retaining only the coefficients for s^0/μ and s^1/μ in that equation.)

- Eliminate a number of variables corresponding to the number of equations which are rendered algebraic in x_1 and λ_1 as the result of the previous step, via substitution.

- Apply eigenvalue decomposition (or matrix Riccati equation solution) technique to the resulting reduced Euler-Lagrange equations (refer to pages A-5 to A-7 of Appendix A). Notice that the form of the filter-observer solution must be modified to allow for differentiation of the measurements. Multiple differentiation may be required.

- Use the algebraic equations identified in the next-to-last step to obtain estimates of the remaining states.

APPENDIX F

EFFECT OF AUGMENTING PROCESS NOISE INTENSITIES ON FILTER EIGENVALUES AND RMS ESTIMATION ERROR

Data for three filter design passes is summarized in this appendix. The filter is for the longitudinal dynamics of the UH-1H helicopter in 100 kt cruise. All measurements are noise free. The nine measurements include airspeed error and integral airspeed error as appropriate for cruise. The third and final filter design has acceptable rms estimation error and closed-loop eigenvalues which are within the acceptable range.

TABLE F-1. INITIAL FILTER DESIGN, 100 KT

Q MATRIX DIAGONAL, FILTER 1

4.24	1 PUG
2.92	2 PWG
1.00	3 PHC
0.100E-03	4 P U
0.100E-03	5 P W
0.100E-03	6 P Q
0.100E-03	7 PTH
0.100E-03	8 PDB
0.100E-03	9 PDC
0.100E-03	10 PHE
0.100E-03	11 PXB
0.100E-03	12 PSE

CLOSED LOOP EIGENVALUES, FILTER 1

126. 180.	1 E13
0.392 180.	2 E01
0.331E-02 180.	3 E02

RMS STATE EST ERROR, FILTER 1

0.482	1 X01
0.128	2 X02
0.000	3 X03
0.482	4 X06
0.254E-01	5 X07
0.000	6 X08
0.406E-13	7 X09
0.000	8 X10
0.000	9 X11
0.000	10 X12
0.117E-01	11 X13
0.000	12 X14

K12 GAIN MATRIX, FILTER

1 HD	2 Q	3 TH	4 DB	5 DC	6 HDI	7 HDE	8 ASI	9 ASE	
-0.386E-01	-0.285	6.52	0.000	0.000	0.144E-07	-0.308E-07	-0.449E-06	0.180E-03	1 E13
6.72	-0.048	-0.113E+04	0.000	0.000	0.862E-05	0.535E-05	-0.287E-03	-0.969	2 E01
-125.	2.23	0.211E+05	0.000	0.000	0.359E-06	-0.995E-04	-0.126E-04	-0.836E-01	3 E02

TABLE F-2. SECOND FILTER DESIGN, 100 KT

Q MATRIX DIAGONAL, FILTER 1

4.24	1 PUG
2.92	2 PWG
1.00	3 PHC
0.100E-01	4 P U
0.000	5 P W
0.100E-03	6 P Q
0.100E-05	7 PTH
0.100E-03	8 PDB
0.100E-03	9 PDC
0.100E-03	10 PHE
0.000	11 PXB
0.100E-03	12 PSE

CLOSED LOOP EIGENVALUES, FILTER 1

0.333	1
180.	E13
240.	2
180.	E01
0.116E-01	3
180.	E02

RMS STATE EST ERROR, FILTER 1

0.875	1 X01
0.934E-01	2 X02
0.000	3 X03
0.875	4 X06
0.462E-01	5 X07
0.000	6 X08
0.736E-13	7 X09
0.000	8 X10
0.000	9 X11
0.000	10 X12
0.000	11 X13
0.000	12 X14

K12 GAIN MATRIX, FILTER

1 HD	2 Q	3 TH	4 DB	5 DC	6 HDI	7 HDE	8 ASI	9 ASE	
0.433E-05	-0.814E-08	-0.731E-03	0.000	0.000	0.696E-19	0.587E-12	0.493E-14	-0.228E-08	1 E13
13.1	0.765E-02	-0.221E+04	0.000	0.000	0.284E-04	0.178E-05	-0.944E-03	-0.904	2 E01
-238.	0.450	0.402E+05	0.000	0.000	0.158E-05	-0.323E-04	-0.502E-04	0.472E-01	3 E02

TABLE F-3. FINAL FILTER DESIGN, 100 KT

Q MATRIX DIAGONAL, FILTER 1

4.24	1 PUG
2.92	2 PWG
1.00	3 PHC
10.0	4 P U
0.000	5 P W
0.100E-03	6 P Q
0.100E-05	7 PTH
0.100E-03	8 PDB
0.100E-03	9 PDC
0.100E-03	10 PHE
0.000	11 PXB
0.100E-03	12 PSE

CLOSED LOOP EIGENVALUES, FILTER 1

0.333	1 E13
180.	
25.1	2 E01
180.	
0.111	3 E02
180.	

RMS STATE EST ERROR, FILTER 1

2.03	1 X01
0.277	2 X02
0.000	3 X03
2.03	4 X06
0.107	5 X07
0.000	6 X08
0.171E-12	7 X09
0.000	8 X10
0.000	9 X11
0.000	10 X12
0.000	11 X13
0.000	12 X14

K12 GAIN MATRIX, FILTER

1 HD	2 Q	3 TH	4 DB	5 DC	6 HDT	7 HDE	8 ASI	9 ASE	
0.130E-06	-0.207E-07	-0.220E-04	0.000	0.000	-0.155E-12	0.134E-13	0.518E-11	-0.629E-09	1 E13
1.53	1.39	-259.	0.000	0.000	0.153E-03	0.156E-05	-0.508E-02	-0.120	2 EC1
-24.7	4.41	0.417E+04	0.000	0.000	0.081E-05	-0.254E-05	-0.296E-03	1.18	3 E02

1. Report No.	2. Government Accession No.	3. Recipient's Catalog No.
NASA CR-3275		

4. Title and Subtitle	5. Report Date
PRACTICAL OPTIMAL FLIGHT CONTROL SYSTEM DESIGN FOR HELICOPTER AIRCRAFT. Volume I - Technical Report	May 1980
	6. Performing Organization Code
7. Author(s)	8. Performing Organization Report No.
L. G. Hofmann, Susan A. Riedel, and Duane McRuer	TR-1127-1-I
	10. Work Unit No.
9. Performing Organization Name and Address	11. Contract or Grant No.
Systems Technology, Inc. 13766 South Hawthorne Boulevard Hawthorne, California 90250	NAS2-9946
	13. Type of Report and Period Covered
12. Sponsoring Agency Name and Address	Contractor Report
National Aeronautics and Space Administration Washington, D. C. 20546	14. Sponsoring Agency Code

15. Supplementary Notes

Ames Technical Monitor: Heinz Erzberger

16. Abstract

A method by which modern and classical control theory techniques may be integrated in a synergistic fashion and used in the design of practical flight control systems is presented here. A general procedure is developed, and several illustrative examples are included. Emphasis is placed not only on the synthesis of the design, but on the assessment of the results as well.

The first step here is to establish the differences, distinguishing characteristics and connections between the modern and classical control theory approaches. Ultimately, this uncovers a relationship between bandwidth goals familiar in classical control and cost function weights in the equivalent optimal system. In order to obtain a practical optimal solution, it is also necessary to formulate the problem very carefully, and each choice of state, measurement and output variable must be judiciously considered. These so-called "engineering art" matters allow us to bridge the gap between the optimal control theory and its practical application.

Once design goals have been established and problem formulation completed, the control system is synthesized in a straightforward manner. Three steps are involved: filter-observer solution, regulator solution and the combination of those two into the controller. Assessment of the controller, which is obten the bulk of the task at hand, permits an examination and expansion of the synthesis results. Often, the composite picture which results may lead to a revised design which is simpler and more practical.

Key contributions in this work include the solution of the singular Kalman filter problem, presented in an appendix, and the development of a user-oriented computer software package for the design and assessment of optimal flight control systems. Volume II of this report contains the software details in the form of a user's guide. Volume II is available as a high contractor report number 152306 on microfiche.

17. Key Words (Suggested by Author(s))	18. Distribution Statement
Optimal Control-Theory, Helicopter Flight Control Systems, Singular Kalman Filter, Optimal Control-Software, Optimal Control-Application, Cost Function Weights, Classical Control Analysis	Unclassified - Unlimited STAR CATEGORY - 08

19. Security Classif. (of this report)	20. Security Classif. (of this page)	21. No. of Pages	22. Price*
Unclassified	Unclassified	271	$10.75

*For sale by the National Technical Information Service, Springfield, Virginia 22161

NASA-Langley, 1980